



EANDC (E) 89 "U"

**INDC(EUR)-001/u**

PROGRESS REPORT  
ON NUCLEAR DATA RESEARCH IN THE  
EURATOM COMMUNITY

for the period January 1 to December 31, 1967

Submitted by the Joint Euratom Nuclear Data  
and Reactor Physics Committee

(Secretariat : Central Bureau for Nuclear  
Measurements, Euratom, Geel, Belgium)

February, 1968

**LEGAL NOTICE :**

The information contained in this progress report has a preliminary character.

No data contained in this report may be used without the permission of the responsible authorities.

It is suggested that experimentators should be contacted in this respect.

EANDC(E) 89 "U"

PROGRESS REPORT  
ON NUCLEAR DATA RESEARCH IN THE EURATOM COMMUNITY  
for the period January 1 to December 31, 1967

Submitted by the Joint Euratom Nuclear Data  
and Reactor Physics Committee

(Secretariat : Central Bureau for Nuclear  
Measurements, Euratom, Geel, Belgium)

February, 1968

EUROPEAN AMERICAN NUCLEAR DATA COMMITTEE

## I N D E X

I.	Kernforschungszentrum Karlsruhe (Germany) Institut für Angewandte Kernphysik	1
II.	Physik-Department, Technische Hochschule München (Germany)	35
III.	Institut für Festkörper - und Neutronenphysik, Kernforschungsanlage Jülich	55
IV.	Institut für Kernphysik, University of Frankfurt/ Main (Germany)	58
V.	Physikalisches Staatsinstitut, I. Institut für Experimentalphysik, Hamburg (Germany)	59
VI.	Institut für Reine und Angewandte Kernphysik der Universität Kiel	63
VII.	Reactor Centrum Nederland, Petten (Netherlands) F.O.M. Groups	64
VIII.	Reactor Instituut Delft (Netherlands)	67
IX.	Laboratorio di Fisica Nucleare Applicate, Centro di Studi Nucleari del C.N.E.N., Casaccia (Roma) (Italy)	68
X.	Sottosezione di Firenze dell'Istituto Nazionale di Fisica Nucleare - Istituto di Fisica dell'Università', Firenze (Italy)	72
XI.	Centro Siciliano di Fisica Nucleare, Istituto Nazionale di Fisica Nucleare, Sezione Siciliana - Istituto di Fisica della Università', Catania (Italy)	78
XII.	Gruppo di Ispra per le Misure di Sezione d'Urto del C.N.E.N. Ispra (Varese) (Italy)	83
XIII.	Laboratorio dati Nucleari, Centro di Calcolo del C.N.E.N., Bologna (Italy)	85
XIV.	Gruppo di Ricerca del Contratto Euratom-CNEN-INFN - Istituto di Fisica dell'Università', Bologna (Italy)	92
XV.	Gruppo di Ricerca del Contratto Euratom-CNEN-INFN- di Fisica dell'Università', Genova (Italy)	94

XVI.	Gruppo di Ricerca del Contratto Euratom-CNEN-INFN - Istituto di Fisica dell'Universita', Pavia (Italy)	97
XVII.	Gruppo di Ricerca del Contratto Euratom-CNEN-INFN - Istituto di Fisica dell'Universita', Roma (Italy)	100
XVIII.	Gruppo di Ricerca del Contratto Euratom-CNEN-INFN - Istituto di Fisica dell'Universita', Padova (Italy)	112
XIX.	Centre de Physique Nucléaire de l'Université de Louvain (Belgium)	116
XX.	Laboratoire Van de Graaff, Université de Liège (Belgium)	118
XXI.	Centre d'Etude de l'Energie Nucléaire (CEN-SCK), Mol (Belgium)	119
XXII.	Central Bureau for Nuclear Measurements, EURATOM, Geel (Belgium)	129
XXIII.	Section des Mesures Neutroniques Fondamentales, C.E.A. - Saclay (France)	171
XXIV.	Département de Physique Nucléaire, C.E.A. - Saclay (France)	206
XXV.	Sections de Mesures Fondamentales du Commissariat à l'Energie Atomique (France)	215
XXVI.	Service de Physique Générale du Commissariat à l'Energie Atomique (France)	233
XXVII.	Laboratoire de Physique Nucléaire, Centre d'Etudes Nucléaires de Grenoble - Commissariat à l'Energie Atomique, et Université de Grenoble (France)	234



KERNFORSCHUNGSZENTRUM KARLSRUHE (GERMANY)  
INSTITUT FÜR ANGEWANDTE KERNPHYSIK

1. 3 MeV Van de Graaf

1.1. High Resolution Resonance Spectroscopy

G. Rohr, K-N. Müller

The measurements of the total neutron cross section of separated isotopes with high resolution were continued. The elements  $^{53}\text{Cr}$  and  $^{49}\text{Ti}$  were measured in the energy range of 20 - 250 keV, the copper isotopes in the range of  $40 \sim 250$  keV.

Figures 1 - 4 show the cross sections as a function of the energy for these elements. The pronounced energy dependent background at 20 keV for the  $^{49}\text{Ti}$  - probe (enriched to 76 %) is due to resonances of the  $^{48}\text{Ti}$  isotope.

The analysis of the  $^{57}\text{Fe}$  and  $^{53}\text{Cr}$  data with the one channel multi-level formula was started but not completed. In the cross sections of these elements we find broad structures with one or more resonances superposed on them (see KFK 452 (1966)):  $^{57}\text{Fe}$  at the energies 60 and 135 keV,  $^{53}\text{Cr}$  at 72 and 93 keV). Until now we have not yet achieved a satisfactory interpretation of these phenomena. In the case of  $^{57}\text{Fe}$  we have to check the influence of a possible inelastic scattering channel for the compound states  $J = 1$  on the shape of the cross section.

A further broad structure one can see in  $^{53}\text{Cr}$  at 137 keV, but in contrast to the above mentioned structures we find a resolved resonance with spin 2 at 125 keV which shows a strong interference effect. The shape of this resonance can be explained only by interference with an underlying broad resonance of the same spin. The maximum cross section of the broad structure however corresponds

more to a resonance with spin 1 than with spin 2; but the existence of the incoherently superposed resonance at 146 keV indicates spin 2 for the broad structure. This inconsistency may be explained by a doorway structure with  $\Gamma^{\rho} \approx \Gamma^{\delta}$ . The resolution of our spectrometer is not sufficient to resolve all the small compoundresonances and we measure the average cross section, the maximum of which depends on the ratio  $\Gamma^{\delta}/\Gamma_{\rho}$ .

### 1.2. Measurement of Radiative Capture Cross Sections

D. Kompe, W. Poenitz and H. Menlove

In 1967 three measurements were performed for the accurate determination of the energy dependence of the capture cross section of gold which is frequently used as cross section standard. Each of these measured cross section shapes was normalized to an absolute value  $\sigma_{n,\gamma}^{Au}$  (30 KeV) = .596 barn [1].

One of these shape measurements [1] uses an energy independent "grey neutron detector" [2] as flux monitor for monoenergetic neutron pulses and a large liquid scintillator [3] for the detection of capture events in the gold sample. Two other shape measurements with the large liquid scintillator referred to the  $^{10}B(n,\alpha,\gamma)$  [4] and  $^6Li(n,\alpha)$  [5] cross sections using a Li-glass detector and a  $^{10}B$  -slab viewed by 4 NaI-cristalls. Fig. 5 shows the results of these three measurements. The full line represents an average curve through the experimental points of the "grey neutron detector" measurement.

The new standard cross section for Au ( $n,\gamma$ ) (Fig. 17) was used to renormalize our preliminary capture cross section data for Nb, Mo, Pd, Ag, Cd, In, Co, Hf, Ta, W and Re [3]. Fig. 6 - 17 show the results of this revaluation and the data of other authors. Fitted curves and the contributions from the single partial waves  $l = 0, 1, 2$  are represented by full lines; inelastic scattering effects were not taken into account in the calculated curves. The p- and d-wave strength functions derived from these least square fits are shown in the following table I.

Table I : Strength functions for p- and d-waves.

Element	A	$S_1 \cdot 10^4$	$S_2 \cdot 10^4$
Nb	93	$11 \pm 3,2$	$0,30 \pm 0,25$
Mo	95,5	$7,4 \pm 2,0$	$0,43 \pm 0,13$
Pd	106,4	$5,8 \pm 0,8$	$1,3 \pm 0,3$
Ag	107,9	$7,4 \pm 0,9$	$2,0 \pm 0,5$
Cd	112,4	$5,4 \pm 1,2$	$1,4 \pm 0,5$
In	114,8	$3,8 \pm 0,6$	$0,93 \pm 0,6$
Cs	133	$3,3 \pm 0,6$	$0,29 \pm 0,25$
Hf	178,6	$0,1 \pm 0,06$	$2,9 \pm 1,0$
Ta	181	$0,1 \pm 0,04$	$0,78 \pm 0,3$
W	183,9	$0,21 \pm 0,06$	$1,0 \pm 0,4$
Re	186,2	< 0,1	$5,4 \pm 0,7$
Au	197	$0,23 \pm 0,04$	$0,73 \pm 0,2$

A remeasurement of the  $^{238}\text{U}$  capture cross section by essentially the same technique as for the  $^{197}\text{Au}$  capture cross section was also performed [14]

References :

- [1] W.P. Poenitz, D. Kompe, H.O. Menlove  
-to be published in Journal of Nucl. Energy-
- [2] W.P. Poenitz - EANDC (E) 80 "S" (1967)
- [3] D. Kompe, Conf. on Nucl. Data for Reactors, CN-23/10 (1966)
- [4] J. Spaepen " " " " " , CN-23/119 (1966)
- [5] A. Bergström, S. Schwarz, L.G. Strömberg, CCDN-NW 3 (1966)
- [6] J. H. Gibbons, R.L. Macklin, P.D. Miller, J.H. Neiler  
-Phys. Rev. 122/1, 182 (1961)
- [7] R.L. Macklin, J.H. Gibbons, Phys. Rev. 159/4, 1007 (1967)
- [8] B.C. Diven, J. Terrell, A. Hemmendinger, Phys. Rev. 120/2 556 (1960)
- [9] W.P. Poenitz, Conf. on Nuclear Data for Reactors, CN-23/6 (1966)
- [10] Yu. P. Popov, F.L. Shapiro, Soviet Phys. JETP 15, 683 (1962)
- [11] R. Booth, W.P. Ball, M.H. Mac Gregor, Phys. Rev. 112/1 226 (1958)
- [12] R.L. Macklin, J.H. Gibbons, T. Inada, Phys. Rev. 129, 2695 (1963)
- [13] D.C. Stupegia, M. Schmidt, A.A. Madson,  
J. Nucl. Energy A/B 19, 767 (1965)
- [14] W.Pönitz and H. Menlove, Nucl. Sci. Eng (In Press).

### 1.3. Fission Cross Sections

E. Pfletschinger

Preliminary measurements of the fission cross section ratio of  $^{239}\text{Pu}$  to  $^{235}\text{U}$  were done in the energy range from 30 keV to 300 keV by time-of-flight technique with Xenon scintillation fission detectors. Till now no relevant results could be obtained due to the difficulties of discriminating fission against background caused by response of the multipliers to neutrons and by  $\alpha$ -pile up.

New detectors were prepared which allow to observe both fission products in coincidence and in the very near future measurements will be done with these detectors, trying also to enlarge the energy range in both directions.

### 1.4. Operation of the Machine

H. Miessner

The pulsed 3 MeV Van de Graaff worked without any serious breakdowns during the period covered by this report and only routine repairs were necessary. The total weekly operation time of the machine was about 130 hrs; 85% of this ~~time~~ was effectively used as measuring time.

A high vacuum test pumpstand including the whole terminal equipment of the machine (ion source, deflection chamber, pulsing device and power supply) was installed. Some improvements of the ion source system let us hope that it will be possible to increase the beam current by 30.- 50%.

## 2. $(n,\gamma)$ - Spectroscopy

W. Michaelis, U. Fanger, G. Markus, H. Ottmar, H. Schmidt

### 2.1. Introduction

At the Karlsruhe research reactor FR-2 the excited states of several nuclei have been investigated by thermal neutron capture using a 5-crystal Ge (Li) pair spectrometer [1], a Ge (Li) anti-Compton device [2,3], a Ge (Li) - NaI (Tl) coincidence system [1] and an angular correlation spectrometer. Studies were made both in the region of nearly spherical nuclei and in the region of strongly deformed nuclei. A summary of the experimental results has been presented at the Tokyo conference on nuclear structure [4].

### 2.2. Level Structure of $^{58}\text{Fe}$ and $^{62}\text{Ni}$

Since the isotopic abundance of  $^{57}\text{Fe}$  and  $^{61}\text{Ni}$  is low in the natural elements (2.19 % and 1.19 %, respectively), highly enriched samples of 90.73 %  $^{57}\text{Fe}$  and 92.11 %  $^{61}\text{Ni}$  were used as a target.

Level energies for  $^{58}\text{Fe}$  and  $^{62}\text{Ni}$  are summarized in Table II. The transition diagrams are shown in Figs. 18 and 19, respectively. Large dots indicate experimentally established coincidence relationships. Gamma rays entering a level and dotted at their arrowheads have been shown to be in coincidence with at least one gamma ray leaving the same level and dotted at its origin.

The first excited level at 810.5 keV in  $^{58}\text{Fe}$  is the well known one-phonon vibrational state. A new level with spin and parity  $0^+$  has been introduced at 2256.6 keV. This level together with the  $2^+$  state at 1674.6 keV belongs to the two-phonon triplet.

The levels at 2133.9 keV and 2781.8 keV possibly contain marked admixtures from the three-phonon excitations. This may be concluded from the branching of transitions deexciting these states. In terms of the vibrational model the assignment of the 2133.9 keV level to the two-phonon triplet must be ruled out since a transition to the second  $2^+$  state is forbidden.

Table II : Excited states in  $^{58}\text{Fe}$  and  $^{62}\text{Ni}$ .

$^{58}\text{Fe}$				$^{62}\text{Ni}$			
E [keV]	Jπ	E [keV]	Jπ	E [keV]	Jπ	E [keV]	Jπ
810.5	$2^+$	4296	$1, 2$	1172.3	$2^+$	3268.6	$1^+, 2^+$
1674.1	$2^+$	4322	$1, 2$	2047.7	$0^+$	3368.6	$1^+, 2^+$
2133.4	$3^+, 4^+$	4353		2300.9	$2^+$	3517.8	$1^+, 2^+$
2256.8	$0^+$	4444	$1, 2$	2335.2	$4^+$	3961.9	$1^+, 2^+$
2781.5	$1^+(2^+)$	4550	$(0^+)1^+, 2^+$	2889.9	$2^+, 3^+$		
2876.0	$(0^+, 1^+)2^+$	5001	$(1^+), 2^+$	3057.6	$2^+, 3^+$		
3083.8	$2^+$	5221.5	$(1^+), 2^+$	3156.8			
3244.0	$0^+(1^+, 2^+)$	5295	$(1^+, 2^+)$	3256.0			
3536.6	$1^+(2^+)$	5414					
3630	$(0^+, 1^+)2^+$	5522	$0^+(1^+, 2^+)$				
3881	$1, 2$						
4139	$1, 2$						

In  $^{62}\text{Ni}$  the levels at 1172.3, 2047.7, 2300.0 and 2335.2 keV correspond to the one- and two-phonon excitations, respectively. From the levels observed at higher energies the excited states at 3057.6, 3268.6 and 3368.6 keV show enhanced transitions to the vibrational triplet. These states therefore may be regarded as possible candidates for states with strong admixtures from the three-phonon quintuplet.

A comparison of the experimental excitation energies with the predictions of pure vibrational models [5-8] remains unsatisfactory both for  $^{58}\text{Fe}$  and  $^{62}\text{Ni}$ .

For  $^{62}\text{Ni}$  Kerman and Shakin [5] who have included cubic terms in the nuclear vibrational Hamiltonian achieved a good fit to the two-phonon levels. However, when their formulas and parameters are used to compute the three-phonon quintuplet a comparison with Fig. 19 gives no promising results. One might speculate about more realistic models such as the microscopic approaches made by Hsu and French [9] and indeed, the spectra calculated for  $^{62}\text{Ni}$  in the seniority approximations seem to give the right trend, at least as concerns the level sequence.

Angular correlation measurements on  $^{58}\text{Fe}$  and  $^{62}\text{Ni}$  are in progress. These experiments are expected to allow more precise spin determinations.

### 2.3. Gamma-Gamma Angular Correlations in $^{88}\text{Sr}$ .

Gamma-gamma angular correlations have been measured for various cascades from the reaction  $^{87}\text{Sr}(n,\gamma)^{88}\text{Sr}$ . Natural strontium was used as a target. The cross section contribution of  $^{87}\text{Sr}$  is 87.4 %. Due to the complex structure of capture spectra angular correlation measurements are extremely difficult. In order to minimize systematic errors extensive use was made of the capabilities of an on-line computer system. Some results are summarized in Table III. Column 1 gives the gamma-ray cascade. Column 2 and 3 list the coefficients for an expansion in Legendre polynomials together with the experimental errors which include both statistical and systematic uncertainties. Excitation energy, spin and parity of the initial states are given in column 4 and 5. Possible shell model configurations for the initial states are listed in column 6.

A transition diagram for  $^{88}\text{Sr}$  may be found in a recently published study [10] on neutron capture in  $^{87}\text{Sr}$ .

Table III      Angular Correlations in  $^{88}\text{Sr}$

Cascade [ keV ]	$A_2$	$A_4$	Initial state $E_i$ [ keV ]	$J_i \pi_i$	Possible structure
850 - 897	-(0.083 ± 0.010)	-(0.009 ± 0.016)	3583	4-, 5-	(p3/2) (g9/2) or (f5/2) (g9/2)
897 - 1836	-(0.079 ± 0.013)	-(0.003 ± 0.005)	2733	3-	$Q_3$
3010 - 1836	-(0.089 ± 0.007)	-(0.002 ± 0.011)	4846	3-	(p3/2) (g9/2) or (f5/2) (g9/2)

Table IV : Level structure of isotonic species  $^{165}\text{Dy}$ ,  $^{167}\text{Er}$  and  $^{169}\text{Yb}$ .

Structure	Level energies [ keV ]		
	$^{165}\text{Dy}$	$^{167}\text{Er}$	$^{169}\text{Yb}$
1/2- [ 521 ]	108.2	207.8	24.2
5/2- [ 512 ] + 1/2- [ 510 ] + $Q_{22}$	184.3	346.5	191.4
5/2- [ 523 ]	533.5	667.9	569.9
5/2+ [ 642 ] + 5/2- [ 523 ] + $Q_{30}$			580.5
5/2- [ 512 ] + $Q_{22}$ + 1/2- [ 510 ]	570.3 (a=0.048)	763.5	806.9 (a=0.097)
7/2+ [ 633 ] + $Q_{22}$ + 3/2+ [ 651 ]	538.6	531.5	590.3
3/2- [ 521 ] + 1/2- [ 521 ] + $Q_{22}$	573.6	752.8	659.5
1/2- [ 521 ] + $Q_{22}$ + 3/2- / 521 /	1103.3	(1227)	1262

#### 2.4. Level Structure of Deformed Odd-Mass Nuclei

In the region of deformed odd-A nuclei the nature of various excited states has been determined using neutron capture. The results can be well understood in the framework of theoretical calculations [11] which take into account quasiparticle-phonon interaction. When the spacings of single-particle states are such that levels connected by large E2 matrix elements occur separated by approximately the quadrupole phonon energy, a break-down of the pure single-particle description and considerable mixing are expected.

In Table III bandhead energies are summarized for the isotonic nuclei  $^{165}\text{Dy}$ ,  $^{167}\text{Er}$  and  $^{169}\text{Yb}$ . Enriched samples of 92.71 %  $^{164}\text{Dy}$ , 95.6 %  $^{166}\text{Er}$  and 19.5 %  $^{168}\text{Yb}$  were used as a target.

A striking feature of the quasiparticle-phonon interaction is the appearance of large components of high-lying Nilsson states in the low-energy region. A typical example is the admixture of the  $1/2^-[510]$  state into the K-2 vibration on the  $5/2^-[512]$  state. The observed nonvanishing decoupling parameter may be ascribed to such an admixture. According to the present experimental results the contribution of the  $1/2^-[510]$  state seems to increase from  $^{165}\text{Dy}$  to  $^{169}\text{Yb}$ . In  $^{169}\text{Yb}$  the decoupling parameter and the rotational factor are  $a = 0.097$  and  $t_{1/2}^2 = 13.5$  keV, whereas the rotational factor for the  $5/2^-[512]$  band is 12.4 keV.

For a detailed discussion of the results on  $^{165}\text{Dy}$  see ref. [1]. An extensive analysis of the data on  $^{167}\text{Er}$  and  $^{169}\text{Yb}$  will be published in the near future. A preliminary transition diagram of  $^{169}\text{Yb}$  may be found in refs. [1, 12].

References:

- [ 1 ] G. Markus, W. Michaelis, H. Schmidt and C. Weitkamp  
Z. Physik 206 (1967) 84
- [ 2 ] W. Michaelis and H. Schmidt, KFK 429 (1966)
- [ 3 ] W. Michaelis and H. Küpfer, Nuclear Instr. and Meth.  
56 (1967) 181
- [ 4 ] U. Fanger, G. Markus, W. Michaelis, H. Ottmar and H. Schmidt  
Proc. Int. Conf. Nucl. Structure, Tokyo 1967, KFK 616 (1967)
- [ 5 ] A.K. Kerman and C.M. Shakin, Physics Letters 1 (1962) 151
- [ 6 ] P. Leal Ferreira, I.A. Castiho Alcaras and V.C. Aguilera Navarro  
Phys. Rev. 136 (1964) 1243
- [ 7 ] S.T. Belyaev and V.G. Zelevinskii, Izvest. Akad. Nauk. SSSR,  
Ser. Fiz. 28 (1964) 127; Bull. Acad. Sci. USSR Phys. Ser 28  
(1964) 121
- [ 8 ] D.M. Brink, ANL - 6797 (1963)
- [ 9 ] L.S. Hsu and J.B. French, Physics Letters 19 (1965) 135
- [ 10 ] H. Schmidt, W. Michaelis, C. Weitkamp and G. Markus,  
Z. Physik 194 (1966) 373
- [ 11 ] V.G. Soloviev, P. Vogel and G. Jungklausen,  
Report JINR Dubna E 4 - 3051 (1966)
- [ 12 ] W. Michaelis, U. Fanger, D. Lange, G. Markus, H. Schmidt and  
C. Weitkamp, KFK 562 (1967); JüI-Conf. 1 (1967) 40

### 3. Slow Neutron Inelastic Scattering, Scattering - Law Measurements

W. Gläser, G. Ehret, P.v. Blanckenhagen, K.B. Renker, W. Schott

#### 3.1.1 Zirconium Hydride

The evaluation of the generalized frequency distribution  $\rho(\beta)$  ( $\beta = \frac{\hbar\omega}{k_B T}$ ) for  $ZrH_{1.08}$  has been completed. The weight of the acoustical part ( $\Omega_D \approx 27$  meV) is about 0.006, the total weight of  $\rho(\beta)$  is about 0.785 if only scattering from H is considered. This distribution describes integral thermalization properties in a satisfactory way.

Lit.: W. Gläser, KFK-Report 602 (1967)

G. Ehret, Thesis, Karlsruhe (1968)

#### 3.1.2 Water and Ice

The scattering of cold neutrons ( $E_0 = 5$  meV) from  $H_2O$  at temperatures of  $-12^\circ$  and  $+23^\circ C$  has been measured at angles between  $16^\circ$  and  $110^\circ$ .  $\rho(\beta)$  has been extracted from these data using an iterative correction for multiple scattering. The quasielastic scattering from  $H_2O$  ( $23^\circ$ ,  $45^\circ$  and  $75^\circ C$ ) and  $D_2O$  ( $23^\circ C$ ) has been analysed quantitatively using the LEAP formalism for corrections.

Lit.: P. v. Blanckenhagen and K.B. Renker, Phys. Verh. DPG(7), 1967, 532

#### 3.1.3 Liquid and Solid Hydrogen

The double differential scattering cross sections  $\frac{d^2\sigma}{d\Omega dE}$  f liquid  $H_2$  ( $T=19.8^\circ K$ ) and solid  $H_2$  ( $T=4.4^\circ K$ ) have been measured with incident energies of 21,8 and 87 meV for scattering angles between  $20^\circ$  and  $150^\circ$ . The results deviate considerably from the gas model calculations and have been interpreted with a spectral density  $\rho(\beta)$ .

Lit.: W. Schott and W. Gläser, Phys. Verh. DPG(7), 1967, 534

3.2. Other Experiments.

P. Schweiss, E. Albold

3.2.1 Phonon Dispersion in Iron

Phonon dispersion measurements in the (110)-plane of room temperature iron have been completed. The interatomic force constants of a fifth neighbor Born- von Kármán model have been determined. Using the sampling technique a frequency distribution has been calculated from these data.

Lit.: P. Schweiss et. al., Helvetica Physica Acta 40, 378 (1967)

3.2.2 Doppler Broadening of the 6.68 eV Resonance in  $^{238}\text{U}$

The doppler broadening of the 6.68 eV resonance in metallic  $^{238}\text{U}$  and uranium dioxyde has been measured as a function of temperature between room temperature and 1000°C. The line broadening in  $\text{UO}_2$  is quantitatively explained using a realistic frequency distribution of lattice vibrations in  $\text{UO}_2$  and the scattering law formalism.

Lit.: E. Albold, Thesis, Karlsruhe (1968)

#### 4 . Isochronous Cyclotron

##### 4.1. Development of the T.o.F. Spectrometer

S. Cierjacks, H. Unseld, P. Forti, D. Kopsch, L. Kropp, J. Nebe

During the period covered by this report the time-of-flight spectrometer worked for several operation periods of each about two weeks without serious breakdowns. In the past year several modifications of the apparatus were made [1]. By solving some material problems for the deflection systems which arise under conditions of increased beam intensities the overall reliability was further improved. Additionally the outer deflection plates in March 67 were set to the last remaining hill section of the pole faces. In this new position the much time consuming adjustment, which was necessary previously, could be avoided. For the 3 : 1 frequency divider a new phase stable electronic circuit which is in use since May 67, was constructed by members of the cyclotron laboratory.

The application of a modified version of the AEG ion sources (concerning the material of some components of the sources) now allows an operation of the cyclotron with an unreduced internal beam current of several hundred  $\mu$ A. (these new sources were developed in the cyclotron laboratory too).

In June 67 the CDC 3100 was equipped with an additional 8 U - 24 bit memory. With this extended storage capacity higher input rates (up to  $1 \cdot 10^4$  C/sec for 8.000 time channels in the transmission experiments) or more data channels (mainly important for partial cross section measurements) can be accepted with this new acquisition system. For both deflection systems remotecontrolled deflection plates are under construction and are to be completed in the early 1968.

As a result on the studies concerning the increase of the repetition rate a new concept has been worked out [2]. With a meander shaped upper deflection plate of the outer deflector (used as strip-line) a considerable more economic system (from the power consideration point of view) could be realised. The use of such a deflection system may allow a power eco-

nomization of about a factor 6. The new power pulse generator (the thyratron was replaced by a microwave power-tube) was developed in the last year and should be put in operation also the early 1968. The previously mentioned increase of the flight path is in progress. The present flight path will be increased additionally by 130 m to a total length of 180 m. The new project which must be constructed outside the present territorium of the Karlsruhe Center is to be completed in 1968.

References:

- [1] S. Cierjacks, B. Duelli, P. Forti, D. Kopsch, L. Kropp, M. Löseel  
J. Nebe, M. Schweickert, H. Unseld - Rev Sci Instr. to be published
- [2] H. Unseld, S. Cierjacks, - Fachtagung "Antennen und Elektro-  
magnetische Felder" der NTG und U.R.S.I., Darmstadt, Okt. 67

4.2. Total Cross Section Measurements

S. Cierjacks, P. Forti, D. Kopsch, L. Kropp, J. Nebe

The neutron total cross section of material samples of Bi, Tl, S and Na have been measured from about 0.3-30 MeV generally for two sample thicknesses. Additionally a remeasurement of the total cross section of C, O, I, Ca and Fe with different sample thicknesses and a 1.0 nsec channel width were made. In the latter measurements mainly the statistical accuracy in the lower energy range has been improved considerably. All these data have been taken using the Laben UC - KB digital time-sorter combined with the new CDC 3100 data acquisition system. A statisticul analysis of the data to investigate whether a broader structure is present in addition to the fine structure is under way [1].

For some elements a resonance parameter analysis in the low energy region is in progress.

Reference:

- [1] S. Cierjacks - Thesis 1967

#### 4.3. Partial Cross Sections

S. Cierjacks, P. Forti, D. Kopsch, L. Kropp

Measurements with the fast coincidence apparatus (liquid scintillators) have been completed / 1 / .

The solid state scattering chamber has been equiped with additional semiconductor telescopes. A more sophisticated programm was written which allows the particle assignment and automatic corrections of charged particle time-of-flights during the measurement. By applications of commercial zero-cross-over circuits (EGG 100 M module a further improvement of the time resolution was obtained.

A new approach to measure inelastic neutron scattering would be to use the Karlsruhe cyclotron as the neutron source. Since this source delivers a continuous neutron spectrum the incoming neutron energy as well as the **energy** of the scattered neutrons must be **deduced** from the experiment. Conclusive **results** can be obtained either by a double time-of-flight experiment or by a single time-of-flight experiment using Ge(Li) solid state detectors. In the latter case the total time-of-flight should be measured simultaneously with the  $\gamma$ -energy. Evaluating both the pulse height and the time-of-flight information allows to determine the initial energy as well as the energy of the scattered neutrons. The construction of suitable detectors is under way. An on-line program which will be written, which can be used to store the data as a function of the incident neutron time-of-flight, scattering angle and time-of-flight after scattering or the pulse height of the Ge(Li) detectors respectively.

References:

- [1] O. Meyer, M. Baumgärtner and F. Wüchner  
Nucleonik 10, 4 (1967) 189
- [2] O. Meyer and G. Haushahn,  
Nucl. Instr. and Method 56 (1967) 177
- [3] O. Meyer, 11th Scintillation and Semiconductor Counter  
Symposium, Febr. 1968, Washington
- [4] W. Michaelis,  
Nucl. Instr. and Meth., to be published
- [5] U. Tamm, KFK 509 (1967)
- [6] U. Tamm, W. Michaelis and P. Coussieu  
Nucl. Instr. and Meth. 48 (1967) 301
- [7] W. Michaelis, KFK 617 (1967)
- [8] W. Michaelis  
Nucl. Instr. and Meth. to be published
- [9] W. Michaelis and H. Küpfer  
Nucl. Instr. and Meth. 56 (1967) 181
- [10] F. Horsch, KFK 558 (1967)
- [11] W. Michaelis and D. Lange  
Nucl. Instr. and Meth., in press

## 5. New Developments in Instrumentation

### 5.1. On-line Computers G. Krüger

#### 5.1.1. Small On-line Computers Coupled with Experiments

The electronic design and development of the multiple access system MIDAS were finished during the reporting period. After Connection of some new nuclear physics experiments & facilities are in normal operation with the system.

The total input capacity of MIDAS (Multiple Input Data Acquisition System) amounts to 10 experiments, two of them can be located at remote places. They are connected by fast data transmission lines. During the year most activity concerns the development work in the fields of programming and system organisation [1]. Privat libraries for the measuring programs of the experimentors were established on the IBM 1311 disc. units. The archived programs in the different libraries can be activated by experimentor's command using the command panel at the location of the experiment.

The operation of MIDAS as an on-line-real-time multichannel analyser with a capacity of about 262.000 channels has proven very useful during routine operation. To accumulate multiparameter data directly without delay a new programmed method of list-processing were implemented.

The program package which should ensure system integrity during periods of wrong running experiments was extended. The computer indentifies now immediately experiment malfunctions which overload the computer. Then the safety system closes the erroneous data way without interfering the correct running measurements.

The check point program is now a standard feature of the system. This program in connection with the new **time-of-the-day real-time** clock interrupts the system in regular intervalls. The recent status and all the intermediate results of the different measurements are saved into magnetic tape. Therefore a total breakdown of the system cannot destroy large amount of measuring results.

The library of experiment-oriented measuring programs was considerably extended.

An additional display unit and some control circuitry have been added to the CAE 510 computer at the van de Graaff accelerator. The flexibility of the system and the adaption for further needs should be performed now mainly by programming.

Several new programs for the experiments of the IAK at the isochronous cyclotron - laboratory were designed and tested. The operating system was adapted to the extended configuration of the CDC 3100. The input and multiplex system of the computer was extended so that 4 different experiments can be simultaneously coupled to the CDC-machine. The last parts of the electronic modules shall be added during the next months.

After this data the electronic design work of all on-line data processing systems used by the IAK will be finished. The necessary further increase in data processing capacity for measuring and experimental purposes requires a completely new approach, which shall be handled by the central data processing group of the centre.

#### 5.1.2. Study in the field of programming languages.

The analysis of the basic structure of an experiment oriented real-time programming language progressed during the reporting period / 2 /. At the end of the year the staff of the working group joints the central data processing, which designs and develops a large time-sharing system, in which the small on-line machines will be integrated.

#### Literature

- [1] G. Krüger  
MIDAS-Erfassung und Steuerung kernphysikalischer Messungen durch ein Vielfachzugriffssystem.  
NTG-Tagung "Teilnehmer-Rechensysteme" Erlangen, Sept. 1967 erscheint im Verlag Oldenbourg Anfang 1968.
- [2] V. Haase  
EXOS - Entwurf einer experiment-orientierten Computersprache.  
Externer Bericht 1/67 - 1, IAK

## 5.2 Semiconductor Spectrometers

W. Michaelis, F. Horsch, D. Lange, O. Meyer, U. Tamm

### 5.2.1 Detector Technology

Coaxial Li-drifted germanium detectors have been fabricated with active volumes up to  $33 \text{ cm}^3$  [1]. The energy resolution (3.3 keV for  $E_\gamma = 662 \text{ keV}$ ) is comparable with the energy resolution of planar detectors. The time distribution has been investigated for various detector shapes (circular and trapezoidal cross section, one open end and double-open end detectors).

High-resolution particle detectors are now produced by ion-implantation technique [2]. The improved performance of these counters is due to the fact that well-channeled ions at relative low energy and low ion-concentration minimize bulk damage effects. High-resistivity n-type, p-type and intrinsic germanium and silicon have been bombarded with ions of more than 30 elements in the energy range between 5 and 10 keV [3]. The properties of large-area  $n^+$  and  $p^+$  contacts produced in this way have been studied in detail. Very thin entrance windows are obtained by ion-implantation.

The gamma-ray response characteristics of lithium-drifted germanium detectors have been determined experimentally for several detector geometries [4].

### 5.2.2 Electronic Instrumentation

For high-resolution studies preamplifiers with cooled paralleled field-effect transistors have been applied with great success [5]. A pulse-shape discrimination circuit has been developed which is sensitive to a slow time-constant component in the charge carrier collection of lithium-drifted germanium detectors [6]. Pre-amplifier output pulses containing such a component are rejected. By this method the spectrum shapes can be improved considerably.

The possibilities of threshold reduction in leading edge timing with pulse transformers between detector and preamplifier have been studied by means of a fast low-noise preamplifier for the time signals [7]. Since this method proved to be insufficient for large volume germanium detectors a timing circuit was developed which is applied between charge-sensitive preamplifier and main amplifier [8]. The timing system has no influence on the energy resolution of high precision semiconductor spectrometers.

High-resolution studies with semiconductor counters are now aiming at an accuracy of 100 eV or better in the particle or gamma-ray energy [9]. For calibration and/or gain stabilisation such measurements require pulse generators of extremely high linearity and stability. A precision pulser has been developed which has an accuracy and stability of 20 ppm and better [10].

### 5.2.3 New Spectrometers

For applications in radiative neutron capture spectroscopy a Ge(Li) anti-comptonspectrometer has been designed for the energy range up to 3 MeV [9]. The instrument allows for the special conditions of  $(n,\gamma)$  spectroscopy and gives improved performance compared to previous devices. The system consists of a planar  $4.9 \text{ cm}^3$  Ge(Li) diode, a 50 cm dia.  $\times$  40 cm plastic scintillator and a 4" dia.  $\times$  6" NaI (Tl) detector at scattering angle  $0^\circ$ . The anti-coincidence method together with a pulse-shape discrimination technique very effectively suppress the compton background under the peaks. The energy resolution is 2.15 keV fwhm at 662 keV.

A new type of internal pair formation spectrometer has been developed which makes use of the high-resolution capabilities of semiconductor diodes [11]. The instrument consists of two silicon detectors forming a  $dE/dx + dE$  telescope for the positron-electron pair and two NaI (Tl) scintillation counters for detecting the positron annihilation quanta. With present techniques the optimum energy resolution is 0.07 % at 10 MeV. The spectrometer has been designed for application in neutron capture spectroscopy.

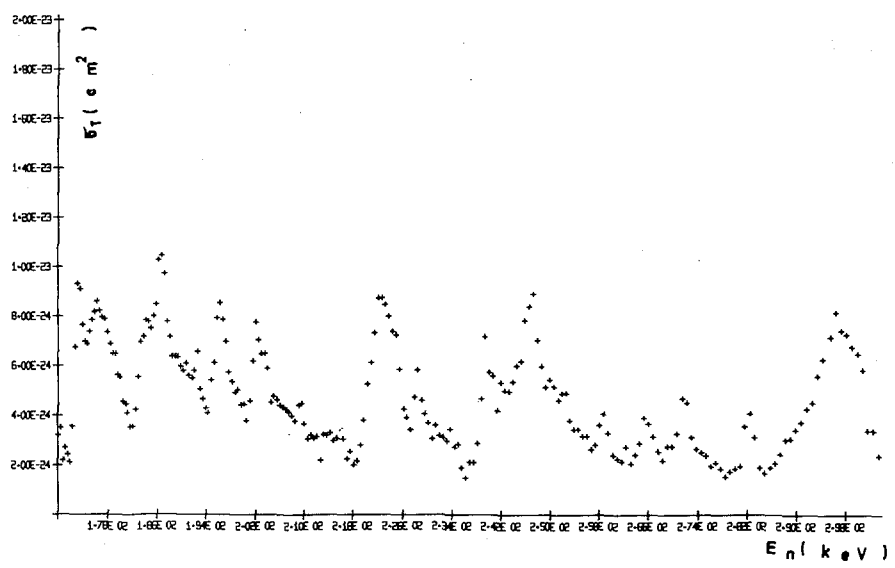
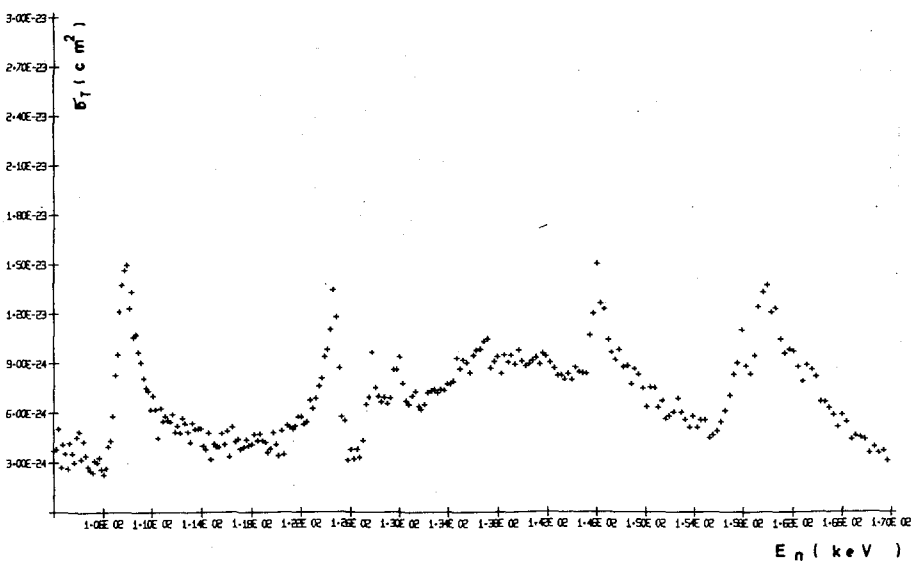
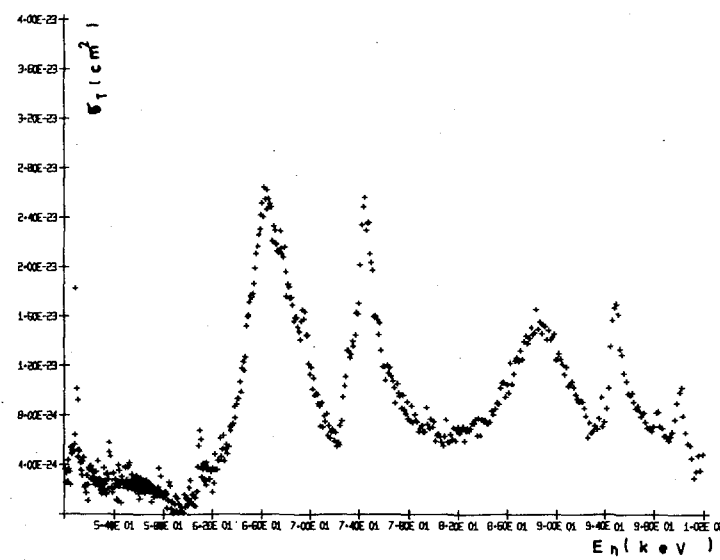
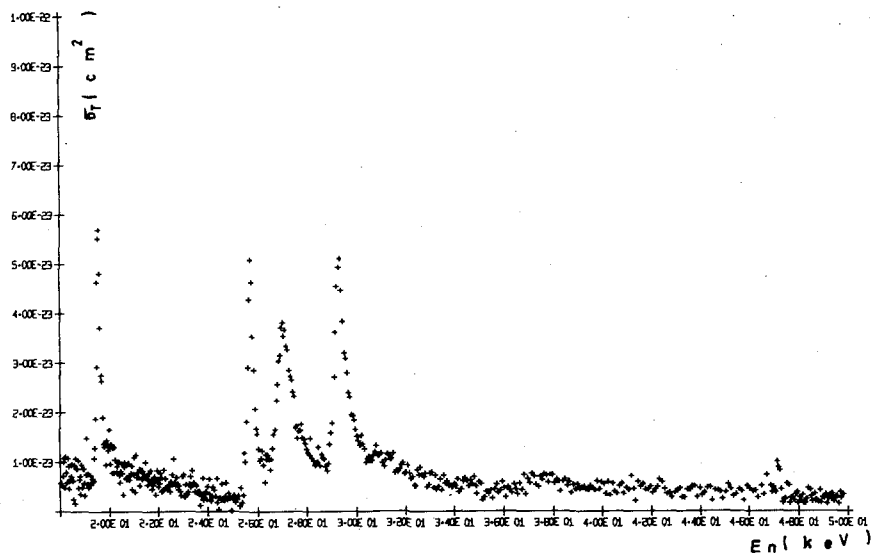


Fig.1 Total neutron cross section curve for  $^{53}\text{Cr}$

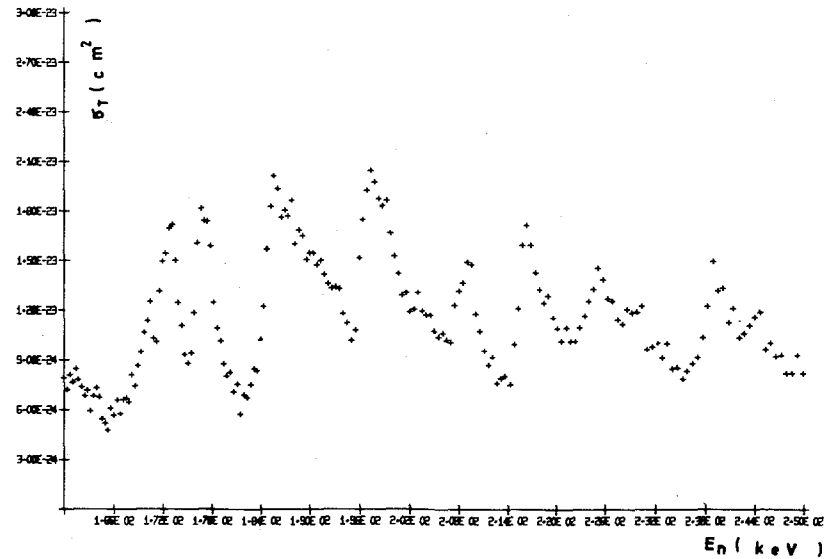
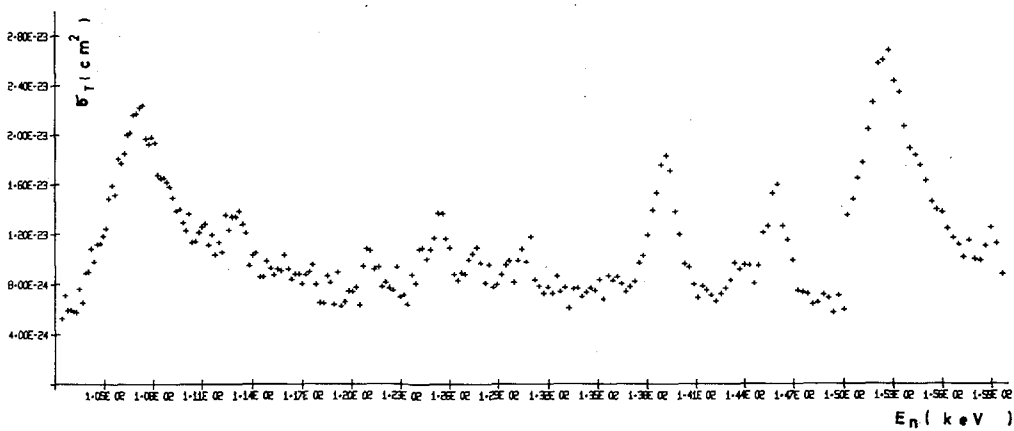
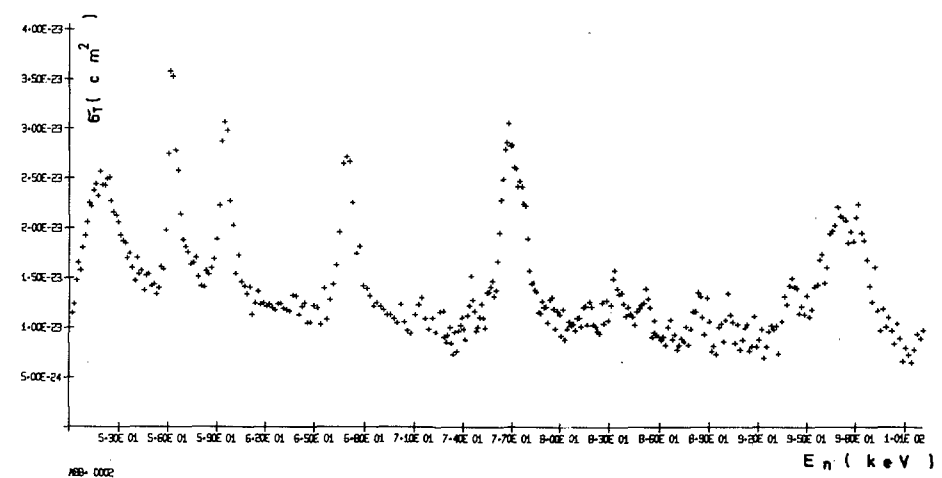
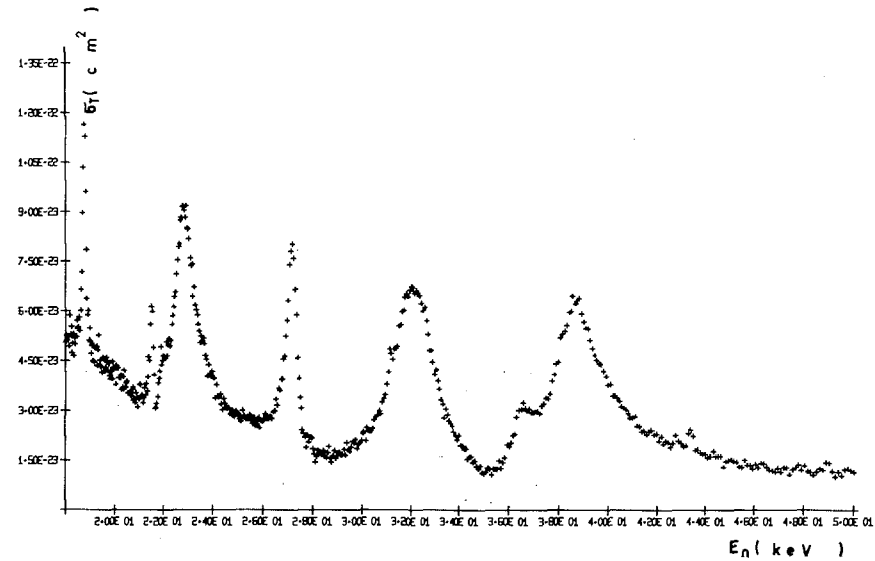


Fig.2 Total neutron cross section curve for  $^{46}\text{Ti}$

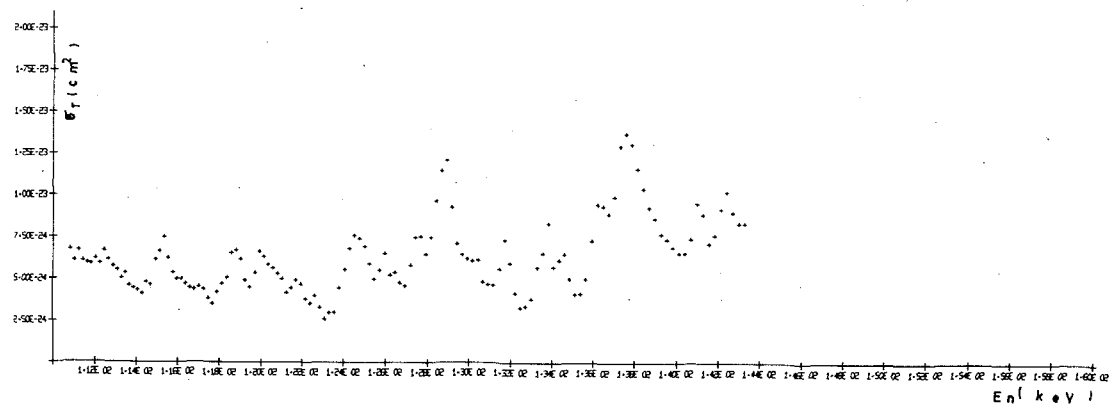
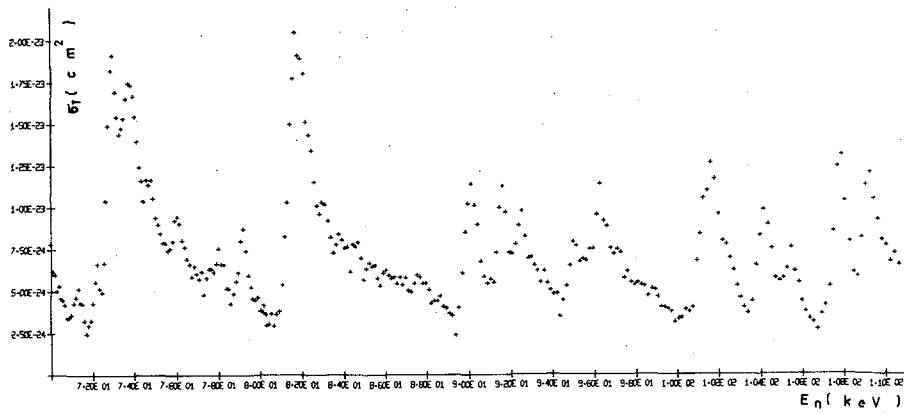
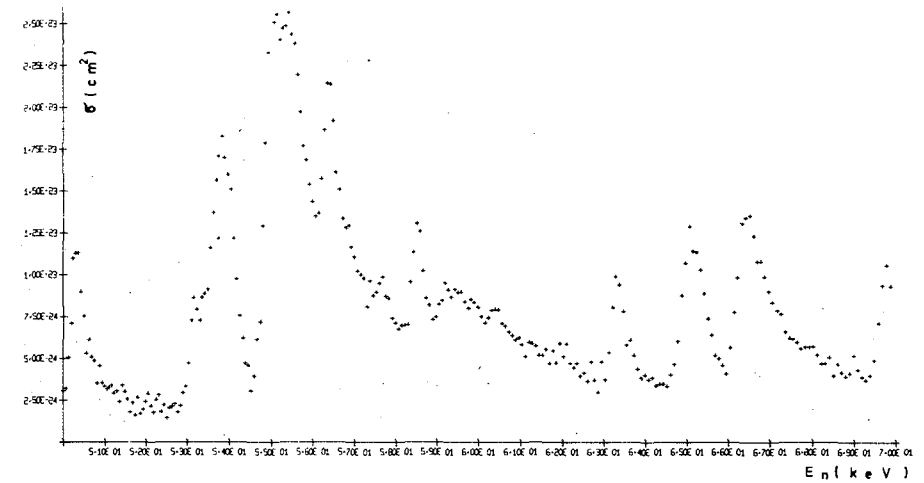
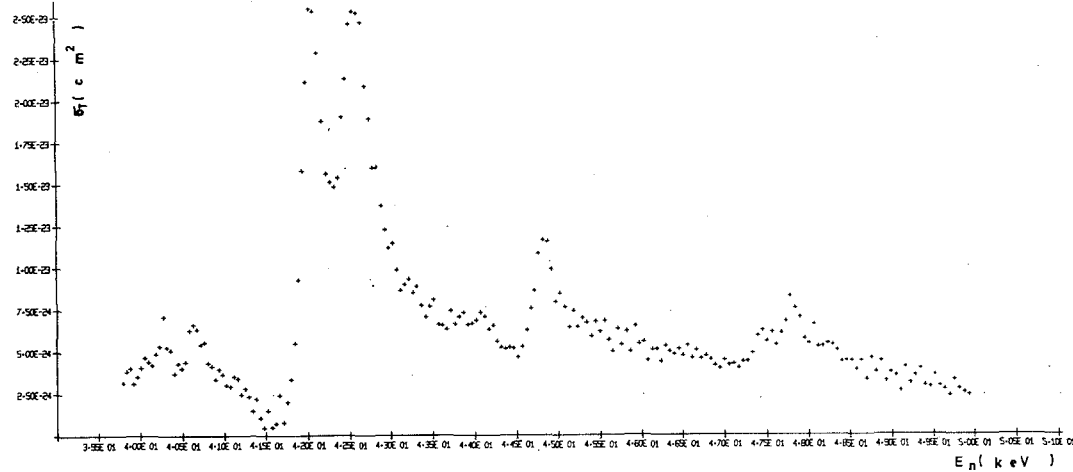


Fig.3 Total neutron cross section curve for  $^{63}\text{Cu}$

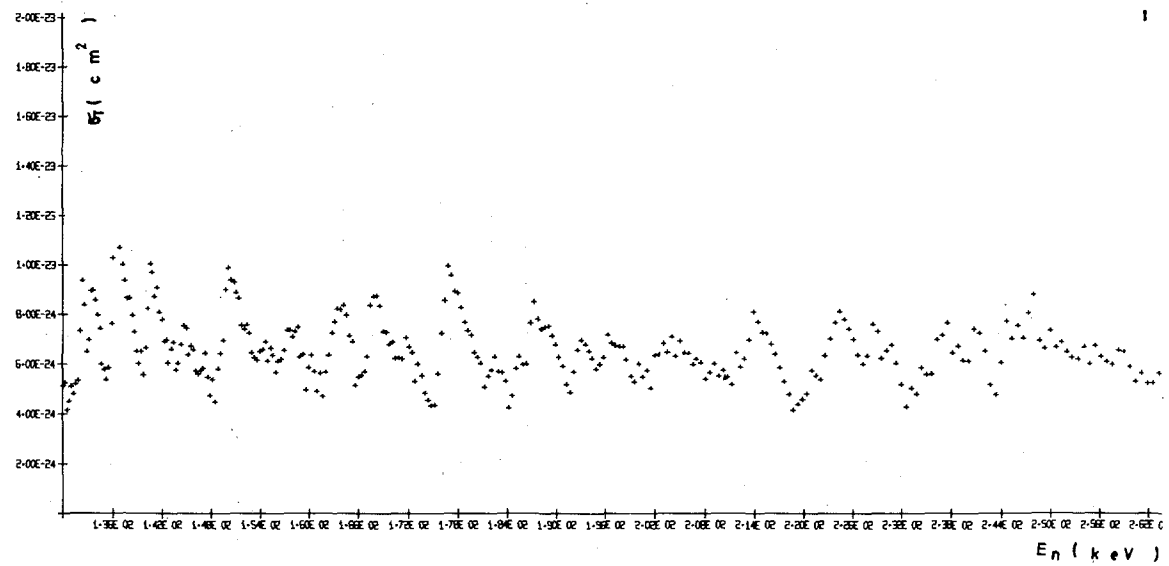
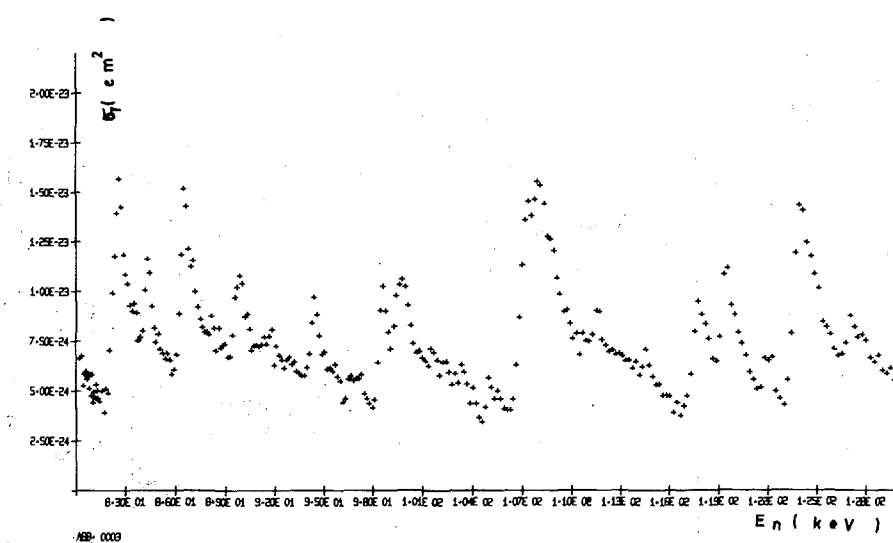
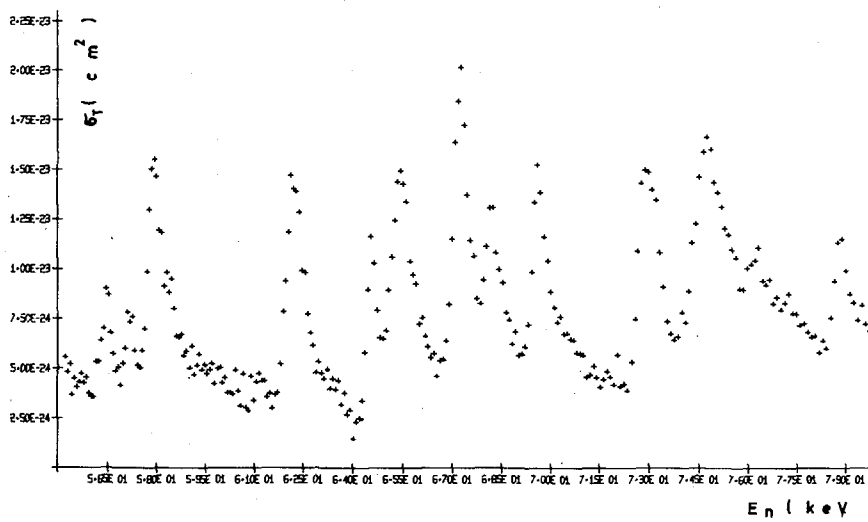
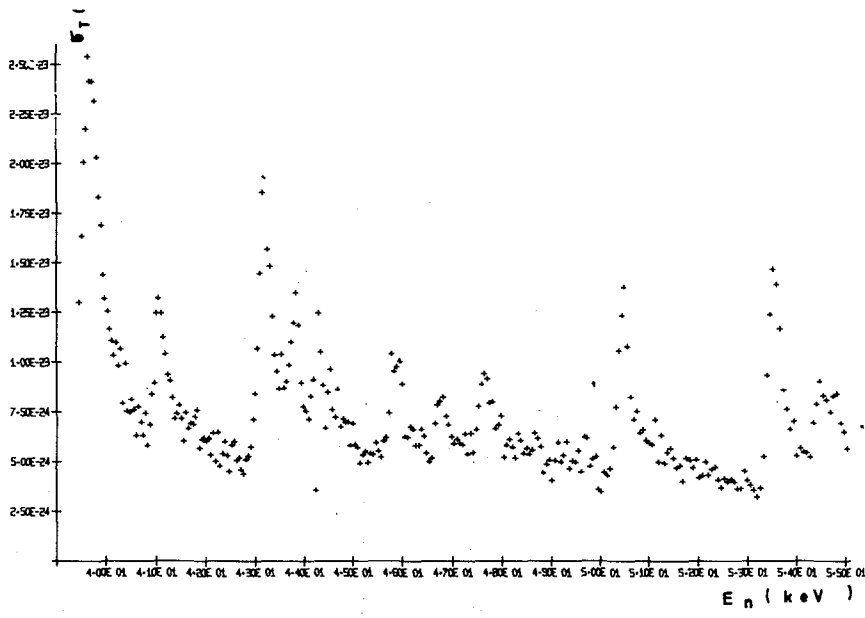


Fig. 4 Total neutron cross section curve for  $^{65}\text{Cu}$

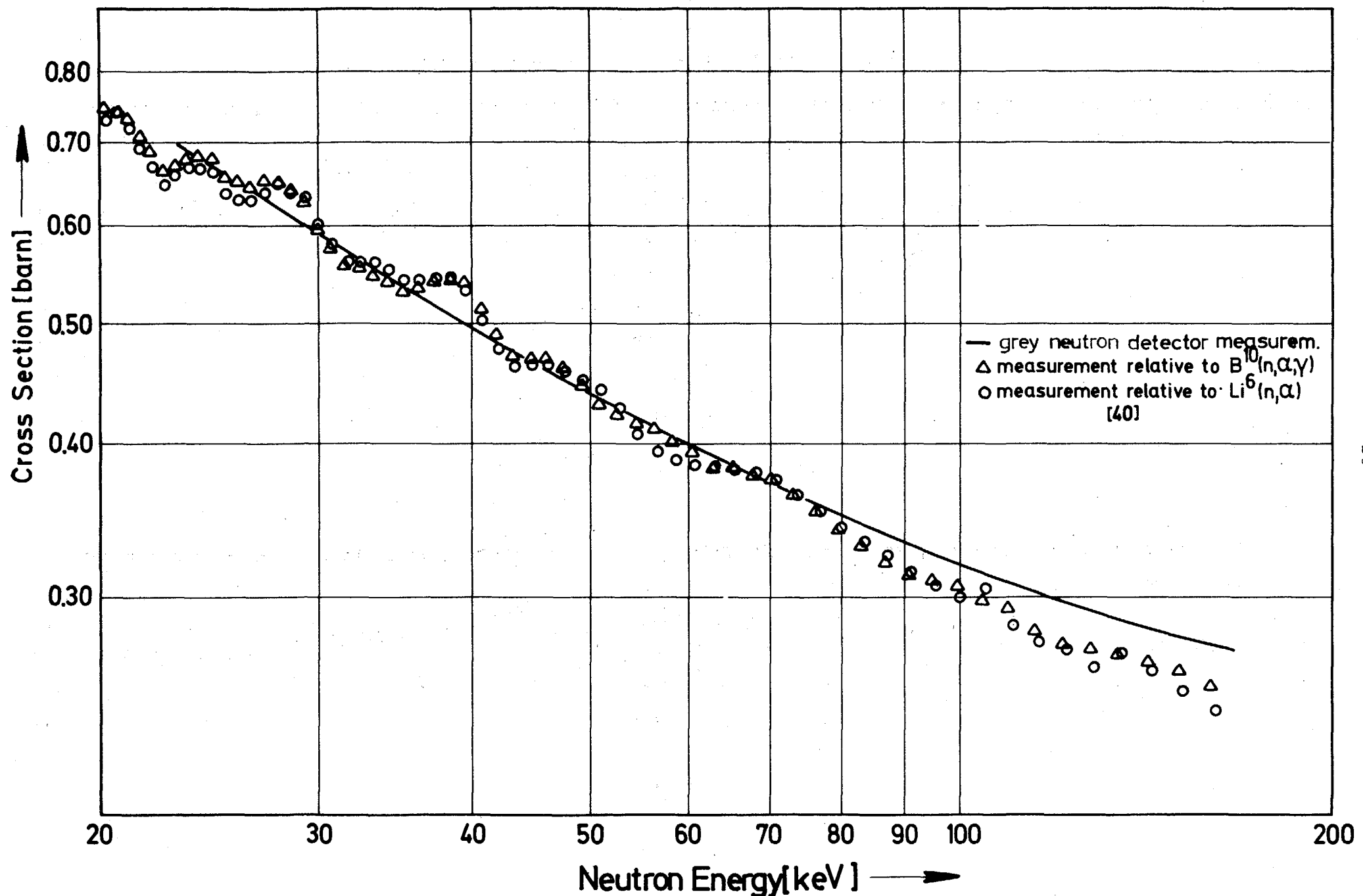


Fig. 5 Results of the measurements of the capture cross section of Au

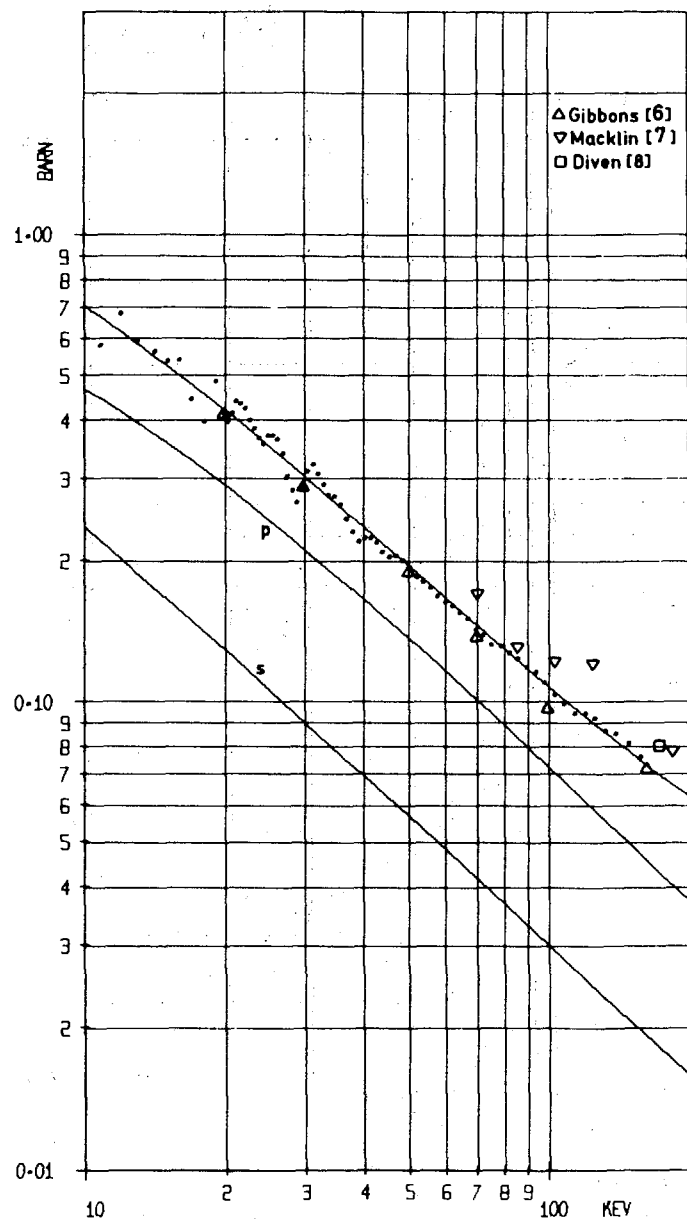


Fig. 6  $\sigma_{n,\gamma}^{\text{Nb}}$

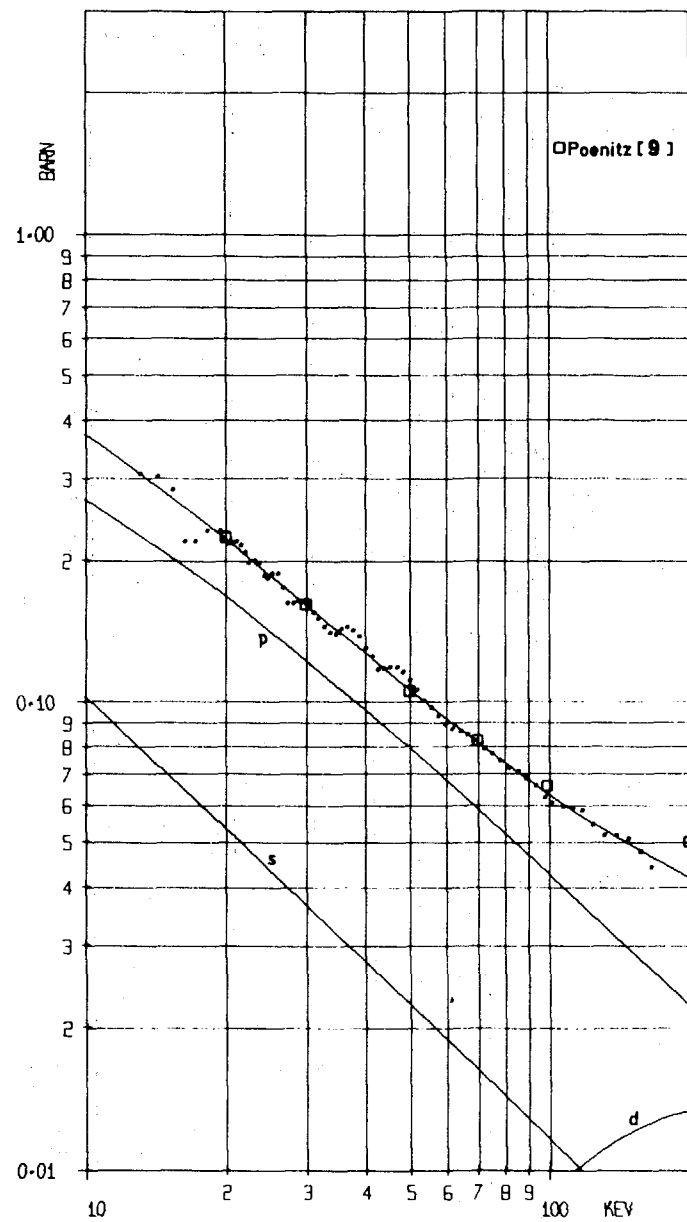


Fig. 7  $\sigma_{n,\gamma}^{\text{Mo}}$

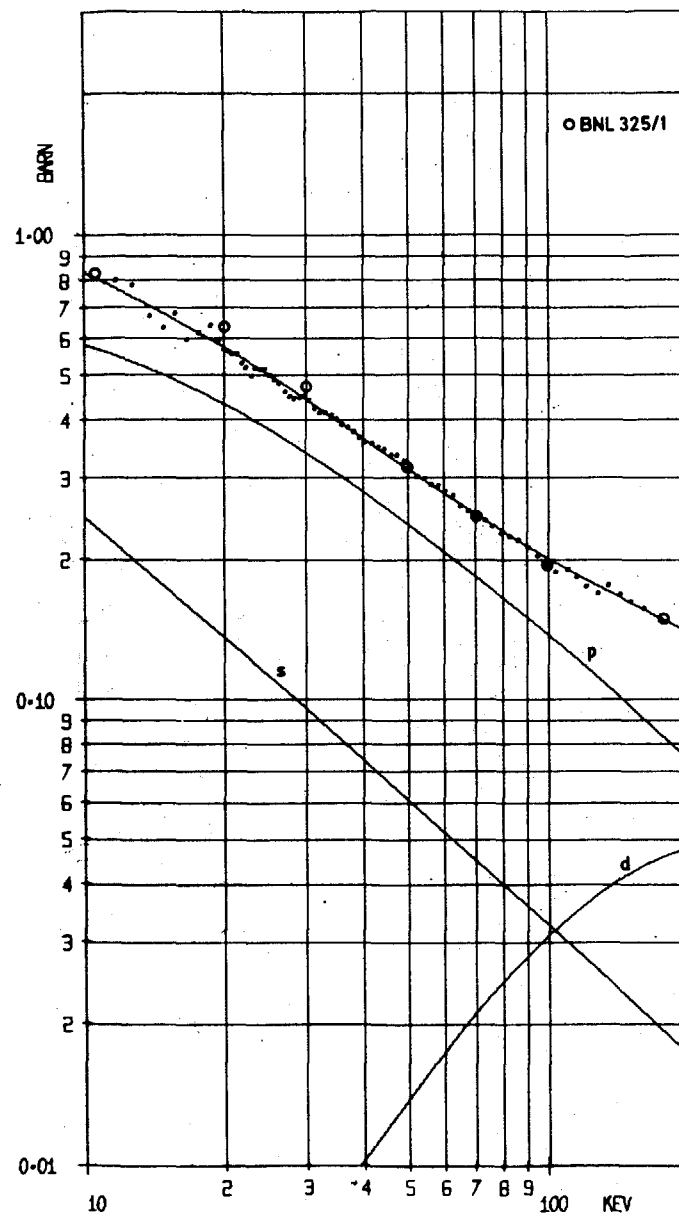


Fig. 8  $\sigma_{n,\gamma}^{Pd}$

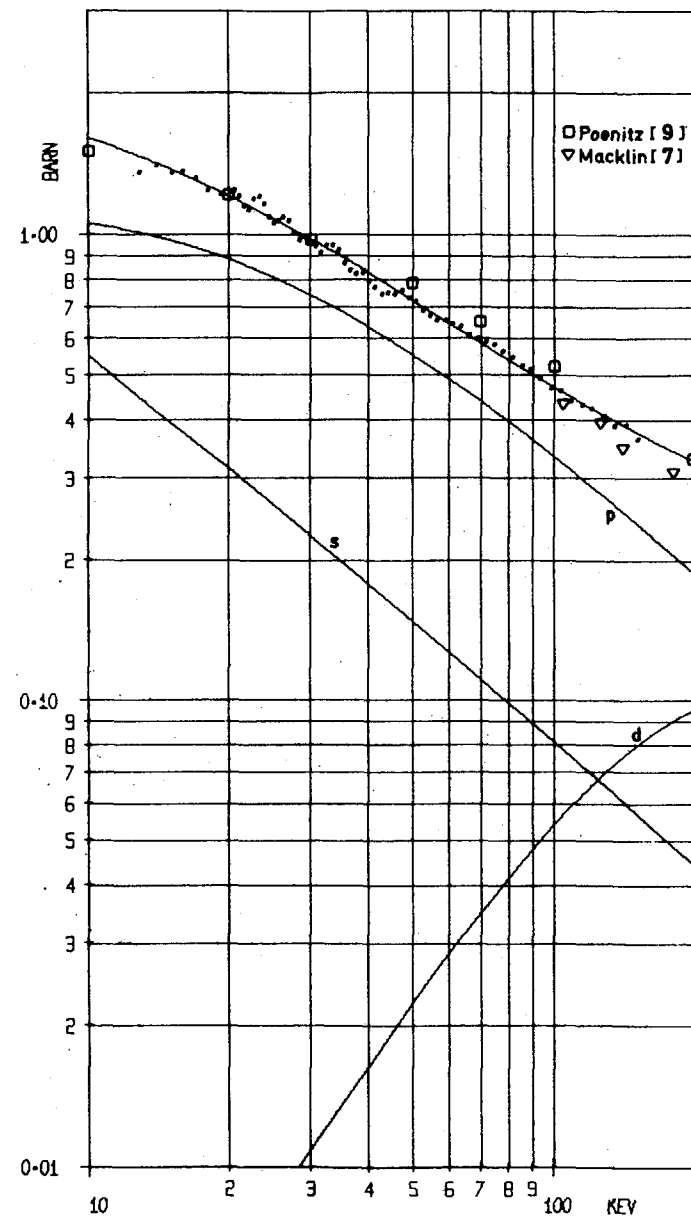


Fig. 9  $\sigma_{n,\gamma}^{Ag}$

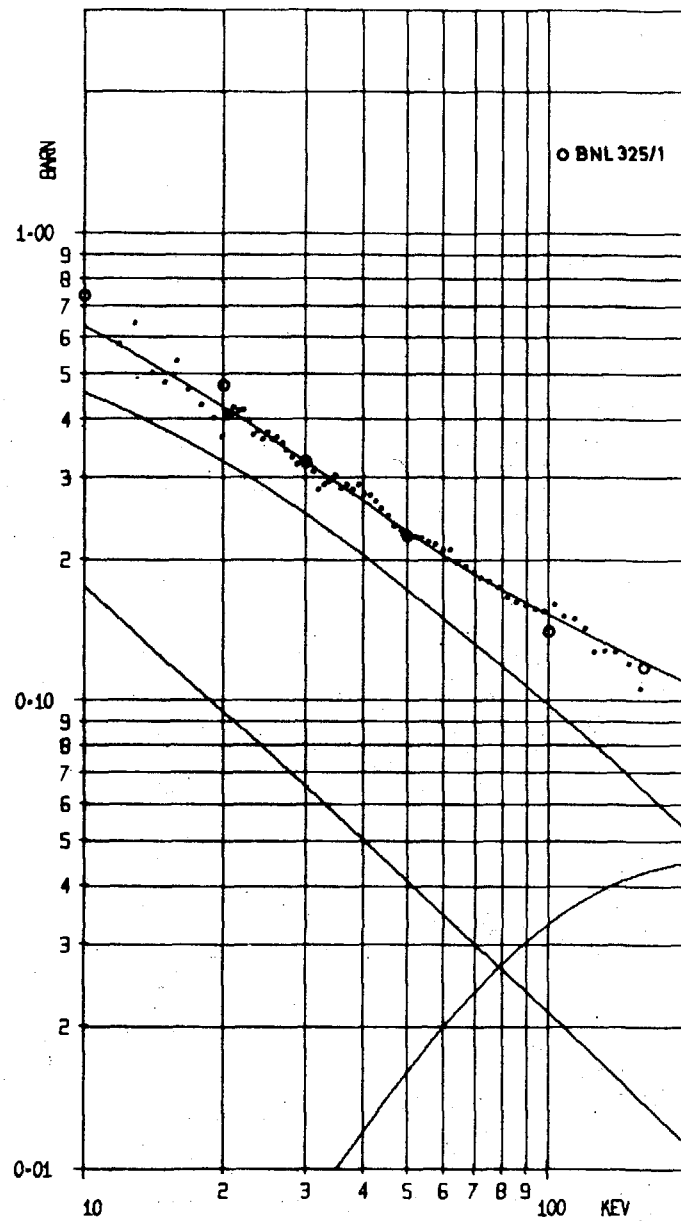


Fig. 10  $\sigma_{n,\gamma}^{Cd}$

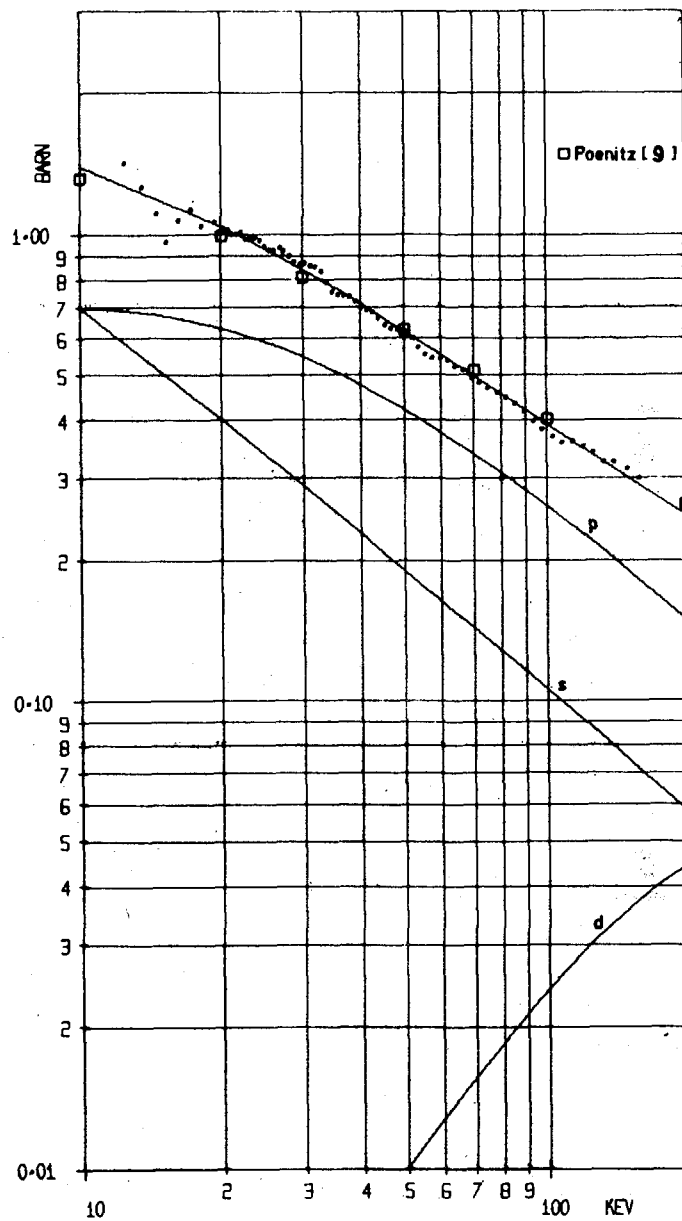


Fig. 11  $\sigma_{n,\gamma}^{In}$

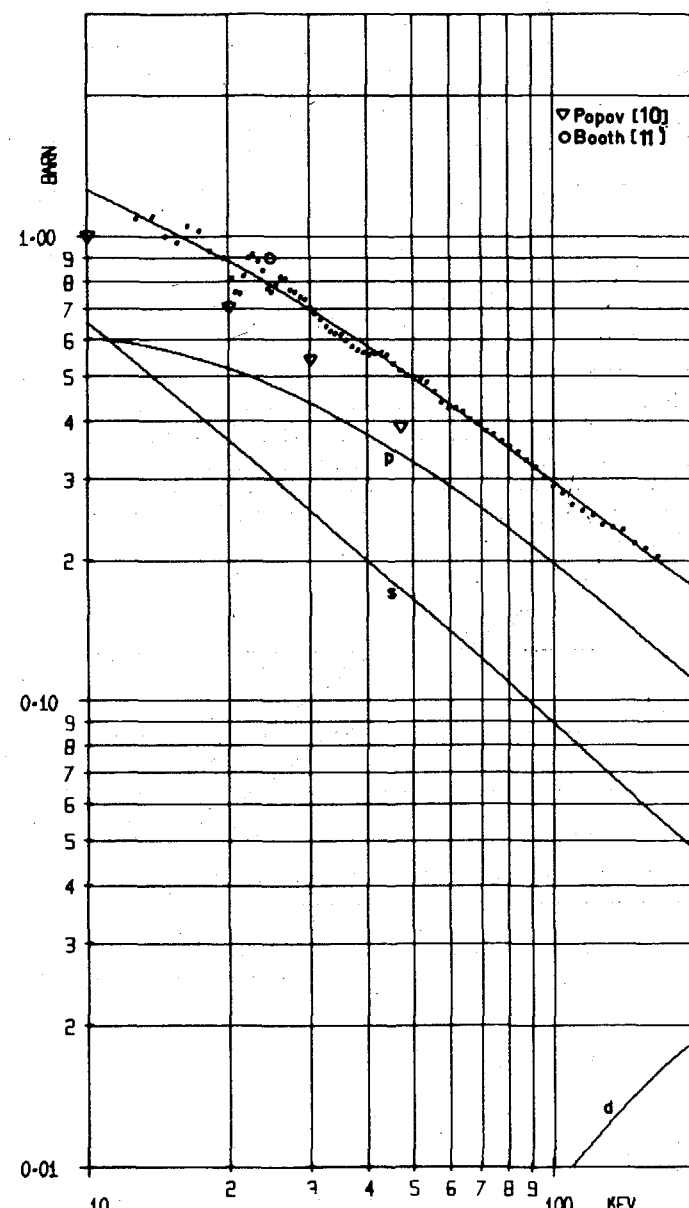


Fig.12  $\sigma_{n,\gamma}$   
Cs

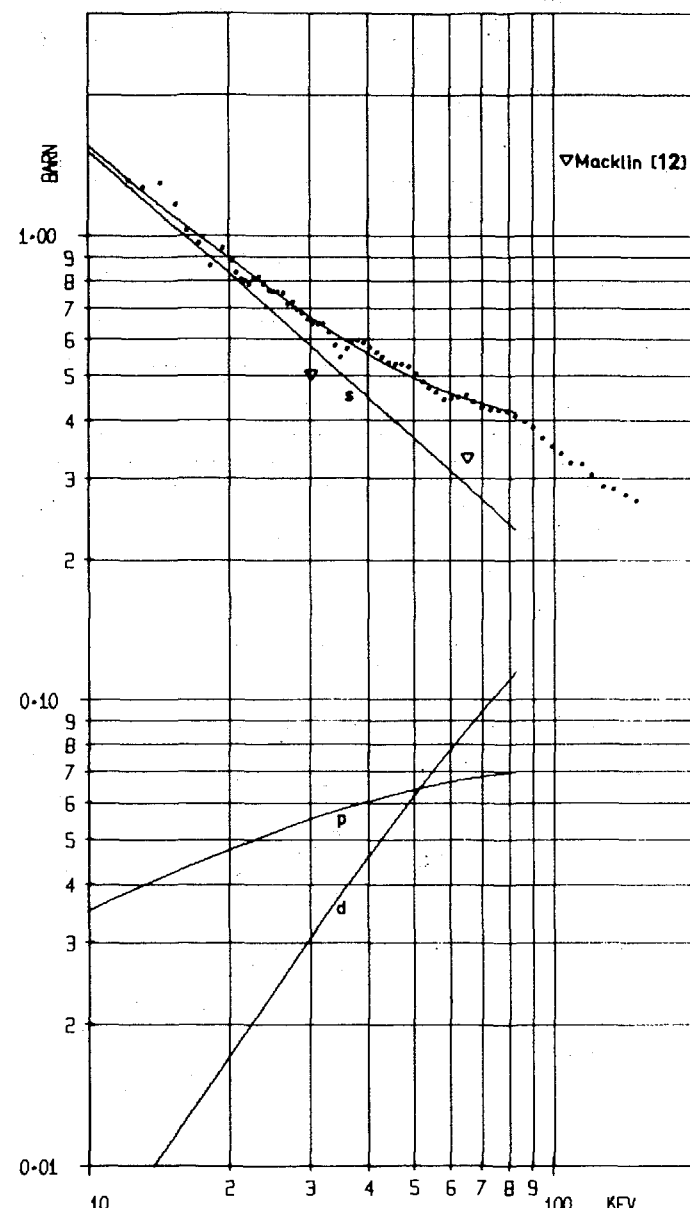


Fig.13  $\sigma_{n,\gamma}$   
Hf

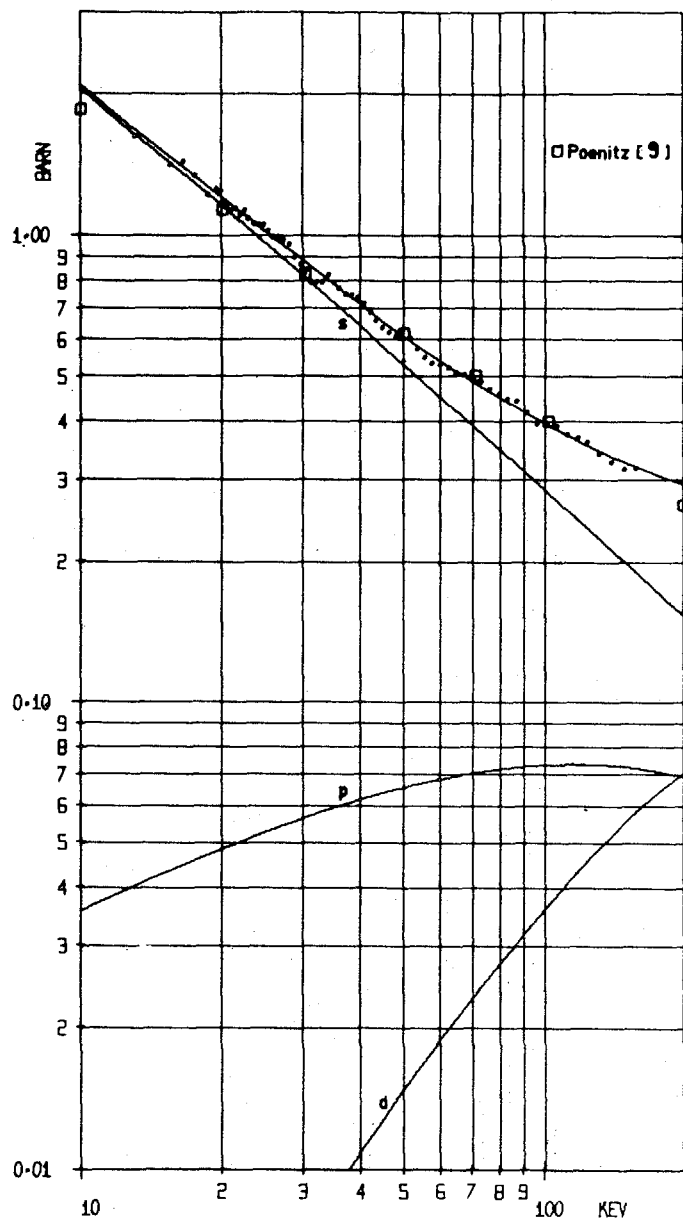


Fig.14  $\sigma_{n,\gamma}^{Td}$

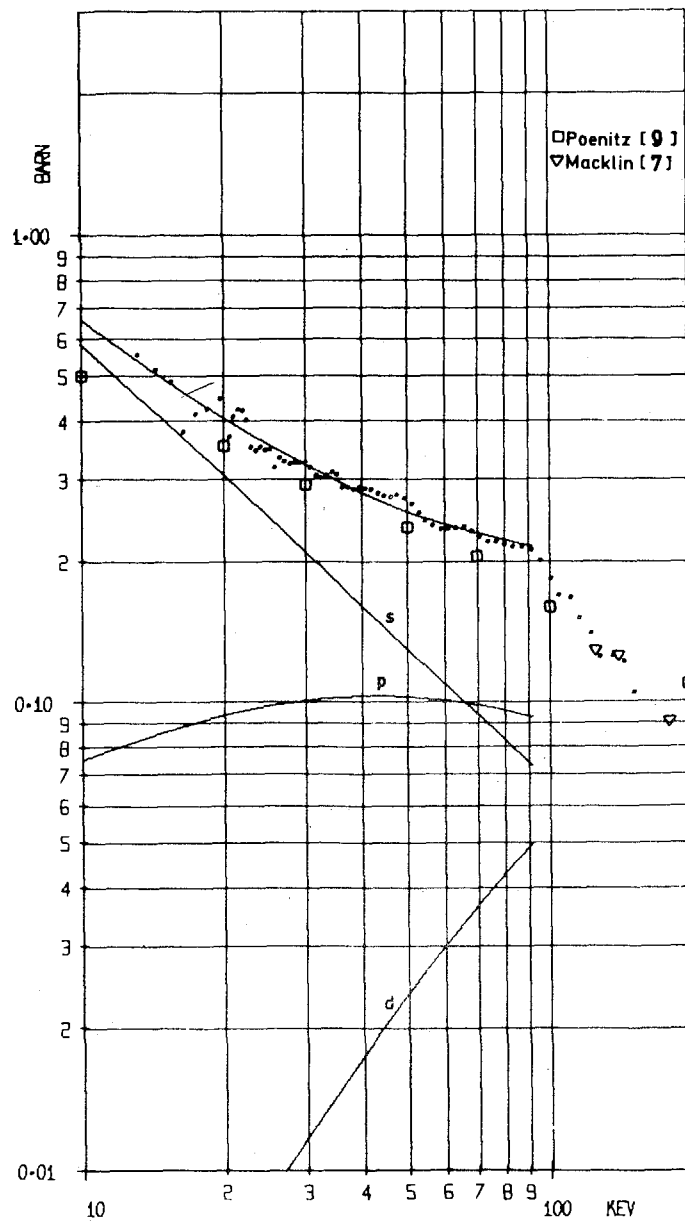


Fig.15  $\sigma_{n,\gamma}^W$

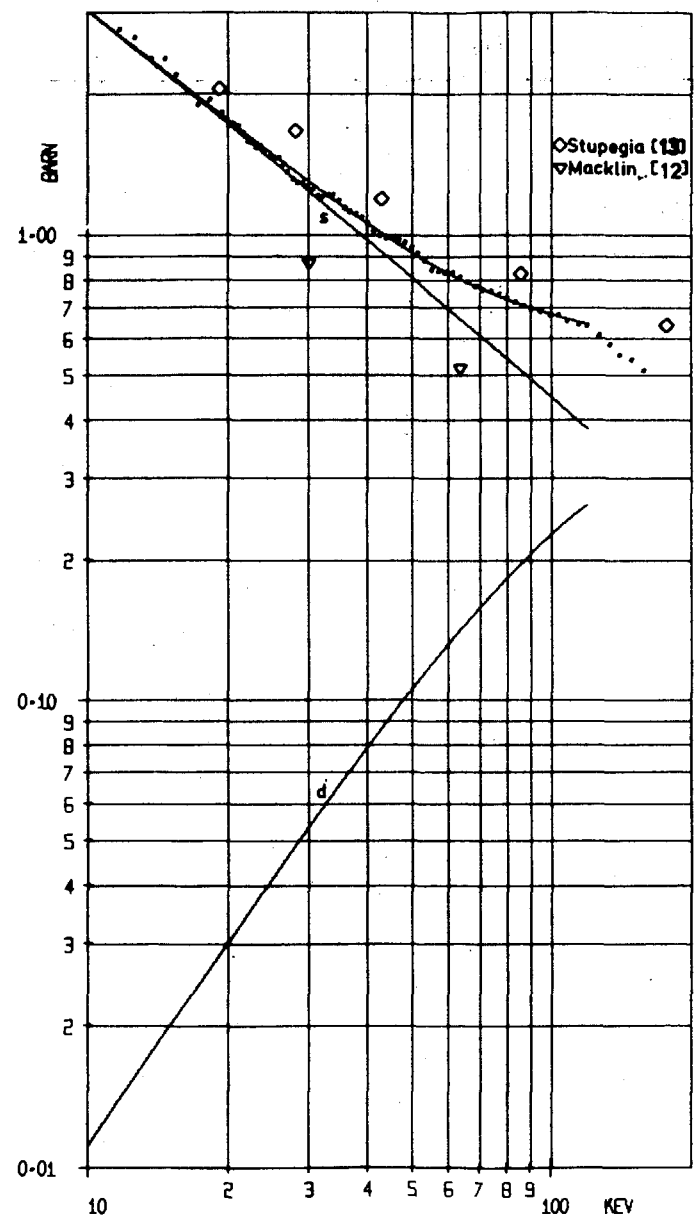


Fig. 16  $\sigma_{n,\gamma}^{re}$

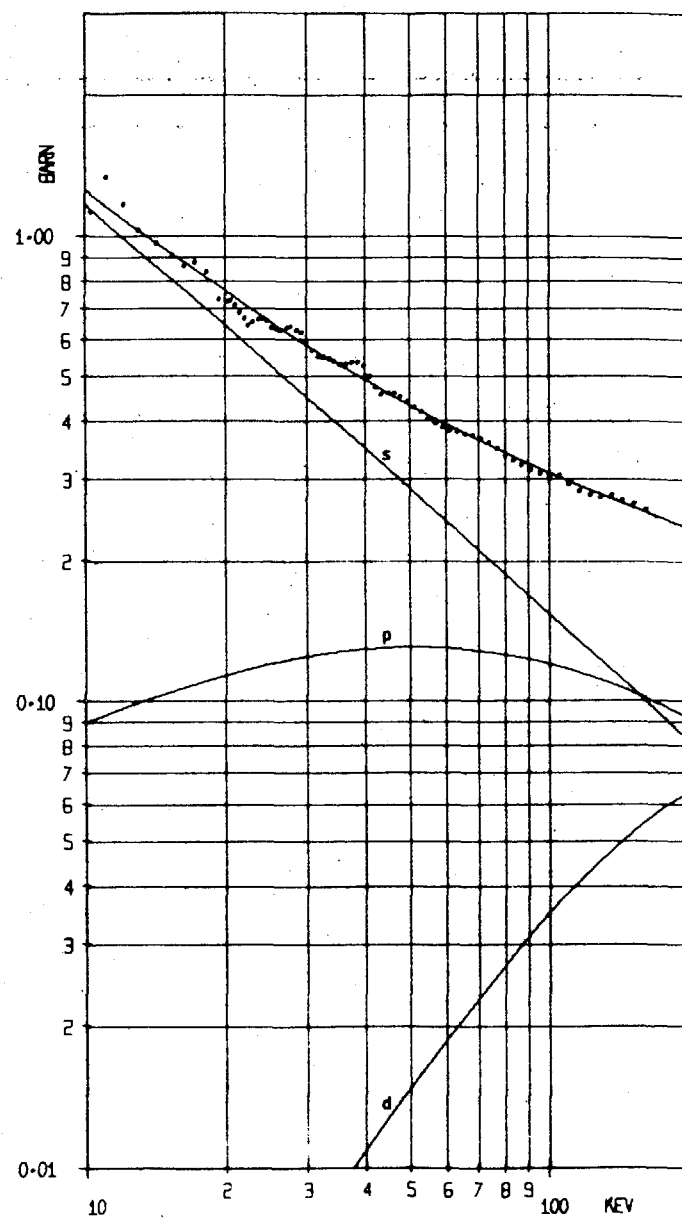
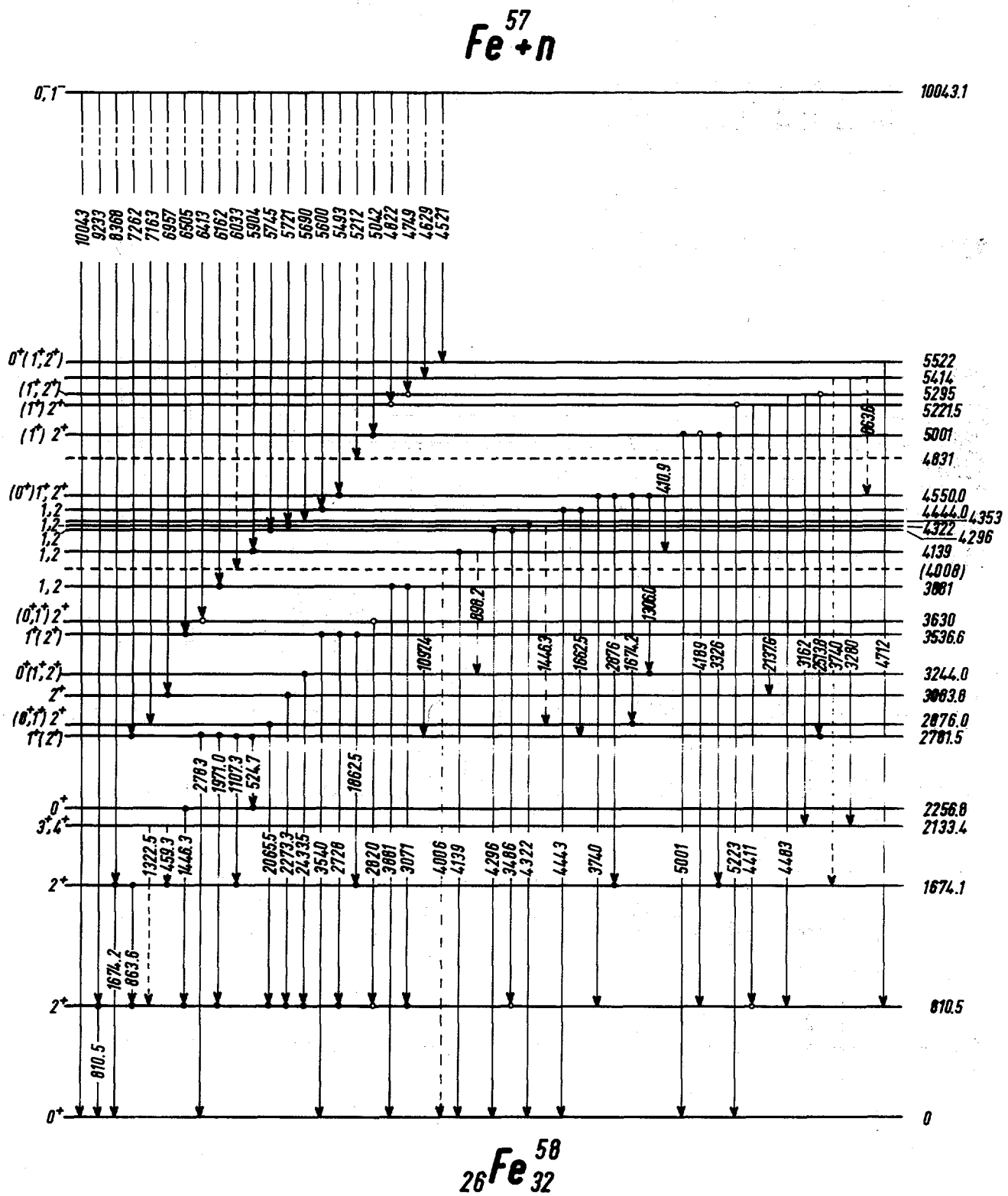


Fig. 17 Standard Cross Section



**Fig. 18**

$Ni^{61}$

10596

1<sup>-</sup>2<sup>-</sup>

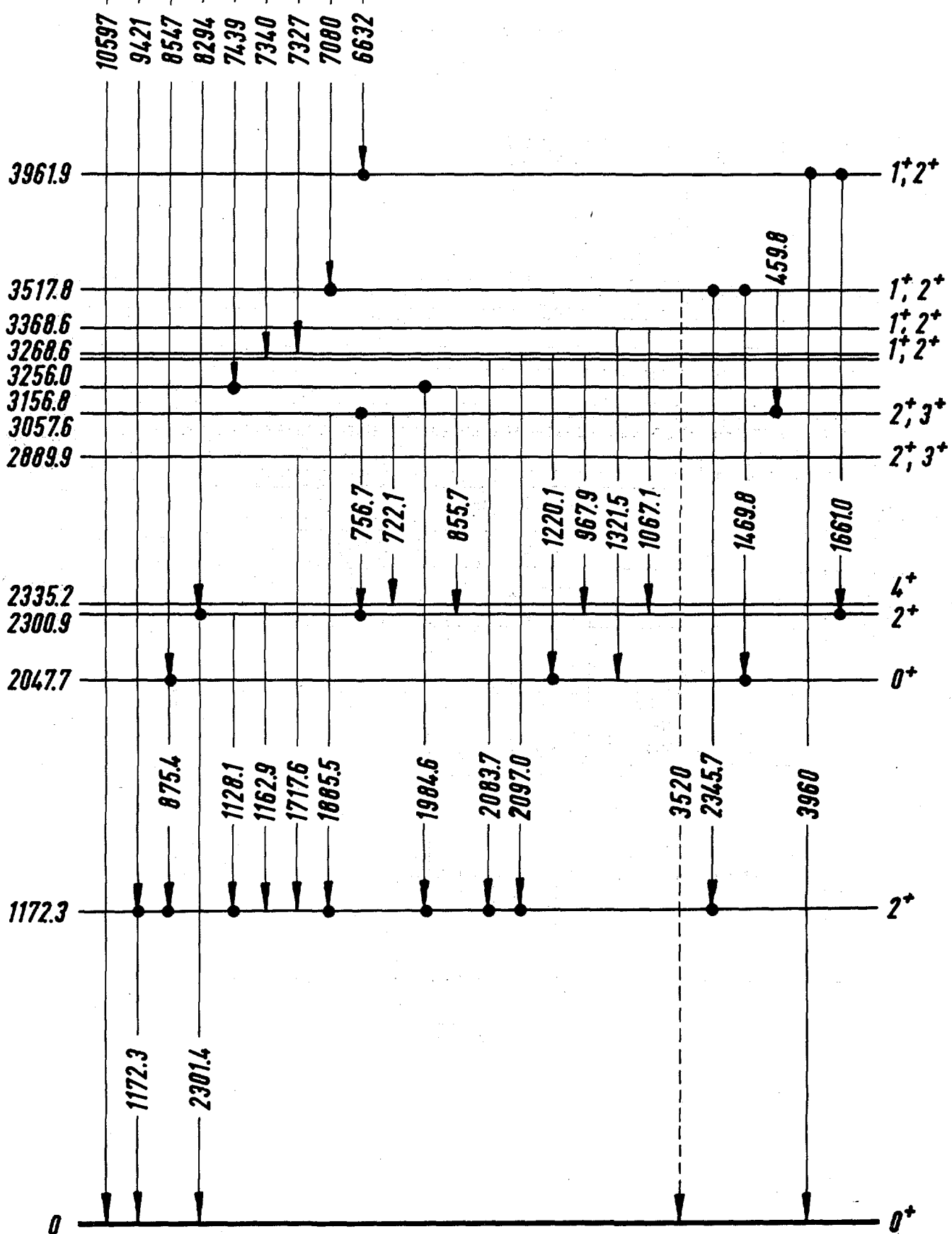


Fig. 19

$28Ni^{62}_{34}$

II. PHYSIK-DEPARTMENT, TECHNISCHE HOCHSCHULE MÜNCHEN (GERMANY)

1. Fast Neutron Cross-sections.

1.1. Measurements of (n,2n) Cross-Sections at 14.7 MeV by activation.

W. Dilg and H. Vonach

Activation measurements of (n,2n) cross-sections at 14.7 MeV were performed for 16 nuclei with mass 140 to 204 using neutrons from the D-T reaction. Such target nuclei were selected for which the (n,2n) reaction lead to product nuclei decaying predominantly electron capture. Thus the absolute measurement of the activities produced was done in all cases by K-X-ray counting (photopeak area) with a thin (3mm) NaJ crystal calibrated with standardized sources.<sup>+</sup>

Electron capture activities were calculated from the X-ray intensities taking into account fluorescence yield and K to L and M capture ratio. In cases where electron capture decay lead to excited states of the final nucleus for X-rays emitted after internal conversion or produced by external conversion of gammarays in the target material and for summing effects in the NaJ-crystal were applied. The neutron flux was determined by means of aluminum monitor foils activated with the sample using a cross-section of 111.5 m b/17 for the monitor reaction  $^{27}\text{Al}$  (n, $\alpha$ )  $^{24}\text{Na}$ . Table I gives the measured cross-sections with errors (including the statistical and all systematic errors) and the ratio of the measured (n,2n) cross-sections to the reaction cross-section. As the table shows the (n,2n) cross-sections amount to 80 - 100 % of the non elastic cross-section for all nuclei investigated. No dependence of the ratio  $\sigma(n,2n) / \sigma_{\text{nonelast}}$  on target mass especially no shell effects can be detected withing the experimental errors of about 10 %.

Lt. /1/ W. Nagel, Thesis, University of Amsterdam (1966)

<sup>+</sup>from the Zentralbüro für Kernmessungen - Geel

Table I

(n,2n) Cross-Sections and Ratios of (n,2n)  
Cross-Sections to the Total Reactions at 14.7 MeV

Reaktion	(n, 2n)	(n, 2n) / nonelast.
	at 14,7 MeV	
	mb	
$^{140}\text{Ce}(n,2n)^{139}\text{Ce}$	1780 $\pm$ 135	0,85
$^{142}\text{Nd}(n,2n)^{141}\text{Nd}$	1695 $\pm$ 120	0,80
$^{154}\text{Gd}(n,2n)^{153}\text{Gd}$	1850 $\pm$ 140	0,84
$^{160}\text{Dy}(n,2n)^{159}\text{Dy}$	1985 $\pm$ 150	0,88
$^{165}\text{Ho}(n,2n)^{164\text{i+g}}\text{Ho}$	2185 $\pm$ 300	0,95
$^{165}\text{Ho}(n,2n)^{164\text{i}}\text{Ho}$	1225 $\pm$ 170	
$^{166}\text{Er}(n,2n)^{165}\text{Er}$	2230 $\pm$ 170	0,97
$^{169}\text{Tm}(n,2n)^{168}\text{Tm}$	1925 $\pm$ 150	0,84
$^{170}\text{Yb}(n,2n)^{169}\text{Yb}$	2035 $\pm$ 155	0,88
$^{175}\text{Lu}(n,2n)^{174\text{g}}\text{Lu}$	1285 $\pm$ 140	0,82
$^{175}\text{Lu}(n,2n)^{174\text{i}}\text{Lu}$	655 $\pm$ 55	0,82
$^{176}\text{Hf}(n,2n)^{175}\text{Hf}$	2300 $\pm$ 175	0,97
$^{182}\text{W}(n,2n)^{181}\text{W}$	2200 $\pm$ 170	0,92
$^{191}\text{Ir}(n,2n)^{190\text{g}}\text{Ir}$	1730 $\pm$ 135 (i:367mb)	0,85
$^{197}\text{Au}(n,2n)^{196\text{i+g}}\text{Au}$	2405 $\pm$ 15	
$^{198}\text{Hg}(n,2n)^{197\text{i+g}}\text{Hg}$	2425 $\pm$ 220	0,96
$^{203}\text{Tl}(n,2n)^{202}\text{Tl}$	2240 $\pm$ 170	0,88
$^{203}\text{Pb}(n,2n)^{202}\text{Pb}$	2110 $\pm$ 160	0,83

1.2. Precision Measurements of Excitation Functions of  
(n,p), (n, $\alpha$ ) and (n,2n) Reactions Induced by  
13.5 - 14.7 MeV Neutrons.

H.K. Vonach, W.G. Vonach, H. Münzer (Universität München) und P. Schrammel (Ges. f. Strahlenforschung, Neuherberg)

Excitation Functions for the reactions  $^{19}\text{F}$  (n,2n),  $^{24}\text{Mg}$  (n,p),  $^{27}\text{Al}$  (n, $\alpha$ ),  $^{48}\text{Ti}$  (n,p),  $^{51}\text{V}$  (n, $\alpha$ ),  $^{65}\text{Cu}$  (n,2n),  $^{107}\text{Ag}$  (n,2n),  $^{106\text{m}}\text{Ag}$ ,  $^{115}\text{In}$  (n,2n),  $^{114\text{m}}\text{In}$ ,  $^{181}\text{Ta}$  (n,2n),  $^{108\text{m}}\text{Ta}$  and  $^{197}\text{Au}$  (n,2n),  $^{196}\text{Au}$  were determined in 30 - 50 KeV steps in the energy range 13.50 - 14.7 MeV using the activation method. Neutrons from the D - T reactions (deuteron energy 0.12 MeV) were used to irradiate the samples. The gamma-activities produced by the reactions were measured with a large NaJ well crystal (statistical accuracy 0.2 - 0.5 %). Systematic errors were minimized by use of an accurate geometry (target sample distance  $100 \pm 0.15$  mm) and by use of an extremely light air-cooled target assembly minimizing the contribution of elastically scattered neutrons to the activation of the samples and by the use high-purity metallic samples. The attenuation of neutrons in the target and target assembly as well the intensity of the neutrons scattered elastically by target and target assembly was calculated as a function of the neutron emission angle (and corresponding neutron energy) and appropriate corrections applied. In this way an overall accuracy of about 1 % could be obtained for the relative cross-section  $\sigma(\text{En})\sigma(14.7\text{MeV})$ . The excitation functions are shown in fig. 1 to 8, cross-sections are arbitrarily normalized to unity at 14.7 MeV, the size of the data points corresponds to the statistical errors. The smooth curves are least square fits of first or second degree polynomials except for the  $^{24}\text{Mg}$  (n,p) and Al (n, $\alpha$ ) where definitely fine structure is present and the smooth curves were drawn according to "eye-inspection".

Numerical values of these fit curves describing the relative cross-sections are given in table II in 0.1 MeV steps.

Also shown in the figures are the [1] excitation functions reported by Strohal et al., Csikai [2] and Bormann and Riehle [3]. Our data as well as Bormann's definitely show that the large fluctuations found by Strohal and Csikai do not exist and are probably due to systematic errors. Only in the two reactions  $^{24}\text{Mg}$  ( $n, p$ ) and  $\text{Al}$  ( $n, \alpha$ ) some structure (however completely different from Strohal's results) seems to be definitely present. For all reactions, involving nuclei heavier than aluminium no fine structure is detectable within the experimental errors of about 1 %.

In addition ratios of the cross-sections to the  $^{27}\text{Al}$  ( $n, \alpha$ ) cross-section were determined for 8, of the reactions investigated at 14.7 MeV.

An accuracy of 2 - 3 % (including all systematic errors) was obtained by means of careful efficiency calibrations of the well crystal used. The experimentally determined ratios as well as the absolute cross-sections obtained with a value of 111.5 mb for the  $^{27}\text{Al}$  ( $n, \alpha$ ) cross-section are given in table III. The value of 111.5 mb was obtained, as we weighted average of all previously reported measurements by Nagel. [5].

#### Literature

- [1] P. Strohal et al. Phys. Letters 6 (1963) 205
- [2] J. Csikai Proc. Int. Conf. on the Study of Nuclear Structure with Neutrons Antwerpen 1965
- [3] M. Bormann and I. Riehle Z. f. Physik 207, 64 (1967)
- [4] J.M. Ferguson and I.C. Albergotti N.P. A98 (1967) 65
- [5] W. Nagel, Thesis University of Amsterdam (1966)

Table II

Relative Cross-sections  $\sigma(E_n)/\sigma(14.7 \text{ MeV})$  for the reactions investigated in steps of 0.1. MeV, all values accurate to  $\pm 1\%$ .

Reaktion	$E_n$ (MeV)										
		13.6	13.7	13.8	13.9	14.0	14.1	14.2	14.3	14.4	14.5
$^{19}_{24}\text{Fe}(n, 2n)$	$^{18}_{24}\text{F}$	0.613	0.648	0.683	0.718	0.754	0.779	0.824	0.859	0.894	0.930
$^{24}_{24}\text{Mg}(n, p)$	$^{24}_{24}\text{Na}$	1.177	1.135	1.082	1.065	1.095	1.110	1.115	1.110	1.095	1.075
$^{27}_{27}\text{Al}(n, \alpha)$	$^{24}_{24}\text{Na}$	1.112	1.105	1.092	1.077	1.077	1.080	1.080	1.072	1.045	1.025
$^{48}_{48}\text{Ti}(n, p)$	$^{48}_{48}\text{Sc}$	0.937	0.952	0.965	0.976	0.985	0.992	0.998	1.002	1.004	1.004
$^{51}_{51}\text{V}(n, \alpha)$	$^{48}_{48}\text{Sc}$	0.820	0.836	0.852	0.867	0.885	0.902	0.918	0.934	0.951	0.967
$^{56}_{56}\text{Fe}(n, p)$	$^{36}_{36}\text{Mn}$	1.074	1.072	1.070	1.066	1.062	1.056	1.049	1.042	1.033	1.023
$^{65}_{65}\text{Cu}(n, 2n)$	$^{64}_{64}\text{Cu}$	0.856	0.871	0.887	0.903	0.918	0.932	0.945	0.958	0.969	0.980
$^{107}_{107}\text{Ag}(n, 2n)$	$^{106m}_{106m}\text{Ag}$	0.879	0.893	0.906	0.919	0.931	0.943	0.954	0.964	0.974	0.983
$^{115}_{115}\text{In}(n, 2n)$	$^{114m}_{114m}\text{In}$	0.932	0.938	0.944	0.950	0.957	0.963	0.969	0.975	0.981	0.987
$^{181}_{181}\text{Ag}(n, 2n)$	$^{180m}_{180m}\text{Tal}$	0.014	1.013	1.011	1.010	1.009	1.008	1.006	1.005	1.004	1.003
$^{196}_{196}\text{Au}(n, 2n)$	$^{196}_{196}\text{Au}$	0.99	0.991	0.992	0.993	0.994	0.995	0.995	0.996	0.997	0.998

Table III

Experimental cross-section ratios  $\sigma/\sigma^{27}\text{Al}$  ( $n, \alpha$ ) and absolute cross-sections based on a value of 111.5  $\pm 2$  mb for the  $^{27}\text{Al}(n, \alpha)$  reaction for 14.7 MeV neutrons.

Reaction	$\sigma/\sigma^{27}\text{Al}(n, \alpha)$	$\sigma[\text{mb}]$
$^{19}\text{F} (n, 2n) ^{18}\text{F}$	$0.398 \pm 3\%$	$44.4 \pm 2$
$^{24}\text{Mg} (n, 2n) ^{24}\text{Na}$	$1.61 \pm 1\%$	$179.7 \pm 4$
$^{48}\text{Ti} (n, p) ^{48}\text{Sc}$	$0.601 \pm 2\%$	$67. \pm 2.5$
$^{51}\text{V} (n, \alpha) ^{48}\text{Sc}$	$0.1462 \pm 2\%$	$16.3 \pm 0.6$
$^{56}\text{Fe} (n, p) ^{56}\text{Mn}$	$0.912 \pm 3\%$	$101.8 \pm 4$
$^{65}\text{Cu} (n, 2n) ^{64}\text{Cu}$	$7.84 \pm 2\%$	$874 \pm 35$
$^{107}\text{Ag}(n, 2n) ^{106m}\text{Ag}$	$5.37 \pm 2\%$	$599 \pm 20$
$^{197}\text{Au}(n, 2n) ^{196}\text{Au}$	$18.83 \pm 5\%$	$2100 \pm 140$

### 1.3. Averaged Cross-Section of the Reaction $^{89}\text{Y}$ ( $n,2n$ ) $^{88}\text{Y}$

G. Rau

Samples of  $\text{Y}_2\text{O}_3$  were irradiated for about 300 hours in a central position of the FRM-reactor to measure the cross-section of the reaction  $^{89}\text{Y}$  ( $n,2n$ )  $^{88}\text{Y}$  averaged over a fission neutron spectrum.

$$(1) \quad \langle \sigma \rangle = \frac{\int_{E_T}^{\infty} \sigma(E) \psi(E) dE}{\Phi_{eq}}$$

Eq. (1) is only valid in a region, where the reactor spectrum has about the same shape as a fission neutron spectrum [1].

This condition is fulfilled in the case of  $^{89}\text{Y}$  ( $n,2n$ )  $^{88}\text{Y}$  because of its high threshold. The equivalent fission flux  $\Phi_{eq}$  was determined by the reaction  $^{46}\text{Ti}$  ( $n,p$ )  $^{46}\text{Sc}$  with  $\langle \sigma \rangle = 12,6 \text{ mb}$  [2].

After a post-irradiation cool-off time of about 30 days, the  $^{88}\text{Y}$  - and  $^{46}\text{Sc}$  - activities were measured  $\nu$ -spectroscopically by means of a calibrated  $3 \times 3"$  NaI(Tl)-crystal [3].

An averaged cross-section,  
 $\langle \sigma \rangle_{n,2n} (^{88}\text{Y}) = 0,2 \pm 0,01 \text{ mb}$

was found.

#### References:

- [1] Cranberg, L. et al.: Phys. Rev. 103, 662 (1956)
- [2] Köhler, W.: Nukleonik 8, 9 (1966)
- [3] Rau, G., K. Knopf: FRM 90 (1967)

2. Thermal Cross-Section of the Reaction  $^{34}\text{S}(\text{n},\nu)^{35}\text{S}$ [1]  
W. Köhler , K. Knopf

Samples of  $(\text{NH}_4)_2\text{SO}_4$  and  $\text{K}_2\text{SO}_4$  were irradiated in the graphite reflector of the FRM-reactor. Thermal flux was measured by activation of  $20\mu$  gold foils ( $\sigma_0 = 98,8 \text{ mb}$ ). The  $^{35}\text{S}$ -activity was determined by  $4\pi\beta$ -counting. A thermal cross-section

$$\sigma_0 = 33,7 \pm 3,6 \text{ mb}$$

was found.

References

- [1] W. Köhler, K. Knopf: Nukleonik 10, 278 (1967)

3. Resonance Activation Integrals of  $^{98}\text{Mo}$ ,  $^{103}\text{Rh}$  and  $^{191}\text{Ir}$

E. Schneider

The resonance activation integral

$$(1) \quad I_{\text{res}} = \int_{E_c}^{\infty} \frac{\sigma(E) dE}{E}$$

of a sample (index 1) relative to that of a reference standard was measured by two methods:

a) the absolute (activity) method

$$(2) \quad I_{\text{res1}} = I_{\text{res2}} \frac{A_1 N_2}{A_2 N_1}$$

( $A_i$  = activity;  $N_i$  = number of target nuclei)

b) the cadmium-ratio method

$$(3) \quad I_{\text{res1}} = I_{\text{res2}} \frac{\sigma_{01} (R_{c2}^{-1})}{\sigma_{02} (R_{c1}^{-1})}$$

( $\sigma_{0i}$  = thermal activation cross-section;  $R_{ci}$  = cadmium-ratio).

In the usual manner, the  $1/v$  - component

$$(4) \quad I_{1/v} = \int_{E_c}^{\infty} \sigma_0 \frac{E_0}{E} \cdot \frac{dE}{E}$$

can be separated from  $I_{\text{res}}$ , and thus the true resonance integral

$$(5) \quad I_{\text{res}} = I_{\text{res}} - I_{1/v}$$

is obtained.

In the following work, the resonance activation integrals of  $^{98}\text{Mo}$ ,  $^{103}\text{Rh}$  and  $^{191}\text{Ir}$  were determined. As reference standards, gold wires were used with the following data;  
 $\sigma_0 = 98,6 \pm 0,3 \text{ b}$ ;  $I_{\text{res}} = 1507 \pm 20 \text{ b}$

With a cadmium-cutoff  $E_c = 0,55 \text{ eV}$ , we obtain  $I_{1/v} = 42 \pm 0,2 \text{ b}$  and  $I_{\text{res}} = 1549 \pm 20 \text{ b}$ .

For shielding against thermal neutrons, Cd-capsules of 0.5 mm thickness were used. With the data given in

[1-4], the cadmium-cutoff  $E_c$  was calculated.

Samples and reference standards were irradiated in the pneumatic rabbit system of the FRM-reactor [5]; the determination of activity was done with a calibrated  $3 \times 3"$  NaI(Tl)-crystal [6]. For elimination of self-shielding correction factors were determined..

The results of the measurements are compiled in the following table IV.

Table IV : Resonance activation integrals.

Reaction	$E_c$ [eV]	$\sigma_0$ [b]	$I_{1/v}$ [b]	$I_{res}$ [b]	$I_{r\acute{e}s}$ [b]
$^{98}\text{Mo}(n,\gamma)^{99}\text{Mo}$	0,55	$0,18 \pm 0,02$	0,076	$6,45 \pm 0,14$	$6,38 \pm 0,15$
$^{103}\text{Rh}(n,\gamma)^{104m}\text{Rh}$	0,55	$11 \pm 1$	4,23	$83 \pm 5$	$78 \pm 7$
$^{103}\text{Rh}(n,\gamma)^{104g}\text{Rh}$	0,55	$157 \pm 3$	57	$1114 \pm 65$	$1054 \pm 74$
$^{191}\text{Ir}(n,\gamma)^{192m}\text{Ir}$	0,62	$300 \pm 30$	120	$1060 \pm 150$	$940 \pm 162$
$^{191}\text{Ir}(n,\gamma)^{192(m+g)}\text{Ir}$	0,62	$910 \pm 90$	360	$4440 \pm 250$	$4080 \pm 285$

### References

- [1] Takeda, R., K. Inoue: JAERI-1052 (1963)
- [2] Maunders, E.D.: J.Nucl.Energy 2, 959 (1965)
- [3] Stroughton, R.W. et al: ORNL 2823 (1960)
- [4] Yasuno, T.: J.Nucl.Energy 2, 427 (1965)
- [5] Rau, G: FRM 50 (1963)
- [6] Rau, G: Nukleonik 2, 228 (1967)

4. Measurements of Coherent and Scattering Length

L. Koester, N. Nücker, W. Nistler, H. Ungerer, P. Schacht

- 4.1. With the neutron gravitation refractometer at the FRM, the coherent scattering length was measured for the bound atom of bismuth.

The result is:

$$a_{coh}(\text{bound atom}) = +(8,5682 \pm 0,0012) F$$

For the determination of the coherent scattering length it was necessary to measure the density of the liquid metal at different temperatures. With a pycnometer a density of  $d = (10,049 \pm 0,001) \text{ gcm}^{-3}$  has been found for bismuth at  $271^\circ\text{C}$ . By the same method the density of Pb at  $327,3^\circ\text{C}$  was measured:

$$d(\text{Pb}) = (10,661 \pm 0,004) \text{ gcm}^{-3}$$

- 4.2. New measurements have been started to find the precise scattering length of elements in organic liquids.

The first results for bromine, chlorine and carbon are:

$$\text{C} : a = + (6,66 \pm 0,02) F \text{ former results } (6,648 \pm 0,004) F$$

$$\text{Cl} : a = + (9,640 \pm 0,007) F " " (9,633 \pm 0,006) F$$

$$\text{Br} : a = + (6,871 \pm 0,012) F$$

- 4.3. Furthermore, experiments have been started in order to measure the coherent scattering length of elements which are not available in liquid form for direct measurements at the refractometer.

As already described [1] the method is based on the small angle scattering of a mixture of powdered material and a liquid with known scattering length.

First measurements have been performed with powdered tungsten in a mixture of  $\text{C}_2\text{Cl}_4$  and  $\text{C}_6\text{H}_5\text{Cl}$ . Now these experiments are continued with a system of powdered tungsten and  $\text{D}_2\text{O}/\text{H}_2\text{O}$ .

An accuracy of  $\pm 1\%$  for the determination of scattering length by this method seems to be within reach.

[1] L. Koester, W. Trüstedt; Physikertagung Berlin, Okt. 1967

5. Measurement of Free Cross-Sections for slow neutrons

P. Fehsenfeld, L. Koester

Together with the precise value of the coherent scattering length of Bi it is necessary to measure the free cross-section of Bi with great accuracy in order to determine the neutron-electron-interaction.

For this purpose a resonance detector made of Rh respectively Ag has been developed which is working in a continuous fashion. Moreover a filter difference method is applied, so that the fraction of all neutrons with an energy above 1000 eV contributing to the cross-section measurement is less than  $2 \cdot 10^{-5}$ . The first results have been obtained with two Bi-samples of different thickness

$$(1,25\text{eV}) = (9,16 \pm 0,04) \text{ b}$$

$$(1,25\text{eV}) = (9,19 \pm 0,04) \text{ b}$$

The final accuracy is expected to be somewhat better than  $10^{-3}$ .

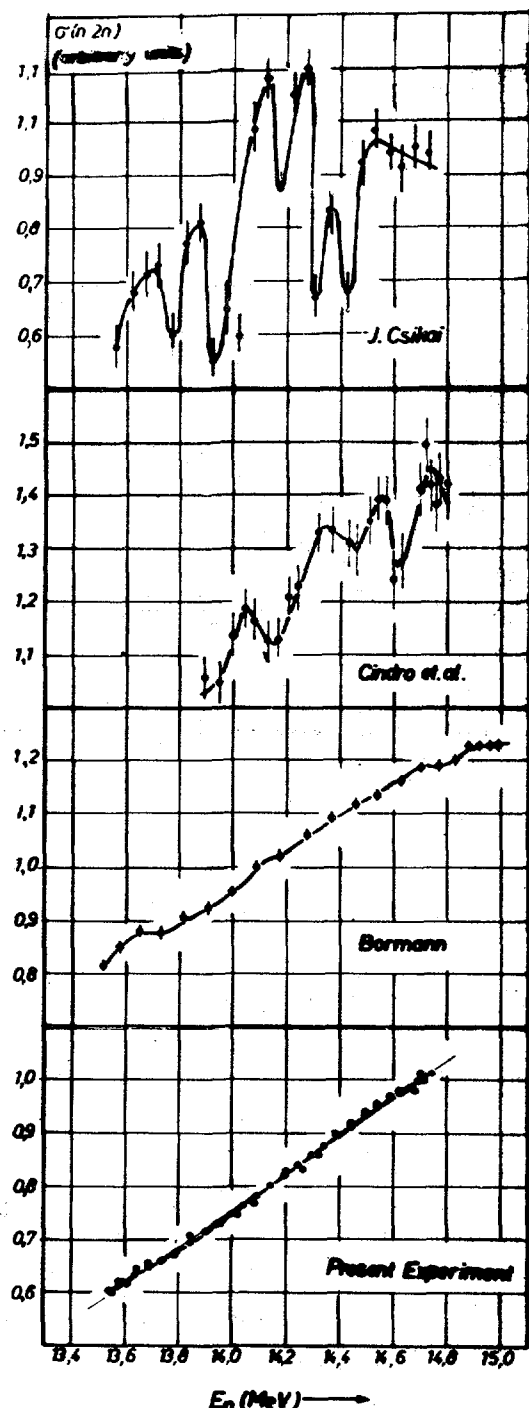


Fig.1 Excitation function of  
the reaction  $F^{19}(n,2n)F^{19}$

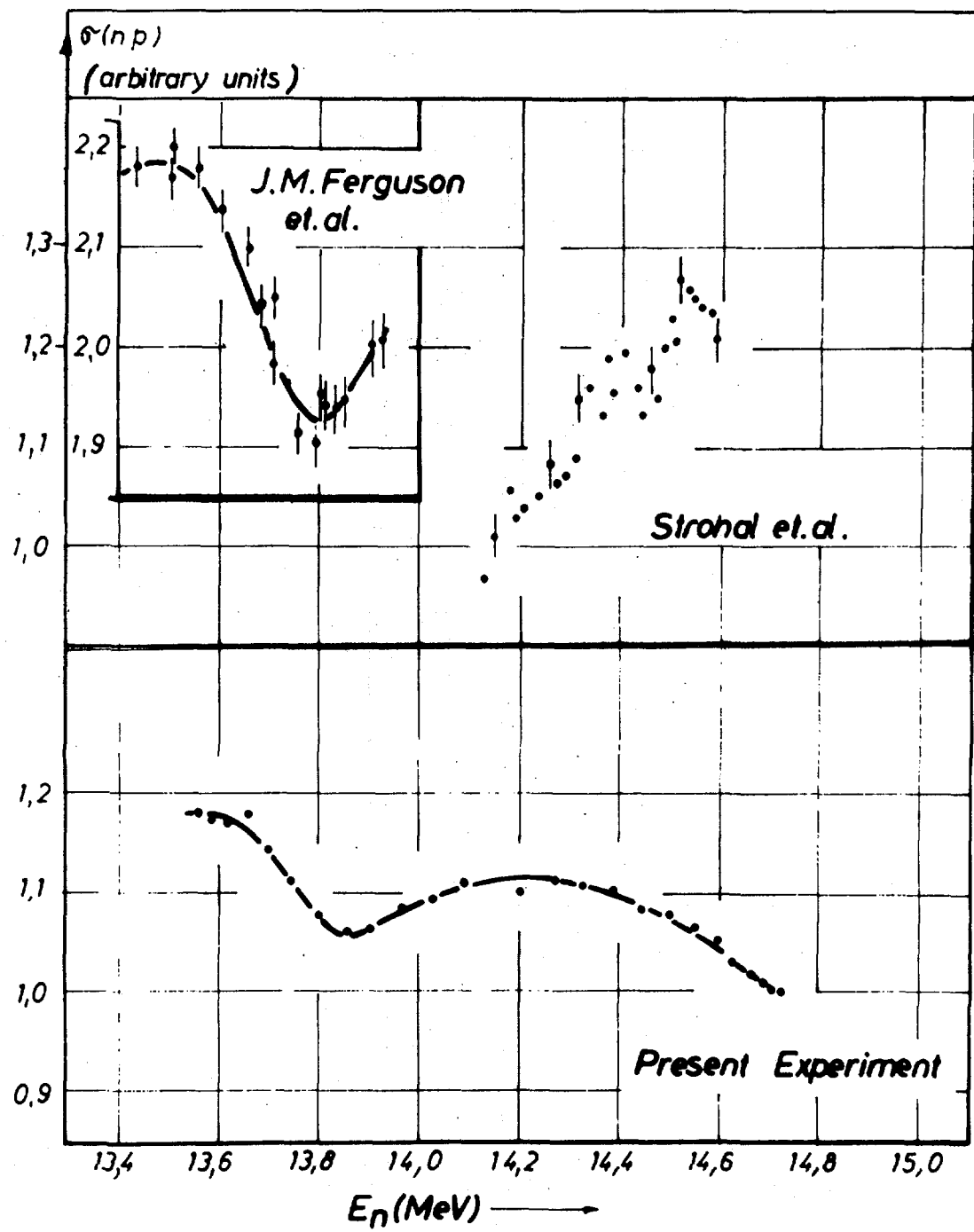


Fig.2 Excitation function of the reaction  $\text{Mg}^{24}(n,p)\text{Na}^{24}$

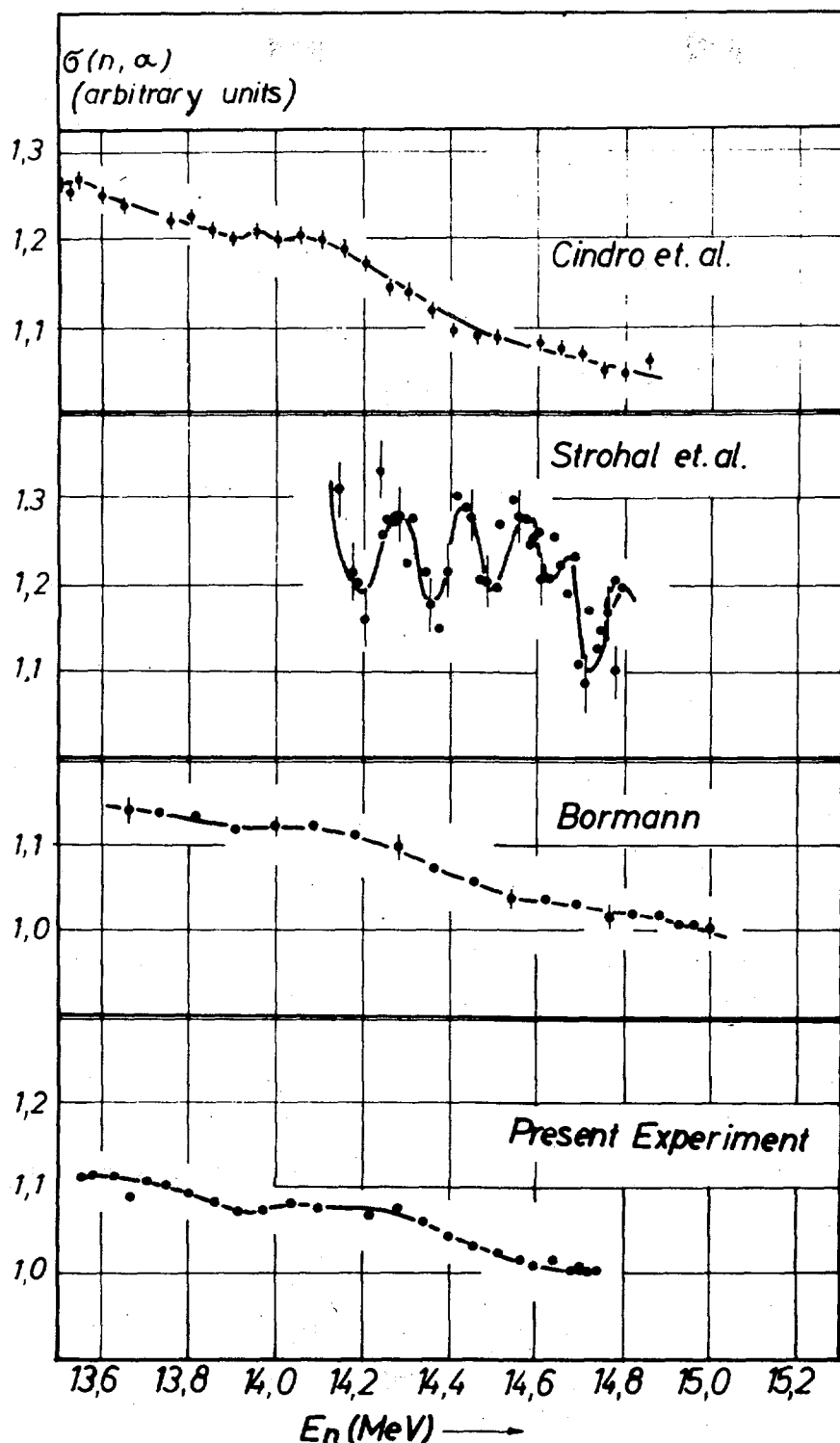


Fig.3 Excitation function of  
the reaction  $At^{27}(n, \alpha)Na^{24}$

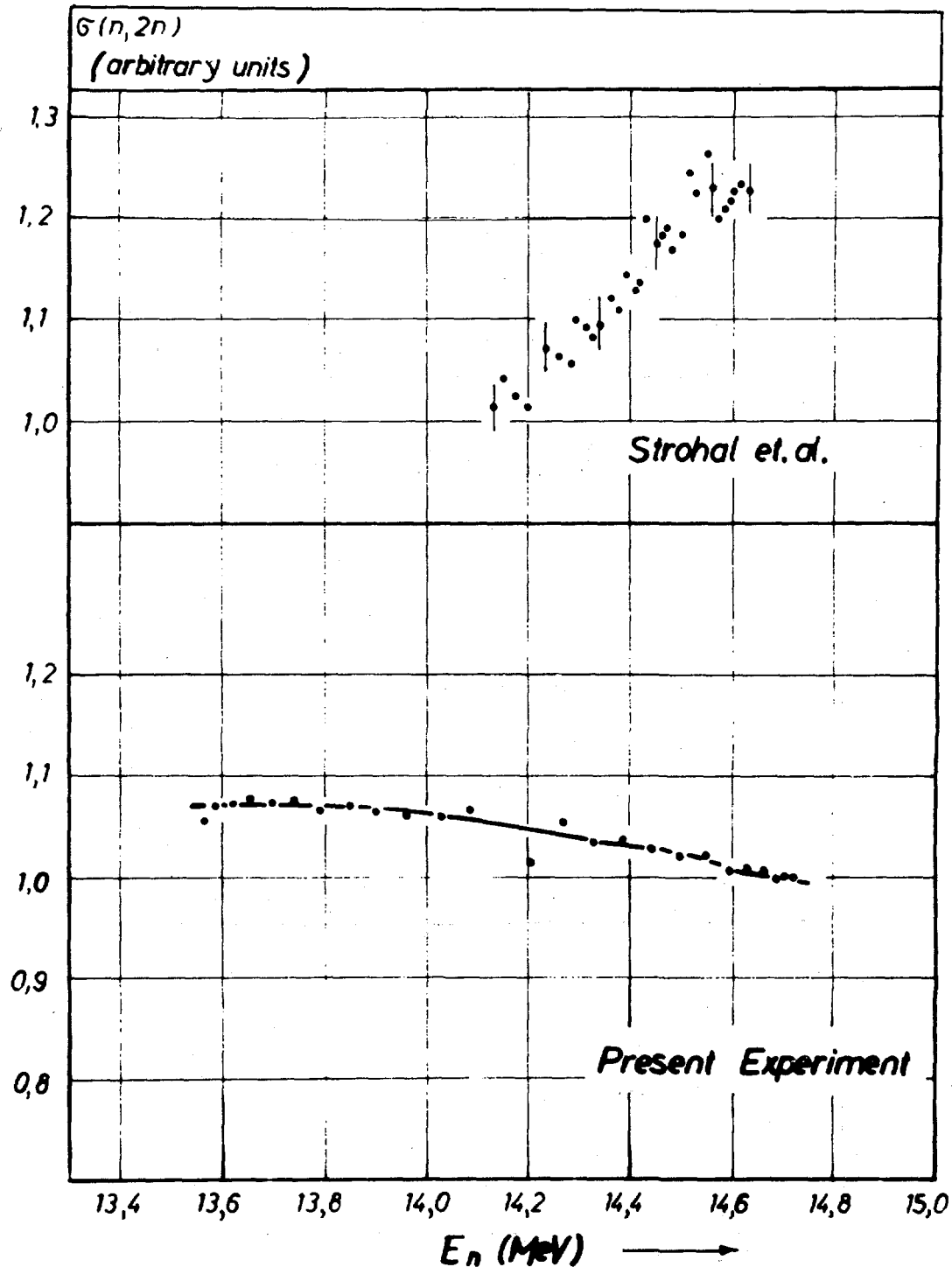


Fig. 4 Excitation function of the reaction  $\text{Fe}^{56}(n,p)\text{Mn}^{56}$

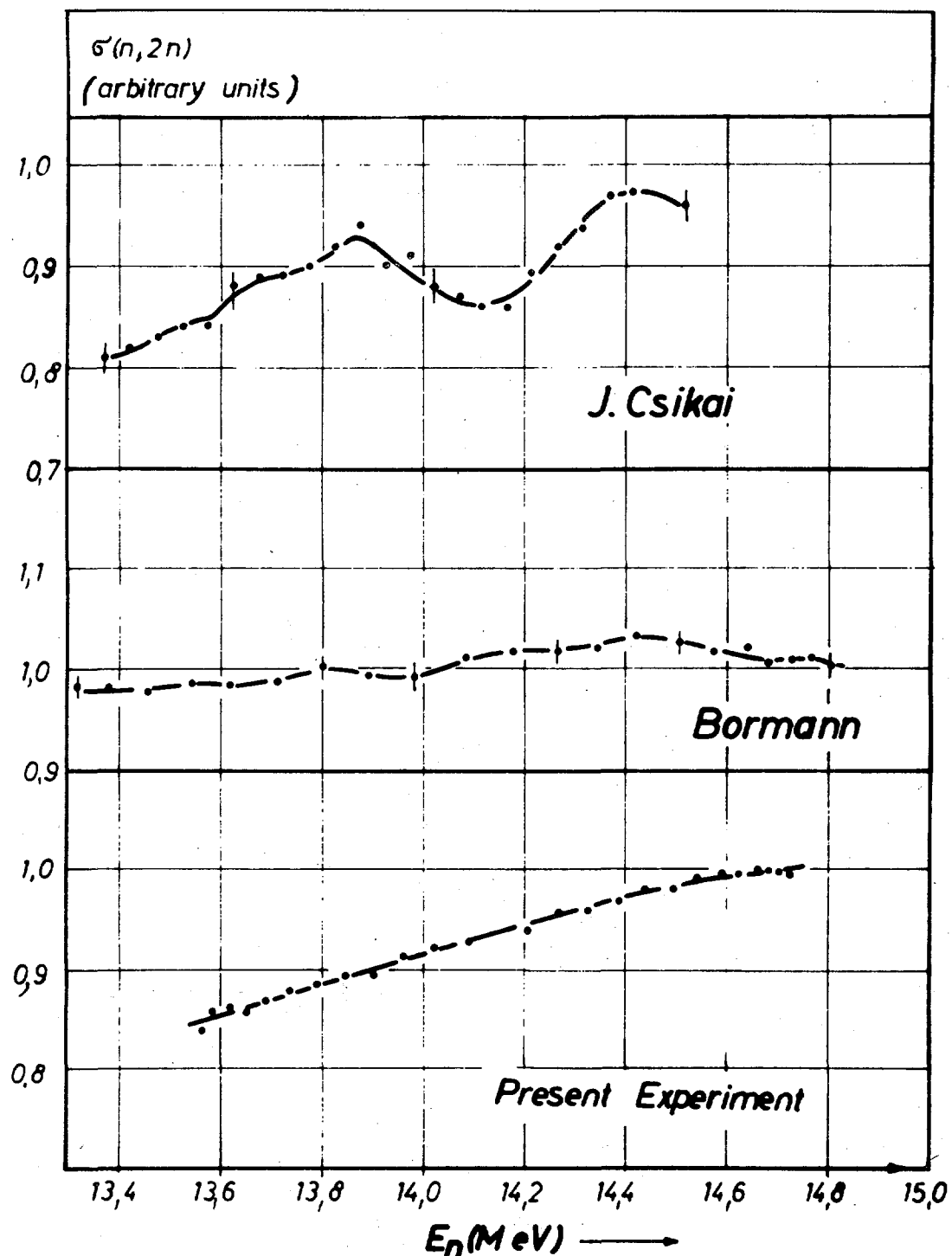


Fig. 5 Excitation function of the reaction  $\text{Cu}^{65}(n,2n)\text{Cu}^{64}$

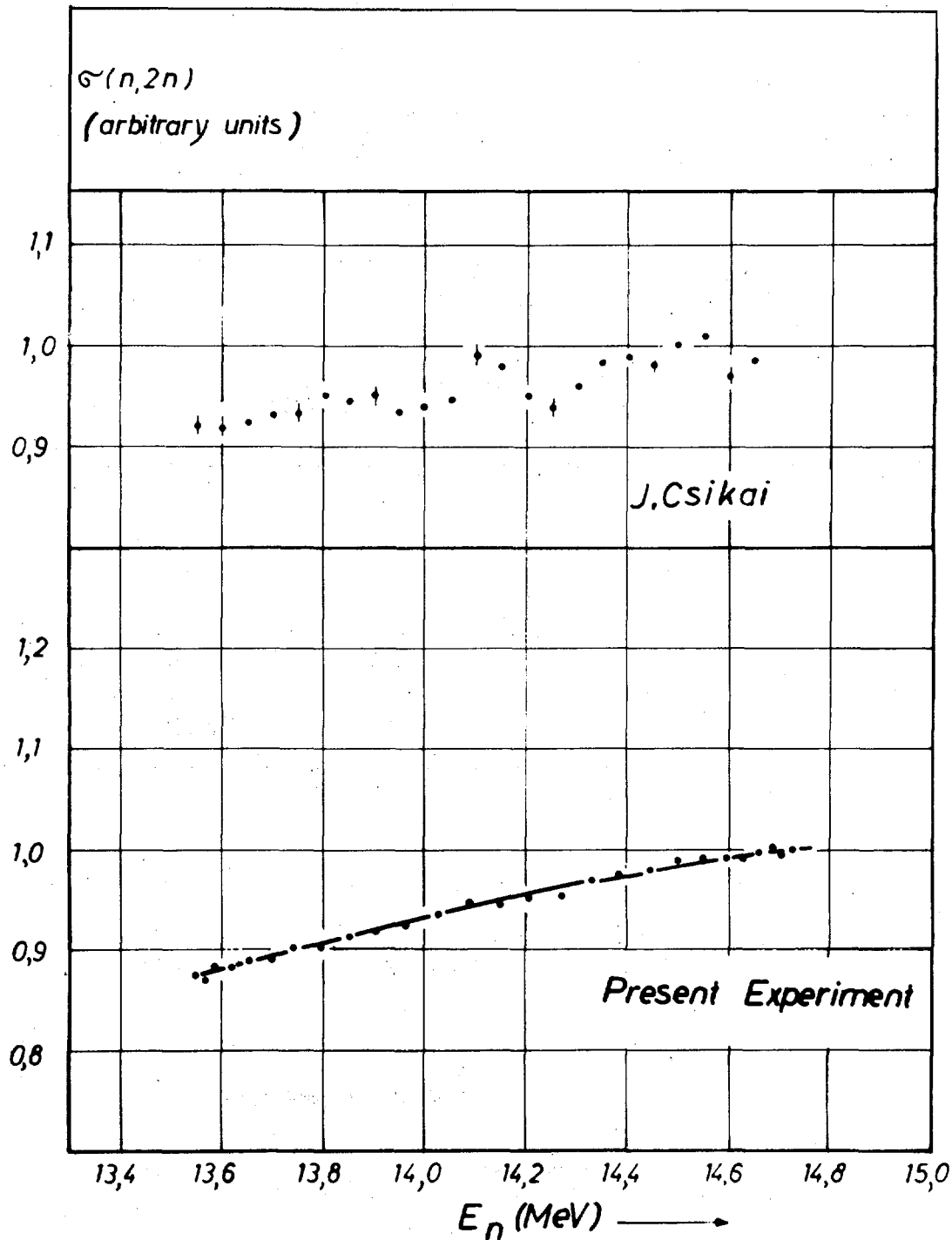


Fig.6 Excitation function of the reaction  $\text{Ag}^{107}(n,2n)\text{Ag}^{106m}$

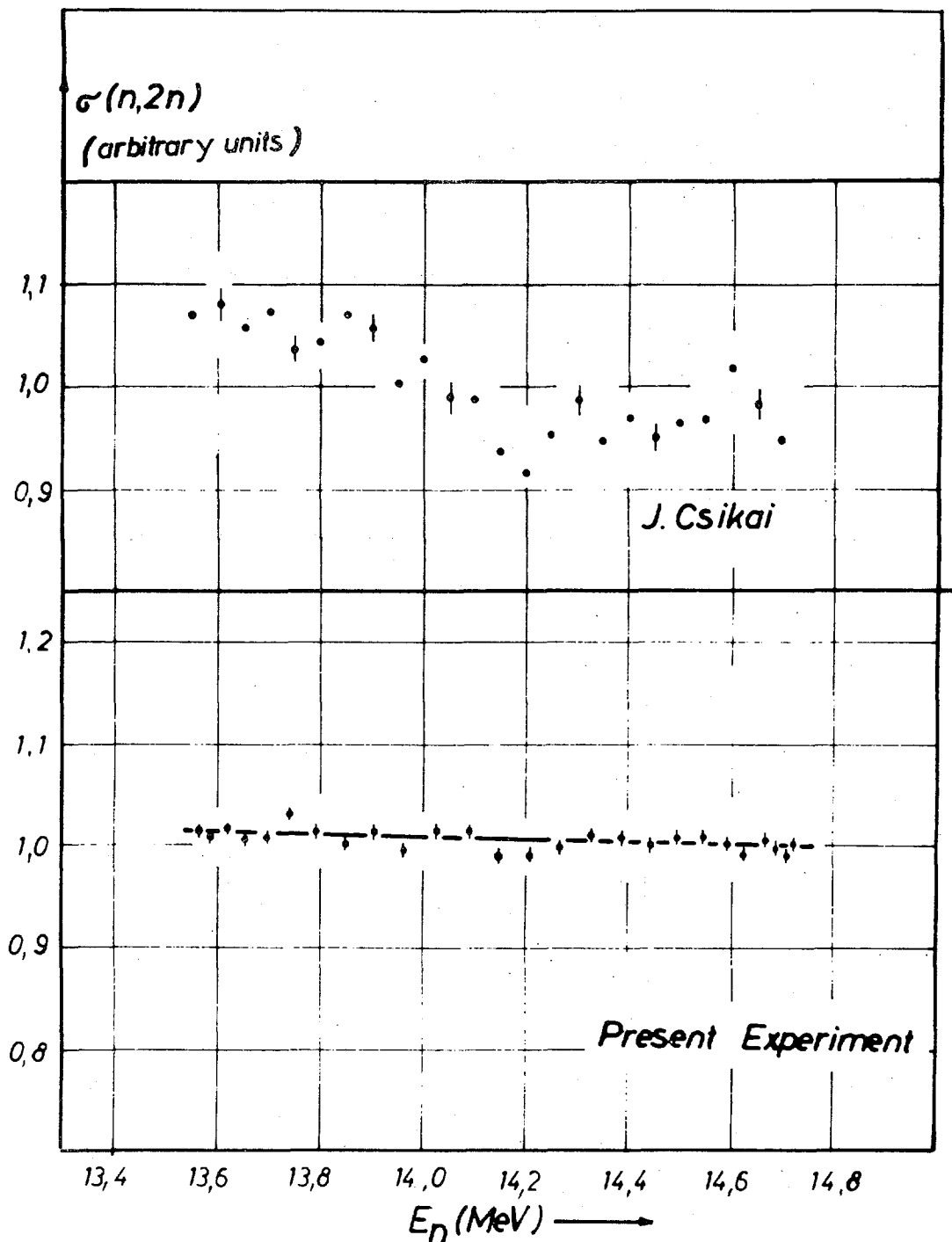


Fig.7 Excitation function of the reaction  $Ta^{181}(n,2n)Ta^{180m}$

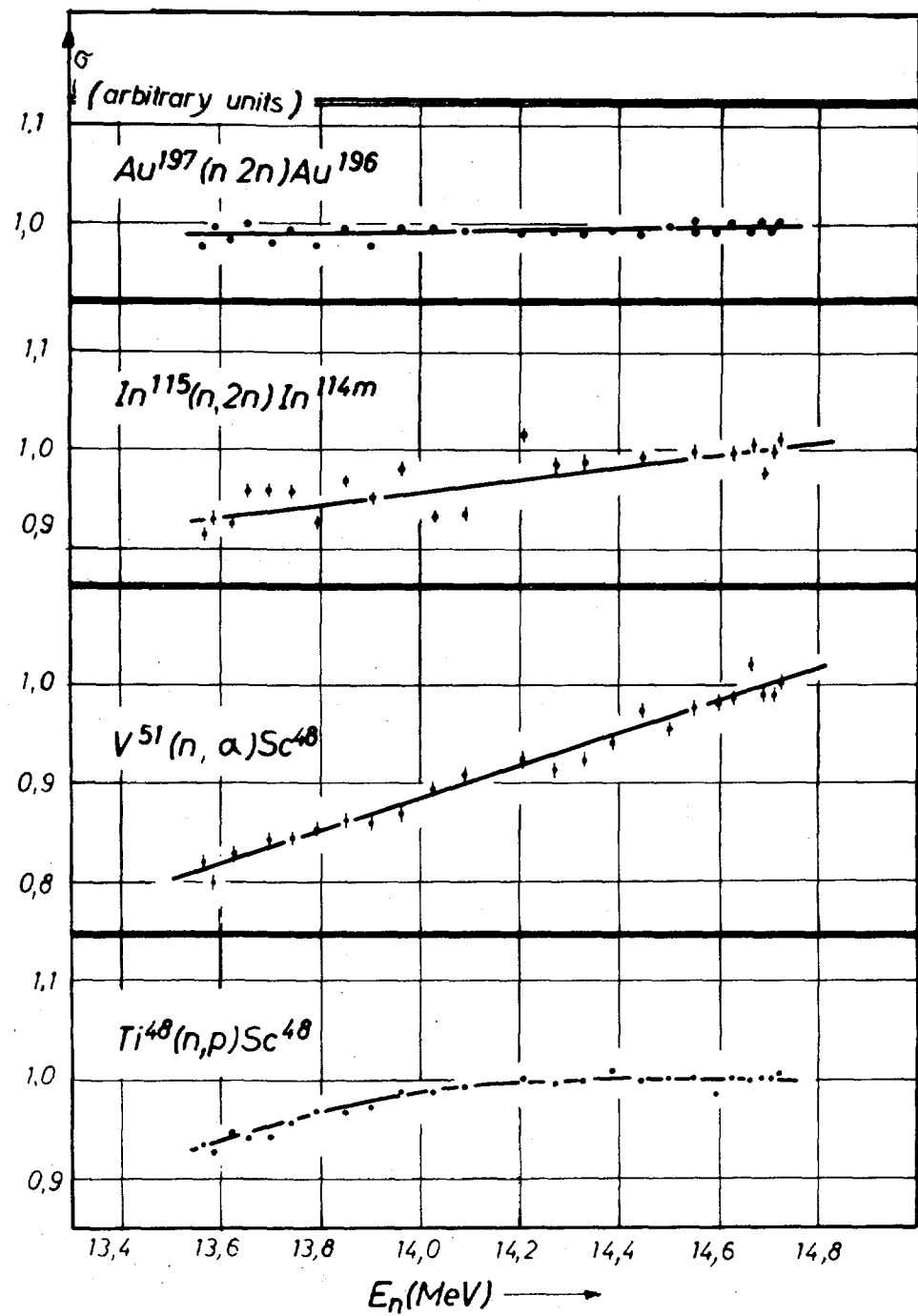


Fig. 8 Excitation function of the reactions  $In^{115}(n,2n)In^{114m}$ ,  $V^{51}(n,\alpha)Sc^{48}$ ,  $Ti^{48}(n,p)Sc^{48}$ ,  $Au^{197}(n,2n)Au^{196}$ .

III. INSTITUT FÜR FESTKÖRPER - UND NEUTRONENPHYSIK, KERNFORSCHUNGS  
ANLAGE JULICH .

The Measurement of the Incoherent Scattering Cross Sections of  
Lead and Bismuth

R. Scherm

A precise measurement of the spin- and isotopic incoherent scattering cross sections  $\sigma_{inc}$  of lead and bismuth has been performed by determining the intensity of the neutrons scattered by the sample in a large solid angle. The detectors have been calibrated using a vanadium sheet as a reference sample.

Very low neutron energies in the range of 0.4 - 1.3 mev were used to suppress elastic Bragg and inelastic energy loss scattering. To avoid energy gain scattering the samples were cooled to temperatures between 3 and 50°K (fig. 1). At the lowest temperatures the inelastic scattering vanishes and the scattered intensity is only due to  $\sigma_{inc}$ . The results are given in table I. Geometrical effects due to different sizes of the sample and the vanadium standard as well as the absorption of the neutrons in the samples were corrected by calculations and additional experiments. The values of the last row of table I were obtained after correction for hydrogen impurities. Oxygen and metallic impurities contribute only a negligible amount to the disorder scattering.

By this method scattering cross sections as small as  $10^{-4}$  barn can be measured. The method can also be extended to materials with high absorption or to materials which are available only in very small amounts. The experiments have been performed in connection with a program for the re-determination of the electrostatic neutron electron interaction.

A full account of this work will be found in an internal JÜL-report.

Table I  
Disorder Scattering Cross Sections of Pb and Bi  
(1mbarn =  $10^{-3}$  barn)

	Pb	Bi
measured scattering cross section	$3.26 \pm 0.22$	$8.14 \pm 0.43$ mbarn
Hydrogen impurity	$0.12 \pm 0.01$	$0.062 \pm 0.008$ weight ppm
incoherent cross section	$1.3 \pm 0.5$	$7.1 \pm 0.6$ mbarn

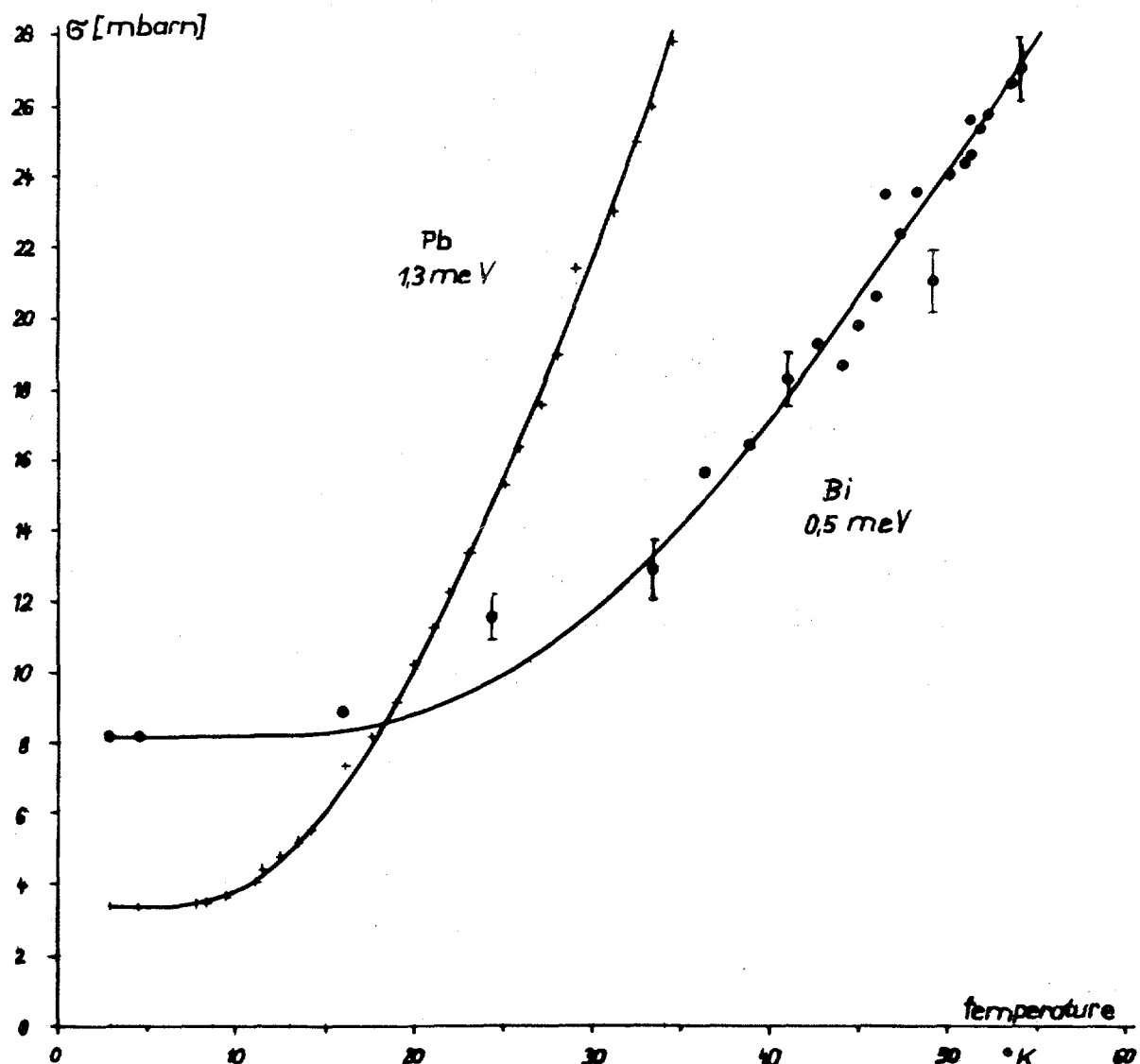


Fig. 1 Scattering cross section as a function of sample temperature.

Scattering angle:  $60 - 120^\circ$ . The solid curve is calculated using a single phonon energy corresponding to  $53^\circ\text{K}$  for Pb and  $105^\circ\text{K}$  for Bi.

IV. INSTITUT FÜR KERNPHYSIK, UNIVERSITY OF FRANKFURT/MAIN (GERMANY)

1. Fast Neutron Cross Sections by Activitation Techniques

(R. Bass and R. Wechsung)

The reactions  $^{88}\text{Sr}(n,p)^{88}\text{Rb}$  ( $E_n = 8.0-9.2$  MeV,  $\delta E_n = 0.05$  MeV and  $E_n = 14$  MeV) and  $^{208}\text{Pb}(n,p)^{208}\text{Tl}$  ( $E_n = 17.0-18.4$  MeV,  $\delta E_n = 0.10$  MeV and  $E_n = 14$  MeV) have been investigated. The neutron energy spread was approximately 100 keV and absolute cross sections were obtained with an estimated uncertainty of about  $\pm 20\%$ . Numerical tables of the results are available on request.

2. Inelastic Neutron Scattering on  $^6\text{Li}$

(R. Bass and G. Presser)

The reaction  $^6\text{Li}(n,n'\gamma)^6\text{Li}$  (3.56) was investigated using a ring scatterer which consisted of 96 % enriched metallic  $^6\text{Li}$ . Time of flight techniques were employed to reduce background due to room-scattered neutrons. The cross section rises from threshold to  $E_n \approx 5$  MeV, and remains approximately constant at  $8 \pm 2$  mb over the neutron energy range 5 - 7 MeV.

V. PHYSIKALISCHES STAATSINSTITUT, I. INSTITUT FÜR EXPERIMENTAL-PHYSIK, HAMBURG (Germany)

Excitation Function Measurements for (n,2n) and (n,p) Reactions.

M.Bormann, A.Behrendt and O.Vogel

Excitation functions for some (n,2n) and (n,p) reactions were measured in the neutron energy region 13-19 MeV using the activation technique. Gamma activities were detected by means of a NaJ-well crystal, the annihilation radiation from  $\beta^+$ -activities was observed with a coincidence spectrometer consisting of two NaJ crystals and  $\beta^-$ -activities were measured with a Methane-flow-counter. Neutrons were produced via the reaction  $H^3(d,n)He^4$  in thin titanium-tritium targets with the deuteron beam of a 3 MeV Van de Graaff Generator. The neutron flux was measured with a Stilbene recoil proton spectrometer.

The results are given in Table I. In most cases the half-lives of the activities produced have been remeasured. These values are stated in Table I with error indications.

Table I. Cross Sections in mb

Reaction $E_n$ (MeV)	$\text{Cd}^{106}(\text{n}, 2\text{n})\text{Cd}^{105}$	$\text{Sn}^{112}(\text{n}, 2\text{n})\text{Sn}^{111}$	$\text{Sb}^{121}(\text{n}, 2\text{n})\text{Sb}^{120g}$	$\text{Sb}^{121}(\text{n}, 2\text{n})\text{Sb}^{120m}$	$\text{Sb}^{121}(\text{n}, 2\text{n})\text{Sb}^{120}$
19.42 $\pm$ 0.12	1429 $\pm$ 142	1138 $\pm$ 128	786 $\pm$ 74	680 $\pm$ 63	1466 $\pm$ 97
18.56 $\pm$ 0.15	1426 $\pm$ 142	1164 $\pm$ 131	875 $\pm$ 82	672 $\pm$ 62	1547 $\pm$ 103
17.78 $\pm$ 0.17	1521 $\pm$ 152	1205 $\pm$ 135	950 $\pm$ 90	735 $\pm$ 68	1694 $\pm$ 113
16.85 $\pm$ 0.18	1535 $\pm$ 153	1255 $\pm$ 139	1029 $\pm$ 97	713 $\pm$ 66	1742 $\pm$ 117
16.18 $\pm$ 0.18	1600 $\pm$ 160	1256 $\pm$ 141	1046 $\pm$ 98	731 $\pm$ 68	1777 $\pm$ 119
15.51 $\pm$ 0.17	1614 $\pm$ 162	1253 $\pm$ 141	1080 $\pm$ 101	679 $\pm$ 64	1759 $\pm$ 119
14.87 $\pm$ 0.17	1589 $\pm$ 159	1217 $\pm$ 138	1014 $\pm$ 96	695 $\pm$ 64	1709 $\pm$ 115
14.11 $\pm$ 0.15	1358 $\pm$ 136	1110 $\pm$ 127	935 $\pm$ 90	611 $\pm$ 58	1546 $\pm$ 107
13.44 $\pm$ 0.13	1072 $\pm$ 108	998 $\pm$ 110	919 $\pm$ 86	601 $\pm$ 55	1520 $\pm$ 102
12.78 $\pm$ 0.11	834 $\pm$ 84	724 $\pm$ 82	817 $\pm$ 77	552 $\pm$ 51	1369 $\pm$ 93
$T_{1/2}$	54.98 $\pm$ 0.55m	35 m	15.91 $\pm$ 0.08m	5.77 $\pm$ 0.05d	* $\sigma_g + \sigma_m = \sigma$

Table I. (continued)

$E_n$ (MeV) Reaction	$Sb^{123}(n,2n)Sb^{122}$	$Pr^{141}(n,2n)Pr^{140}$	$Sm^{144}(n,2n)Sm^{143}$
19.42 $\pm$ 0.12	1131 $\pm$ 124	1804 $\pm$ 174	1637 $\pm$ 160
18.56 $\pm$ 0.15	1209 $\pm$ 132	1853 $\pm$ 178	1706 $\pm$ 166
17.78 $\pm$ 0.17	1214 $\pm$ 133	1905 $\pm$ 183	1856 $\pm$ 181
16.85 $\pm$ 0.18	1340 $\pm$ 147	1872 $\pm$ 180	1703 $\pm$ 168
16.18 $\pm$ 0.18	1335 $\pm$ 147	1801 $\pm$ 174	1703 $\pm$ 168
15.52 $\pm$ 0.17	1358 $\pm$ 149	1787 $\pm$ 172	1637 $\pm$ 160
14.87 $\pm$ 0.17	1277 $\pm$ 137	1700 $\pm$ 164	1629 $\pm$ 160
14.11 $\pm$ 0.15	1263 $\pm$ 135	1614 $\pm$ 159	1371 $\pm$ 137
13.44 $\pm$ 0.13	1247 $\pm$ 132	1485 $\pm$ 143	1081 $\pm$ 106
12.78 $\pm$ 0.11	1113 $\pm$ 122	1496 $\pm$ 144	890 $\pm$ 88
T 1/2	2.82 $\pm$ 0.05 d	3.4 $\pm$ 0.02 m	8.57 $\pm$ 0.08 m

Table I (continued)

$\text{Ho}^{165}(n, 2n)\text{Ho}^{164m}$		$\text{Ta}^{181}(n, 2n)\text{Ta}^{180m}$		$\text{Cd}^{106}(n, p)\text{Ag}^{106g}$	
$E_n$ (MeV)	(mb)	$E_n$ (MeV)	(mb)	$E_n$ (MeV)	(mb)
19.47 $\pm$ 0.08	811 $\pm$ 91	18.25 $\pm$ 0.10	438 $\pm$ 35	19.42 $\pm$ 0.12	132 $\pm$ 22
19.33 $\pm$ 0.10	897 $\pm$ 101	17.78 $\pm$ 0.13	474 $\pm$ 37	18.56 $\pm$ 0.15	143 $\pm$ 23
18.62 $\pm$ 0.16	944 $\pm$ 107	17.22 $\pm$ 0.15	510 $\pm$ 41	17.78 $\pm$ 0.17	134 $\pm$ 21
18.82 $\pm$ 0.19	1287 $\pm$ 145	16.75 $\pm$ 0.16	639 $\pm$ 51	16.85 $\pm$ 0.18	127 $\pm$ 20
16.87 $\pm$ 0.21	1392 $\pm$ 158	16.18 $\pm$ 0.17	735 $\pm$ 59	16.18 $\pm$ 0.18	144 $\pm$ 23
15.52 $\pm$ 0.21	1599 $\pm$ 180	15.64 $\pm$ 0.17	916 $\pm$ 74	15.52 $\pm$ 0.17	97 $\pm$ 16
14.10 $\pm$ 0.18	1782 $\pm$ 204	15.09 $\pm$ 0.17	1065 $\pm$ 85	14.87 $\pm$ 0.17	102 $\pm$ 16
13.42 $\pm$ 0.16	1701 $\pm$ 192	14.60 $\pm$ 0.16	1157 $\pm$ 94	14.11 $\pm$ 0.15	85 $\pm$ 14
12.75 $\pm$ 0.12	1604 $\pm$ 182	14.10 $\pm$ 0.15	1146 $\pm$ 93	13.44 $\pm$ 0.13	76 $\pm$ 12
		13.57 $\pm$ 0.14	1125 $\pm$ 90	12.78 $\pm$ 0.11	70 $\pm$ 11
		12.96 $\pm$ 0.11	1139 $\pm$ 92		
	$T_{1/2} = 42.4 \pm 0.3 \text{ m}$		$T_{1/2} = 7.99 \pm 0.05 \text{ h}$		$T_{1/2} = 24 \text{ m}$

VI. INSTITUT FÜR REINE UND ANGEWANDTE KERNPHYSIK DER UNIVERSITÄT

---

KIEL

---

1. Fast Chopper

H.H. Jung, H.G. Priesmeyer

The new Fast Chopper facility has been installed at the FRG-1; it is operating since Dec. 1. Technical details of the new spectrometer are as following:

The rotor material is steel and has a uranium core. Diameter of the rotor is 318 mm; diameter of the uranium core is 80 mm. The rotor has seven cigar-shaped slits with 0.2 mm width at the ends and 1.0 mm width at the center of the slit. Maximum speed is 12,000 rpm. Minimum burst width is 0.5  $\mu$ s.

The collimators are made of nickel and are 600 mm long each. Flight paths of 21 and 95 meters are installed. Seven lithium glass detectors (NE 912) viewed by one photo-multiplier each are used as neutron detectors. The glass detectors have dimensions 2.5"  $\varnothing$  and 1" thickness.

The flight time is measured by a 4096-channel analyser by TELEFUNKEN. Channel width: from 0.1 to 19.2  $\mu$ s. The resolution of the spectrometer above 50 eV is 27 ns/m at the 21 meter station and lower at lower energies, as the rotor has to be slowed down.

Total cross section measurements on radioactive isotops are planned: Cs 135/137, Pm 147, Tc 99 and others.

2. Crystal Spectrometer

K. Brand, M. Saad

There has been no progress in 1967 since the reactor FRG-1 was shut down. Since November, measurements of total neutron cross sections have been performed on  $\text{BaH}_2$  and  $\text{CaH}_2$ .

Further measurements are planned to determine the vibration energies of heavy metal hydrides.

VII. REACTOR CENTRUM NEDERLAND, PETTEN (NETHERLANDS)

F.O.M. groups.

1. Nuclear orientation experiments with reactor neutrons.

H. Postma, E.R. Reddingius, J.F.M. Potters\*, J. Mellema, and R. Kuiken.

The measurements on the anisotropy of the directional distributions of neutron-capture gamma rays from aligned nuclei have been extended. For this purpose a 6.5 cc Ge(Li)-detector has been used. The apparatus is considerably improved by installing a much larger cryostat and by fully automating the process of adiabatic demagnetization together with the collection of data. The isotopes studied are  $^{149}\text{Sm}$  and  $^{59}\text{Co}$ . Information about spins of several excited states of  $^{150}\text{Sm}$  and  $^{60}\text{Co}$  could be obtained from these measurements.

In cooperation with Harwell a study of the anisotropy of fission fragments from aligned  $^{235}\text{U}$  has been started. A preliminary measurement is in reasonably good agreement with former measurements carried out by J. Dabbs in Oak Ridge.

Publications.

H. Postma and E.R. Reddingius - Directional distribution of neutron capture gamma rays from aligned  $^{143}\text{Nd}$ - and  $^{145}\text{Nd}$  nuclei, *Physica* 34 541 (1967).

E.R. Reddingius, J.F.M. Potters and H. Postma - A study of gamma ray spectra of thermal neutron capture in  $^{143}\text{Nd}$  and  $^{145}\text{Nd}$ ; including directional anisotropy and linear polarization measurements of such gamma rays from aligned  $^{143}\text{Nd}$ , *Physica* 37 (1967).

---

\* till 1-8-1967.

2. Thermal-neutron capture  $\gamma$ -ray spectroscopy.

P. Spilling, H. Gruppelaar, A.M.F. Op den Kamp and A.M.J. Spits.

A thermal-neutron beam from the horizontal radial beam hole of the Dutch High Flux Reactor is obtained with a filter method. The thermal-neutron flux is about  $10^7 \text{ cm}^{-2}\text{s}^{-1}$ . The  $\gamma$ -rays from several  $(n,\gamma)$  reactions were studied with a high-resolution Ge(Li) spectrometer and a 4096-channel analyser. From the measurements the following physical information was obtained:  $\gamma$ -ray energies and intensities, excitation energies, Q-values and decay schemes. The reactions, which have been studied, are:  
 $^{24}\text{Mg}(n,\gamma)^{25}\text{Mg}$ (ref.1),  $^{25}\text{Mg}(n,\gamma)^{26}\text{Mg}$ (ref.1),  $^{40}\text{Ca}(n,\gamma)^{41}\text{Ca}$ (ref.2),  
 $^{12}\text{C}(n,\gamma)^{13}\text{C}$ (ref.3),  $^{17}\text{F}(n,\gamma)^{20}\text{F}$ (ref.3) and  $^{44}\text{Ca}(n,\gamma)^{45}\text{Ca}$ (ref.4).

These investigations are a part of the program of the Dutch Foundation for Fundamental Research on Matter ("Stichting voor Fundamenteel Onderzoek der Materie", F.O.M.).

References

- 1) P. Spilling, H. Gruppelaar and A.M.F. Op den Kamp,  
Nucl. Physics A 102 (1967) 209.
- 2) H. Gruppelaar and P. Spilling,  
Nucl. Physics A 102 (1967) 226.
- 3) P. Spilling, H. Gruppelaar, H.F. de Vries and A.M.J. Spits,  
to be published.
- 4) H. Gruppelaar, P. Spilling and A.M.J. Spits,  
to be published.

3. Circular polarization of gamma rays after capture of polarized neutrons in S, Ca, Ti, Cr, Co, Hg and Pb.

K. Abrahams and W. Ratynski<sup>\*</sup>.

The circular polarization of gamma rays after capture of polarized thermal neutrons in natural targets of S, Ca, Ti, Cr, Co, Hg and Pb has been measured using two Ge(Li) detectors with a volume of 15 cm<sup>3</sup> and 30 cm<sup>3</sup>, respectively. As a source of polarized neutrons a system of 52 cobalt mirrors, each one meter long, was used. Circular polarization was measured by transmission through two 10 cm long cylinders of magnetized permendur. Every 10 sec. the neutron spin was reversed. The measuring time per sample was on the average two weeks. Several new spin assignments could be made and many old spin assignments could be confirmed.

---

\* On leave from the Institute for Nuclear Research, Świerk, Poland.

VIII. REACTOR INSTITUUT DELFT (NETHERLANDS)

W. Hoekstra

Using the tangential radiation facility of the H.O.R. reactor  
the gamma ray spectra of  $^{232}\text{Th}(n,\gamma)$ ,  $^{233}\text{Th}$  and of  $^{185},^{187}\text{Re}(n,\gamma)$ ,  
 $^{186},^{188}\text{Re}$  have been measured with the aid of a Ge(Li) detector.

Results will be published.

IX. LABORATORIO DI FISICA NUCLEARE APPLICATA, CENTRO DI STUDI  
NUCLEARI DEL C.N.E.N., CASACCIA (ROMA) (ITALY)

1. Introduction

In the last year the Nuclear Physics Group of the "Centro Studi Nucleari della Casaccia" was engaged in the following activities:

- 1) Nuclear resonant scattering experiment.
- 2) Gamma-ray spectroscopy and thermal neutron radiative capture experiment.
- 3)  $(n, n'\gamma)$  directional correlation measurements on Mg and Si.
- 4) Development of techniques for the elaboration of experimental data with computers.
- 5) Theoretical studies on the nuclear wave functions.

Later on the progresses we obtained in this year will be briefly described.

2.1. Experimental studies

The running of the TRIGA Mark II reactor of the "Centro Studi Nucleari della Casaccia" (Applied Nuclear Physics Laboratory) was stopped in September 1965 for a power increasing from 100 kW to 1 MW.

In this occurrence a new facility was planned and executed, consisting in a beam hole tangential to the reactor core and going through the whole biological shield. The main features of this new facility were described in our preceding reports.

The reactor will work again regularly at the beginning of 1968. However some preliminary measurements have been performed in the last months.

2.2. Nuclear resonant scattering experiment

The aim of nuclear resonant scattering experiments is both to measure the radiative widths of nuclear levels with energy near to the binding energy for particles emission and to study in-

elastic scattering processes to extract some information about level scheme. Such a study is included in a systematic research done by nuclear physics group on the radiative widths for E1 electromagnetic transition [1], [2]. Our previous results are reported in references [3], [4] and [5].

With respect to our preceding measurements, our experimental apparatus has been improved. The new tangential beam hole is used, which allows a great reduction of gamma and neutron background. Without source and with a borated paraffin filter (total thickness ~ 50 cm) we have no detectable gamma flux above ~3 MeV and a neutron flux of a few n/cm<sup>2</sup> sec. A goniometer was built for directional correlation analysis between scattered and incident gamma-rays and for cascade gamma-rays angular correlations. The gamma-spectra are analysed with 5"x5" (NaI(Tl) and 30 cc Ge(Li) detectors. For correlation measurements a Ge(Li) detector pair spectrometer or an anti-Compton spectrometer can be used. All detectors are shielded by lead and full external apparatus is inclosed in a large borated paraffin and concrete bunker.

### 2.3. Gamma-ray spectroscopy and thermal neutron radiative capture experiment

Two Ge(Li) gamma-ray detectors (a 30 cm<sup>3</sup> sensitive volume Ge(Li) coaxial detector and a 3 cm<sup>3</sup> sensitive volume planar detector from Princeton) are in use from the summer of 1967.

The best line width obtained for the <sup>137</sup>Cs 661 KeV gamma-rays is less than 4 KeV. The gamma-rays from the decay of <sup>152</sup>Eu ( $T_{\frac{1}{2}} = 9.3$ h for the isomeric state decay and  $T_{\frac{1}{2}} = 12.5$ y for the ground state decay) have been studied. New transitions and new levels have been identified.  $\gamma-\gamma$  coincidences with NaI(Tl)-Ge(Li) detectors and Ge(Li)-Ge(Li) detectors are in progress, as well as  $\gamma-\gamma$  angular correlations measurements. The same detection chain will be employed to study the thermal neutron radiative capture. During 1967 since the reactor was

not running, the activity was limited to build a new collimator in order to have a collimated thermal neutron without  $\gamma$  and fast neutron background. A Bi single crystal randomly oriented will be used to filter the neutron beam.

2.4. (n,n' $\gamma$ ) directional correlation measurements on Mg and Si

During the year 1967, a first collection of experimental data on directional correlations (n,n' $\gamma$ ) has been completed. The targets utilized were natural magnesium and silicon, the incident neutrons beam was obtained by the d(d,n)<sup>3</sup> He reaction at deuterons energy of 390 KeV.

The measurements have been interrupted for about four months in order to replace the accelerating column and high voltage stabilizer of PN Van de Graaff.

A computer program based on "Montecarlo" method is being developed in order to elaborate the experimental data.

2.5. Development of techniques for the elaboration of experimental data with computers

A Montecarlo program for the detector efficiency calculation of high energy (0+15 MeV gamma-rays in NaI(Tl) scintillators has been studied. Such a program allows efficiency calculations for cylindrical detectors and for ellipsoidal sources, out of the detector axis. Our results have been compared with both experimental measurements and calculations of previous authors. A report is being prepared.

Moreover a computer program to analyse complex gamma-ray spectra has been studied. The method permits automatic identification of peaks of high resolution spectra in the presence of background, provided that the data are stored in a way suitable for computer input (i.e. on magnetic or paper tape). The program reads the entire spectrum, locates the peaks and determines their amplitudes, centroids and widths with their

hamiltonian can be handled by employing shell model wave functions without giving rise to spurious effects deriving from the motion of the center of mass (11). The method provides an approach to the study of very light nuclei alternative to the usual variational method.

An application of the method to the calculation of the  $1^-$  levels of  $^{208}\text{Pb}$  in Tamm-Dancoff approximation has been performed. It has been found that in the usual calculations the spuriousity can have very large effects on transition probabilities but very small effects on the eigenvalues. The method provides indeed eigenfunctions which are practically free from spuriousity.

#### References

- [1] P. Oliva and D. Prosperi - Nuovo Cimento 49 (1967) B 161.
- [2] D. Prosperi and S. Sciuti: Ricerche di Fisica dei nuclei con raggi quasi monocromatici. Relazione su invito presentata al 52° congresso della SIF, Trieste Ottobre 1966 - DOC/SEFIN (1962) 10.
- [3] M. Giannini, P. Oliva, D. Prosperi and S. Sciuti - Nuovo Cimento 34 (1964) 344.
- [4] M. Giannini, P. Oliva, D. Prosperi and S. Sciuti - Nuclear Physics 65 (1965) 344.
- [5] M. Giannini, P. Oliva, D. Prosperi and G. Toumbev - Nuclear Phys. A 101 (1967) 145.

X. SOTTOSEZIONE DI FIRENZE DELL'ISTITUTO NAZIONALE DI FISICA  
NUCLEARE - ISTITUTO DI FISICA DELL'UNIVERSITA', FIRENZE (ITALY)

1.1.  $\beta$  and  $\gamma$  spectroscopy

The Group for  $\beta$  and  $\gamma$  spectroscopy has been studying the decays of some nuclei with solid state detectors.

1.2. Decay of  $^{138}\text{Ba}$

The relative gamma-ray intensities in the decay of  $^{133}\text{Ba}$  have been determined by means of Germanium detectors. A reasonable value of long ft of an EC second forbidden transition is obtained. The experimental electromagnetic transition strengths connecting 3 excited states and the ground state of  $^{133}\text{Cs}$  are found to agree fairly well with the theoretical estimates of the Kisslinger-Sorensen model [1].

1.3. Decay of  $^{176m}\text{Yb}$

The isomeric level ( $T_{\frac{1}{2}} = 11.7$  sec) of  $^{176m}\text{Yb}$  [2], obtained by bombarding an enriched sample of  $^{176}\text{Yb}$  isotope with 14 MeV neutrons, has been studied. The energies of the single transitions have been determined to a precision of about 0.3 KeV by fixing the isomeric state at  $1050.1 \pm 0.6$  KeV. A study by means of Germanium detectors and  $\gamma$ - $\gamma$ coincidence measurements supplied a good value of the total conversion coefficient of the isomeric transition of 95.9 KeV, thus establishing the E1 nature of this transition. Hence the value  $8^-$  for the spin and the parity of the isomeric level is also established. The level, therefore, must certainly be interpreted as due to the coupling, according to the rules of Gallagher and Soloviev, of two neutrons in Nilsson's orbits  $7/2^-$  [514] and  $9/2^+$  [624].

1.4. Decay of  $^{143}\text{Sm}$  and the  $^{143}\text{Pm}$  levels

By means of a Germanium detector the  $\gamma$  transitions among some levels of  $^{143}\text{Pm}$  (populated in the decay of  $^{143}\text{Sm}$ ) have been

corresponding errors by non-linear least squares fitting.

Doublets are handled automatically.

### 3.1. Theoretical studies on the nuclear wave functions

#### 3.2. Excited levels of odd-odd deformed nuclei

During this year we have concentrated on the study of the effects of a tensor component in the neutron-proton residual interaction.

By fitting a large body of experimental data we have been able to show that such a component exists and has important effects on the energy levels of these nuclei.

A report of our results will soon be submitted for publication, together with some calculations in which we apply our new residual interaction to the investigation of the level schemes of some nuclei which have received extensive experimental attention ( $^{166}\text{Ho}$ ,  $^{170}\text{Tm}$ ,  $^{182}\text{Ta}$ ).

#### 3.3. Generalized Hartree-Fock equations

Our investigation of the technique suggested by M. Jean for the study of the nuclear many-body problem has led us to the formulation of an equation which is equivalent to the usual Hartree-Fock equations, but contains an additional term, representing both second order effects and rearrangement effects. A perturbation expansion of this term can lead to the determination of an improved single-particle basis.

We are now performing a systematical analysis of the various ways of solving this equation.

#### 3.4. Study of intrinsic motion wave functions in shell-model calculations

The nuclear hamiltonian has been substituted with one equivalent with regard to the intrinsic motion of the nucleons, that is the motion of the nucleons in their center of mass. The new

studied. We have observed transitions of 274, 1056, 1242, 1516 KeV. The intensities balance, the coincidence measurements and the systematics of the neighbouring nuclei suggest the presence of levels at 274, 1056 and 1516 KeV. The 274 KeV level may probably be identified with that foreseen by Kisslinger and Sorensen in the semimagic nuclei ( $N=82$ ) whose presence in the other nuclei with  $N=82$  has already been observed experimentally.

### 1.5. $^{49}\text{Ti}(p,n\gamma)$ reaction and the $^{49}\text{V}$ levels

In the frame of the researches carried out with the Van de Graaff accelerator of the University of Padua, a first work concerning the levels of  $^{49}\text{V}$  in collaboration with the Trieste Group has been calculated. The reaction used was  $^{49}\text{Ti}(p,n\gamma)$  on target of enriched  $^{49}\text{Ti}$  isotope. All the  $\gamma$  transitions among the low-lying levels have been determined and this has allowed us to give some assignments on the possible spins of the levels according to the intensity relations among transitions to levels of known spin and parities. In particular we can observe that the  $11/2^-$  and  $9/2^-$  assignments to the 1022 KeV and 1155 KeV levels would be in very nice agreement with the theoretical spectrum recently calculated by Malik and Scholz on the basis of the Coriolis coupling model. Besides, the 1141 KeV level has probably positive parity. In this case it could be attributed to the coupling of the  $1d_{\frac{3}{2}}^3$  hole state to the core configuration. It is interesting to note that the determination of the energies within 0.1 KeV has allowed us to determine the position of the various lines in the decay scheme with certainty and more rapidly than with the usual coincidence methods. The results have been published in "Nuovo Cimento" [4].

Similar researches on the levels of higher energy of  $^{49}\text{V}$  and on the low levels of  $^{50}\text{V}$  are in progress. A program of lifetime measurements of excited levels both with the usual electronic methods and with methods based on Doppler shift has also been started.

In collaboration with the Trieste Group we have in course measurements of neutron spectra, aiming at levels spectrometry, and at a search of analogue states as resonances of compound nucleus.

2.1. (n,2n) reactions on  $^{80}\text{Br}$ ,  $^{91}\text{Mo}$ ,  $^{112}\text{In}$ ,  $^{143}\text{Sm}$

The cross-section ratios for the production of the isomeric pairs  $^{80m}\text{Br}$ ,  $^{91m}\text{Mo}$ ,  $^{112m}\text{In}$ ,  $^{143m}\text{Sm}$  through the (n,2n) reaction have been measured by the activation method. The experimental data of this activity and those available from the literature have been analysed by the Huizenga-Vandenbosch method, and the spin cutoff parameter has been extracted.

3.1.  $^{16}\text{O}$  (n, $\alpha$ )  $^{13}\text{C}$  reaction (in collaboration with the Bologna Group)

About 5000 two prong events produced by 14 MeV neutrons in a Wilson chamber Oxygen filled were observed and measured. About 70% of these events is attributable to  $^{16}\text{O}$  (n, $\alpha$ )  $^{13}\text{C}$  reactions. The attribution was made by a suitable cinematical fit. Each event was also checked for (n,p) and (n,d) reactions, both energetically possible.

The range-energy relation for  $^{13}\text{C}$  in Oxygen has been obtained in good agreement with that found in a previous experiment for  $^{13}\text{C}$  in Neon.

The spectrum of the excitation energy shows, well separated, the fundamental and first excited level of  $^{13}\text{C}$ . The second and third ones, on the contrary, are not resolved. The angular distributions for all the events and for distinct levels have been constructed.  $\alpha$ - particles show, in the rest frame of  $^{17}\text{O}$ , a well definite peak in the backward direction, for fundamental and first excited level. This behaviour suggests that also for  $^{16}\text{O}(\text{n},\alpha)$   $^{13}\text{C}$  reactions direct interactions such as heavy stripping mechanism are present.

This result is in very good agreement with previous experiments

made with visual techniques. It is however noticeable that the  $^{16}\text{O}(n,\alpha)$   $^{13}\text{C}$  reaction at the same energy, studied with counter techniques, gives, for the angular distributions, results quite in disagreement with ours. For the first levels the angular distributions show, in fact, forward asymmetry. The results will soon be published. The results on the  $^{20}\text{Ne}(n,2\alpha)$   $^{13}\text{C}$  reaction have been published in "Nuovo Cimento" [5].

#### 4.1. Ericson's fluctuations

Following a first work where we analysed the method of the maxima counting to determine the correlation width, we have extended the research to include the effect of the finite energy resolution. We have then calculated the bias introduced by various types of experimental resolution (rectangular, Gaussian, Lorentzian) and presented the coefficients to be used in the different experimental situations to obtain  $\Gamma$  by means of the maxima counting. We have also made a comparison of the influence of the finite resolution on the various methods to determine  $\Gamma$ . The results have been presented to LIII S.I.F. Meeting and are in the press [7].

#### 5.1. Montecarlo calculations on the "Blocking" effects in single crystals

It is known that the angular distribution emitted from a lattice centre of a single crystal shows narrow minima in the direction of main crystal strings.

According to a suggestion by Tulinov, this "blocking" effect of lattice strings could be exploited to measure the lifetime of highly excited nuclear states produced in nuclear reactions. In fact, the depth of minimum is expected to decrease with increasing distance of the emission point from the lattice centre, so that the average recoil distance could be deduced from the

angular distribution.

This possibility has been investigated by means of detailed numerical calculations with a "Montecarlo" method, using the IBM 7090 of CNUCE. The model is based on Feldman's approximations on the atomic scattering in a crystal, and takes the thermal vibration into account. According to preliminary results [presented at S.I.F. 53th Meeting, Oct. 1967], the method should be sensitive to lifetimes of the  $10^{-17}$  order.

#### References

- [1] P. Blasi, M. Bocciolini, P.R. Maurenzig, P. Sona - Nuovo Cimento Serie X 50B (1967) 298.
- [2] M. Bocciolini, A. Cambi, T.F. Fazzini, P.R. Maurenzig - Nuovo Cimento Serie X 52B (1967) 229.
- [3] P. Blasi, M. Bocciolini, P. Sona - LIII S.I.F. Meeting Bologna 1967.
- [4] P. Blasi, P.R. Maurenzig, R.A. Ricci, N. Taccetti, R. Giacomich, M. Lagonegro, G. Poiani - Nuovo Cimento Serie X 51B (1967) 241.
- [5] S. Petralia, G. Di Capriacco, M. Mandò, G. Parrini - Nuovo Cimento 44 (1966) 225-228.
- [6] P.G. Bizzeti and P.R. Maurenzig - Il Nuovo Cimento Serie X 47B (1967) 29.
- [7] P.G. Bizzeti and P.R. Maurenzig - LIII S.I.F. Meeting - Bologna 1967 - To be published in "Il Nuovo Cimento".

XI. CENTRO SICILIANO DI FISICA NUCLEARE, ISTITUTO NAZIONALE DI  
FISICA NUCLEARE, SEZIONE SICILIANA - ISTITUTO DI FISICA DELLA  
UNIVERSITA', CATANIA (ITALY).

1.1. Experimental research work on nuclear structure and reactions

1.2. Nuclear fission

The angular distributions of fragments of neutron-induced fission of thorium have been measured with nuclear emulsions loaded with thorium nitrate and exposed to monoenergetic neutron beams in the energy range  $1.7 < E_n < 5.3$  MeV. From the measured angular distributions we have deduced the values of the parameter  $K_0^2$ , whose dependence on the excitation energy we have compared with that of other even-mass target nuclei. The results have been published on "Nuclear Physics" [1]. Measurements on the angular distributions for neutron energy near the  $^{232}\text{Th}(n, f)$  threshold are in progress. The mono-energetic neutrons are obtained by means of the  $^{12}\text{C}(\text{d}, n)$  reaction with 2 MeV deuterons. The preliminary results show a strong dependence of the angular distributions on the neutron energy in the range  $1.35 < E_n < 1.55$  MeV. The anisotropy ratio  $N(0^\circ)/N(90^\circ)$  in this range decreases from 0.9 at  $E_n = 1.35$  MeV to 0.25 at  $E_n = 1.5$  MeV [2].

The aim of experiments is to ascertain the strength of various states through which likely the fissioning nucleus passes at the "saddle-point" configuration.

1.3.  $^{19}\text{F}(\text{d}, \text{p}\gamma)^{20}\text{F}$  reaction

$(\text{d}, \text{p}\gamma)$  angular correlations of the proton group corresponding to the 0.65 MeV level of  $^{20}\text{F}$  produced in the reaction  $^{19}\text{F}(\text{d}, \text{p}_1)^{20}\text{F}$  have been measured at  $E_d = 1.6$  MeV.

The measurements have been carried out in the reaction plane and in two azimuthal planes for a proton emission angle of  $45^\circ$ .

The experimental points have been fitted by a sum of even order Legendre polynomials. The best fits obtained including polynomials to the 6th order seem to agree better with the experimental points.

Taking into account this result, a possible presence of more reaction mechanism is suggested.

#### 1.4. Neutrons from Am-Be sources

The neutron energy spectrum of an Am-Be source has been measured using a particular fast-neutron spectrometer. High efficiency and good energy resolution ( $\Delta E_n \approx 0.3$  MeV at  $E_n = 10$  MeV) was achieved.

The preliminary results evidenced the detailed structure of the spectrum.

Measurements are in progress in order to obtain the neutron spectrum with high accuracy and very good statistics. Results are compared with other measurements obtained with Pu-Be [3] and Po-Be [4] sources.

#### 1.5. Time of flight spectrometer

A time of flight neutron spectrometer has been realized in order to study elastic and inelastic neutron scattering on various nuclides with our 2 MeV Van de Graaff. The incoming neutron beam is obtained by means of the d-d reaction in a gas target.

The associate particle method is used as a start signal using solid state detectors with suitable time pick-off. Neutrons are detected by a liquid organic scintillator with  $\gamma$ -n discrimination.

Resolving time of a few ns has been obtained and we are trying to improve it.

#### 1.6. A diffraction model applied to the reaction $^{26}\text{Mg}(^3\text{He},\alpha)^{25}\text{Mg}$

Angular distributions have been measured for the five groups

of alpha particles in the reaction  $^{26}\text{Mg}(^3\text{He}, \alpha)^{25}\text{Mg}$ , in the energy range of the incoming  $^3\text{He}$  4+6 MeV, using the 6 MeV Van de Graaff of Frankfurt am Main University. A diffractional model has been derived by using complex angular momenta methods which fit the experimental data extremely well. [10].

Work is under way to ascertain the limits of validity for such a model.

#### 1.7. Analysis of nuclear reactions with the $^{29}\text{Si}$ as intermediate system [5]

The statistical fluctuations in the excitation functions of some nuclear reactions ( $^{27}\text{Al}+\text{d}$ ,  $^{28}\text{Si}+\text{n}$ ,  $^{26}\text{Mg}+^3\text{He}$ ) having the  $^{29}\text{Si}$  as intermediate system, have been analyzed in order to estimate the values of  $D_0 = D_J(2J+1)$  and  $\Gamma$  of the C.N. levels. It is shown that these quantities are simply related by

$$\langle \sigma_{ft} \rangle = \frac{\chi^2}{2(2I+1)(2i+1)} \frac{D_0}{\Gamma R_0}$$

where  $\langle \sigma_{ft} \rangle$  is the average fluctuating cross section and  $R_0$  the normalized variance of the fluctuations.

The obtained values of  $D_0$  and  $\Gamma$  agree with theoretical predictions based on the Fermi gas nuclear model.

#### 1.8. The $^7\text{Li}+\text{d}$ reactions

Measurements of bidimensional spectra and angular correlations between the two alpha particles are in progress. The alpha particles from the  $^7\text{Li}+\text{d} \rightarrow \alpha + \alpha + \text{n}$  are detected by means of solid state detectors and pulses analyzed by a 4096 channels LABEN analyzer.

Preliminary results were given at the 53rd meeting of the Italian Society of Physics [6]. These results allowed to give an estimate of the three body direct break-up in the reaction.

1.9. Statistical fluctuations analysis of the  $^{26}\text{Mg}(^3\text{He},\alpha)^{25}\text{Mg}$  reaction

The  $^{26}\text{Mg}(^3\text{He},\alpha)$  reaction has been studied at  $E_{^3\text{He}} = 4.6 \text{ MeV}$  for the  $\alpha_0$ ,  $\alpha_1$ ,  $\alpha_2$ ,  $\alpha_3$  and  $\alpha_4$  groups. The excitation functions were measured in steps of 50 KeV with  $^3\text{He}$  energy resolution better than 25 KeV and at angles between  $15^\circ$  and  $165^\circ$  in steps of  $5.5^\circ$ .

The data have been analysed on the basis of statistical fluctuation theory, obtaining information on some nuclear parameters. Methods of statistical mathematics not so far utilized on the fluctuation analysis have been used in order to evaluate the compound nucleus contribution in the presence of large direct effects.

2.1. Theoretical research work on nuclear structure and reactions

2.2. The electric levels of  $^{12}\text{C}$ ,  $^{16}\text{O}$  and  $^{28}\text{Si}$  nuclei and the corresponding g.s. transition rates have been calculated [7] in the TD and extended TD (ETD) approximations.

The results have been compared with the predictions of a schematic model [8], with other TD or RPA calculations and with experiment.

The differences between the TD and ETD eigenvalues came out to be quite important ( $\sim 2 \text{ MeV}$ ) for some even-parity levels.

Taking into account the continuous spectrum tends, in general, to give results, for the e.m. transition probabilities, in better agreement with the available experimental data.

2.3. The elastic and inelastic scattering amplitudes for nucleon-nucleus reactions on  $^{15}\text{N}$  have been computed in the framework of the ETD approximation [9].

It has been found that the average behaviour of the elastic cross sections can be reproduced by the "orthogonality scattering".

Some properties of the resolvent operator for the total hamiltonian have been investigated with special emphasis on the nuclear structure dependence of the calculated resonances.

References

- [ 1 ] S. Lo Nigro and C. Milone - Nucl. Phys. A96 (1967) 617.
- [ 2 ] S. Lo Nigro and C. Milone - Boll. SIF 55 (1967) 66.
- [ 3 ] A. Rubbino and D. Zubke - N. Cim. 44 (1966) 179.
- [ 4 ] R. Potenza and A. Rubbino - Nucl. Instr. & Meth. 25 (1963) 77.
- [ 5 ] G. Corleo, G. Pappalardo and A. Rubbino - N. Cim. B52 (1967) 248.
- [ 6 ] G. Calvi, C. Milone, S. Notarrigo and R. Potenza - Boll. SIF 55 (1967) 36.
- [ 7 ] F. Catara, M. Di Toro and O. Stazi - Nucl. Phys. in press.
- [ 8 ] A. Agodi, F. Catara, M. Di Toro and O. Stazi - N. Cim. 48 (1967) 237.
- [ 9 ] A. Agodi, F. Catara and M. Di Toro - Boll. SIF 55 (1967) 8 and to be submitted to Annals of Physics.
- [ 10 ] S. Notarrigo, A. Rubbino, S. Sambataro and D. Zubke - Boll. SIF 55 (1967) 36.

XII. GRUPPO DI ISPRA PER LE MISURE DI SEZIONI D'URTO DEL C.N.E.N.

ISPRA (VARESE) (ITALY)

1.1. Analysis of neutron resonances

C. Coceva, F. Corvi, P. Giacobbe and M. Stefanon

A work describing the experimental and analysis methods employed for the determination of slow-neutron resonance parameters has been accepted for publication on Nuclear Instruments and Methods. The abstract is the following: Methods of analysis of neutron transmission data in time-of-flight spectrometry are examined, with particular attention to the experimental conditions which should be satisfied for a correct estimation of resonance parameters and errors. To improve the applicability of the shape-analysis method in the work performed with the fast neutron chopper of Ispra, the resolution function of this spectrometer was determined in a detailed way.

The main features of the analysis methods applied to the experimental data obtained at Ispra are presented and illustrated by examples.

2.1. Spin assignement of neutron resonance

C. Coceva, F. Corvi, P. Giacobbe and G. Carraro<sup>(\*)</sup>

These measurements have been performed at the Linac of the C.B.N.M. Euratom, Geel (Belgium); an account of them can be found in the chapter C.B.N.M. activities.

3.1. Numerical simulation of the  $\gamma$ -ray cascade

P. Giacobbe, M. Stefanon

In connection with the experiments performed by the group on the Linac of B.C.N.M. EURATOM of Geel, the  $\gamma$ -decay process has

---

(\*) C.B.N.M., EURATOM, Geel.

been studied from the theoretical point of view, in order to have a support for the hypothesis underlying the method of spin assignment. A numerical simulation of the process has been performed, exploiting existing experimental data on the low-excitation levels and the theories for the level density of higher excitation energy, and for transition probabilities of the different multipolarities. Particular care has been devoted to the influence of the limitations in the detecting apparatus, such as the varying efficiency of NaI crystals as a function of the energy, and the effect of the energy thresholds which are artificially set to the gamma detection. In this way the result of the comparison between computation and experiment depends only on the consistency of the model used with the real nuclear process. The calculation gives results which are directly comparable with experiments related to the  $\gamma$ -decay from neutron capture states. The experiment of spin assignment involves some integral features of the  $\gamma$ -decay, such as mean multiplicity and the integral of the  $\gamma$ -spectrum above a given energy. In this respect the model works well, the accordance with the experiment being satisfactory. A more crucial test would be a systematic comparison with measurements of the detailed shape of the  $\gamma$ -energy spectra. The comparison performed in the particular case of  $^{177}\text{Hf}$  has shown a good accordance, but has also indicated some deficiencies of the model, when low-lying levels are involved. Such deficiencies can be explained with the general uncertainties of the theory. The results of the calculation can also be compared with other possible experiments, such as absolute multiplicity of isomeric cross section ratio measurements.

XIII. LABORATORIO DATI NUCLEARI, CENTRO DI CALCOLO DEL C.N.E.N., BOLOGNA (ITALY)

- 1.1. Theoretical calculation of neutron capture cross-sections
- 1.2. Neutron fission product cross-sections for radiative capture in 1 KeV-10 MeV energy range

The neutron radiative capture cross-section in the energy range 1 KeV-10 MeV for several elements and nuclei has been evaluated or re-evaluated on the basis of the latest experimental data available.

The following elements and their stable isotopes have been considered: Zr, Mo, Ru, Rh, Pd, Ag, Co, La, Ce, Pr, Nd, Sm, Eu, Gd. The results are available through the ENEA ND C in Saclay (UK format).

1.3. Collective and direct radiative captures

The expression for the nucleon radiative capture cross-section by nuclei via collective mechanism has been completed in order to take into account the spin-orbit interaction [1]. The direct and collective cross-sections for  $^{208}\text{Pb}(n,\gamma)$  and  $^{208}\text{Pb}(p,\gamma)$  reactions have been calculated. A good agreement between calculated and measured cross-sections has been obtained by using optical parameters which describe quite accurately experimental differential elastic scattering, reaction cross-sections, and polarization data. Further, the results have been improved taking into account the effects of the interference between the direct and the collective captures.

- 2.1. Theoretical calculations of neutron elastic and inelastic scattering cross-sections
- 2.2. Adiabatic coupled-channel calculations of fast neutron scattering by  $^{238}\text{U}$ .

Several analyses of  $n-^{238}\text{U}$  scattering at low energies have been

performed in the past [2], [3], taking into account the coupling between the  $2^+-0^+$  (ground state) levels [4] (model I). The agreement between theory and experiment was found quite good for the angular distributions; however, in the energy range of a few MeV it was not possible to obtain a very good agreement for the total cross-section. This may be due to the fact that  $^{238}\text{U}$  is a rather deformed nucleus, so that an expansion of the potential truncated at the first power of  $\beta$  may not be sufficient to describe the deformation. In addition, levels with  $I \geq 4$  may give some contribution to  $\sigma_T$ . Both these effects can be estimated using the method of the adiabatic coupled-channel calculations [5], [6] (in this way the coupling of all the levels of the rotational band is automatically taken into account) and expanding the deformed potential in terms of Legendre polynomials rather than in powers of  $\beta$  (model II).

Some calculations with the two models have been performed using the same potential parameters as in [2], but  $V_{SO} = 6.5$  MeV. The theoretical total cross-section obtained with model II is in better agreement with the experimental one (fig. 1).

At some MeV, no significant differences were found in the angular elastic + direct inelastic distributions given by the two methods. This is shown in fig. 2 in which curve a) was obtained by means of model II, whereas curve b) was obtained using model I. Even at few MeV the differences were small.

### 2.3. Elastic and inelastic scattering based on microscopic description of the nucleus

The elastic and inelastic scattering processes of neutron from deformed nuclei described by microscopic models have been studied. In particular odd mass number nuclei with  $A \leq 40$  have been considered.

The wave functions for different nuclear states are obtained in

the hypothesis of an inert axially symmetric even-even core plus a single nucleon which can be excited from a self-consistent Hartree-Fock orbit ( $\varphi_k$ ) to another ( $\varphi'_k$ ). Thus the model allows to take into account the inelastic diffusion process from levels belonging to rotational bands different from the ground state band.

The diffusion cross-sections will be calculated with the DWBA and coupled channel methods.

2.4. Photoreaction calculations in the giant resonance energy region for doubly closed shell light nuclei

The particle-hole model with continuum excitation by means of the photoreactions cross-sections of  $^{12}\text{C}$  and Ca has been analyzed [7] and extended to the calculations of  $^{28}\text{Si}$  photoreactions.

Results of this analysis have been presented at the International Conference on Nuclear Structure - Tokyo, September 1967 [8].

In fig. 3 is given the total photo-absorption cross-section of  $^{28}\text{Si}$ . The data on  $^{12}\text{O}$ ,  $^{40}\text{Ca}$ ,  $^{28}\text{Si}$  photoreactions obtained assuming a charge dependence of the interaction have been compared with the charge independent data. A strong effect of the Coulomb interaction has been observed.

Calculations with a finite-range force and a full antisymmetrization of the interaction are envisaged.

2.5. Scattering cross-sections of even-even nuclei with a microscopic model

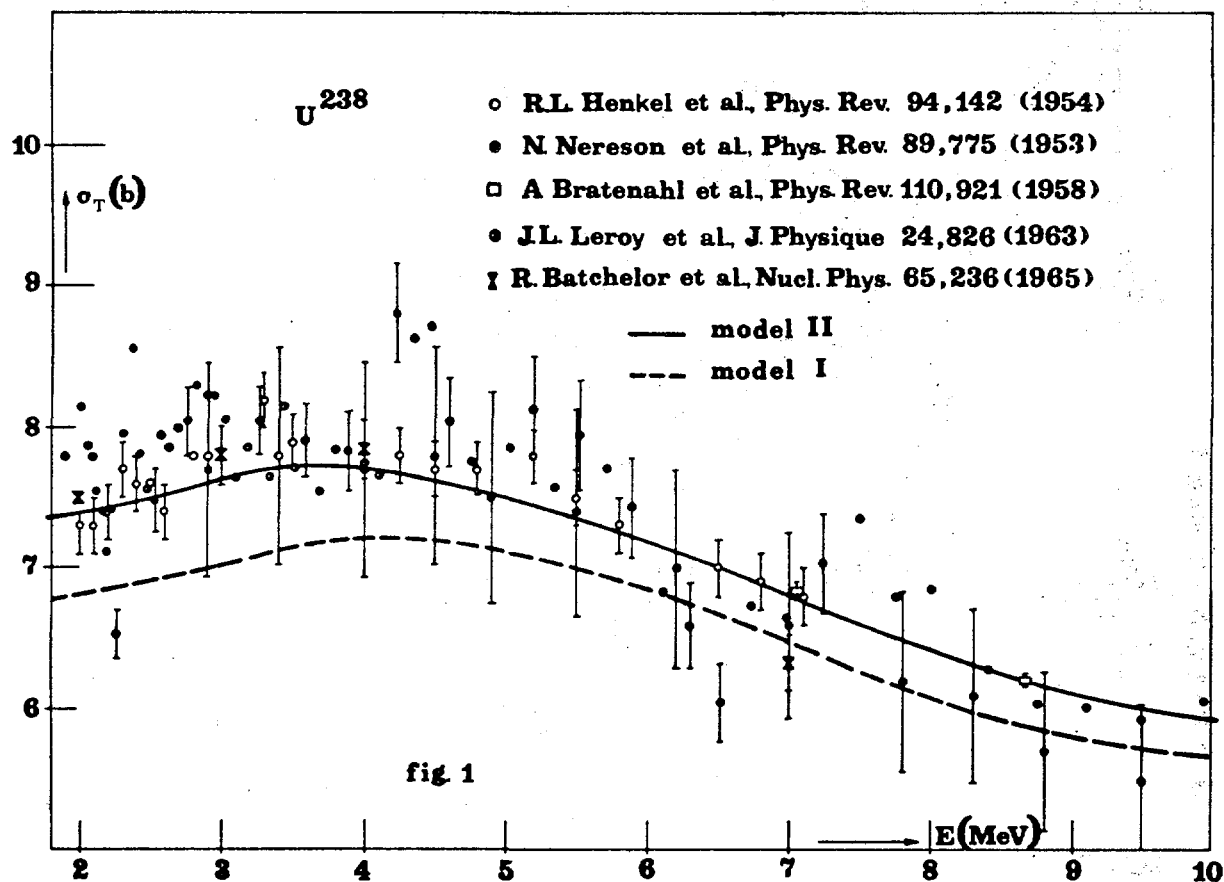
A coupled-channel programme for the scattering analysis of even-even nuclei described by a microscopic wave-function has been written for IBM-7094 computer. The programme has been checked in the case of the DWBA on the results given by Schaepper (\*) of Saclay (S.P.T.).

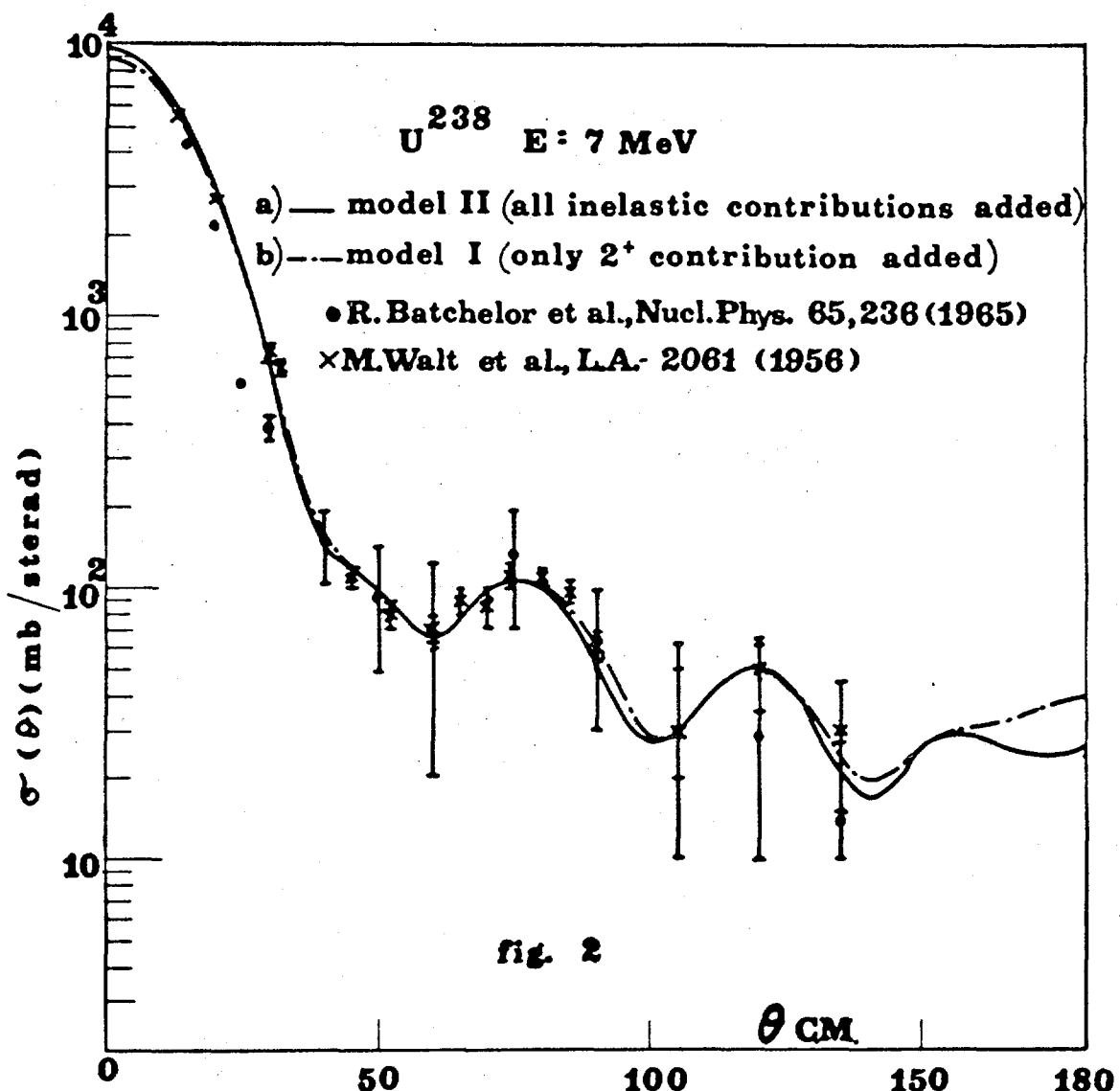
---

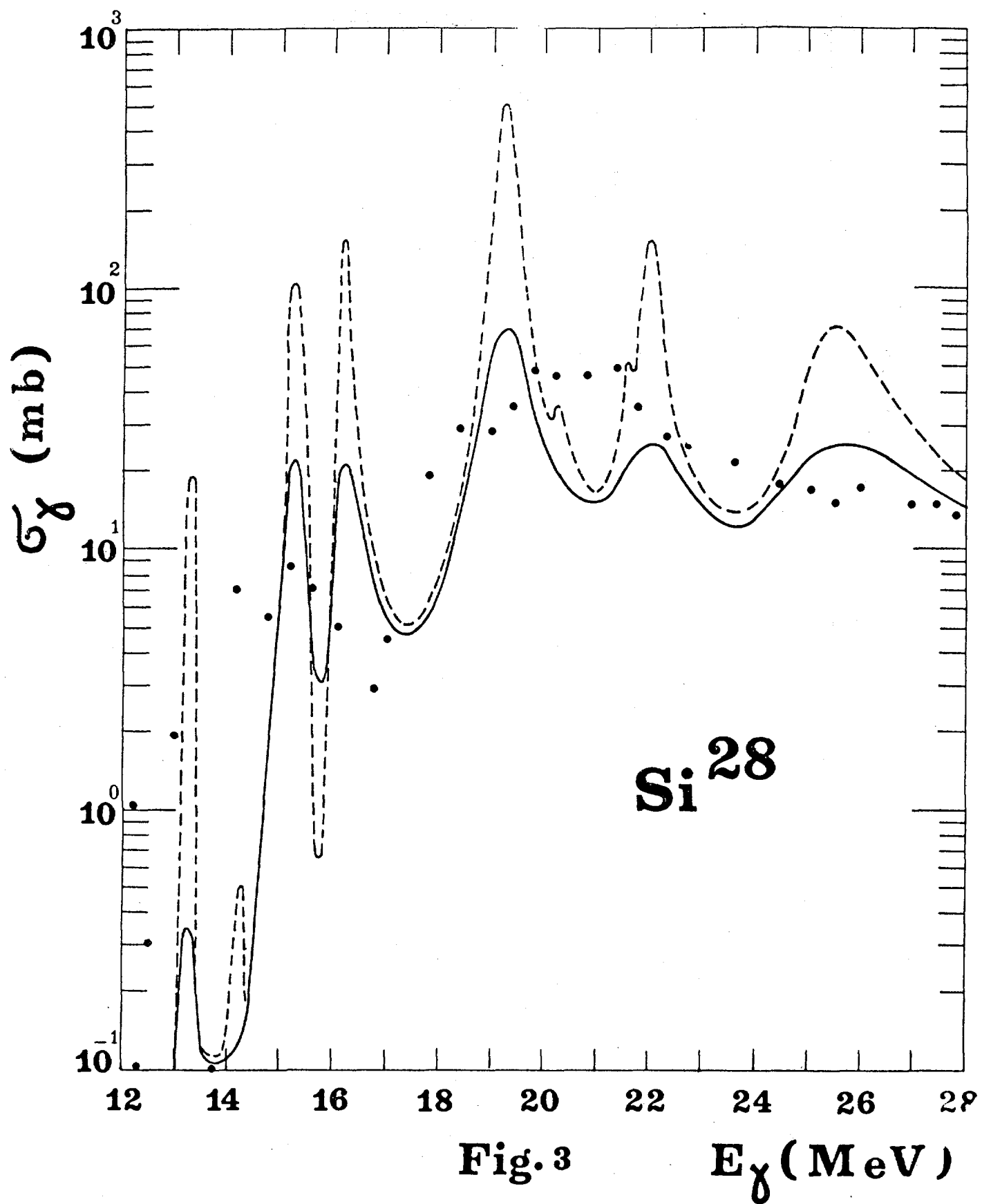
(\*) Private communication.

References

- [1] G. Longo, F. Saporetti - Nuovo Cimento 52B (1967) 539.
- [2] B. Baldoni, A.M. Saruis - Nuovo Cimento 33 (1964) 1145.
- [3] C.L. Dunford - NAA-SR-MEMO-11456 (1965).
- [4] B. Buck - Phys. Rev. 130 (1963) 712.
- [5] B.C. Barret - Nuclear Phys. 51 (1964) 27.
- [6] T. Tamura - Rev. of Mod. Phys. 37 (1965) 679.
- [7] M. Marangoni, A.M. Saruis - Phys. Lett. 24B (1967) 218.
- [8] M. Marangoni, A.M. Saruis - Coupled Channel Calculation of Si<sup>28</sup> Photoreactions.







XIV. GRUPPO DI RICERCA DEL CONTRATTO EURATOM-CNEN-INFN - ISTITUTO DI  
FISICA DELL'UNIVERSITA', BOLOGNA (ITALY)

1.1. The cross-section for the  $^3\text{H}(n, ^2\text{H})2\text{n}$  has been measured at neutron energy  $E_n = 15.1 \text{ MeV}$ . For  $\theta = 0^\circ$ , the value of  $29 \pm 4 \text{ mb/sr}$  was found for the cross-section integrated between 5.47 and 7.68 MeV [1]. For the same energy, measurements have been performed for the reactions  $^3\text{H}(n, ^3\text{H})\text{n}$  and  $^3\text{H}(n, p)3\text{n}$  at  $\theta = 0^\circ$  and  $\theta = 15^\circ$  (laboratory system). The results of these measurements are given in table I; it must be noted that the values for the  $^3\text{H}(n, p)3\text{n}$  reaction are referred to the cross-section integrated between 3.5 and 6 MeV proton energy at  $\theta = 0^\circ$  and between 3.5 and 5.74 MeV proton energy at  $\theta = 15^\circ$  [2].

References

- [1] E. Fuschini et al.: to be published in Nuclear Physics.
- [2] E. Fuschini et al. - Nuovo Cimento  $^{48}\text{B}$  (1967) 190.

TABLE I : cross-section values  $\sigma_{^3\text{H}(n, ^3\text{H})n}$  and  $\sigma_{^3\text{H}(n, p)3n}$  reactions  
at 15 MeV.

Reaction ( $E_n = 15.1$ MeV)	$\sigma (\vartheta_{LS} = 0^\circ)$ (mb/sr)	$\sigma (\vartheta_{LS} = 15^\circ)$ (mb/sr)
$^3\text{H}(n, ^3\text{H})n$	$228 \pm 4$	$124 \pm 1$
$^3\text{H}(n, p)3n$	$25 \pm 6$	$10 \pm 3$

XV. GRUPPO DI RICERCA DEL CONTRATTO EURATOM-CNEN-INFN - ISTITUTO  
DI FISICA DELL'UNIVERSITA', GENOVA (ITALY)

1.1. Photonuclear studies

1.2. Measurements of the cross-section for photoprottons production  
in  $^{12}\text{C}$  using  $\gamma$  rays of energy between 30 and 80 MeV

The energy spectra of photoprottons produced in the reaction  $^{12}\text{C}(\gamma, p)$  are measured using a scintillation telescope counter. The telescope consists of two counters, one for the measurement of the specific ionization of the incoming particles, the other for the measurement of the residual energy. Using some care in the design of the counters, an over-all energy resolution better than 5% was obtained even if the counters have a relatively large area ( $150 \text{ cm}^2$ ). The associated electronics was designed to meet the following requirements: a) to be able to discriminate a few protons in a very large number of electrons ( $10^7 + 10^8$  electron/s), b) to have a good over-all linearity also for fast signals ( $5 \cdot 10^{-9}\text{s}$ ). The apparatus gives a discrimination between protons and electrons with a mixing lower than a few percent. With our apparatus protons with energy above 25 MeV can be recorded. In this way we confine ourselves to the analysis of an energy region above the giant resonance. By doing a series of spectra at various maximum energies of the bremsstrahlung  $\gamma$  beam, information can be obtained regarding the two possible processes: 1) direct emission of protons to the continuum with or without excitation of the residual nucleus, 2) emission of protons following the excitation of nuclear energy levels above the giant resonance.

The experiment has not yet been completely performed. The results just obtained show an interesting discontinuity in the high energy region of the proton spectrum, that seems to be due to the s-shell and p-shell structure of the nucleus.

The electronics designed for this experience was described in [1] [2].

1.3.  $\gamma$ -n reaction in the nuclei  ${}^6\text{Li}$ - ${}^7\text{Li}$

A  ${}^6\text{Li}$  and a  ${}^7\text{Li}$  targets were exposed to the  $\gamma$  beam of a betatron (30 MeV maximum energy).

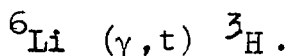
The resulting neutrons were recorded using nuclear plates.

The energy spectra of the neutrons gave a measurement of the energy of the possible excited states for nuclei  ${}^6\text{Li}$  and  ${}^7\text{Li}$ .

The results obtained are in good agreement with other measurements previously done. The detailed results of this experiment are given in [3][4].

1.4. Photodisintegration of  ${}^6\text{Li}$  in  ${}^3\text{H} + {}^3\text{He}$ .

After some preliminary experiments, nuclear plates doped with  $\text{Li}^6$  were used to study the reaction



The scanning of the emulsions is now performed.

We hope to verify in this way some predictions that come out of a cluster model of the nucleus  ${}^6\text{Li}$ .

2.1. High resolution, high efficiency  $\gamma$ -ray spectrometer

A spectrometer for  $\gamma$ -rays in the energy region between 20 and 100 MeV, having a 2% resolution and a mean 6% efficiency, was assembled using two large NaI(Tl) crystals (see [5]). The dimensions of the two crystals are 230 mm diameter x 160 mm height, and 148 mm diameter x 93 mm height.

The smaller crystal has a central hole in which the incident beam is collimated. The systems act as a  $4\pi$  spectrometer but with two separate crystals it is possible to impose supplementary condition to improve the resolution. The spectrometer is now completely assembled and preliminary measurements were

done to test its good performances.

The spectrometer is intended to be used in measurements of spectra of scattered  $\gamma$  rays, and in measurements of total absorption cross-section.

### 3.1. Monoenergetic $\gamma$ rays

Theoretical calculations were performed to establish the best geometrical condition in which it is possible to obtain a quasi monocromatic  $\gamma$  beam from positrons annihilating in flight in a suitable target. A careful examination of the bremsstrahlung contamination of the  $\gamma$  beam, suggested that, to minimize this contribution, relatively large angles must be chosen. A detailed design of a beam handling system to be used with the positron beam available at the Frascati Linac was also performed. The results of the theoretical calculations about these subjects are reported in [6].

### References

- [1] G. Manuzio, L. Racca - Apparecchiatura elettronica transistorizzata per l'elaborazione veloce degli impulsi di un telescopio di contatori a scintillazione - Rapporto INFN/TC 67/1.
- [2] G. Manuzio, L. Racca - Tunnel diode inverter - Electronic Letters 3 (1967) 45.
- [3] G. Paoli, M. Scotto, A. Wataghin - Reactions in Li<sup>7</sup> - Nuovo Cimento 40 (1965) 441.
- [4] G. Paoli, M. Scotto, A. Wataghin - Energy spectrum of photo-neutrons from Li<sup>6</sup> - Nuovo Cimento 43 (1966) 189.
- [5] B. Zeigler, J.M. Wyckoff, H.W. Koch - Nucl. Instrument Meth. 24 (1963) 301.
- [6] R. Malvano, E. Mancini, G. Ricco, M. Sanzone - Gamma da annichilazione di e<sup>+</sup> su idrogeno - Rapporto INFN/BE 67/7.

XVI. GRUPPO DI RICERCA DEL CONTRATTO EURATOM-CNEN-INFN - ISTITUTO  
DI FISICA DELL'UNIVERSITA', PAVIA (ITALY)

1.1. The Low Energy Group of the Nuclear Physics Institute of the University of Pavia has begun the study of the emission of long-range alpha-particles and light nuclei during nuclear fission, in order to achieve more detailed and accurate information about the fission problem and the nuclear matter in general [1], [2], [3], [4], [5]. In this year, it has been measured the energy spectrum of the alpha-particles and identified the helium isotopes from thermal neutron induced fission of  $^{239}\text{Pu}$ , using a neutron beam extracted from the Triga Mark II reactor of the University of Pavia.

In order to identify the various light charged particles, a DE-E solid state telescope, allowing simultaneous determination of the total kinetic energy and energy loss of the incident particles, has been employed [6].

The energy spectrum of the 11.300 detected long-range alpha-particles above 13 MeV; corrected for loss in the Nickel absorber, is shown in fig. 1.

The gaussian curve has its maximum at 16 MeV and a 4,66 MeV HWHM. The peak energy is slightly less than reported in the only  $^{239}\text{Pu}$  experiment known to us which was performed by Perfilov and coll. [7] with very poor statistics.

The He isotopes recorded are the following [8]:

- 47 events of  $^6\text{He}$  with energy above 17 MeV giving an intensity of 0,4 relative to emission of 100 alpha-particles
- 42 events attributable to  $^3\text{He}$  above 12 MeV with a yield relative to emission of alpha-particles of  $2.6 \cdot 10^{-3}$
- 7 events attributable to  $^8\text{He}$ .

References

- [1] S.L. Whetstone jr. and T.D. Thomas - Phys. Rev. Lett. 15 (1965) 298.
- [2] S.W. Cosper, J. Cerny and R.C. Gatti - Phys. Rev. 154 (1967) 1193.
- [3] S.L. Whetstone jr. and T.D. Thomas - Phys. Rev. 154 (1967) 1174.
- [4] M. Marshall and J. Scobie - Phys. Lett. 23 (1966) 583.
- [5] J. Chwaszczecka, M. Dakowski, T. Krogulski, E. Piasecki, W. Przyborski and M. Sowinski - Phys. Lett. 24 (1967) B 87.
- [6] F.S. Goulding, D.A. Landis, J. Cerny and R.H. Pehl - Nucl. Instr. and Meth. 31 (1964) 1.
- [7] N.A. Perfilov, Z.I. Solov'eva, R.A. Filof and G.I. Khlebnikov Sov. Phys. JEPT 17 (1963) 1932.
- [8] D. Bollini, M. Cambiaghi, F. Fossati and T. Pinelli - Nuovo Cimento 51 (1967) 235.

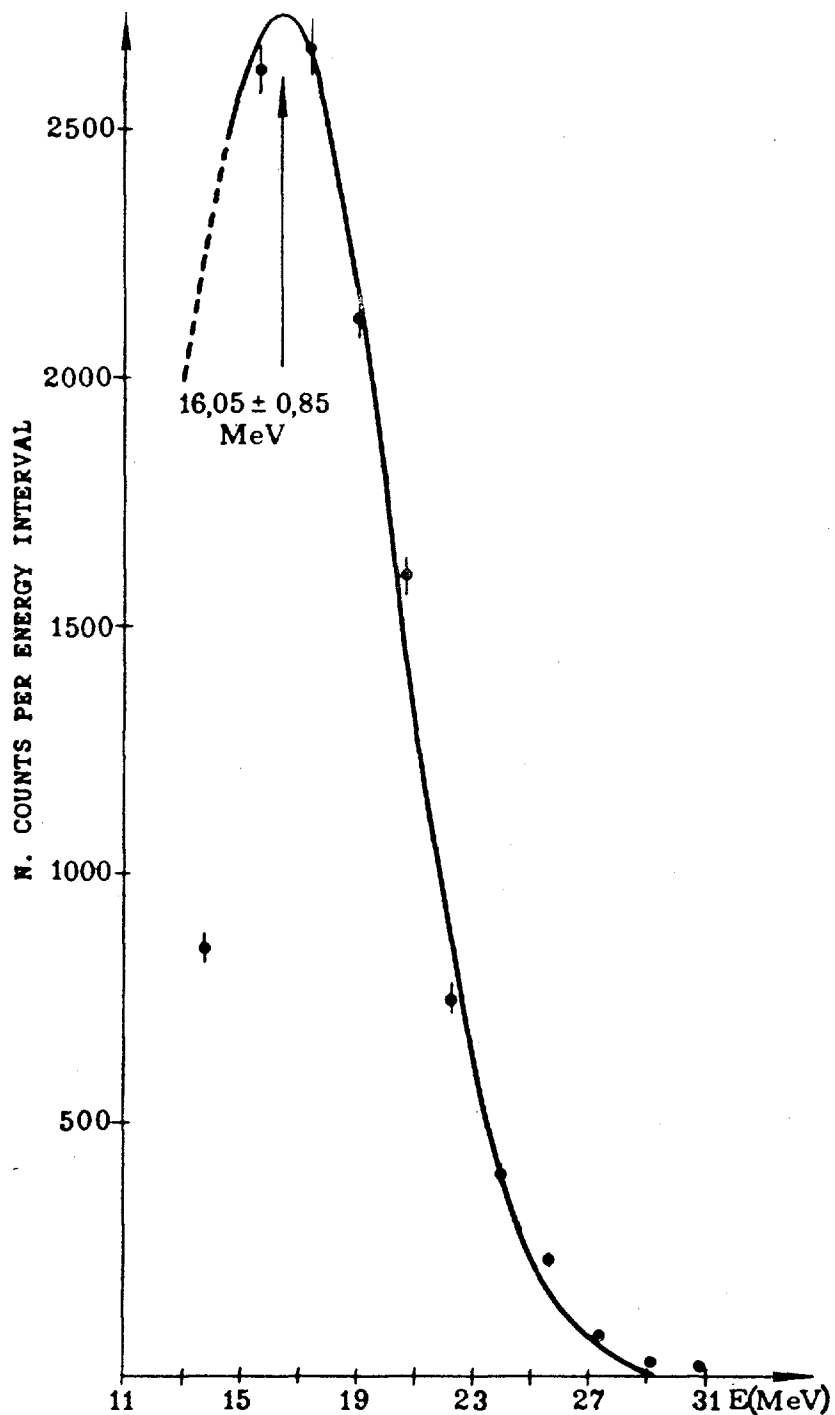


Fig. 1 - Energy spectrum of the long-range alpha particles emitted from  $\text{Pu}^{239}$  neutron induced fission. Energies have been corrected for energy loss in the Ni foil.

XVII. GRUPPO DI RICERCA DEL CONTRATTO EURATOM-CNEN-INFN - ISTITUTO  
DI FISICA DELL'UNIVERSITA', ROMA (ITALY)

I. Works on photofission

(L. Fiore, A. Manfredini, M.C. Ramorino)

1.1. Angular distribution of  $^{238}\text{U}$

We have concluded and analysed angular distribution measurements in the  $^{238}\text{U}$  photofission induced by monochromatic  $\gamma$  rays, whose energy slightly exceeds the fission barrier, for 12 energies of  $\gamma$  in the interval  $5.4 \leq E \leq 9.0$  MeV. As  $\gamma$  source we have used some  $(n, \gamma)$  reactions on elements chosen so that the  $\gamma$  spectrum has a line of predominant intensity above 5 MeV (threshold of photofission), eventually together with few lines of much lower intensity.

Nuclear emulsions loaded with a complex of  $^{238}\text{U}$  have been used. The technical and geometrical conditions of the exposure have already been discussed in papers [1] and [2]. The distribution of the projected angles on the plane of emulsion (being  $0^\circ$  the  $\gamma$  rays direction) was recorded, confining the measurements to tracks whose dip angle was less than a prefixed value  $\beta_0$ . The distribution  $W(\alpha, \beta \leq \beta_0)$  can be easily transformed into the distribution  $W(\theta)$  of the space angles, with  $\theta = 0^\circ$  for the direction of the  $\gamma$  beam. We suppose that the form of the angular distribution to be measured is

$$W(\theta) = a + b \sin^2 \theta + c \sin^2 \theta \cos^2 \theta$$

To obtain the  $W(\theta)$  from the measured  $W(\alpha, \beta \leq \beta_0)$  two corrections are to be made because of the efficiency of detection of each scanner  $\epsilon_i(\alpha)$  and of the background of neutrons in the beam. If  $F_i(\alpha, \beta \leq \beta_0)$  is the angular distribution and  $\epsilon_i(\alpha)$  the efficiency function measured for the  $i^{\text{th}}$  scanner, the real angular distribution is given by

$$w_i(a, \beta < \beta_o) = \frac{F_i(a, \beta \leq \beta_o)}{\varepsilon_i(a)}$$

Now the  $w_i(a, \beta < \beta_o)$  can be added together and geometrically transformed into the  $\Phi(\theta)$  distribution of the space angles, normalized so that  $\int \Phi(\theta) \sin \theta d\theta = 1$ .

The angular distribution  $W(\theta)$  due only to  $\gamma$ -rays is given by

$$W(\theta) = [\Phi(\theta) - p_n w_n(\theta)] \frac{1}{1-p_n}$$

where  $p_n$  is the percentage of fission tracks due to neutrons, as calculated in papers [3] and [4], and  $w_n(\theta)$  is the angular distribution of fissions produced by neutrons, measured by us using emulsions exposed with Bi target, whose  $\gamma$  spectrum has a maximum energy at 4.17 MeV, under enough the photofission threshold. We have obtained

$$w_n(\theta) = (1.03 \pm 0.07) - (0.04 \pm 0.07) \sin^2 \theta$$

The values of  $a$ ,  $b$  and  $c$  in the  $W(\theta)$  distribution, obtained after corrections, are reported in Table I.

In fig. 1 are reported some measured angular distributions compared with the  $W(\theta)$  calculated with the  $a$ ,  $b$  and  $c$  values. The values reported in Table I can be handled so as to establish a set of equations, in the same approximation as made in paper [4] for the cross-section measurements (column 1). The set of equations is

$$\sum_i I_i \sigma_i a_i = \left( \frac{F}{\Phi_U} \right) a$$

where  $\frac{F}{\Phi_U}$  is the fission tracks density by unity of  $\gamma$ -ray flux and uranium nuclei, as measured in paper [4];  $I_i$  is the relative intensity of the  $i^{th}$  line,  $\sigma_i$  the corresponding fission cross-section and  $a_i$  the value of the constant term  $a$  for the corresponding  $\gamma$ -energy. With the same approximation of paper [4] the set of linear equations can be solved and the solution further

approximated by linear interpolation.

The errors in Table I take into account the statistical errors on the fission tracks measure and the errors due to all introduced corrections.

The behaviour of the a and b coefficients with energy is that provided by Bohr's hypothesis near photofission threshold [6]. The coefficient c is small but different from zero; statistical errors are too big to give its behaviour with energy.

We have made also a quantitative analysis of the angular distribution coefficients introducing the following simplifying hypothesis: The states which can contribute to the photofission in our energy interval are  $1^- k=0$ ,  $1^- k=1$  dipole absorption, and  $2^+ k=0$ , quadrupole absorption ( $k$  is the projection of the total angular momentum of the nucleus on the symmetry axis), but the state  $2^+ k=0$  gives a constant contribution, in our energy interval, corresponding to 0.06 of  $\sigma_{tot}$ ; indicating with  $\sigma_0^-$ ,  $\sigma_1^-$  respectively the cross-sections for the states  $1^- k=0$ ,  $1^- k=1$ ; the coefficients a and b of the angular distribution  $w(\theta)$  can be expressed by

$$a = \frac{3}{4} \frac{\sigma_1^-}{\sigma_{tot}}$$

$$b + \frac{1}{2} a = \frac{3}{4} \frac{\sigma_0^-}{\sigma_{tot}}$$

Using, besides, the fission cross-section formula available for energies near fission threshold, see papers [7] and [8],

$$\sigma = \text{const} \int_0^E e^{-\frac{U_f}{T}} / (1 + \frac{B-U_f}{E_p}) dU_f \quad (1)$$

where the first factor in the integral measures the chance of concentrating an amount of energy  $U_f$  on the fission oscillation rather than on the other degrees of freedom, and the second factor is the fission barrier penetration given by Hill and

Wheeler [9], we can express  $a$  and  $b$  through the  $T$ ,  $B$  and  $E_p$  parameters which characterize the nucleus. Fitting the functions  $a$ ,  $b + \frac{1}{2}a$  and  $\frac{b}{a}$  separately, for the parameters  $T$ ,  $B$  and  $E_p$  we have obtained the values reported in Table II.

The values reported in Table II are calculated using the values of  $a$  and  $b$  of Table I.

In fig. 2 are shown the experimental and calculated behaviour of the fitted functions with energy and the agreement of the experimental  $^{238}\text{U}$  photofission cross-section with that calculated with formula 1) and the parameters of Table II as far as about 6.5 MeV. Hereafter the competition of the  $(\gamma, n)$  process does not render our formulas available.

#### 2.1. Cross-section of $^{232}\text{Th}$ .

Thorium loaded nuclear emulsions have been exposed to monochromatic  $\gamma$ -rays obtained from  $(n, \gamma)$  reactions on the following elements: S, Dy, Y, Ca, Ti, Be, Mn, Pb, Fe, Al, Cu, Ni. As far as details are concerned, we refer to our previous papers whether for obtaining monochromatic  $\gamma$ -rays [13, 14], or for loading nuclear emulsions with fissile materials [10, 15], or finally for experimental data handling [11, 12].

Here we report the experimental results that are summarized in Table III: column 1 lists the reactor targets; column 2 the main line energies; column 3 the corresponding  $\gamma$ -rays fluxes; column 4 the ratio  $N_f / \Phi_m$  Th, that is the fission tracks density by unity of  $\gamma$ -ray flux and thorium nuclei; and column 5 the cross-section values obtained after correction for neutron background and for the secondary lines contribution.

These last values are also shown in fig. 3 together with the corresponding  $U$  values. The behaviour of the two cross-sections is roughly the same and is explained with the growth of the  $(\gamma, n)$  reaction which starts at about 6 MeV and at about 7 MeV becomes competitive with fission process. That the minimum

happens for Th and U at the same energy does not necessarily mean that the ( $\gamma$ ,n) thresholds for the two nuclei coincide. The position of the minimum may depend in fact on the behaviour and absolute value of the two cross-sections; with respect to Uranium, Thorium has actually a much less photofission cross-section, while his ( $\gamma$ ,n) cross-section grows very sharply [16]. The ratio  $\sigma_{\text{Th}}/\sigma_{\text{U}}$  is reported in fig. 3 as a function of energy. Disregarding the first point because of the large error it is affected by, this ratio shows a broad maximum at about 7 MeV which agrees with the Huizenga et al. results [16] and which is explained by these authors in terms of the competitiveness of ( $\gamma$ ,n) reactions with fission, together with the different thresholds of Uranium and Thorium ( $\gamma$ ,n) reactions.

#### References

- [1] H.G. De Carvalho, A. Manfredini, M. Muchnik, M. Severi, R. Bösch, J. Lang, R. Müller, W. Wolfli - N. Cim. 25 (1962) 534.
- [2] H.G. De Carvalho A. Manfredini, M. Muchnik, M. Severi, R. Bösch, W. Wolfli - N. Cim. 29 (1963) 463.
- [3] A. Manfredini, M. Muchnik, L. Fiore, C. Ramorino, H.G. De Carvalho, J. Lang, R. Müller - Nucl. Phys. 74 (1965) 377.
- [4] A. Manfredini, M. Muchnik, L. Fiore, C. Ramorino, H.G. De Carvalho, R. Bösch, W. Wolfli - N. Cim. 44B (1966) 218.
- [5] A. Bohr - Int. Conf. on the Peaceful Uses of Atomic Energy Vol. 2 (1956) 911.
- [6] I. Halpern - Annual Revue of Nucl. Sci. 9 (1956) 245.
- [7] T. Kivikas, B. Forkman - Nucl. Phys. 64 (1965) 420.
- [8] D.L. Hill, J.A. Wheeler - Phys. Rev. 89 (1953) 1102.
- [9] H.G. De Carvalho, A. Manfredini, M. Muchnik, M. Severi, R. Bösch, J. Lang, R. Müller, W. Wolfli - N. Cim. 25 (1962) 534.
- [10] A. Manfredini, M. Muchnik, L. Fiore, C. Ramorino, H.G. De Crvalho, J. Lang, R. Müller - Nucl. Phys. 74 (1965) 377.

- [12] A. Manfredini, M. Muchnik, L. Fiore, C. Ramorino, H.G. De Carvalho, R. Bösch, W. Wolfli - N. Cim. 44B (1966) 218.
- [13] L. Jarezyk, J. Lang, W. Wolfli, R. Müller - Helv. Phys. Acta 34 (1961) 488.
- [14] L. Jarezyk, J. Lang, H. Knoepfel, R. Müller, W. Wolfli - Nucl. Instr. and Meth. 13 (1961) 287.
- [15] H.G. De Carvalho - Prog. Nucl. Tech. and Instr. - Vol. 1 (North Holland, Amsterdam) 247 (1965).
- [16] J.E. Gindler, J.R. Huizenga, R.A. Achmitt - Phys. Rev. 104 (1956) 425.

TABLE I : Coefficients for angular distribution in U-238 photo-fission.

Target	E (MeV)	a	b	c
Dy	5.58	.05 $\pm .06$	1.37 $\pm .05$	.30 $\pm .21$
Y	6.09	.007 $\pm .03$	1.34 $\pm .03$	.74 $\pm .13$
Ca	6.37	.23 $\pm .04$	1.04 $\pm .04$	.53 $\pm .18$
Ti	6.75	.40 $\pm .03$	.85 $\pm .03$	.23 $\pm .14$
Be	6.80	.55 $\pm .11$	.41 $\pm .10$	1.11 $\pm .41$
Mn	6.94	.63 $\pm .04$	.56 $\pm .04$	-.04 $\pm .18$
Pb	7.34	.65 $\pm .06$	.41 $\pm .06$	.61 $\pm .23$
Fe	7.71	.63 $\pm .05$	.45 $\pm .05$	.49 $\pm .23$
Al	7.41	.75 $\pm .05$	.30 $\pm .05$	.37 $\pm .21$
Cu	7.66	.62 $\pm .06$	.49 $\pm .06$	.38 $\pm .24$
S	7.96	.69 $\pm .06$	.33 $\pm .06$	.71 $\pm .24$
Ni	8.63	.83 $\pm .05$	.20 $\pm .06$	.30 $\pm .19$

TABLE II : Values of the parameters  $T, B, E_p$  which appear in Eq.(1).

	State 1 <sup>-</sup> k=0	State 1 <sup>-</sup> k=1
T	.55 MeV	.65 MeV
B	5.6 MeV	6.54 MeV
$E_p$	.12 MeV	.15 MeV

TABLE III : Coefficients for angular distribution in Th-232 photofission.

Target 1	E (MeV) 2	$\frac{\Phi}{\gamma} \cdot \text{cm}^{-2}$ 3	$\frac{N_f}{\Phi} \frac{\gamma}{\text{Th}}$ (mb) 4	$\sigma$ (mb) 5
S	5.43	3.32	.59± .16	.16± .16
Dy	5.58	2.62	.79± .07	.73± .07
Y	6.07	2.18	1.90± .15	1.60± .16
Ca	6.42	2.16	5.13± .44	4.73± .44
Ti	6.75	1.16 9.21	12.20± .82	7.94± .89
Be	6.80	.96 1.01	2.40± .25	2.40± .25
Mn	7.16	2.39	7.14± 1.11	3.67± .74
Pb	7.38	.65	3.81± .56	3.25± .56
Fe	7.64	1.40	6.38± .51	4.86± .53
Al	7.72	5.11 3.14	5.45± .34	4.47± .34
Cu	7.91	.71	12.31± 2.53	6.89± 2.55
Ni	8.86	1.29	12.05± 1.03	5.79± .91

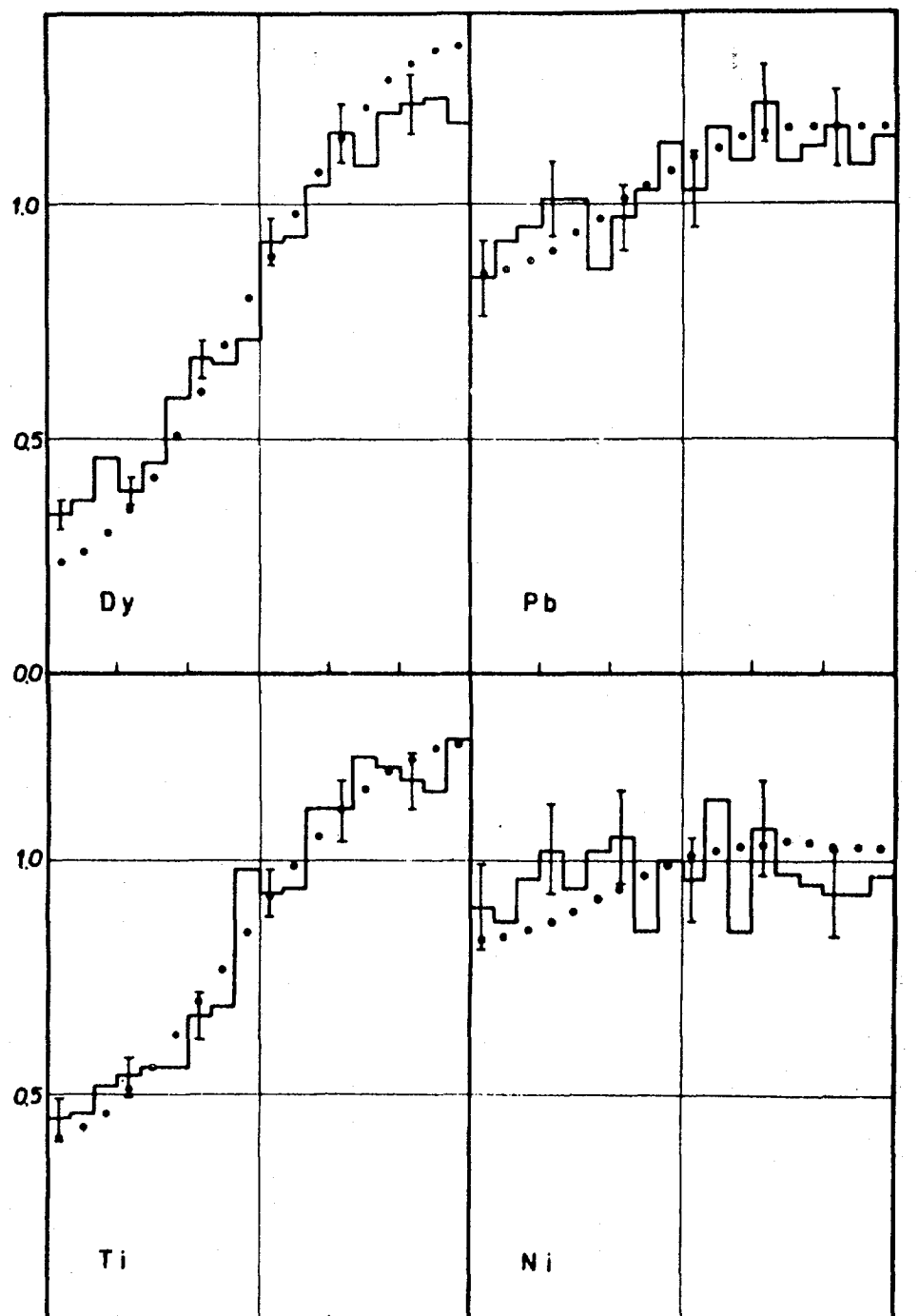


Fig. 1

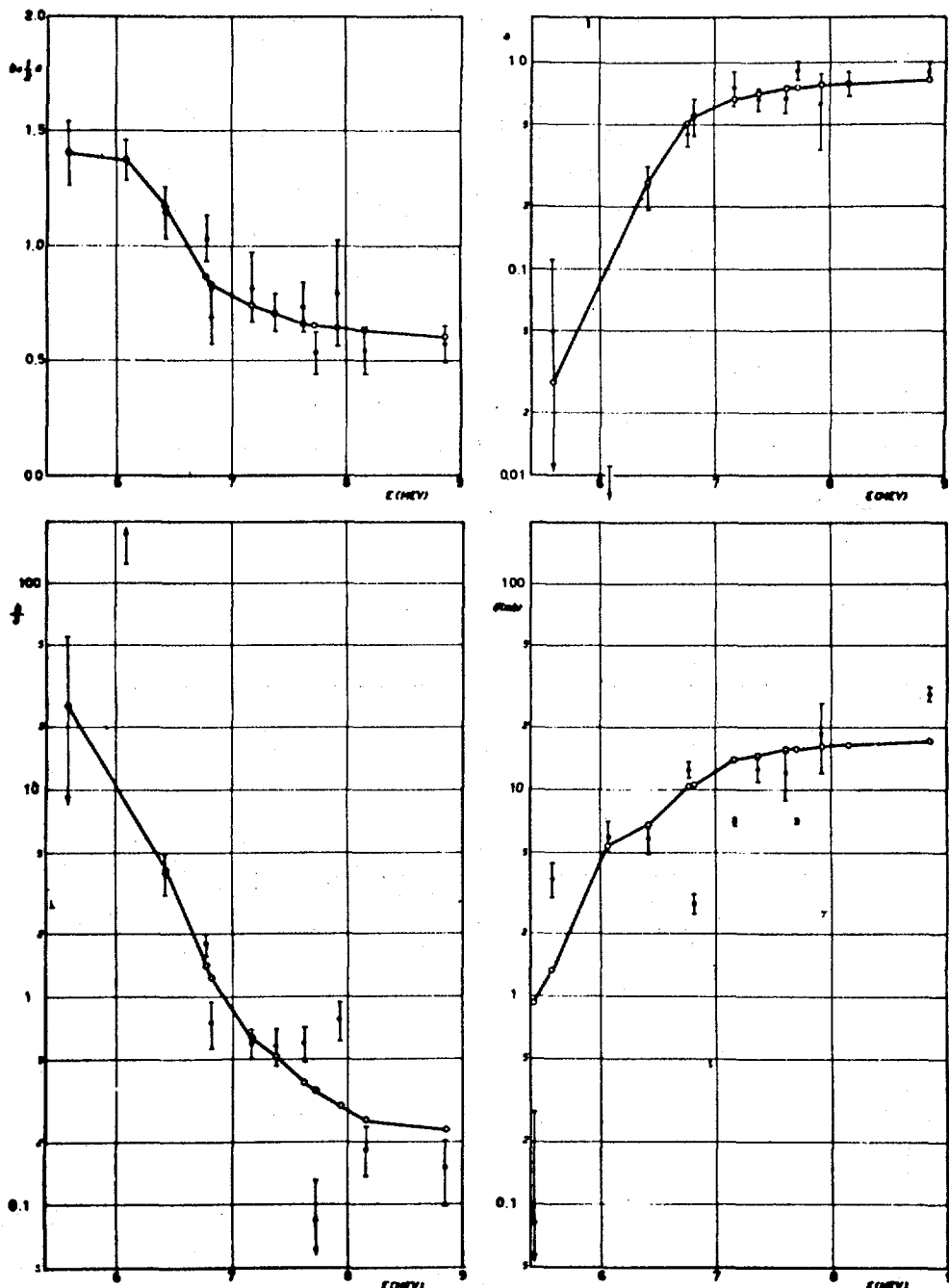


Fig. 2

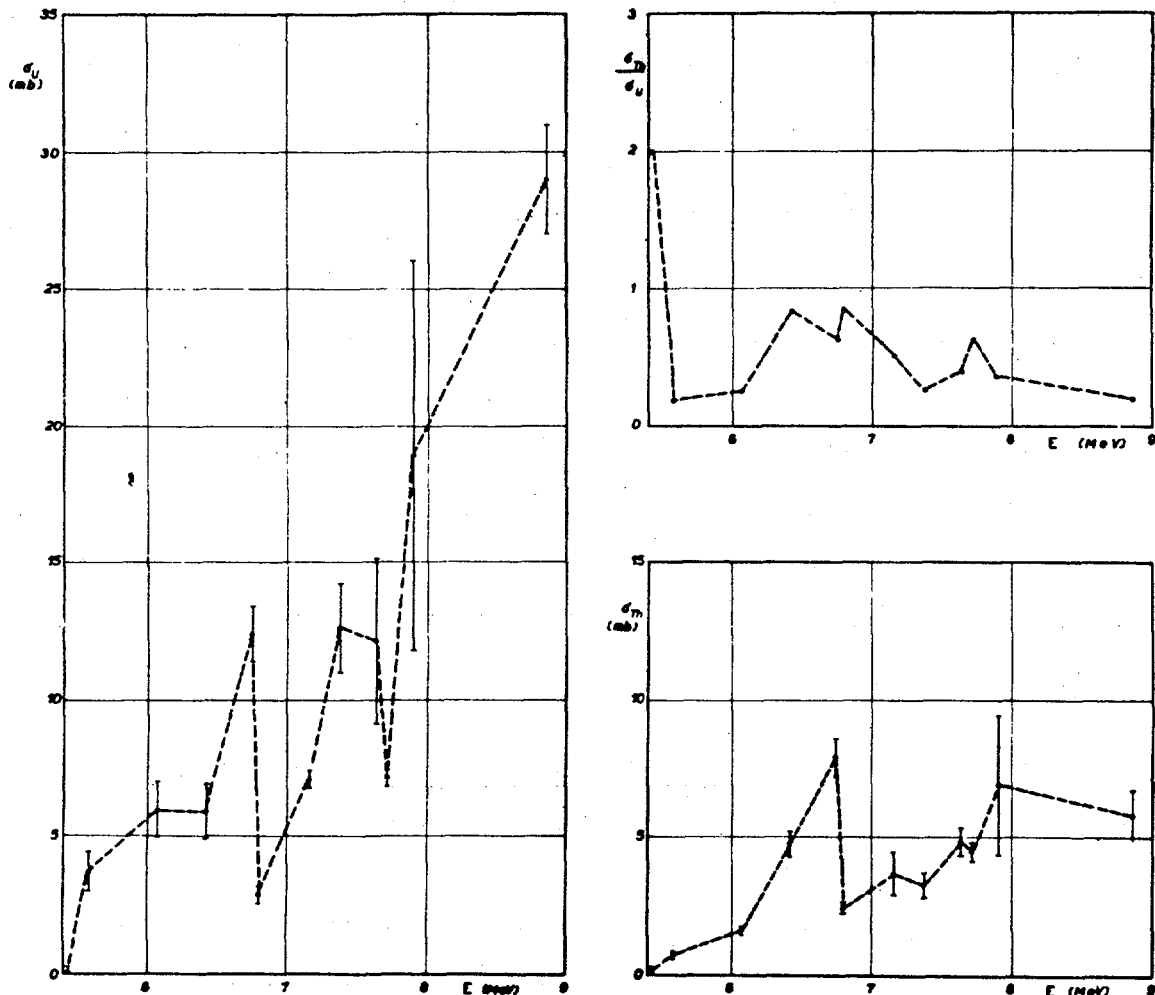


Fig 3

XVIII. GRUPPO DI RICERCA DEL CONTRATTO EURATOM-CNEN-INFN - ISTITUTO DI FISICA DELL'UNIVERSITA', PADOVA (ITALY)

1. Elastic and inelastic scattering of fast neutrons from  $^{165}\text{Ho}$   
(U. Fasoli, P.P. Sambo, D. Toniolo, G. Zago)

A measurement has been performed of angular distribution of elastic and inelastic scattering from  $^{165}\text{Ho}$  at the following energies: 3.0, 4.3, 6.0, 7.5 MeV, using the time-of-flight technique. The nuclear temperature of  $^{165}\text{Ho}$  and the level density deduced from the neutron inelastic scattering are in good agreement with the statistical model previsions. The analysis of the elastic scattering is beeing carried out using an optical model which considers also the nuclear deformation.

2. Elastic and inelastic scattering of fast neutrons from  $^{23}\text{Na}$   
(U. Fasoli, P.P. Sambo, D. Toniolo, G. Zago)

The elastic and inelastic cross sections of each level of  $^{23}\text{Na}$  have been measured using the time-of-flight technique at the energies 1.5, 2.5, 4.0, 6.5 MeV. A complete analysis of the data with the optical model is underway.

3. Total cross section of neutrons on Mg, Cl, K in the energy interval 5.0+8.5 MeV  
(U. Fasoli, P.P. Sambo, D. Toniolo, G. Zago)

The total cross section of neutrons on Mg, Cl, K has been measured in the energy interval 5.0+8.5 MeV, with steps of 25 KeV, energy resolution of about 30 KeV and a statistical error of 1+2%. The Mg cross section shows strong fluctuations, Cl and K cross section fluctuations are less pronounced.

The Mg cross section has been partially remeasured both with higher (about 10 KeV) and smaller (about 200 KeV) energy resolution to study the dependence of the fluctuations amplitude from the averaging interval.

An analysis of the fluctuations is in progress also from the point of view of the "intermediate structures".

4. Use of the PDP-8 computer

A PDP-8 computer has been used for the analysis of all our measurements. In particular, a Montecarlo code has been figured out and successfully used for the correction due to multiple scattering in neutron scattering.

An interface has been constructed in order to use on line the computer for experiments of neutron physics.

5. Analysis of the p-<sup>3</sup>He low energy interaction (\*)

(L. Drigo and G. Pisent, Nuovo Cimento 51B, 419 (1967))

The elastic scattering of protons from <sup>3</sup>He nuclei is analyzed at the very low energies. A phase shift analysis on the cross section and polarization data between 2.38 and 4.46 MeV leads to the determination of four solution sets (see Tables I,II,III). These mathematical solutions are examined in the light of a nucleon-nucleus potential model. The structure of the spin-dependent interaction which is necessary to assume in order to reproduce the experiments is widely discussed. Some elements on the discrimination between phase shift ambiguities are also given by the potential calculation, but, for a clear-cut conclusion on this point, further high energy analyses, and perhaps triple scattering experiments will be probably needed.

(\*) Work carried out under Contract EURATOM-CNEN-INFN

TABLE I : Phase shift sets extracted from cross section and polarization experiments below 5 MeV.

	E (MeV)	$-\delta_{00}^0$	$-\delta_{10}^0$	$\delta_{01}^1$	$\delta_{11}^0$	$\delta_{11}^1$	$\delta_{11}^2$	$\Delta$
(a)	2.38	36.0°	35.4°	12.8°	4.4°	15.3°	18.8°	1.89
	2.61	36.2°	39.6°	15.8°	5.9°	18.1°	21.1°	0.56
	2.89	38.8°	39.3°	17.6°	5.7°	19.5°	26.4°	0.87
	3.22	44.6°	41.0°	19.7°	5.7°	23.4°	32.0°	0.46
	3.54	43.1°	45.5°	22.0°	8.9°	24.4°	36.1°	1.00
	3.84	45.5°	47.6°	23.4°	8.2°	27.2°	39.5°	0.98
	4.15	46.8°	48.8°	23.4°	8.8°	31.3°	43.7°	0.85
	4.46	49.8°	51.4°	22.8°	11.6°	33.3°	45.8°	1.82
(b)	2.38	38.0°	33.4°	14.8°	21.2°	8.2°	21.0°	1.88
	2.61	37.2°	38.6°	16.8°	20.2°	9.5°	22.0°	0.62
	2.89	40.8°	37.3°	19.6°	23.5°	8.7°	28.0°	0.92
	3.22	44.6°	39.0°	21.7°	28.5°	11.5°	34.0°	0.56
	3.54	42.1°	44.5°	23.0°	28.0°	13.0°	37.0°	1.08
	3.84	42.5°	44.6°	26.4°	33.5°	13.0°	42.0°	1.08
	4.15	44.8°	46.8°	25.4°	36.4°	15.7°	46.0°	1.14
	4.46	45.8°	49.4°	24.8°	42.0°	16.0°	48.0°	2.15
(c)	2.38	36.2°	34.7°	19.1°	4.3°	14.7°	18.5°	1.83
	2.61	41.3°	37.9°	20.1°	5.0°	16.1°	19.8°	0.55
	2.89	39.6°	39.1°	24.5°	7.6°	14.6°	24.7°	0.86
	3.22	38.2°	43.8°	29.3°	4.3°	18.8°	28.0°	0.48
	3.54	46.7°	44.3°	33.2°	8.4°	19.3°	32.6°	0.94
	3.84	47.7°	45.6°	37.5°	3.4°	23.1°	36.0°	0.70
	4.15	52.8°	46.8°	43.1°	5.3°	23.6°	38.1°	0.73
	4.46	55.2°	49.6°	46.7°	7.0°	26.0°	38.8°	1.73
(d)	2.38	37.1°	33.7°	20.1°	17.7°	7.2°	19.5°	1.89
	2.61	42.3°	36.9°	21.1°	19.2°	8.2	20.8°	0.57
	2.89	40.6°	38.1°	25.5°	17.0°	10.0°	25.7°	0.90
	3.22	36.2°	43.8°	29.3°	23.5°	9.7°	30.0°	0.52
	3.54	45.7°	43.3°	34.2°	20.5°	12.0°	33.6°	0.98
	3.84	49.7°	41.6°	41.5°	30.0°	8.0°	38.0°	0.74
	4.15	51.8°	43.8°	46.1°	28.0°	10.2°	39.1°	0.68
	4.46	58.2°	46.6°	49.7°	26.5°	15.5°	39.8°	1.41

TABLE II : Extrapolation of the phase shift of Table I to higher energies.

	E MeV	$-\delta_{00}^0$	$-\delta_{10}^1$	$\delta_{01}^1$	$\delta_{11}^0$	$\delta_{11}^1$	$\delta_{11}^2$	$\delta_{02}$	$\delta_{12}$	$\epsilon$	$\Delta$
(a)	5.51	53.2°	59.9°	24.3°	13.8°	38.6°	54.4°	-5.4°	-1.2°	-0.9°	0.56
	6.82	59.0°	67.5°	23.1°	16.7°	46.2°	59.8°	-9.9°	-0.3°	-4.7°	0.67
(b)	5.51	53.5°	57.0°	25.5°	53.0°	20.0°	57.0°	-3.0°	-2.0°	6.0°	1.13
	6.82	62.0°	65.0°	27.0°	61.0°	27.0°	63.0°	-4.0°	-2.0°	8.0°	1.98
(c)	5.51	61.0°	60.0°	57.0°	14.0°	31.0°	40.0°	0.0°	-2.0°	8.0°	0.51
	6.82	70.5°	65.0°	67.0°	16.5°	34.0°	45.0°	-2.0°	-2.0°	8.0°	0.71
(d)	5.51	62.0°	59.0°	57.0°	35.0°	22.0°	42.0°	0.0°	-2.0°	8.0°	0.46
	6.82	69.0°	66.0°	63.0°	42.0°	24.5°	48.0°	1.0°	-3.0°	10.0°	0.69

TABLE III : S-wave effective range parameter (in fermis).

	$a_s$	$r_{0s}$	$a_t$	$r_{0t}$	$a_s^n$	$a_t^n$
p - ${}^3\text{He}$ (sol.a)	8.45	1.38	8.45	1.62	3.50	3.72
p - ${}^3\text{He}$ (sol.c)	7.94	1.96	7.89	1.62	3.89	3.60
n - ${}^3\text{H}$ (ref. 12)	--	--	--	--	3.38	3.25

XIX. CENTRE DE PHYSIQUE NUCLEAIRE DE L'UNIVERSITE DE LOUVAIN (Belgium)

---

VAN DE GRAAFF DEPARTMENT

---

The pulsed 4 MeV Van de Graaff has been utilized for the study of different reactions involving neutron detection.

1. Elastic and inelastic scattering of 15-20 MeV neutrons on  $^{12}\text{C}$ .

G. DECONNINCK and J.P. MEULDERS

The pulsed deuteron beam is allowed to enter in a tritium gas cell; the energy of the neutrons from the  $\text{T}(\text{dn})^4\text{He}$  reaction varies between 16 and 20 MeV when detected at  $0^\circ$ .

A 2 meters iron collimator mounted on a rotating frame has been utilized for elastic scattering measurements. The sample is a cylinder of high density graphite.

Angular distributions have been measured at 4 different energies between  $30^\circ$  and  $145^\circ$  by a technique combining time-of-flight and pulse shape discrimination. The aim of this work is to remove discrepancies in the 14 MeV existing data and to extend measurement up to 20 MeV.

Large variations in the cross section suggest the existence of resonances which are analysed with a program involving optical and resonant theories.

Inelastic scattering cross sections on the 4,43 MeV level are also determined by these measurements. Handling of the results is in progress.

Efficiency of the neutrons detectors in the 9-20 MeV region.

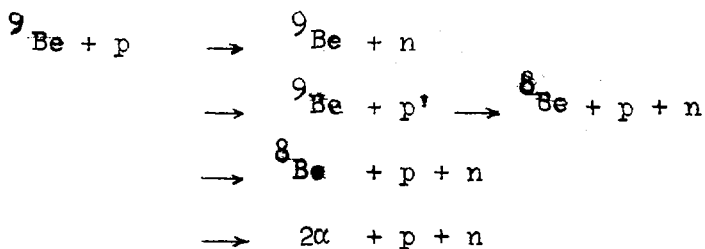
Large liquid scintillators are utilized in the preceding experiments. The efficiency is measured with the known angular distribution of the  $\text{T}(\text{dn})^4\text{He}$  reaction but also by scattering of neutrons on an hydrogenous material. The sample was a cylinder of NE 102 mounted on a photo-

multiplier and coincidences between the time-of-flight signal and the proton signal are taken. A special program of calculation has been written to calculate corrections on the measured efficiency, these corrections are necessary to take into account the absorption in the scintillator.

## 2. Neutrons from the bombardement of Beryllium by proton.

F. BODART and G. DECONNINCK

Protons on Beryllium gives the following reactions:



These reactions have been carefully studied at incident energies ranging between 2.7 and 4 MeV. Angular distributions are measured at 5 energies between 0° and 160°.

The first reaction is by far the most intense. Calculations are still in progress..

### The ${}^9\text{Be}(p, n){}^8\text{B}$ as a source of mono-energetic neutrons.

Contribution has been presented at the "Meeting on Accelerator Targets for the Production of Neutrons", held in Liège in September 1967. The possibility of producing high fluxes of monoenergetic neutrons is discussed and cross sections are presented.

## 3. The study of ${}^{51}\text{V}(p, n){}^{51}\text{Cr}$ reaction.

G. DECONNINCK and J. ROYEN

Angular distribution measurements are in progress for this reaction in connection with the study of analogue states in  ${}^{52}\text{Cr}$ .

XX. LABORATOIRE VAN DE GRAAFF, UNIVERSITE DE LIEGE (Belgium)

Prof. L. WINAND

Differential scattering cross section of  $^{16}\text{O}$  (d,p)  $^{17}\text{O}$

The Van de Graaff Laboratory has been studying the problem of the detection of oxygen at the surface of metals, using protons from the  $^{16}\text{O}$  (d,p)  $^{17}\text{O}$  reaction.

For the study of surface layers containing low quantities of oxygen it is necessary to know with a good accuracy the differential cross-section of the  $^{16}\text{O}$  (d,p) reaction for low  $E_d$  values.

We have undertaken to study this reaction for deuteron energies lower than 800 keV.

It is necessary to consider the equilibrium that establishes itself between the residual oxygen in the chamber and the oxygen of the target. This equilibrium is a function of residual pressure, partial pressures, incoming beam intensity, (which modifies the surface temperature of the target), the carbon deposits from vacuum pumping systems etc..

A systematic study of these factors has been undertaken, in order to measure  $\frac{d\sigma}{d\Omega}$  and to determine the minimum amount of oxygen that can be detected.

The accurate knowledge of  $\frac{d\sigma}{d\Omega}$  as a function of  $E_d$  will allow the oxygen concentration to be measured as a function of the distance from the target surface.

2. Long-range particles from Po sources

The determination of the nature of the long range particles emitted by Po sources has been done by multiple scattering measurements on their tracks in nuclear emulsions. The result is consistent with the one obtained previously by ionisation loss measurements and indicates that these particles are protons. Their origin is still unexplained.

XXI. CENTRE D'ETUDE DE L'ENERGIE NUCLEAIRE (C.E.N.-S.C.K.) Mol, Belgium

---

1. Slow Neutron Spectroscopy

1.1. Crystal Spectrometer

F. POORTMANS

Two Be single crystals, fabricated by the Metallurgy Department of CEN, Saclay, have been tested on the neutron diffractometer. One of the crystals may possibly be used as a monochromator but further tests will be performed after the crystal blank has been cut.

The BR2 neutron crystal spectrometer has been used for activation cross section measurements of  $^{151}\text{Eu}$  in the energy range 0.01 eV - 0.5 eV.

The gamma activities are measured with a single NaI crystal spectrometer or a  $\gamma$ - $\gamma$  coincidence spectrometer consisting of two 4" x 4" NaI crystals. The neutron flux is measured by activating a thin gold foil. The data are currently being analysed.

1.2. Resonance Cross Section Analysis

H. CEULEMANS +

Following an extended stay at Columbia University, New York, N.Y., with the Neutron Velocity Selector group \* some of the experimental data on Nd isotopes obtained during the last run will be further analysed. To this end the computer codes which were used at Columbia have been adapted to the IBM 360/40 at ACEC, Charleroi, which is used under the terms of a contract between our institute and this company.

---

+ on leave of absence from S.C.K. until 1.9.67

\* See e.g. the Report WASH-1074 p. 26 or the Pogram Nuclear Physics Laboratories Progress Report NYO-GEN-72-132

### 1.3. Publications

Spins of Slow Neutron Resonances in Sm, Gd, Ta, Re and Ir Isotopes

F. Poortmans and H. Ceulemans, Nucl. Phys. A97, 657 (1967)

Spin Measurements of the 8.8 eV and 12.4 eV neutrons Resonances in  $^{235}\text{U}$

F. Poortmans, H. Ceulemans and M. Nève de Mévergnies, Nuclear Data for Reactors, Vol II, 211, 1967 IAEA, Vienna 1967.

## 2. Fission Physics and Chemistry

### 2.1. Fission cross-section measurements with fission track detectors

M. NEVE de MEVERGNIES and P. del MARMOL

To measure the fission cross-section of  $^{232}\text{Th}$  for thermal neutrons, a sandwich consisting of a thin  $^{232}\text{Th}$  deposit \* and a plastic disk used as a fission-track detector is irradiated in the thermal column of the BR1 graphite reactor, inside a thick lead container so as to minimize photo-fission reactions. The deposit has a thickness of 0.90 mg/cm<sup>2</sup> Th. on an Al backing. The detector is a polycarbonate known as Makrofol E. The measurements are in progress.

### 2.2. Identification of $^{83}\text{As}$ and $^{84}\text{As}$ in fission and nuclear charge distribution in this mass region

P. del MARMOL

The study of  $^{83}\text{As}$  and  $^{84}\text{As}$  in thermal neutron fission of  $^{235}\text{U}$  through milking of their granddaughter products yielded the following results:

$^{83}\text{As}$      $t_{1/2} = (14.1 \pm 1.1)\text{s}$ ; cumulative yield:  $81 \pm 9\%$  of chain 83.

$^{84}\text{As}$      $t_{1/2} = (5.8 \pm 0.2)\text{s}$ ; cumulative yield:  $17 \pm 2\%$  of chain 84.

Using Wahl's method the most probable charge ( $Z_p$ ) was calculated for both chains and gave  $32.95 \pm 0.27$  for mass 83 and  $34.04 \pm 0.10$  for mass 84.

---

\* supplied by BCMN, Euratom, Geel.

The latter result shows a striking fine structure in the otherwise smooth empirical function of  $Z_p$  versus mass number and is probably caused by the closed shell of 50 neutrons.

### 2.3. Publications

P. del Marmol and M. Nève de Mévergnies, J. Inorg. Nucl. Chem.  
29, (1967) 273

P. del Marmol, Arkiv för Fysik, 36 (1967) 205

### 3. Inelastic Scattering of Slow Neutrons

S. HAUTECLER

In order to explain the lattice dynamics of bcc and fcc metals, KREBS has developed a force model in which the metal is considered as a lattice of spherical ions, of uniform charge distribution, embedded in an electron sea. The physical content of this model has been applied to the case of hexagonal close-packed metals. The elements of the dynamical matrix have been deduced by assuming, on one hand, central "spring" interactions extending up to the sixth neighbours and, on the other hand, screened Coulomb interactions between all ions. The relations between the parameters introduced in the model and the five elastic constants have been obtained by means of the method of long waves. Calculations of the phonon dispersion curves along the symmetry axes for Be, Mg and Zn are in progress.

An experimental investigation of the lattice dynamics of Zn has been performed; scattering curves in the (001) plane have been deduced for three different scattering angles. Our program is being extended

to the calculation of the scattering curves so that these experimental curves could be used directly to check the model. Some preliminary measurements have also been done on the paramagnetic scattering by  $\text{UO}_2$ ,  $\text{KMnF}_3$  and  $\text{MnS}$ .

During the last quarter, measurements have been stopped in order to install 9 evacuated flight paths moving inside a shielded room.

#### 4. Joint Research by CEN and BCMN on Fission Cross Sections.

A joint program of research of CEN and BCMN was started in 1966 and has been pursued in 1967.

The measurements are reported elsewhere in this Report, under the following heading :

##### Fission in the Resonance Region:

2.1. Normalization of relative  $^{235}\text{U}$  fission cross-sections in the resonance region.

2.2. Ratio of Binary-to-Ternary Fission in  $^{235}\text{U}$ .

#### 5. Properties of $^{235m}\text{U}$ .

M. NEVE de MEVERGNIES and P. del MARMOL

The possibility of measuring the fission cross section of  $^{235m}\text{U}$  ( $1/2^+$ ) has been investigated. This isomeric state is fed by the  $\alpha$ -decay of  $^{239}\text{Pu}$ , so a  $^{235m}\text{U}$  source can be prepared, using a catcher foil to collect the recoils from a thin  $^{239}\text{Pu}$  layer. Preliminary estimates show that by subsequent irradiation of such a  $^{235m}\text{U}$  source, in contact with a Makrofol fission track detector, in a thermal flux of about  $5 \cdot 10^{14} \text{ n/cm}^2 \text{ s.}$ , the fission cross section of this isomer could be measured if it is of the order of or larger than about 500 b. These measurements are underway. As the isomer decays to the  $^{235}\text{U}$  ground state by a 25 eV-transition fully converted in the P and Q layers, a study of the chemical or "environmental

effect on the half-life of  $^{235m}U$  ( $T_{1/2} = 26\text{min}$ ) has been undertaken.

Preliminary results indicate a very large effect, amounting to about 6% between two extreme cases.

## 6. Integral cross sections measurements and nuclear data related to reactors.

### 6.1. Evaluation of nuclear data for activation detectors.

A. FABRY, P.P. DAMLE, D.LANGELA, H. VANDENBROECK

The application of the spectral index technique in thermal and fast reactors requires an accurate description of differential energy cross section for activation detectors.

Excellent papers have been published on nuclear data related to fissile and structural materials considered in reactor calculations, but no counterpart seems to exist for activation detectors, except in the case of threshold reactions. A systematic compilation and evaluation effort has therefore been undertaken to fulfill the requirement, in close connection with reactor physics programmes. The report Blg 421 [1] presents recommendations for the reactions :  $^{164}\text{Dy}(n, \nu)^{165g}\text{Dy}$ ,  $^{151}\text{Eu}(n, \nu)^{152m}\text{Eu}$ ,  $^{176}\text{Lu}(n, \nu)^{177g}\text{Lu}$ ,  $^{191}\text{Ir}(n, \nu)^{192g}\text{Ir}$ ,  $^{193}\text{Ir}(n, \nu)^{194g}\text{Ir}$ ,  $^{115}\text{In}(n, \nu)^{116m}\text{In}$ ,  $^{197}\text{Au}(n, \nu)^{198}\text{Au}$ ,  $^{175}\text{Lu}(n, \nu)^{176m}\text{Lu}$  and  $^{186}\text{W}(n, \nu)^{187}\text{W}$  in view of their use in thermal reactors (energy below about 50 eV).

A further paper [2] soon to be published gives both differential and multigroup recommended cross section sets for the reactions  $^{115}\text{In}(n, \nu)^{116m}\text{In}$ ,  $^{197}\text{Au}(n, \nu)^{198}\text{Au}$ ,  $^{186}\text{W}(n, \nu)^{187}\text{W}$ ,  $^{139}\text{La}(n, \nu)^{140}\text{La}$ ,  $^{55}\text{Mn}(n, \nu)^{56}\text{Mn}$ ,  $^{198}\text{Pt}(n, \nu)^{199g}\text{Pt}$  and  $^{63}\text{Cu}(n, \nu)^{64}\text{Cu}$  over the whole neutron energy range 0,001 eV - 10 MeV for the application in fast reactor spectra.

6.2. Activation cross section measurements in the uranium-235 thermal fission neutron spectrum.

A. FABRY

This study has led to a publication [3] whose abstract follows :

"Absolute measurements of fission-spectrum averaged cross sections for a few threshold and capture reactions have been performed by the activation technique under experimentally controlled conditions of neutron background. These measurements indicate, in agreement with other integral studies reported recently at Los Alamos [4], that the uranium-235 thermal fission neutron spectrum is significantly harder than according to differential data based on n-p scattering"

Table 1 compares the measured absolute average fission spectrum cross sections with the values computed by weighting the best differential energy cross sections with two representations of the uranium-235 fission neutron spectrum.

The method developed in that paper has been further refined and is being applied to systematic measurements of average capture cross sections for a number of nuclides, with the aim to supersede older unreliable data [5][6], to renormalize or complete differential measurements and to compare with the statistical model of nuclear reactions.

6.3. Use of intermediate standard neutron spectra for the improvement of nuclear data basic to fast reactors.

A. FABRY, P. VANDEPLAS

The main idea in that project is to generate intermediate non  $1/E$  standard neutron spectra by selected interactions of fission spectrum neutrons with materials arranged in a one-dimensional geometry, the significant processes involving only nuclear reactions which are considered as

standard for differential energy cross section measurements [7], in such a way that the resulting neutron spectra can be predicted accurately by sophisticated transport calculations.

In addition to their use for a standardization effort of in-pile neutron spectrometry techniques, these spectra make possible interesting contributions to the improvement of nuclear data for fast reactors.

This is developed in a recent paper [8]; the abstract follows :

"The possibility of generating intermediate standard neutron spectra through partial moderation of the uranium-235 thermal fission spectrum within a cavity in a conventional thermal column has been investigated. Multigroup transport calculations on simple spherical arrangements of source and moderator have shown that a family of well predictable neutron spectra can be produced and that fast reactor spectra are sufficiently well simulated, in the useful energy range.

A highly flexible mock-up of such a system has been realized in a spherical cavity hollowed out of the protruding end of the graphite thermal column of the BR1 reactor.

Preliminary measurements by the activation technique are compared with theory.

It is shown that the device can be used as a tool for better assessment of neutron spectrometry techniques and for accurate integral testing of basic nuclear data. Attention is finally drawn upon a modified version of the spherical shell transmission technique, which will tentatively be applied to improve multigroup inelastic and capture cross section sets for some important materials."

Table I : Average fission spectrum cross sections (mb.)

Reaction	Measured	Computed		Reference for preferred differential energy cross section
		WATT's analytical description [a]	GRUNDL's multigroup fit. [b]	
$^{197}\text{Au}(n,\gamma)^{198}\text{Au}$	74 $\pm$ 3	89 $\pm$ 7	82 $\pm$ 7	PONITZ 1966, 67 below 1 MeV [c] GRENCHE 1966 above 1 MeV [d]
$^{115}\text{In}(n,\gamma)^{116m}\text{In}$	122 $\pm$ 6	136 $\pm$ 11	128 $\pm$ 10	GRENCH 1967 [e]
$^{115}\text{In}(n,n')$ $^{155m}\text{In}$	200 $\pm$ 10	182 $\pm$ 20	201 $\pm$ 21	GRENCH 1967 [e]
$^{32}\text{S} (n,p) ^{32}\text{P}$	74 $\pm$ 3	67 $\pm$ 7	79 $\pm$ 8	LISKIEN 1967 [f]
$^{27}\text{Al}(n,\alpha)^{24}\text{Na}$	0,78 $\pm$ 0,03	0,68 $\pm$ 0,04	0,76 $\pm$ 0,05	LISKIEN 1967 [f]

References for Table I :

- [a] WATT B.E. (1952) Phys. Rev. 87, 1037
- [b] GRUNDL J.A. (1967) to be published in Nucl. Sci. Eng.
- [c] PONITZ W. (1966) Report KFK 454  
PONITZ W. (1967) Report KFK
- [d] GRENCHE H.A. et al. (1966) Report WASH - 1068
- [e] GRENCHE H.A. et al. (1967) Report WASH - 1071
- [f] LISKIEN H. (1967) IAEA Panel on "Nuclear Standards needed for Neutron Cross-Section Measurements" Brussels, May. To be published.

6.4. Method for measurement of in-pile neutron angular distributions and check of the differential neutron cross sections of the  $^{6}\text{Li}(\text{n},\text{t})^{4}\text{He}$  reaction relative to a narrow neutron energy group.

G. and S. DE LEEUW

A method for the measurement of the neutron angular distribution in-pile has been described in paper SM 101-45 of the "Symposium on Fast Reactor Physics and Related Safety Problems" at Karlsruhe in November 1967.

In an isotropic neutron flux, this method based on the simultaneous measurement, by means of solid state detectors, of the  $E_t$  and  $E_\alpha + E_t$  spectra relative to the collimated particles, allows also the determination of the differential neutron cross sections. The cross section is deduced from the measured monoenergetic triton distribution. The definition of the neutron energy, selected in the  $E_\alpha + E_t$  spectrum by means of a single channel, depends on the window width of the channel and the resolution of the spectrometer.

The optimal resolution obtainable till now being 60 keV (FWHM of the thermal peak) the determination of the angular differential neutron cross section is only possible in the high energy region (above about 500 keV), below only a check of the existing ones makes sense.

References for §. 6.

- [1] P.P. DAMLE, A. FABRY, H. VANDENBROECK (1967) Report Blg 421 in print
- [2] A. FABRY, D. LANGELA (1967) To be published.
- [3] A. FABRY (1967) Nukleonik 10 Bd., Heft 5, 280 - 282
- [4] J.A. GRUNDL (1967) To be published in Nucl. Sci. Eng.
- [5] D.J. HUGHES, W.D. SPATZ, N. GOLDSTEIN (1953) Phys. Rev. 91, 1423
- [6] A.A. DRUZHININ, A.A. LBOV, P.P. BILIBIN (1967) Sov. Journ. Nucl. Phys. Vol. 4 n° 3, 366
- [7] IAEA Panel on "Nuclear Standards needed for Neutron Cross Section Measurements" Brussels, May 1967. To be published.
- [8] A. FABRY, P. VANDEPLAS (1967) IAEA symposium on "Fast Reactor Physics and Related Safety Problems" Paper SM-101/25 (Karlsruhe 30 October - 3 November).

XXII. Central Bureau for Nuclear Measurements, EURATOM,  
Geel (Belgium)

1. 3 MeV Van de Graaff Accelerator

1.1. Measurement of Neutron Fluxes

H. Liskien, A. Pauisen

For the study on fast neutron flux density standards the following detectors are now available:

a) An Associated Particle Counting Set-Up

Particle identification is carried out with a solid state detector, (sensitive to E), an electro-static analyser (sensitive to Z/E) and with time-of-flight measurements (sensitive to M/E) (E = kinetic energy; Z = charge; M = mass).

b) A Recoil Proton Telescope

Discrepancies detected this year gave rise to a re-determination of the hydrogen content of thin radiator foils and to a study of their long time behaviour.

c) A Methane Filled Proportional Counter

A cross-check between our counter and a similar one lent from Aldermaston was carried out. The computer programs WALL END and FITPRO A needed for the flux evaluation are running. The aim is to achieve an accuracy of better than  $\pm 3\%$  in the application ranges of the different counters. Possible cross-checks between the different methods at some fixed neutron energies may be seen from the following table. Cross-checks already carried out are indicated by arrows.

Neutron energy	reaction	ass.part. meth.	teles- cope	prop. counter
0.5 MeV	T(p,n) <sup>3</sup> He	X		X
1.0 MeV	T(p,n) <sup>3</sup> He	X	<----->	X
2.0 MeV	D(d,n) <sup>3</sup> He/ T(p,n) <sup>3</sup> He		X	X<----> X
5.0 MeV	D(d,n) <sup>3</sup> He	X		X
15.0 MeV	T(d,n) <sup>4</sup> He	X	<---->X	

In addition a solid state proton-recoil counter (as suggested by G. Dearnaley) was bought from Aldermaston. Tests for the counter itself and the corresponding computer programs for flux evaluation are running. Furtheron a new proportional counter for the use of pure hydrogen as counting gas and a new proton-recoil counter which is essentially based on the well-known "Perlow" counter were constructed and tested.

1.2. Cross Sections for Neutron Induced Threshold Reactions

H. Liskien, A. Paulsen

Measurements of the excitation functions for the reactions  $^{93}\text{Nb}(n,2n)^{92}\text{Nb}$  and  $^{103}\text{Rh}(n,2n)^{102}\text{Rh}$  are prepared. Measurements of absolute cross sections for the reactions  $^{31}\text{P}(n,p)^{31}\text{Si}$ ,  $^{32}\text{S}(n,p)^{32}\text{P}$ ,  $^{58}\text{Ni}(n,p)^{58}\text{Co}$  and  $^{64}\text{Zn}(n,p)^{64}\text{Cu}$ , for which relative values were already published, will be performed when the flux standard program has been carried out.

Supplement sheets for the compilation EUR 119.e Vol.2 were prepared and are in press. Also the older contents of this compilation were brought up to date with respect to all included reactions.[1][2][3][4]

1.3. Scattering Measurements

M. Coppola, H.H. Knitter

1.3.1. On  $^6\text{Li}$

The evaluation of the final absolute differential and total elastic scattering cross sections of  $^6\text{Li}$  in the energy range from 1.0 to 2.3 MeV was completed.

Fig. 1 shows the total elastic scattering cross section in comparison with measurements of other authors [5].

1.3.2. On  $^7\text{Li}$

The evaluation of the final absolute neutron differential elastic and inelastic scattering cross sections of  $^7\text{Li}$  in the energy range between 1.12 and 2.30 MeV

is made. The total and the total inelastic cross sections are calculated from the experimental results and are shown in figs. 2 and 3.

### 1.3.3. On Natural Silicon

At the end of 1966, angular distributions of neutrons elastically and inelastically scattered by natural silicon were measured at eight energies between 4.00 and 5.75 MeV. The final absolute neutron differential elastic and inelastic ( $Q = 1.77$  MeV) scattering cross sections were evaluated. At the highest primary neutron energy of 5.75 MeV also the cross sections for neutron differential inelastic scattering leading to the second ( $Q = 4.61$  MeV) and to the third ( $Q = 4.97$  MeV) excited states of the  $^{28}\text{Si}$  nucleus were extracted from the measurements [6]

### 1.3.4. Neutron Angular Distributions from the $^{14}\text{C}(\text{d},\text{n})^{15}\text{N}$ and $^{15}\text{N}(\text{d},\text{n})^{16}\text{O}$ Reactions [7]

A typical time-of-flight spectrum for the reaction  $^{14}\text{C}(\text{d},\text{n})^{15}\text{N}$  is shown in fig. 4.

### 1.3.5. On Carbon

Since the total cross section of Carbon is a monotonic function of the neutron energy below 2.0 MeV and since only neutron elastic scattering is possible in the same energy region, the differential neutron scattering cross section of Carbon is especially well suited as a standard for neutron scattering in this region. For this reason accurate determination of the differential elastic scattering cross sections is necessary. So far angular distributions at eight primary neutron energies between 0.8 and 1.5 MeV were measured. Up to now at each energy, measurements were taken between  $20^\circ$  and  $150^\circ$  in angle steps of  $10^\circ$ .

### 1.3.6. On $^{239}\text{Pu}$

A series of neutron scattering measurements on  $^{239}\text{Pu}$  were started at low primary neutron energies. For these experiments an especially developped "low threshold" neutron time-of-flight detector is in use. The detection threshold corresponds to a neutron energy of about 40 keV. For the evaluation of the neutron scattering cross sections it is necessary to subtract from the measured spectra the contribution of the fission neutrons. The fission spectrum was measured with primary neutron energies around 60 keV. So far angular distributions of neutrons from  $^{239}\text{Pu}$  have been measured at incoming energies of 0.4, 0.3 and 0.2 MeV.

### 1.3.7. Experimental Equipment

A detecting system consisting of four counters for simultaneous detection of neutrons scattered at different angles was brought into operation. So far only three counters were used for measuring neutron angular distributions, while the fourth was used as a neutron time-of-flight monitor. The general lay-out of the experimental arrangement is shown in fig. 5.

## 1.4. Ion Source Test Facility

K.H. Böckhoff, A. Crametz

The first stage of the 150 keV accelerator was put in operation. Protons of about 1 mA have been accelerated to 30 keV and sharply focussed onto a graphite target.

## 2. Linear Accelerator

### 2.1. Total Cross Sections

#### 2.1.1. Resonance Range

Total Cross Section of  $^{240}\text{Pu}$

K.H. Böckhoff, W. Kolar

The measurements and analysis of the neutron total

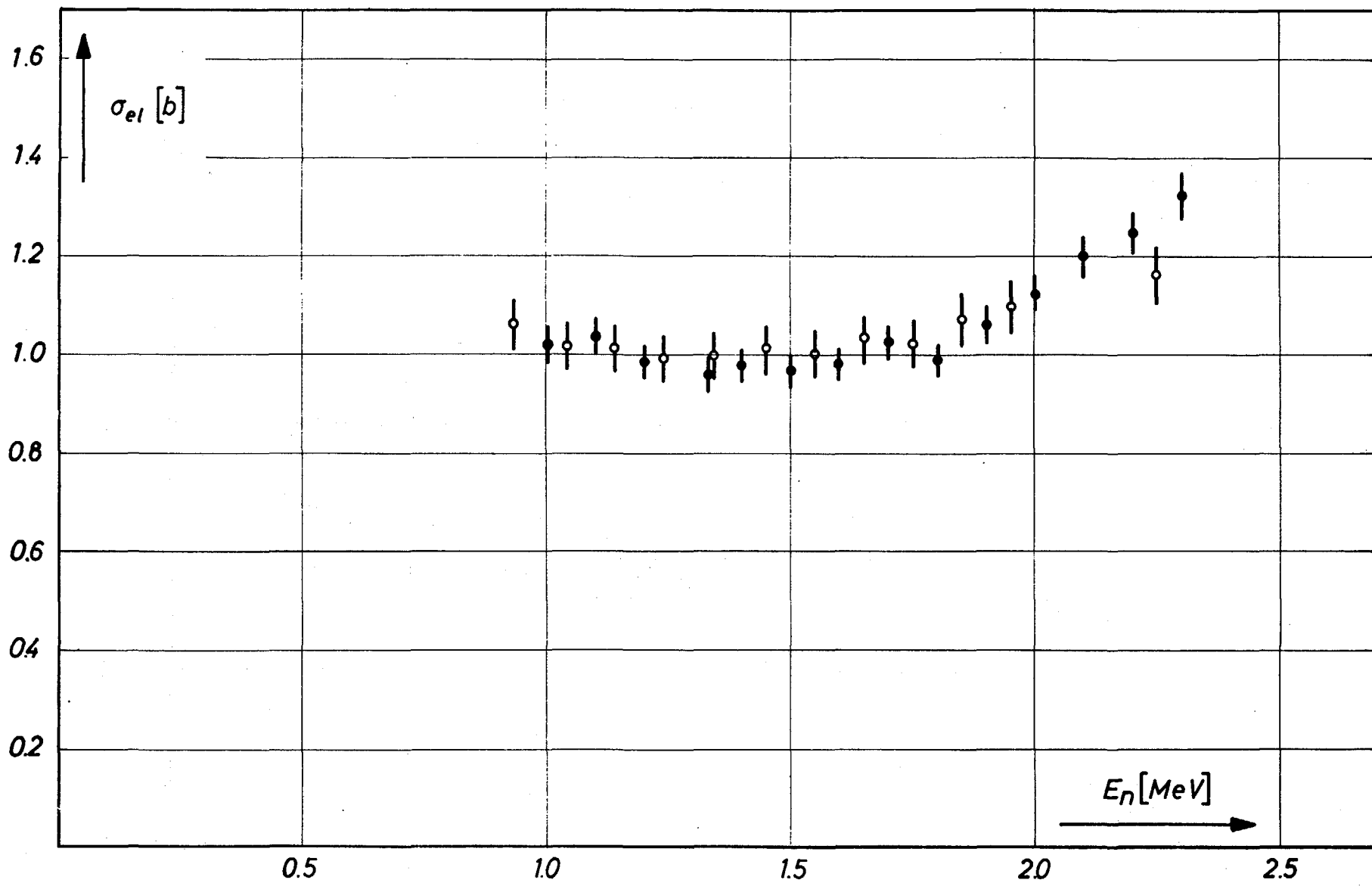


Fig.1 Integrated elastic cross sections.

- present work
- Lane et al. (6)

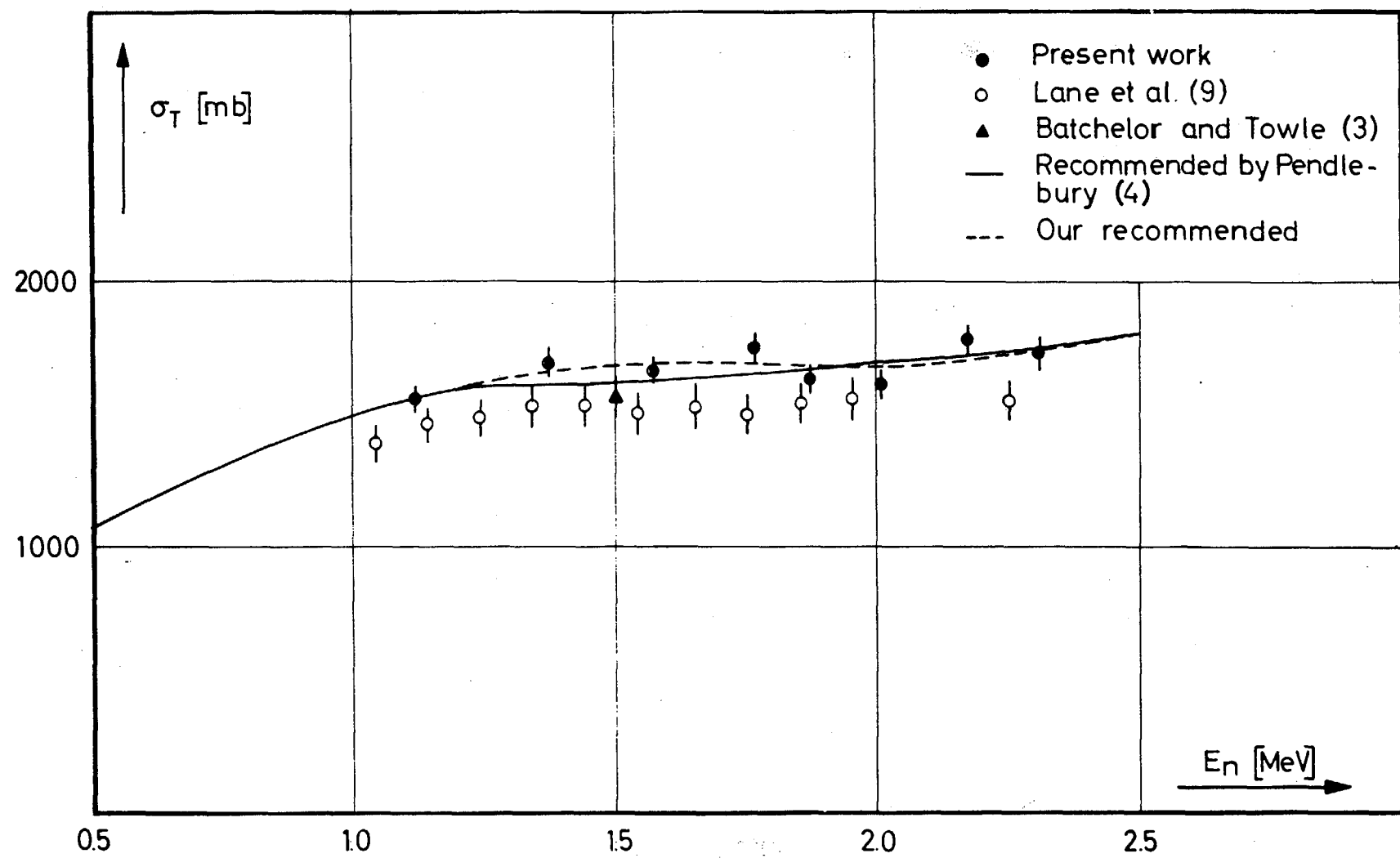


Fig. 2 Total neutron cross sections of  ${}^7\text{Li}$ .

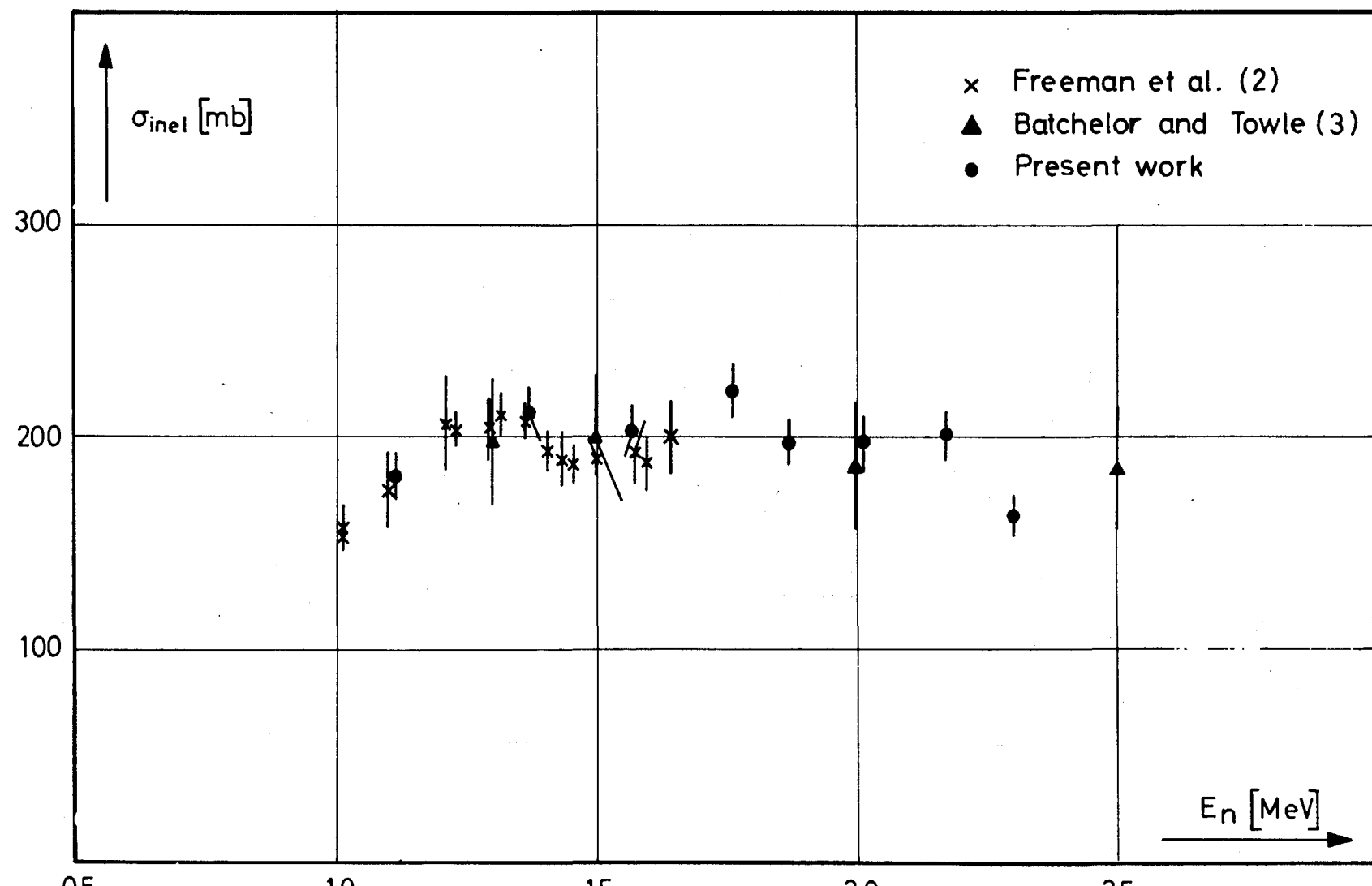


Fig.3 Integrated inelastic neutron scattering cross sections of  ${}^7\text{Li}$ .  $Q = -0.478 \text{ MeV}$ .

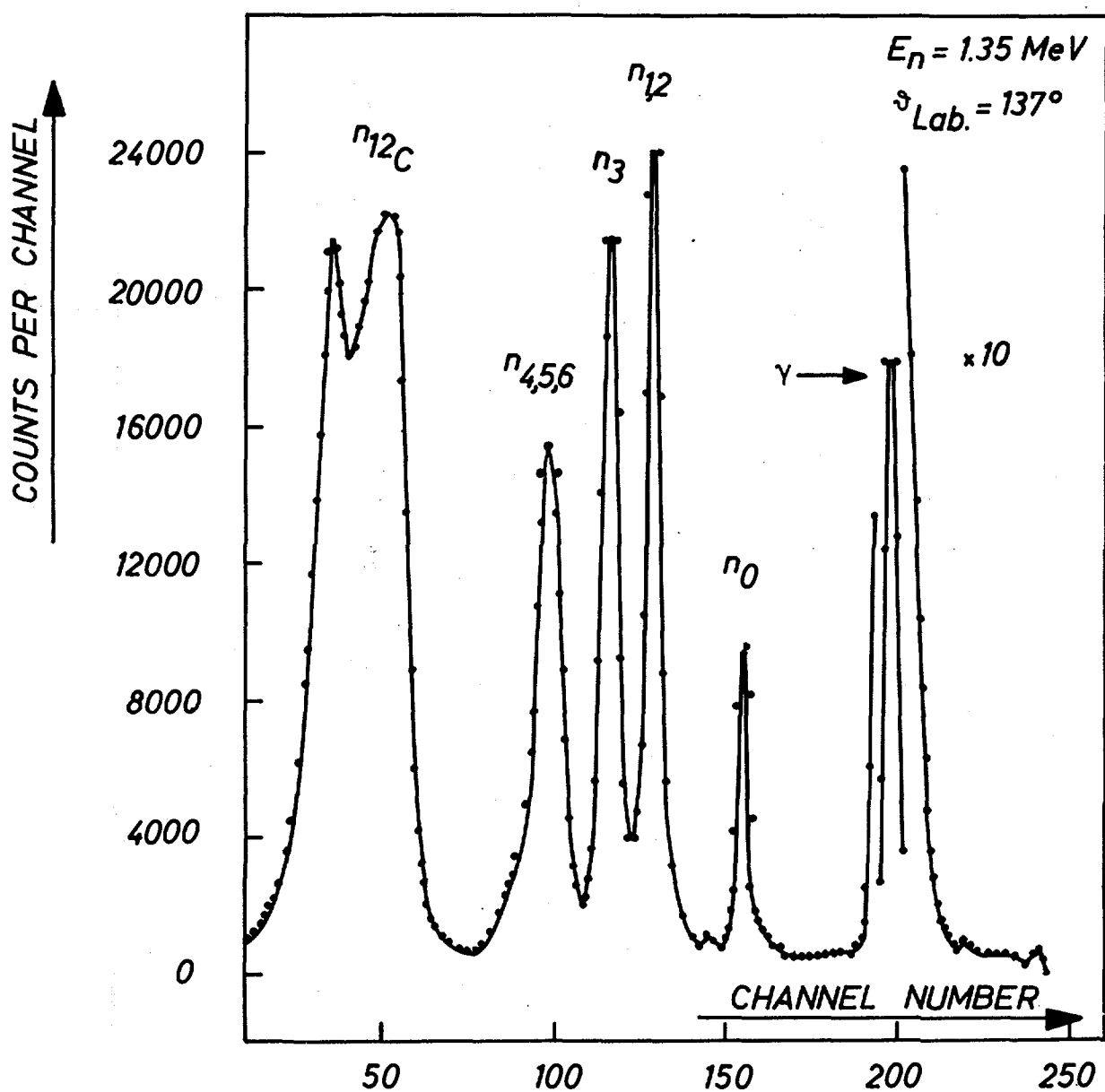


Fig. 4  $^{14}\text{C}(\text{d},\text{n})^{15}\text{N}$  reaction. Typical time-of-flight spectrum.

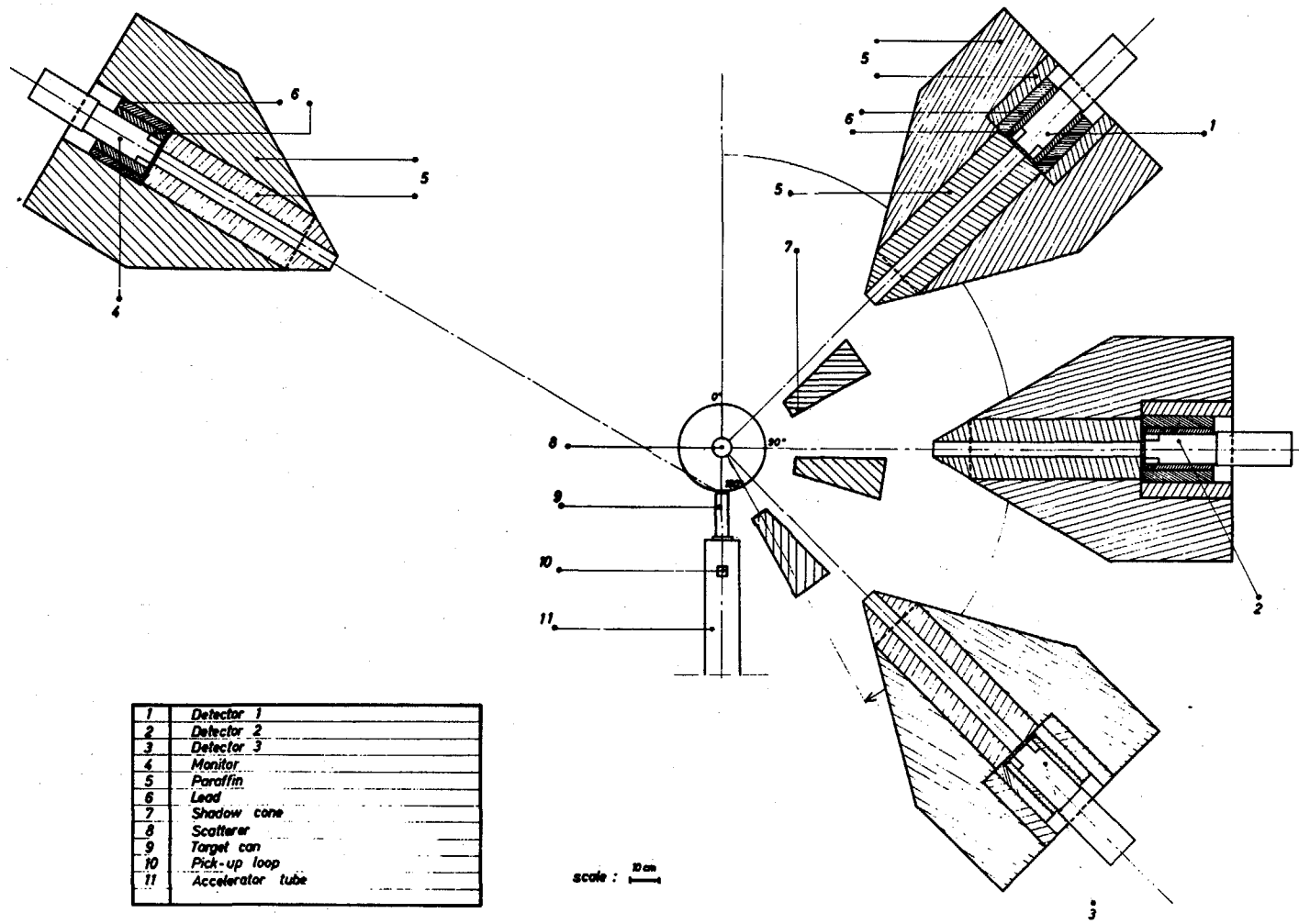


Fig.5 General lay-out of the experimental arrangement

cross section of  $^{240}\text{Pu}$  have been terminated. 264 resonances between 20 eV and 5.7 keV have been analysed with respect to  $\Gamma_n$  using the area analysis program of Atta and Harvey.

Combining the results of this transmission measurement with those of a capture experiment (see 2.7.1.), a full set of resonance parameters ( $E_0$ ,  $\Gamma_n$  and  $\Gamma_Y$ ) for 32 resonances between 38 eV and 820 eV has been determined. The first 100 resonances of the resolved resonance range (20 eV - 1500 eV) have been used to evaluate their statistical properties with the following results:[8][8a]

Mean level spacing:  $\langle D \rangle = 15.7 \pm 0.8$  eV

Mean reduced neutron width:  $\langle \Gamma_n^o \rangle = 1.54 \pm 0.22$  meV

S-wave strength function:  $S_0 = (1.05 \pm 0.16) \cdot 10^{-4}$

#### Total Cross Section of $^{233}\text{U}$

K.H. Böckhoff, G. Carraro, W. Kolar

This measurement was prepared, especially by testing a  $^6\text{Li}$ -glass detector. At low neutron energies this detector gives a 3 to 4 times higher response than the  $^{10}\text{B}$  detector. The signal-to-background ratio was the same in both cases up to energies of about 400 eV.

#### 2.1.2. High Energy Range ( $E_n > 200$ keV)

##### Total Cross Sections of C and Na

K.H. Böckhoff

The experimental set-up, described in the previous progress report, is now operating. The time of flight spectra from water- or mercury-cooled targets showed a structure, due to resonances of the stainless steel canning material (besides the one from oxygen for water-cooled ones). Air-cooled graphite targets produced no structure up to 2 MeV but the neutron yield was low. A tungsten target produced only a slight

structure at low energies with a higher neutron yield.

Low resolution transmission determinations have been carried out on carbon, together with a high-resolution one (45 ps/m), the latter with the W-target. This showed several very sharp resonances which seem not to be reported until now.

Another experiment with the W-target was carried out on Na. Also here some new very sharp resonances were observed. Data reduction and evaluation are in progress.

## 2.2. Fission Data

E. Migneco, J. Theobald

### 2.2.1. Fission Cross Section of $^{235}\text{U}$

The cross section of the  $^{235}\text{U}(\text{n},\text{f})$  reaction has been measured with a high energy resolution for neutrons between 6 eV and 3 keV. A fission fragment and a fission neutron detector were used simultaneously. The obtained  $\sigma_{n,f}$  values obtained are in good agreement with the data of Michaudon. The data obtained with the fission fragment detector agree within a few percent with the results of the fission neutron detector.

A fit of data with the single level formalism has been reached without assuming a contribution of residual fission. Resonance parameters for 78 levels between 6 and 150 eV could be determined. Their statistical properties can be summarized as follows:

- 1) A correlation between the  $\Gamma_f$  and  $\Gamma_\gamma$  values cannot be found.
- 2) The  $\chi^2$  distribution of  $\Gamma_f$  has a number  $v \approx 4$  of degrees for freedom. For the  $\Gamma_\gamma$  values we find  $v \approx 40$  for resonances below 50 eV and  $v \approx 30$  for resonances between 50 and 150 eV.
- 3) In the distribution of  $\alpha$  (the capture to fission ratio) we find a grouping of resonances with

$\langle\Gamma_f\rangle = 100$  meV below  $\alpha = 0.6$  and with  $\langle\Gamma_f\rangle = 27$  meV for  $\alpha$ -values higher than 1.0 [9].

#### 2.2.2. Subthreshold Fission Cross Section of $^{240}\text{Pu}$ [10]

The subthreshold neutron induced fission cross section of  $^{240}\text{Pu}$  has been measured with the fission neutron detector in the energy range between 200 eV and 9 keV. The resonance parameters have been determined with an area analysis program. The fission spectrum obtained shows a periodical appearance of clusters of resonances with particularly high fission widths (Fig. 6). This result is of special interest in relation to the theory of Strutinsky who introduces shell effects into nuclear deformation energies (Nucl. Phys. A95 (1967) 420-442).

#### 2.2.3. Fission Cross Section of $^{233}\text{U}$

The measurement of this fission cross section is being prepared with a spark chamber as fragment- and the liquid scintillator as neutron-detector. The spark chamber detector for fission fragment detection of highly  $\alpha$ -active fissile isotopes consists of six wire-to-plate chambers ( $20 \times 20 \text{ cm}^2$ ). Nitrogen circulates at a pressure of 250 Torr.

#### 2.3. $\gamma$ -Measurement and Determination of Neutron Multiplicities

The mechanical construction of a large liquid scintillator tank is ready. The realisation of a heavy shield for this detector is continuing.

#### 2.4. Normalization of Relative $^{235}\text{U}$ Fission Cross-Sections in the Resonance Region

A.J. Deruytter (CBNM), C. Wagemans\*

These measurements are carried out at the CBNM linac by a joint CBNM-SCK-team with the view to extend the

\* Belgian research fellow NFWO (University of Gent)

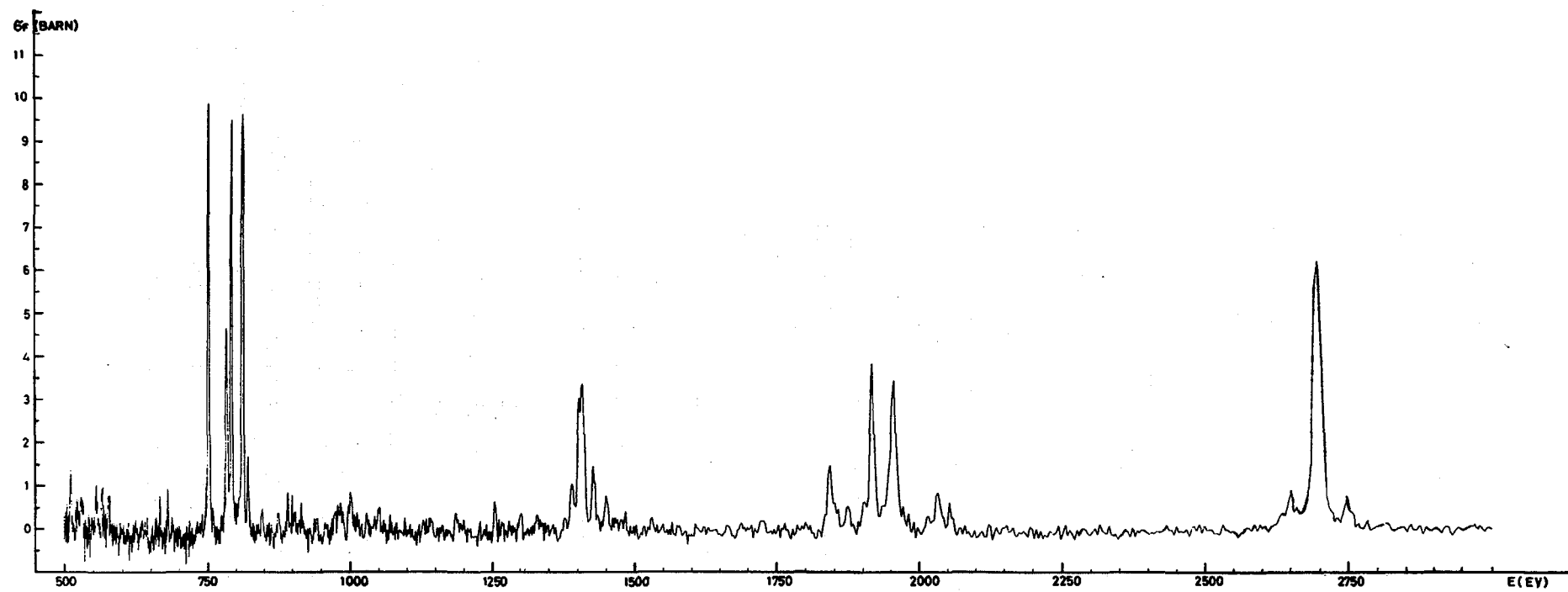


Fig.6 Subthreshold fission cross section of neutron induced fission of  $^{240}\text{Pu}$

Linac fission cross-sections down to below thermal energy for a direct normalisation to the absolute 2200 m/s reference cross-section. A well-collimated short flight-path (about 8 meter) with low repetition rate (50 c/s) and long burst time (2  $\mu$ sec) of the Linac is used. Also a run at 10 c/s was performed to check the influence in the low energy-region of overlap neutrons. The comparison of the induced reaction-rates in a back-to-back  $^{235}\text{U}$ - and  $^{10}\text{B}$ -foil is made simultaneously with two sets of solid-state detectors and registered in two halves of a 4096 channels time-of-flight analyser. Based on the normalisation at 2200 m/s a few resonance integrals will be later calculated.

## 2.5. Scattering Cross Sections

E. Migneco, J. Theobald

### Scattering Cross Section of $^{240}\text{Pu}$

A scattering cross section measurement on  $^{240}\text{Pu}$  has been performed between 18 eV and 3 keV [11]. A  $^{10}\text{B}$ -loaded liquid scintillator has been used as detector for scattered neutrons with a pulse shape discriminator against  $\gamma$ -rays. Fig. 7 shows a time-of-flight spectrum of the scattering yield. The analysis of the resonance parameters is under way.

### Other Measurements

Measurements of the scattering cross section on Cu, Nd and Hf relatively to Pb are in preparation. For determination of the scattering cross section of fissile isotopes a big scintillator tank, to be used as an anti-fission detector, has been constructed and the shielding is going to be built. The  $^{10}\text{B}$ -loaded liquid scintillator for the scattered neutron detection has been successfully tested during the  $^{240}\text{Pu}$  scattering experiment.

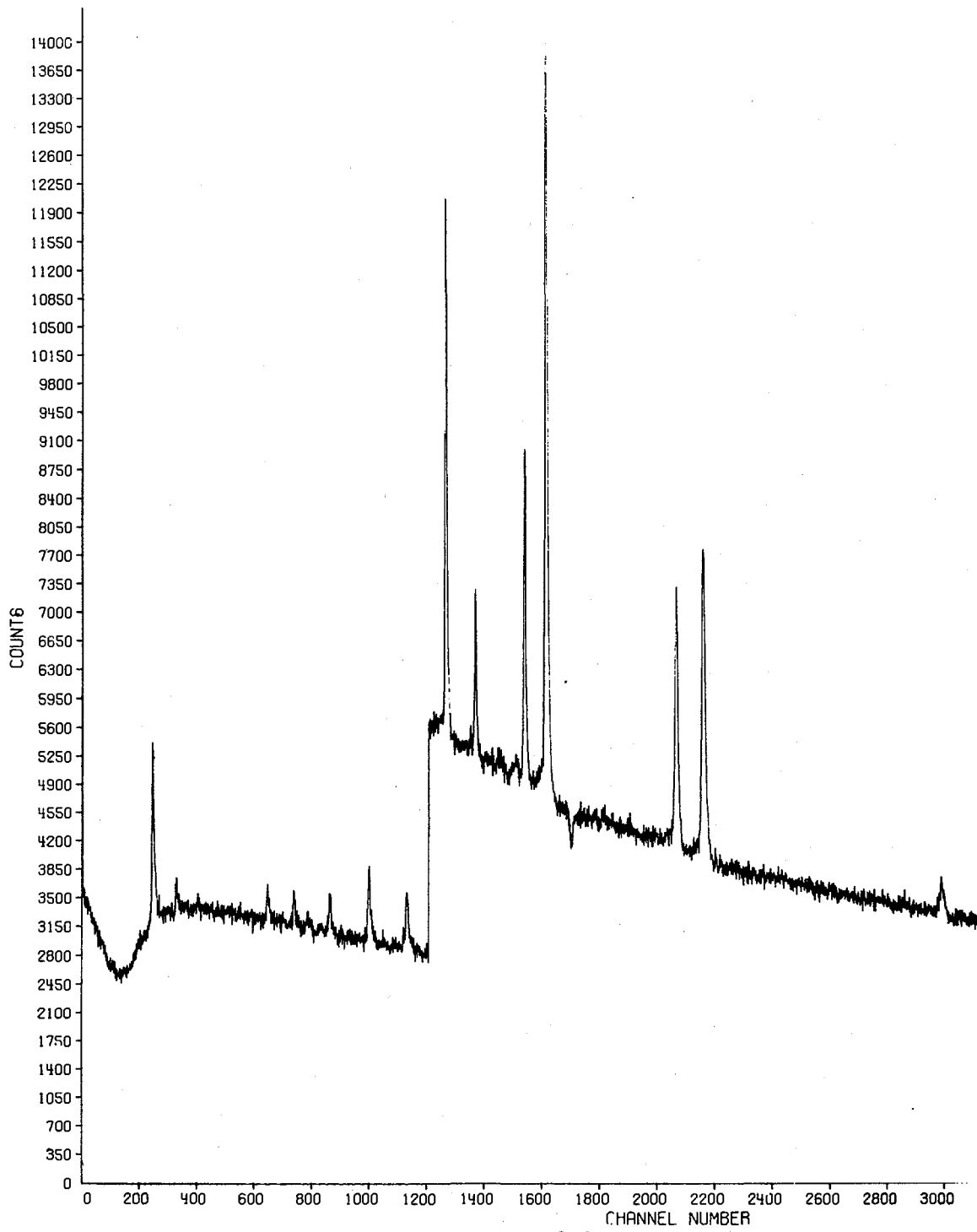


Fig. 7 Time of flight spectrum of the  $^{240}\text{Pu}$  scattering experiment (20-300 eV)

## 2.6. Neutron Capture Cross Sections

H. Weigmann, J. Winter

### 2.6.1. Capture Cross Sections

The detector [12] for neutron capture cross section measurements which was described in the last Annual Progress Report has been used for measurements on natural Mo,  $^{240}\text{Pu}$ , natural Cu, and natural Nd.

#### Measurements on Natural Mo

Data for natural Mo have been obtained in the neutron energy range from 10 eV to 25 keV [13]. An area analysis which contains a Monte-Carlo subroutine to calculate the multiple scattering contribution to the capture areas, has been applied to resonances with known isotopic assignment; it yields  $g\Gamma_n$  for small resonances and  $\Gamma_\gamma$  for large ones. Above 1 keV neutron energy, the observed capture rate has been averaged to give the mean capture cross section which is in good agreement with earlier measurements. For the final attribution and analysis of some resonances to specific isotopes of Mo, measurements on separated isotopes are planned.

#### Measurements on $^{240}\text{Pu}$

Neutron radiative capture in  $^{240}\text{Pu}$  has been studied in the neutron energy range from 38 eV to 820 eV [14]. The resonance area analysis of the capture data has been combined with the transmission area analysis (see above) to obtain the resonance parameters. The radiative widths of 32 resonances have been determined yielding a mean value of  $\langle\Gamma_\gamma\rangle = (23.2 \pm 2.0)$  meV. The observation of unusual large radiative widths for some resonances at the upper limit of the analysed energy range has been interpreted as being due to the presence of subthreshold fission in these resonances. This interpretation has been confirmed in a measure-

ment of the subthreshold fission cross section with the aid of a fission neutron detector of Migneco and Theobald (see 2.2.).

#### Other Measurements

Data on neutron capture in Cu and Nd have been collected. The analysis of the Cu data between 200 eV and 16.5 keV is under way.

#### 2.7. Standard Data [15][16][17]

##### 2.7.1. Cross Section Ratio $^{10}\text{B}(n,\alpha)$ to $^6\text{Li}(n,\alpha)$ between 1 keV and 50 keV

E. Migneco, J. Theobald

The experimental set-up consists of an eight meter long collimated flight path. The neutron beam is collimated down to 15 cm by water and boron-carbide and to 5.5 cm by a sequence of boron-carbide loaded plastic hollow cylinders. A precisely known sample of  $^{10}\text{B}$  and  $^6\text{Li}$  is to be placed into a sample changer in the neutron beam. The outgoing particles are detected by 4 Si surface barrier detectors of  $500 \text{ mm}^2$  each. The different parts of the detection system have been installed in the flight-path and tested. Up to now the  $\gamma$ -flash from the linac target induces in the detectors pulses, which have a time- and amplitude dependence different from what we have expected. This limits at the moment our useful energy range to values lower than the zone of interest.

##### 2.7.2. Shape of the $^{10}\text{B}(n\alpha,\gamma)$ Cross Section in the Energy Range 1 to 100 keV

K.H. Böckhoff

A feasibility study is being prepared about the measurement of  $\sigma_{n,\alpha\gamma}(E)/\sigma_{n,\alpha\gamma}(E')$ , where  $E' = \frac{1}{9} E$ . The different energies can be obtained by using neutrons scattered from the linac beam by a hydrogenous foil under two different angles. The method

is flux-independent and yields the relative shape of the  $^{10}\text{B}(\text{n},\alpha_0\gamma)$  cross section. This could be normalized to absolute values at the low energy end where the capture cross section is known to be  $1/v$  and by direct methods at the higher energy end (proton recoil counters).

## 2.8. Spin Determinations

### 2.8.1. Spin Measurements of Fissile Nuclei

A.J. Deruytter, C. Wagemans<sup>+</sup>, C. Furetta<sup>++</sup>

A measurement was made of the ratio of binary fission to ternary fission (two heavy fragments and a long-range particle) in  $^{235}\text{U}$  at the CBNM linac with a flight-path of 8 meter length. The useful energy-range extends from 0.18 eV to 21 eV. The time-of-flight-spectra are recorded with and without a 20  $\mu$  thick aluminium absorber between target and detectors. The target is a layer of  $2 \text{ mg/cm}^2$ , 99.5%  $^{235}\text{U}$  on both sides of a thin aluminium support (0.5 mm thick). On each side a bank of surface-barrier detectors (Au-Si) detects the fission fragment (no absorber) or the long-range particles (absorber in). The ratio of the surfaces of the resonances in both measurements was taken. Fluctuations from resonance to resonance are seen. The sign of the fluctuations is in agreement with the results of Michaudon et al. (Saclay).

### 2.8.2. Spin Assignments of Neutron Resonances of Stable Nuclides

G. Carraro, C. Coceva<sup>+++</sup>, F. Corvi<sup>+++</sup> and P. Giacobbe<sup>+++</sup>

The measurements are carried out by a joint CNEN-CBNM team. The experimental set-up outlined in the preceding progress report has been used and measurements

<sup>+</sup> Belgian research fellow NFWO (University of Gent)

<sup>++</sup> Euratom research fellow

<sup>+++</sup> CNEN, Italy

have been performed on natural samples of Pd, Ru, Mo and Hf. For Pd, Ru and Mo capture gamma-ray spectra have been observed to select the resonances due to odd nuclei. The resonance peaks in time-of-flight spectra of singles and coincidences have been analysed by measuring their integral or partial areas. In the more complicated case of Hf, the known parameters have been used to obtain with a best fit procedure the relative strength of the resonances. To this end our shape analysis program has been modified to take into account multiple scattering effects. The spin could be assigned to 50 resonances of  $^{105}\text{Pd}$ , 36 resonances of  $^{99,101}\text{Ru}$ , 24 resonances of  $^{95,97}\text{Mo}$  and 46 resonances of  $^{177}\text{Hf}$ . The assignments are listed in the following tables (I, II, III, IV).

## 2.9. Miscellaneous

### 2.9.1. Kinematics of Nuclear Reactions

M. Coppola, H. Horstmann, H.H. Knitter, H. Liskien, H. Schmid, J. Winter

Several calculations have been performed on the kinematics of nuclear reactions, especially for the production of monoenergetic neutrons [18] and of the non-relativistic [19] and relativistic [20] parameters of nuclear reactions.

### 2.9.2. Instrumentation of Analog Signals and Analog-to-Digital Conversions; Pulse Height Converter

H. Verelst, H. Meyer

A servostabilized pulse height converter of great linearity, stability and speed, especially useful for precision  $\gamma$ -spectroscopy with germanium detectors was developed. Because of the analog controlled sliding energy window foreseen, the system allows to measure also high energy  $\gamma$ -spectra with high resolution, if small memories are used for storage. In such a case

Table I

Spin assignment of  $^{105}\text{Pd}$  resonances

$E_0$ (eV)	J	$E_0$ (eV)	J
55.23	3	377.36	2
68.27	3	389.2	3
77.73	2	401.7	3
86.68	3	431.1	2
104.04	3	449.6	3
126.29	3	466.7	2
134.17	3	532.2	3
141.18	2	547.2	3
150.06	2	568.0	2
154.70	3	578.7	3
158.74	2	591.0	3
168.29	3	593.3	2
184.02	2	605.1	3
202.58	2	621.0	3
226.99	3	663.0	2
252.20	2	682.4	3
252.80	3	696.8	3
260.13	2	700.4	2
287.04	3	712.1	3
305.40	2	724.4	3
313.64	2	757.2	3
327.86	3	780.4	3
347.07	3	789.3	2
354.40	3	794.3	3
370.54	2	807.8	2

Table II  
Spin assignment of  $^{99}\text{Ru}$  and  $^{101}\text{Ru}$  resonances

$E_0$ (eV)	Isot.	J	$E_0$ (eV)	Isot.	J
25.22	99	3	262.70	99	3
42.28	101	3	311.06	101	2
52.13	101	3	313.61	101	3
57.11	99	3	325.17	101	3
61.81	101	2	334.6	99	3
66.82	101	2	336.87	101	2
81.62	99	2	342.17	99	2
100.15	101	3	346.21	101	2
104.09	99	3	378.3	101	3
112.51	101	2	401.6	99	3
141.13	101	3	411.6	101	2
154.30	99	3	426.8	101	2
157.04	101	2	433.8	101	3
197.27	101	3	456.8	101	2
198.86	99	2	462.2	101	3
218.39	99	3	485.2	101	2
243.90	101	3	509.7	99	3
251.46	101	2	538.7	101	2

Table III

Spin assignment of  $^{95}\text{Mo}$  and  $^{97}\text{Mo}$  resonances

$E_0$ (eV)	Isotope	J
45.1	95	3
70.8	97	2
117.9	95	2
159.3	95	3
227.4	97	3
267.9	97	3
311.8	97	3
358.4	95	3
380.7	odd	2
396.9	97	3
554.3	95	2
557.9	97	3
661.5	odd	3
680.5	95	3
770	95	3
786	97	3
862	odd	2
899	95	2
981	odd	2
1025	95	3
1134	odd	2
1145	95	2
1204	odd	3
1250	97	3

Table IV

Spin assignment of  $^{177}\text{Hf}$  resonances

$E_0$ (eV)	J	$E_0$ (eV)	J
1.100	3	59.28	3
2.381	4	62.19	3
5.909	3	63.50	4
6.596	4	71.38	4
8.889	4	76.08	4
10.95	3	84.69	4
13.68	4	86.79	4
13.97	3	88.58	3
21.98	4	97.12	4
25.63	3	99.05	4
27.02	3	103.15	3
31.59	3	115.14	3
32.82	4	121.30	3
36.08	3	122.58	3
36.95	4	131.69	3
43.05	4	134.12	4
45.14	4	141.21	4
46.22	4	148.62	3
48.82	3	163.11	3
49.59	4	167.45	3
54.75	4	181.18	4
56.35	3	199.27	4
57.03	4	208.73	4

small conversion times also for the chosen ramp converter principle are possible. The conversion rate is 125 MHZ, i.e., for an analysis window with 1024 channels the mean converter processing time will be about 5  $\mu$ sec. With a laboratory model the minimum channel width is about  $2.5 \cdot 10^{-3}$  % of the maximum energy to be measured. Important characteristics of the converter are also the integral non-linearity ( $\leq \pm 0.02\%$ ) and the differential non-linearity ( $\leq \pm 1\%$ ). The regulation loop of the servostabilized converter includes the amplifier-chain connected to a detector; the overall system stability is determined by two reference pulse generators for gain and threshold regulation which were developed for that purpose (stability, better 0.01% of maximum pulse amplitude over a temperature range of about 10° C).

### 3. Thermal Neutron Data

A.J. Deruytter, P. Pelfer<sup>+</sup>, C. Furetta<sup>+</sup>

The following measurements were carried out by a CBNM-team using the SCK-chopper at the BR2-reactor.

#### 3.1. Intercomparison of Boron Foils

Several layers of natural boron have been intercompared. A computer program has been written for the deduction from the recorded spectra of: (1) the counting-rate per monitor-count, (2) the peak positions (with standard deviations) of the  $\alpha_0$ - and  $\alpha_1$ -particles of the  $^{10}\text{B}(n,\alpha_0)^7\text{Li}$  and  $^{10}\text{B}(n,\alpha_1\gamma)^7\text{Li}$ , (3) the width of the  $\alpha_1$ -peak with standard deviation. From these characteristics a detailed comparison of the amount of  $^{10}\text{B}$  in the layer and of the layer quality (homogeneity, chemical impurities) is possible. Measurements are made with a 1 cm<sup>2</sup> beam and a 5 cm diameter beam (whole target irradiation) and compared as a check for the

<sup>+</sup> Euratom Research Fellow

homogeneity of the layers. Satisfactory results (probably accurate within 0.3%) are found for the comparison of direct weighing in vacuum and relative neutron measurements for layer thicknesses between about 20 and 80  $\mu\text{g/cm}^2$ . These layers will be used as standards for fission cross-section measurements.

### 3.2. Intercomparison of Fissile Layers

The same equipment as used for the boron comparisons is used for the intercomparison of fissile layers. In this case the fission- and  $\alpha$ -particle pulse-height spectra are recorded with beam-on and beam-off. The fission- and  $\alpha$ -counting rates are deduced respectively per monitor count and per unit-time. The ratios of  $\alpha$ - and fission counting-rates can be compared. With non-homogeneous sources they may differ.

Measurements were performed on electro-sprayed uranyl-acetate sources and evaporated  $\text{UF}_4$ -layers made from NBS-930  $^{235}\text{U}$ -material and agreement was found within statistical errors proving their good homogeneity.

Another method to compare the quality of the foils from different preparation methods is to compare the fission spectrum characteristics of foils with the same thickness in the same geometry. A particularly sensitive parameter, e.g., is the ratio  $N_L / N_V$  of the light fragment peak counting-rate to the valley counting-rate. From these spectra also the low energy tailing can be evaluated and possible multiplication effects (at the high energy-side of the spectrum) of the surface-barrier detector used can be detected. They also enabled us to determine the limit thickness of applicability of the preparation methods to be more than 500  $\mu\text{g/cm}^2$  for electrosprayed and probably more than 1  $\text{mg/cm}^2$  for evaporated sources.

### 3.3. 2200 m/s Fission Cross-Sections

The boron standard foils and the evaporated  $^{235}\text{UF}_4$ -

layers have been intercompared and proved to be satisfactory. Also the electrosprayed  $^{239}\text{Pu}$ -foils are ready for measurement. With the slow chopper installed at BR 2 (tangential beam-hole T-7), the definitive comparison of  $\sigma_{n,f}$  of  $^{235}\text{U}$  and  $\sigma$  of  $^{10}\text{B}$  is started.

3.4. Comparison of Spontaneous Fission of  $^{240}\text{Pu}$  and Thermal Neutron Induced Fission of  $^{239}\text{Pu}$

In view of the set-up of similar experiments in the resonance region (Linac) a measurement is under way to compare the kinetic energies and mass-distributions of both fissioning systems - spontaneous fission of  $^{240}\text{Pu}$  and thermal neutron induced fission of  $^{239}\text{Pu}$  - for the study of the influence on these fission parameters of the difference in excitation energy of the same compound nucleus. A computer program was written to calculate the primary mass distributions and energy distributions from a two-dimensional experiment on the coincident fission fragments, registered event by event. The program was tested for the thermal neutron induced fission of  $^{235}\text{U}$ .

3.5. Miscellaneous

The results of a precise determination of the branching ratio and Q-value of the  $^{10}\text{B}(n,\alpha)^7\text{Li}$  reaction and of the Q-value of the  $^6\text{Li}(n,\alpha)^3\text{H}$  reaction, have been published [21]. Measurements of the  $\alpha$ -branchings in the decay of  $^{235}\text{U}$  are under way.

4. Data Handling

4.1. Data Handling Equipment, Computer and Teleprocessing System

A. De Keyser, H. Horstmann

The IBM 1401 computer has been used for checking, reducing, and analysing experimental cross section data, and for preparing data and analysis programs to be handled by the teleprocessing system Geel-Ispra.

The configuration of the IBM 1800 data acquisition and control system has been specified in detail. The IBM 1800 computer will replace the IBM 1401 at the beginning of 1968. The new computer system will allow for on-line data acquisition and supervisory control of the data collection process. Off-line problems can be treated in time-sharing. Suitable interface equipment is under construction.

#### 4.2. Data Analysis and Programming

M.G. Cao, H. Horstmann, G. Nastri, H. Schmid

##### 4.2.1. Reduction and Analysis of Fission and Scattering Cross Section Data

A set of IBM 1401 programs for the reduction of fission cross section data has been written [22]. These programs have been used to process data for  $^{235}\text{U}$  in the energy ranges 0.15 eV - 20 eV and 4 eV - 20 keV, and for  $^{240}\text{Pu}$  in the energy range 200 eV - 3 keV.  $^{240}\text{Pu}$  scattering cross section data in the range 20 eV - 1 keV have been processed.

A modified version of programs SMNF 032S (Saclay) for shape analysis of fission cross section data has been tested and used to determine resonance parameters of  $^{235}\text{U}$  in the energy range 6 - 150 eV.

The correlation coefficient between  $\Gamma_f$  and  $\Gamma_Y$  and the number of degrees of freedom in the Porter-Thomas distributions have been calculated with IBM 1401 programs.

Program GACA (General Atomic) for area analysis of capture cross section data has been modified to be used for fission data.

A program in French FORTRAN (Saclay) for multiple scattering and self-absorption corrections has been rewritten in FORTRAN II, V3 for the IBM 7090 computer.

Some modifications concerning the sample geometry have been made.

#### 4.2.2. Calculations Concerning the Differential Cross Section for Elastic Neutron Scattering

Two FORTRAN IV programs, BLATT-4 and ERRFIT, have been written. BLATT-4 performs a least squares fit of the Blatt and Biedenharn single level formula for the differential elastic scattering cross section. ERRFIT computes the error on the theoretical differential cross section calculated with resonance parameters obtained from BLATT-4 [23].

The program ELIESE-1 (JAERI-1096) has been modified in order to be used in a least squares method to fit the differential elastic neutron scattering cross section by means of optical model and Hauser-Feshbach calculations. The program is being tested.

#### 4.2.3. Multiple Scattering Corrections for Elastic and Inelastic Neutron Scattering Cross Section Data

Detailed tests of the programs MAGGIE and MOULD (Aldermaston) have been made. Several errors in MAGGIE concerning the score calculations have been corrected. MAGGIE has been completed by a subroutine which performs the correction of the measured inelastic neutron peaks for contamination by multiple elastic scatter. The iteration routine for the shape correction of measured elastic angular distribution has been extended to include the inelastic case. Calculations of flux attenuation factors, shape corrections for elastic and inelastic angular distributions, and special score calculations have been performed for Si (4.00 - 5.74 MeV) Polythene (4.00 - 4.78 MeV), and  $^{7}\text{Li}$  (1.10 - 2.30 MeV).

#### 4.2.4. Corrections for Measurements with Proton Recoil Counters

The programs WALLEND, FITPRO, and SERECO (Aldermaston) have been modified and partly corrected. WALLEND has been used on the IBM 7090 (360) for the calculation of the influence of wall- and end corrections for cylindrical counters on the measurement of proton recoil spectra.

With program FITPRO background and dead-time corrections of the experimental proton recoil spectra and comparisons between the corrected spectrum and the theoretical one obtained from WALLEND have been performed.

SERECO has been used for the calculation of geometrical corrections and energy degradation of recoil protons.

An IBM 7090 (360) program in FORTRAN IV for the calculation of complicated integrals for the flux of recoil protons has been written. The program is being tested.

#### 4.2.5. Total Cross Section Data Reduction in the High Energy Range

A FORTRAN program for data plotting, dead-time corrections, calculations of transmissions and total cross sections has been written and used to process carbon data.

#### 4.3. System Analysis and Programming

H. Horstmann, H. Schmid

##### 4.3.1. Programming of the IBM 1800

A system of on-line and off-line data analysis programs for the IBM 1800 is being written and tested. This system includes interrupt routines for digital data input, on-line data reduction and display functions, off-line calculations, a complete set of plotter routines, teleprocessing programs, and many general utility routines.

#### 4.3.2. Programming of the Calcomp Plotter 506

A report about the following programs has been written: an IBM 7090 subroutine PLOT, compatible with the CETIS plotter subroutine package, a translation program for magnetic tape plotter data, and a set of plotter subroutines for the IBM 1401 computer [24].

#### 4.4. Data Handling Instrumentation

F. Colling, B. Idzerda, H. Meyer, W. Stüber

##### 4.4.1. Data Storage Systems

The second data storage system for the recording and handling of time-of-flight and two-parameter spectra has been delivered to the Linac group for experiments.

##### 4.4.2. Data Reduction and Selection

A multirange, one-parameter conditioner [25] for data reduction by selection, integration and code conversion in connection with the handling of T-O-F-spectra of up to 17 bit word-length has been developed and delivered to the Linac group. The equipment is used as an accordian system for T-O-F-analysers or off-line for spectra already on tape but can be applied for other data handling purposes as well. Test mode operation has been foreseen to allow an easy program control.

##### 4.4.3. Storage Display Equipment

After some interruptions a storage display system with a 10" storage tube for the qualitative integration as well as for the visualisation of digital nuclear data with great word length has been completed.

##### 4.4.4. Multiparameter Display Unit

The laboratory model of a display unit for the visualisation of two-parameter spectra in contour and isometric mode has been modified and extended, to allow a direct co-operation with a computer. For automatic display cycles a storage tube oscilloscope has been adapted.

#### 4.4.5. Random Digital Word Generator

A unit generating binary coded digital words with up to 20-bit length, random in distance and address, and simulating therefore experimental conditions has been developed for the overall test of digital data handling equipment. The generated spectrum is equivalent to a white noise spectrum.

### 5. Radionuclides

#### 5.1. Standardization

An international BIPM intercomparison of dilution techniques using  $^{60}\text{Co}$  solutions, in which the CBNM took part, showed that only an error of about 0.05% could be attributed to our source preparation, while no significant error ( $\gtrsim 0.02\%$ ) was found on the dilution of the solutions.

An international intercomparison of threshold detectors and reactor spectra was organized. About 180 sources from about 10 different reactors were compared.

The total decay rates were determined by integral counting with our 3" x 3" NaJ detector, the impurities by our  $1.1 \text{ cm}^3$  Ge(Li)-detector. All measurements are completed, but the calculation will still require some time.

An intercomparison of  $^{241}\text{Am}$  was made using all possible methods: low geometry, liquid scintillation,  $4\pi$  and  $4\pi\alpha-\gamma$ -coincidence. It showed that  $^{241}\text{Am}$  can be standardized with 0.1% accuracy, but also that this is a limit at present, caused by all kinds of noise and physical second order effects. The latter conclusion seems to be a rather general result from our recent work. This  $^{241}\text{Am}$  solution, the activity of which is known to better than 0.1%, is also available to other laboratories, as are several other radioisotopes calibrated with extreme accuracy before.

About 100 special standard sources were prepared for other laboratories, especially sets of  $\gamma$ -standards with energies below 500 keV and  $\alpha$ -standards with accuracies of about 0.1%.

#### 5.2. Improvement and Development of Counting Methods

A series of interchangeable counters, especially with Si(Li)- and Ge(Li)-detectors has been constructed for all kinds of high accuracy coincidence counting.

Various investigations have been performed, in order to increase the accuracy of activity measurements: the sorption in pipettes used for source preparation has been shown to be below 0.01%; Inox wires have been proved to be superior to nearly all other materials for anodes of gas counters with high ionization densities; comparison of ZnS- and plastic detectors lead to an extrapolation method for  $\alpha$ -spectra in  $\alpha$ -low-geometry counting, which assures an accuracy of better than 0.1% for this method; the  $\gamma$ -efficiency of  $\beta$ -gas-counters was reinvestigated and the problems, not recognized before, solved; optimum conditions for the liquid scintillation counting of U were found; a special coincidence-anticoincidence method for liquid scintillation counting of low beta energy emitters was developed, etc. [26][27][28][29].

The possibilities for monitoring pure  $^{241}\text{Pu}$  have been investigated, using liquid scintillation, windowless flow counter and plastic scintillation techniques. Most previously used methods were unsatisfactory. Therefore a coincidence counter with two photomultipliers connected to one plastic detector for the measurement of solid probes and a new coincidence-anticoincidence liquid scintillation technique for liquid samples were developed. Both methods gave very satisfactory results.

### 5.3. Determination of Nuclear Constants

#### 5.3.1. The Fluorescence Yield of Cr

W. Bambynek

The remeasurement of the fluorescence yield of Cr using the  $^{54}\text{Mn}$ -decay and several independent counting methods was completed. The result (0.2793) is accurate to within a few tenths of a percent and shows definitely that the values, at present used, are about 20% lower than the real ones. Fluorescence yield determinations have been started on  $^{65}\text{Zn}$ . The prepared evaporated sources show promising properties and first measurements give very satisfactory results ( $W_k = 0.433$ ). Measurements on  $^{88}\text{Y}$  are under preparation [30], [31].

#### 5.3.2. Decay Scheme of $^{60}\text{Co}$

H. Hansen, A. Spernol

In the presently accepted decay scheme of  $^{60}\text{Co}$  a level of 2.16 MeV of the daughter nucleus  $^{60}\text{Ni}$  predicted by the theory, is missing. A  $\beta$ -spectrometer investigation showed that this level is populated by about 0.15% of the decays. The subsequent  $\gamma$ -radiation of 0.823 MeV was also detected in long term (10 days) Ge(Li)-measurements with about the same intensity. The other low intensity  $\beta$ -decays were also accurately determined. Some theoretical conclusions could be drawn from this new experimental result [32].

#### 5.3.3. Decay of $^{137}\text{Cs}$

H. Hansen, G. Lowenthal<sup>+</sup>, A. Spernol, W. van der Eijk, R. Vaninbroukx

The decay scheme of  $^{137}\text{Cs}$  was redetermined using as many as possible methods. The  $(\beta+e)/\gamma$  ratio has been determined by  $4\pi$ -, liquid scintillation and  $\gamma$ -spectrometer measurements to  $1.288 \pm 0.2\%$ , the  $e/\gamma$  ratio by

<sup>+</sup> Guest from A.A.E.C.

our e-X-coincidence method [33] to  $\alpha_k = 0.092$ . A first preliminary result of the branching to the ground state is 5.1%. The final results, which are under calculation, will yield a few tenths of a percent accuracy on all branchings.

5.3.4. Decay of  $^{58}\text{Co}$

W. Bambynek, E. De Roost, E. Funck<sup>+</sup>

Co-58 sources were prepared by evaporation and electro-deposition and measured with several methods. Promising results were obtained for the EC/ $\beta^+$  and the  $\gamma$ -branching ratios, especially with the  $4\pi$ -pressure, the coincidence and the Ge(Li) counters.

5.3.5. Decay of  $^7\text{Be}$

E. De Roost, A. Spernol, W. van der Eijk, R. Vaninbroukx

Measurements of the branching-ratio of  $^7\text{Be}$  have been prepared. The possible methods for preparation of thinnest sources are under investigation. Disturbances from recoils and secondary processes have been estimated and have to be checked experimentally.

5.3.6. EC/ $\beta^+$  ratios

E. Funck<sup>+</sup>, A. Spernol

A new series of EC/ $\beta^+$  determinations has been started, with extreme attention to second order effects as  $\gamma$ -efficiency of the  $\beta$ -counters, second order modes of annihilation, intervention of atomic shell effects in  $\beta$ -decay, etc.

6. Isotope Standards of Stable and Fissile Nuclides

6.1. Boron

P.J. De Bièvre, G.H. Debus

Certified standard boron samples in the form of boric

<sup>+</sup> Research Fellow EURATOM

acid have been distributed to laboratories in and outside the European Community [34].

A method has been developed to determine the isotopic composition of metallic boron layers [35], prepared by evaporation [36]. It has been possible to define the  $^{10}\text{B}$  concentration in different samples relative to each other to within 0.2%. It is hoped to achieve an accuracy of 0.25%.

6.2. Lithium

P.J. De Bièvre, G.H. Debus

Four methods used for the chemical assaying of Li agree to within 0.02%. The preparation of purified  $^6\text{Li}$  and  $^7\text{Li}$  is started and blends will be prepared during the first quarter of 1968. Different chemical compounds of Li are under examination in the mass spectrometry group in order to obtain stable signals.

6.3. Deuterium

T. Babeliowsky, G.H. Debus

The correlation between density, H/D ratio and O-isotope content of heavy water has been established; the  $\text{D}_2\text{O}$  range covered was 99.02 - 99.82 mole %. An international intercomparison of a reference water samples has been continued. Results from Chalk River were obtained, results from Sweden are awaited.

7. Sample Preparation and Assaying

G.H. Debus, H.L. Eschbach, K.F. Lauer, H. Moret, G. Müschenborn, J. Van Audenhove, V. Verdingh

In 1967 a total of 114 orders, covering 2024 samples were treated. Sample preparation and assaying started at the CBNM in the beginning of 1963, and as a matter of information a survey of the total activity of this group during the last five years is given in table V.

From 558 orders carried out, 48% were covering Euratom needs, 48.3% concerned activities in different labo-

Table V

Applicant	Number of orders	Number of samples
<b>A. <u>Inside the Community</u></b>		
a) <u>Euratom</u>		
Brussels	2	2
CBNM	201	2271
Ispra	62	8478
Mol (BR-2)	3	166
Total	268	10917
b) <u>National laboratories</u>		
Belgium	45	1471
France	80	1034
Germany	49	536
Italy	11	41
Netherlands	11	265
Total	196	3347
c) <u>Universities and other laboratories</u>		
Belgium	5	9
France	12	250
Germany	12	43
Italy	39	158
Netherlands	6	41
Total	74	501
<b>B. <u>Outside the Community</u></b>		
Austria	1	5
Chalk River(Canada)	3	4
Greece	1	1
IAEA	10	800
UKAEA	5	22
Total	20	832
<b>GENERAL TOTAL</b>	<b>558</b>	<b>15597</b>

ratories in the European Community and 3.6% supported projects outside the European Community.

Special attention has been given to the preparation [37],[38], of pure uranium sources and their accurate analysis [39][40][41]. About 50 sources have been prepared for the determination of the half lives of the U-isotopes. These measurements, in cooperation with the radionuclides laboratory, are nearly finished, and will very probably provide an accuracy of a few tenths of a percent.

Publications

1. PAULSEN, A., LISKIEN, H., Cross-sections for some (n,p)-reactions near threshold. Nuclear Data for Reactions near threshold. Nuclear Data for Reactors, Vol. I, 217, Paris 1967. EANDC(E) 92 "AL"
2. PAULSEN, A., Anregungsfunktionen für die Reaktionen  $^{60}\text{Ni}(n,p)^{60}\text{Co}$  und  $^{63}\text{Cu}(n,\alpha)^{60}\text{Co}$ , Nukleonik 10, 91 (1967) EANDC(E) 98 "AL"
3. LISKIEN, H., (n,3n) - Processes and the statistical theory, Nucl. Phys., in press, EANDC(E)101 "AL"
4. PAULSEN, A., The spin cut-off factor for  $^{60}\text{Co}$ . Z. f. Phys. 205, 226 (1967), EANDC(E) 104 "AL"
5. KNITTER, H.-H., COPPOLA, M., Elastic scattering of neutrons from  $^6\text{Li}$ , EUR-3454.e (1967), EANDC(E)100 "AL"
6. KNITTER, H.-H., COPPOLA, M., Neutron scattering from natural silicon, Z.f. Phys. 207, 56 (1967), EANDC(E) 106
7. COPPOLA, M., KNITTER, H.-H.,  $^{14}\text{C}(d,n)^{15}\text{N}$  and  $^{15}\text{N}(d,n)^{16}\text{O}$  reactions, EUR-3492.e (1967)
8. KOLAR, W., BOCKHOFF, K.H., Resonance Parameters of  $^{240}\text{Pu}$ , Part I: Neutron widths, J. Nucl. Eng., in press EANDC(E)86 "AL"
- 8a. BOCKHOFF, K.H., DE KEYSER, A., HORSTMANN, H., KOLAR, W., MARTIN, H., Measurements of the neutron total cross-section of  $^{240}\text{Pu}$ , Nuclear Data for Reactors, Vol. II, 135, Paris, 1967
9. CAO, M.G., MIGNECO, E., THEOBALD, J., WARTENA, J., WINTER, J., Fission cross-section measurement on  $^{235}\text{U}$ , J. Nucl. Eng., in press

10. MIGNECO, E., THEOBALD, J., Resonance grouping structure in neutron induced subthreshold fission of  $^{240}\text{Pu}$ , Nucl. Phys., in press, EANDC(E)110 "AL"
11. MIGNECO, E., THEOBALD, J., Resonance grouping structure in neutron induced subthreshold fission of  $^{240}\text{Pu}$ , Sec. Conf. on Neutron Cross Sections and Technology, Washington, 1968
12. WEIGMANN, H., CARRARO, G., BOCKHOFF, K.H., A new detector for neutron capture cross-section measurements, Nucl. Instr. and Methods 50, 265 (1967)
13. WEIGMANN, H., SCHMID, H., Neutron radiative capture in Mo, Nucl. Phys. A104, 513 (1967)
14. WEIGMANN, H., SCHMID, H., Resonance parameters of  $^{240}\text{Pu}$ , Part II: Radiative widths, J. Nucl. Eng., in press. EANDC(E)87 "AL"
15. SPAEPEN, J., Primary Standard data and standard samples, Nuclear Data for Reactors. Vol. 1, 241, Paris 1967, EANDC(E)93 "AL"
16. SPAEPEN, J.,  $^{27}\text{Al}(n,\alpha)^{24}\text{Na}$  and  $^{32}\text{S}(n,p)^{32}\text{P}$  cross sections as standards.  
Panel on Nuclear Standards Needed for Neutron Cross Sections Measurements, Brussels, 8-12 May, 1967.  
Presented by Liskien, H.
17. SPAEPEN, J., Fission Foils, Panel on Nuclear Standards Needed for Neutron Cross Section Measurements, Brussels, 8-12 May, 1967. Presented by Deruytter, A.J.
18. COPPOLA, M., KNITTER, H.-H., Production of monoenergetic neutrons using particle accelerators, Kerntechnik, 10, 459, 1967

19. WINTER, J., and SCHMID, H., A simplified method for kinematic calculations of nuclear reactions.  
EUR-Report (in press) and Nucl. Instr. and Methods, (in press)
20. HORSTMANN, H., LISKIEN, H., Relativistic calculations of kinematic parameters for nuclear reactions,  
EUR-3668.e (1968)
21. DERUYTTER, A.J., PELFER, P., Precise determination of the branching ratio and Q-value of the  $^{10}\text{B}(n,\alpha)^7\text{Li}$  reaction and of the Q-value of the  $^6\text{Li}(n,\alpha)^3\text{H}$  reaction,  
J. of Nucl. Eng. A/B, 21, 833 (1967) EANDC(E)99 "AL"
22. CAO, M.G., Programmes pour l'évaluation de la section efficace de fission à partir des données expérimentales brutes, EUR-3652.f (1967)
23. CAO, M.G., Analyse de mesures de diffusion élastique de particules neutres, d'après la formule de Blatt et Biedenharn, Euratom Report, in press
24. SCHMID, H., A contribution to the programming of the Calcomp digital incremental plotter for off-line operation, EUR-3534.e (1967)
25. COLLING, F., STUBER, W., A conditioner with integrated circuits for neutron time-of-flight experiment data selection, Nucl. Instr. and Methods, in press
26. VANINBROUKX, R., Precise measurement of extended  $\beta$ -sources, Standardization of Radionuclides, IAEA, Vienna 1967, p. 443
27. BAMBYNEK, W., Precise solid-angle counting, Standardization of Radionuclides, IAEA, Vienna 1967, p. 373

28. SPERNOL, A., The internal gas counter as a precision absolute counting device, Standardization of Radionuclides, IAEA, Vienna 1967, p. 277
29. VAN DER EIJK, W., MORET, H., Precise determination of drop weights, Standardization of Radionuclides, IAEA, Vienna 1967, p. 529
30. BAMBYNEK, W., Precise redetermination of the  $P_K \omega_K$ -value and the fluorescence yield  $\omega_K$  of Cr after electron capture decay of  $^{54}\text{Mn}$ , Z.f. Phys. 206, 66 (1967), EANDC(E)105 "AL"
31. BAMBYNEK, W., REHER, D., The self-absorption of Auger electrons and x-rays in  $^{54}\text{Mn}$  sources prepared by different methods, Int. J. of Appl. 18, 19 (1967)
32. HANSEN, H., SPERNOL, A., Some investigations on the decay of  $^{60}\text{Co}$ , Z.f. Phys. 209, 111 (1968), EANDC(E)108
33. HANSEN, H., M. DELABAYE, Precise coincidence counting of conversion electrons, Standardization of Radionuclides, IAEA, Vienna, 1967, p. 361
34. SPAEPEN, J., Neutron Standard Cross Section Materials Boron Stocks, Panel on Nuclear Standards Needed for Neutron Cross Section Measurements, Brussels, 8-12 May, 1967. Presented by Debus, G.H.
35. LE DUGOU, Y., LAUER, K.F., Etude du titrage des solutions d'acide borique par coulométrie à intensité constante, EUR-3490.f (1967)
36. VAN AUDENHOVE, J., JOYEUX, J., A simple technique for the preparation of ultra-pure boron layers, Nucl. Instr. and Methods 57, 157 (1967)

37. VERDINGH, V. and LAUER, K.F., Equipment for Electro-spraying, Nucl. Instr. Meth. 49, (1967), 179
38. VERDINGH, V., LAUER, K.F., The preparation of uranium layers by high voltage electrophoresis, Nucl. Instr. and Methods, in press
39. LE DUGOU, Y., LAUER, K.F., Détermination précise de l'uranium par coulométrie potentiel contrôle, EUR-3601 (1967)
40. VERDINGH, V., LAUER, K.F., An accurate determination of microgram quantities of uranium by differential polarography, Fresenius Ztschr. f. Analytische Chemie, in press
41. BRUCK, A., LAUER, K.F., The precise compleximetric titration of uranium (VI), Anal. Chim. Acta 37, 325 (1967)

XXIII. SECTION DES MESURES NEUTRONIQUES FONDAMENTALES

C. E. A. -- SACLAY (FRANCE)

R. JOLY

1. GROUPE DES NEUTRONS THERMIQUES

H. NIFENECKER

Ce groupe comprend les physiciens suivants : A. AUDIAS, P. CARLOS, B. MAIER, H. NIFENECKER, N. PANTCHEVA, M. RIBRAG, R. SAMAMA, M. SCHNEEBERGER, C. SIGNARBIEUX.

1.1. Etudes sur la fission

1.1.1. Ensemble d'acquisition de données multiparamétriques sur bande "compatible calculateur".

L'étude du processus de fission nécessite l'analyse corrélée des nombreux paramètres de la réaction tels que vitesses et énergies des fragments, multiplicité et énergie des radiations promptes). La complexité du traitement des données expérimentales rend nécessaire l'utilisation des grands ordinateurs.

Un appareillage d'acquisition des données a été mis en œuvre pour créer autour des expériences des bandes magnétiques pouvant être lues directement par un ordinateur. L'équipement se compose d'un dérouleur de bande magnétique fonctionnant en mode incrémental et d'une unité électronique de commande d'écriture associée au dérouleur. Les performances optima de l'ensemble sont 30 ms pour l'écriture d'une information multiparamétrique de 72 digits soit un taux d'acquisition d'environ 30 informations par seconde (1).

1.1.2. Etude du mode symétrique dans le cas de la fission à basse énergie

L'étude des paramètres cinétiques des fragments est rendue difficile dans la région des masses symétriques par la présence d'événements aberrants. Une méthode tridimensionnelle a été utilisée pour surmonter ces difficultés dans le cas de la fission thermique de l'U 235 (2) (3).

Cette méthode va être reprise pour étudier les cas de la fission thermique de l'U 235 et du Pu 239 ainsi que la fission spontanée du Cf 252.

Pour ces isotopes à forte activité  $\alpha$ , il est nécessaire d'éliminer les empilements  $\alpha$  - fission. Un circuit "Anti-empilements" satisfaisant a été réalisé : sur une voie rapide, un dispositif à "pompe diodes" permet d'interdire l'analyse lorsque deux impulsions se présentent dans un intervalle de temps inférieur à 1,5  $\mu$ s.

1.1.3. Etude de la distribution corrélée angle-énergie des différentes particules

légères dans le cas de la tripartition de l'U 235 induite par neutrons lents

On utilise la technique des coïncidences rapides entre particules légères et fragments de fission ainsi que la technique de l'identification des particules légères par un système ( $E, \frac{dE}{dx}$ ). Le détecteur  $\frac{dE}{dx}$  est un détecteur au Si à barrière de surface de 180  $\mu$  d'épaisseur. Le détecteur E est capable d'arrêter des protons d'énergie de 15 Mev. La corrélation fragment - particule légère est faite pour trois positions angulaires. Cette expérience est en cours.

1.1.4. Etude du ralentissement des fragments de fission dans la matière.

Une expérience a été faite pour mesurer en fonction de la masse des fragments le ralentissement des fragments dans une matière organique (VYNS).

Le principe consiste à enregistrer simultanément les énergies des deux fragments associés, l'énergie de l'un des fragments ayant été dégradée dans une feuille de VYNS d'épaisseur connue : 8 mesures ont été réalisées

correspondantes à 8 épaisseurs de feuille différentes.

Le dépouillement est actuellement en cours : qualitativement les premiers résultats indiquent qu'en début de parcours la perte d'énergie pour les fragments lourds dépend surtout de la vitesse de ces fragments alors que pour les fragments légers elle dépend surtout de la masse.

#### 1.1.5. Emission de rayons X associés à la fission de U 235

Une première mesure multidimensionnelle portant sur 100.000 événements a été réalisée.

Une première analyse des résultats (4) a montré que la parité du numéro atomique des fragments avait une grande influence sur la probabilité d'émission de rayons X. Ce résultat a été récemment confirmé, dans le cas du Cf 252, par H. R. BOWMAN.

Depuis lors, une analyse plus poussée des résultats a été entreprise pour permettre d'évaluer l'influence des variations brusques dans la probabilité d'émission de rayons X sur la détermination des charges des fragments de fission. On a d'autre part, pu montrer que les effets de polarisation de charges de la matière, s'ils existent dans le cas de la fission, sont faibles.

#### 1.1.6. Mesure de la distribution des masses dans les résonances

Cette expérience faite en collaboration avec le groupe des "neutrons intermédiaires" est décrite dans le cadre des activités de ce groupe.

#### 1.2. Méthodes de traitement de l'information

Une méthode d'analyse rapide des courbes de section efficace neutronique a été mise au point (5).

Une méthode de lissage des courbes tenant compte des propriétés statistiques des fluctuations a été mise au point (6)

Enfin on a écrit un programme de déconvolution général qui donne des résultats satisfaisants.

1.3. Spectroscopie nucléaire à l'aide du rayonnement de capture de neutrons thermiques

1.3.1. Coincidences  $\gamma$ - $\gamma$  et corrélations angulaires  $\gamma$ - $\gamma$  dans la réaction  $^{48}\text{Ti}(n,\gamma)^{49}\text{Ti}$  (7).

Nous avons étudié cette réaction à l'aide de détecteurs I Na (Tl), l'un d'entre eux étant un spectromètre anticompton. Les informations élémentaires étaient enregistrées sur bande magnétique et à la lecture de ces bandes nous avons utilisé la méthode de la "double fenêtre" afin d'éliminer les coïncidences entre deux événements dont l'un est un effet Compton.

La figure 1 résume l'ensemble de nos résultats. En particulier, nous avons pu attribuer aux niveaux à 1,38 Mev ; 1,58 Mev et 1,72 Mev, respectivement les spins et les parités  $3/2^-$ ,  $3/2^-$  et  $1/2^-$ .

1.3.2. Etude des rayonnements  $\gamma$  de capture à l'aide de détecteurs au Germanium

a) Utilisation d'une diode seule (8) des spectres directs ont été enregistrés sur les réactions  $^{89}\text{Y}(n,\gamma)^{90}\text{Y}$ ,  $^{86}\text{Sr}(n,\gamma)^{87}\text{Sr}$  et  $^{87}\text{Sr}(n,\gamma)^{88}\text{Sr}$ .

Dans les trois cas, nous avons pu établir le schéma de désexcitation à partir du niveau de capture.

b) Spectrométrie de "paires" et spectrométrie anticompton utilisant une diode au Ge (Li)

Un cristal annulaire I Na (Tl) de  $10'' \times 12''$  a été partagé en six secteurs optiquement isolés et diamétralement opposés. Au centre de cet ensemble scintillant est placée une diode de  $10\text{ cm}^3$  dont la résolution est de 5,4 kev à 1 Mev. Une logique électronique permet d'utiliser le détecteur solide, soit en spectromètre de paires soit en spectromètre anticompton,

les deux utilisations pouvant s'effectuer simultanément.

Nous avons étudié à l'aide de ce dispositif les réactions  $^{60}\text{Ni}(n,\gamma)^{61}\text{Ni}$  et  $^{62}\text{Ni}(n,\gamma)^{63}\text{Ni}$ . La figure 2 résume les résultats obtenus. Nous envisageons d'étudier ces deux réactions en coïncidence, grâce à un ensemble d'enregistrement multiparamétrique sur bande magnétique : les transitions  $\gamma$  de basse énergie seront détectées par un détecteur INa (Tl) de 4" x 4" tandis que celles de haute énergie ( $E_\gamma \geq 3$  Mev) le seront par la diode Ge (Li) utilisée en spectromètre de paires.

2. GROUPE DES NEUTRONS INTERMEDIAIRES.

A. MICHAUDON

Ce groupe comprend les physiciens suivants : J. BLONS, B. CAUVIN, H. DERRIEN (détaché au Centre d'Oak Ridge, U.S.A., en Juillet 1967), C. EGGERMANN, A. LOTTIN, A. MICHAUDON, D. PAYA, P. RIBON (jusqu'en Octobre 1967), Mlle SANCHE, H. TELLIER (à partir d'Octobre 1967), J. TROCHON.

De plus, plusieurs stagiaires ont été présents en 1967 : M. ASGHAR, J. DABBS (détaché par le laboratoire d'Oak Ridge en Juillet 1967), A. FUBINI (détaché par le C.N.E.N. de Bologne jusqu'en Décembre 1967), D. KOENIG (à partir d'Octobre 1967), H. LANDON (détaché par le N.B.S. en Septembre 1967).

2. 1. Implantation générale

Les travaux ont été poursuivis pour équiper la chambre des cibles d'un dispositif télécommandé pour la manutention et le changement de cibles productrices de neutrons. Les éléments suivants ont été construits :

- salle de stockage à l'extérieur du massif de protection de l'accélérateur

- tunnel de liaison entre cette salle de stockage et la chambre des cibles,
- chariot de transfert des cibles,
- plateau de stockage et de sélection télécommandée des cibles.

Les réglages et mises au point définitifs seront faits en 1968 pendant les arrêts de l'accélérateur.

Après le départ de l'équipe du S P N B E, les bases de vol ont été réparties comme suit (voir figure 3) :

- base n° 1 transmission
- base n° 2 anisotropie des fragments de fission émis après capture de neutrons par des noyaux de U 235 alignés.
- base n° 3 fission de Pu 239
- base n° 4 rayons  $\gamma$  de capture (spectre et multiplicité)
- base n° 5 diffusion élastique
- base n° 6 énergie cinétique des fragments de fission de U 235

Les essais de puissance sur la cible en Uranium naturel ont montré qu'elle peut dissiper une puissance de 4 kw.

## 2. 2. Electronique calculateur CAE 510

Le calculateur fonctionne régulièrement en ligne pendant l'utilisation de l'accélérateur linéaire. Généralement, c'est la mesure de section efficace totale qui est couplée directement à la mémoire du calculateur avec un nombre de canaux utiles au plus égal à 16 K.

Le programme d'accumulation en ligne en mode groupé a été essayé. Il permet d'effectuer simultanément l'acquisition en ligne et un certain nombre d'opérations de dépouillement (par exemple le traçage de courbes).

L'électronique nécessaire pour ce mode de fonctionnement a été réalisée.

La version définitive du programme reste à écrire.

Pour permettre de vérifier le bon fonctionnement en ligne du calculateur, indépendamment des expériences qui lui sont couplées, une console de simulation a été réalisée. Elle permet de simuler, par commande manuelle, un certain nombre d'opérations telles que : échanges d'informations avec la baie d'enregistrement, processus complet de lecture de la mémoire des blocs BM 96 etc ...

Par ailleurs, le calculateur CAE 510 est utilisé de plus en plus pour le dépouillement préliminaire des résultats. Les blocs mémoire BM 96 à 4096 canaux à capacité de  $10^5$  coups/canal peuvent être utilisés, lorsqu'ils sont couplés en ligne avec le calculateur, avec  $2 \times 4096$  canaux à capacité réduite ( $10^2$  par canal pour une série de 4096 canaux de  $10^3$  par canal pour l'autre).

Les programmes sont en cours de mise au point sur le calculateur CAE 510 pour que le dépouillement soit compatible avec le nouveau calculateur IBM 360/75. De même, les programmes qui avaient été écrits pour le calculateur IBM 7094 sont en cours de conversion pour être utilisés par le calculateur IBM 360/75. Plusieurs programmes passent déjà en production sur ce dernier calculateur, notamment le programme d'analyse de forme par moindres carrés.

L'ensemble de l'appareillage électronique de temps de vol a peu changé depuis l'an dernier. Il comprend :

- 1 chaîne multiparamétrique complète à bande magnétiques à 16 pistes, de marque Intertechnique,
- 3 chaînes d'enregistrement sur bandes magnétiques à 16 pistes, utilisant des dérouleurs de marque E. M. I.

- 5 blocs mémoires BM 96 à 4096 canaux,
- 6 codeurs de temps de vol (dont 5 à 50 ns et 1 à 10 ns de largeur minimum de canal).

2.3. Mesures (17) (18)

2.3.1. Sections efficaces totales

Aucune modification d'importance a été apportée à l'équipement.

Les noyaux suivants ont été étudiés :

- Xénon, avec des échantillons de Xénon naturel, de Xénon enrichis soit en Xénon léger, soit en Xénon lourd.
- Thulium
- Fer (résonance à 1,15 kev)
- Tellure avec des échantillons de tellure naturel et d'isotopes séparés.

La largeur d'impulsion de l'accélérateur linéaire est réglée pour être à peu près égale à l'incertitude due au temps de ralentissement dans les plaques de polyéthylène, pour la gamme d'énergie étudiée.

La largeur de canal est choisie systématiquement inférieure à ce temps de ralentissement.

La longueur de vol est de 17 mètres (basse énergie et petits échantillons) ou de 50 mètres (moyenne énergie) ou de 100 mètres (haute énergie, grands échantillons).

2.3.2. Sections efficaces de fission

- Np237 -. Le phénomène de groupement de résonances qui avait été observé précédemment avec le scintillateur gazeux demandait à être précisée.

Pour cela, il fallait obtenir du détecteur un bruit de fond plus faible et une efficacité accrue. C'est la raison pour laquelle la mesure a été reprise deux fois dans les conditions suivantes :

- avec une chambre d'ionisation placée à 7,36 mètres de la cible, et contenant 335 mg de Np 237. Pour réduire l'effet de l'éclair des rayons  $\gamma$ , très important à une distance de vol aussi courte, la chambre était compensée.
- avec un scintillateur gazeux placé à 14,7 mètres de la cible et contenant environ 2 grammes de Np 237 répartis en 12 cellules. Pour réduire le bruit de fond, les cellules étaient couplées optiquement 2 par 2 et les photomultiplicateurs correspondants étaient mis en coïncidence. Cette procédure a permis d'augmenter l'efficacité de détection des fragments de fission.

La mesure a été faite jusqu'à 4 kev avec une résolution globale de 18 ns/m à 100 eV.

Les résultats obtenus avec ces deux détecteurs sont tout à fait compatibles, compte tenu de la différence de résolution dans ces deux mesures.

- Pu 239 -. Pour améliorer la mesure faite à Saclay en 1964, un nouveau détecteur a été construit. Il contient environ 1 gramme de Pu 239, réparti en 12 cellules, et placé dans une enceinte porté à la température de 77° K en vue de réduire l'effet Doppler.

La figure 4 représente la section efficace de fission dans la région de 400 eV et obtenue en plaçant le détecteur à 50 mètres de la cible et accumulant environ 200 heures, l'accélérateur fonctionnant à 500 impulsions de 50 ns par seconde. Cette même figure montre l'amélioration apportée par rapport à la mesure précédente; Ces résultats sont encore préliminaires et seront améliorés dans le courant de l'année 1968.

#### 2.3.3. Rayons $\gamma$ de capture

Des essais préliminaires sont en cours, avec une diode au Ge (Li) de 30 cc pour la mesure du spectre des rayons  $\gamma$  de capture dans les résonances.

Ces essais portent principalement sur la réponse de la chaîne électronique à la forte surcharge due à l'éclair de rayons  $\gamma$  produit par l'accélérateur et sur la résolution en énergie pour les rayons

Une autre expérience est en cours, qui consiste à étudier la multiplicité des rayons  $\gamma$  de capture émis dans les résonances. Pour ce faire, les rayons  $\gamma$  sont détectés dans deux cristaux de Na I ( $5'' \times 2''$ ), et l'on enregistre séparément mais simultanément les impulsions au-dessus de 500 kev environ qui sont en coïncidence sur les deux voies d'une part, et les impulsions supérieures à plusieurs Mev sur une seule voie d'autre part.

Le rapport R des taux de comptage obtenus de ces deux façons différentes est d'autant plus élevé que le nombre de rayons  $\gamma$  émis par cascade est plus grand. Il dépend donc du spin de la résonance dans laquelle se produit la capture radiative du neutron.

Plusieurs noyaux ont été étudiés avec une distance de vol de 30 mètres ou de 50 mètres. La différence du rapport R défini plus haut pour les deux états de spin est de : 4 % ( $^{159}\text{Tb}$ ), 5 % ( $^{103}\text{Rh}$ ), 6 % ( $^{157}\text{Gd}$ ), 10 % ( $^{155}\text{Gd}$  et  $^{131}\text{Xe}$ ), 30 % ( $^{95}\text{Mo}$  et  $^{97}\text{Mo}$ ). Nous reproduisons sur la figure 5 le rapport R pour plusieurs résonances de Mo.

#### 2.3.4.

##### Sections efficaces de diffusion élastique

L'activité principale a été consacrée à la mise au point et à l'installation d'un nouveau détecteur de neutrons diffusés, pour remplacer l'ancien banc de compteurs à  $\text{BF}_3$  dont l'efficacité était trop faible et la résolution en temps trop mauvaise.

Plusieurs détecteurs ont été essayés : scintillateur  $\text{S Zn} - \text{B}_2\text{O}_3$ , verres au lithium enrichi en  $^6\text{Li}$ , scintillateurs liquides chargés au  $^{10}\text{B}$ . Après ces essais, le choix s'est porté sur le scintillateur liquide proposé par

J. E. KAKSON et H. THOMAS, disponible chez Nuclear Enterprise sous la dénomination NE 321 A, en particulier parce que la discrimination de forme neutrons - rayons est bonne. Couplé à un photomultiplicateur EMI 9514 SA, et en appliquant une discrimination de forme dérivée de la méthode d'Owen, il donne un taux de réjection des rayons de  $(99,93 \pm 0,03)\%$ , correspondant à une perte d'efficacité pour les neutrons de  $(8,3 \pm 3)\%$ . Avec une cellule de  $\phi = 4,7$  cm et d'épaisseur 1,5 cm, le temps moyen de capture des neutrons dans le détecteur est d'environ 80 ns.

- des mesures préliminaires ont été faites avec deux cellules placées à 10 cm du faisceau et à une distance de vol de 30 mètres. La discrimination de forme évite la pulsation des photomultiplicateurs au moment de l'éclair

$\gamma$ . Les noyaux suivants ont été étudiés :

-  $^{197}\text{Au}$  Epaisseur :  $n = 1,5 \cdot 10^{-5}$  at/barn

Gamme d'énergie: 40 à 70 eV

-  $^{103}\text{Rh}$  Epaisseur :  $n = 5,8 \cdot 10^{-5}$  at/barn

Gamme d'énergie: 100 eV à 2,3 keV

- Gd naturel Epaisseur :  $n = 3,8 \cdot 10^{-5}$  at/barn

Gamme d'énergie: 16 ev à 300 ev

Un très bon accord a été obtenu avec les anciennes mesures faites avec le banc de compteurs à  $\text{BF}_3$  d'une part, et les mesures de multiplicité des rayons d'autre part.

Pour ces trois éléments, les conditions de fonctionnement de l'accélérateur étaient :  $f = 1\ 000$  c/sec,  $t = 25$  ns.

- l'installation définitive est faite sur la base de vol n° 5 à 30 mètres. Le détecteur consiste en 8 cellules du même type que précédemment (5 seulement sont installées pour le moment). Les mesures ont été faites sur les

éléments suivants, l'accélérateur fonctionnant à 500 c/sec., 50 ns.

- Fe

Etude de la résonance à : 1,15 kev

Epaisseur :  $n = 0,02 \text{ at/barn}$

Cette résonance apparaît très bien et très rapidement (après une heure d'accumulation) quand on supprime la discrimination de forme. En revanche, en appliquant la discrimination de forme, elle n'apparaît pas, même après 35 heures d'accumulation. Ceci prouve que la discrimination de forme est efficace et aussi que la mesure de la section efficace de diffusion de cette résonance est difficile, surtout avec un détecteur sensible aux rayons  $\gamma$ .

- Yb

Epaisseur :  $n = 1,04 \cdot 10^{-4} \text{ at/b}$

Gamme d'énergie : 20 ev à 2 kev

Durée d'accumulation : 30 heures

- Te

Epaisseur :  $n = 3,3 \cdot 10^{-4} \text{ at/b}$

Gamme d'énergie : 20 ev à 2 kev

Durée d'accumulation : 50 heures environ.

La figure 6 montre les résultats bruts de 900 à 1900 ev.

Des mesures sont en cours avec un échantillon de tellure fortement enrichi en  $^{125}\text{Te}$ .

2.3.5. Mesures corrélées des énergies cinétiques des fragments de fission

induite dans l'U 235 par des neutrons de résonances.

(Mesure faite en collaboration avec MM. SIGNARBIEUX et RIBRAG du groupe des neutrons thermiques).

Pour des raisons d'efficacité, le détecteur choisi est une chambre d'ionisation à grille double. L'électrode commune est constituée par un dépôt de  $100 \mu\text{g/cm}^2$  d'uranium, enrichi à 95 % en U 235, évaporé sur un film

de VYNS de  $50 \mu\text{g}/\text{cm}^2$  d'épaisseur. La surface du dépôt est de  $100 \text{ cm}^2$  soit au total  $10 \text{ mg}$  d'U 235.

Une bonne spectrométrie des énergies des fragments nécessite une corrélation des trajectoires dans le détecteur. La solution adoptée, se réfère à la détermination du temps de montée de l'impulsion sur l'électrode collectrice, détermination obtenue par une mesure simultanée des amplitudes des réponses d'une voie linéaire et d'une voie différenciée.

Pour remédier aux difficultés inhérentes à l'éclair  $\gamma$  de l'accélérateur linéaire (mauvaise restitution de l'électronique associée aux détecteurs) chaque électrode collectrice de la chambre à grille a été "compensée" électrostatiquement par une électrode supplémentaire. Cette compensation a permis de réduire très notablement la perturbation.

L'expérience se traduit donc par une analyse à 5 dimensions de chaque évènement :  $t_n$ , temps de vol du neutron incident,  $E_1$ ,  $E'_1$ , amplitudes des réponses linéaire et différenciée du fragment 1 ;  $E_2$ ,  $E'_2$ , amplitudes du fragment 2.

Une acquisition de données sur bande magnétique a été réalisée pendant 6 semaines, sur une base de vol de 7,90 m., l'accélérateur fonctionnant à 500 c/sec. - 100 ns ; le taux d'acquisition était de 13 évènements par seconde pour une bande d'énergie de neutrons allant de 1 ev à 40 ev, soit, au total,  $17,5 \cdot 10^6$  évènements à 5 paramètres chacun. Le dépouillement est en cours.

2.3.6. Mesure de l'anisotropie des fragments de fission induite par des neutrons de résonances dans des noyaux de U 235 alignés

L'appareil d'alignement des noyaux de U 235, mis au point par J. DABBS au laboratoire National d'Oak Ridge a été transporté à Saclay et installé

sur la base de vol n° 2 à une longueur de vol de 5 mètres. L'appareil a été testé jusqu'à une température des cristaux de U 235 de  $T = 0,5^\circ \text{K}$ . L'électronique a été construite et essayée pour avoir une bonne réponse à l'éclair  $\gamma$ , permettre l'enregistrement simultané sur deux voies différentes des impulsions données par les détecteurs à  $0^\circ$  et  $90^\circ$ , ainsi que l'enregistrement séparé des rayons  $\alpha$  de la radioactivité naturelle. Des essais préliminaires, à la température ambiante, ont montré que le taux de comptage et la résolution étaient suffisants pour étudier la plupart des résonances depuis la 1ère à 0,29 eV jusque vers 22 eV.

2. 3. 7.

Collaboration à des mesures faites au laboratoire national d'Oak Ridge

Pendant son séjour à O. R. N. L., M. LOTTIN a participé à une mesure de  $\alpha = \frac{\sigma_e}{\sigma_f}$  de Pu 239 entre 20 kev et 600 kev (10). La mesure a été faite à l'aide de l'accélérateur électrostatique Van de Graaff de 5 MeV. Le faisceau de neutrons était collimaté sur un échantillon de Pu 239 placé au centre d'un grand scintillateur liquide chargé au gadolinium. Un événement de capture radiative dans l'échantillon est caractérisé par une impulsion unique dans le scintillateur correspondant à une cascade de rayons  $\gamma$ . Au contraire, une fission provoque non seulement une impulsion due aux rayons  $\gamma$  prompts associés à la fission, mais aussi plusieurs impulsions retardées de quelques  $\mu\text{sec}$ . dues aux rayons  $\gamma$  de capture dans le gadolinium des neutrons de fission ralentis dans le scintillateur.

L'énergie des neutrons en-dessous de 100 kev a été mesurée par la technique du temps de vol avec une résolution de 7 ns/m. Au-dessus de 100 kev, la mesure a été faite avec un faisceau de neutrons monoénergétiques. Les résultats sont portés sur la figure 7.

2.4.

Analyse des résultats.

Fer - L'analyse de forme de la résonance à 1,15 kev montre clairement qu'elle n'est pas induite par des neutrons "S" (fig. 8) (16).

Gadolinium (12) - L'analyse des résonances des deux isotopes  $^{155}\text{Gd}$  et  $^{157}\text{Gd}$ , (y compris la détermination du spin pour ces deux isotopes de spin 3/2 grâce à la section efficace de diffusion et aux mesures de multiplicité de rayons  $\gamma$ ) a permis de connaître la fonction densité So pour chaque isotope et pour chaque état de spin (fig. 9 et 10). On ne constate pas de variation de So en fonction de l'état de spin pour ces deux isotopes, contrairement à ce qui a été trouvé pour d'autres isotopes de même spin (Au, Br, Ba, As).

Xénon - L'analyse a été conduite de la même façon que pour le gadolinium. L'attribution isotopique est plus difficile car les deux échantillons de xénon (l'un enrichi en Xe lourd, l'autre en Xe léger) n'avaient pas des proportions isotopiques très différentes. Néanmoins, la fonction densité So pour les deux états de spin a pu être déterminée pour les deux états de spin pour Xe 129 de spin 1/2 (fig. 11) et Xe 131 3/2 (fig. 12). Pour ces deux isotopes, y compris pour Xe 131 de spin 3/2, on ne décèle pas de variation de So suivant l'état de spin.

Np 237 - Le phénomène de groupements des résonances qui avait été observé dans la section efficace en-dessous du seuil de Np 237 a été confirmé et précisément par les deux mesures décrites plus haut.

La figure 13 montre le premier groupe de résonances qui apparaît vers 40 ev. La deuxième structure apparaît en fission à 118 ev, mais à cette énergie, la résolution n'est plus suffisante pour la séparer en plusieurs résonances (s'il y a plusieurs résonances). Ces pics sont au nombre de

17 jusqu'à 1 kev et on peut encore en déceler beaucoup d'autres jusque vers 4 kev, énergie supérieure de la mesure.

La figure 14 montre sur le même diagramme  $\sum_{\alpha}^E 2g \Gamma_n^{\alpha}$  et  $\sum_{\alpha}^E \Gamma_f^{\alpha}$  qui sont la somme de 0 à E respectivement des largeurs neutroniques réduites et des largeurs de fission ; ces deux quantités sont tracées en fonction de E. On constate que vers 40 ev, la quantité  $\sum_{\alpha}^E \Gamma_f^{\alpha}$  augmente très rapidement alors que l'autre quantité  $\sum_{\alpha}^E 2g \Gamma_n^{\alpha}$  ne présente aucune anomalie. De même, on constate que la section efficace totale ne présente aucune anomalie aux énergies des pics observés en fission au-dessus de 40 ev. On peut donc parler d'une structure intermédiaire qui ne peut pas être expliquée par un mode spécial de formation de noyau composé par l'intermédiaire d'un état porte. Il semble au contraire que ce soit le couplage des états du noyau composé à la voie de sortie de fission qui soit plus intense à certaines énergies discrètes : 40 ev, 118 ev, etc...

La distribution des largeurs de fission pour les résonances situées en-dessous de 80 ev est portée sur la figure 15. Lorsqu'une résonance n'est pas observée en fission, il est néanmoins possible de déterminer une valeur supérieure de sa largeur de fission appelée  $\Gamma_{f_{Max}}$ . Une valeur approximative de  $\Gamma_f$  peut être prise égale à  $\frac{1}{2} \Gamma_{f_{Max}}$ . La distribution ainsi obtenue est incompatible avec une seule famille en  $X^2$ . Il faut admettre l'existence d'au moins deux familles dont les valeurs moyennes sont  $\langle \Gamma_f \rangle = 0,009 \text{ meV}$  pour les petites résonances et  $\langle \Gamma_f \rangle = 0,4 \text{ meV}$  pour les grandes résonances.

Une section efficace de fission artificielle a été calculée à partir de paramètres tirés au hasard mais qui suivent les distributions habituelles pour les espacements et les largeurs neutroniques réduites. Les largeurs de

fission sont supposées suivre la distribution de la figure 15. La variance de cette section efficace artificielle est environ 3 fois supérieure à la section efficace de fission qui a été mesurée, confirmant ainsi la présence d'une structure intermédiaire dans les résultats expérimentaux (11) (14).

Pu 239 - Les mesures faites à Saclay ont été dépouillées, analysées et présentées au Congrès de Paris en Octobre 1966.

La nouvelle mesure de fission est en cours et sera dépouillée après une accumulation plus importante.

Après son séjour à Oak Ridge, M. LOTTIN a analysé les mesures de  $\alpha$  sur le Pu 239 entre 20 kev et 600 kev, à l'aide d'un formalisme basé sur la théorie des voies de sortie du phénomène de fission, en choisissant plusieurs énergies possibles pour la voie de sortie  $1^+$ . Des calculs préliminaires effectués avec plusieurs hypothèses simplificatrices sont portés sur la figure 7.

- Energie de la voie  $1^+$  située à 200 keV au-dessus de l'énergie de liaison de neutron

-  $\hbar\omega = 500$  keV.

L'énergie de la voie  $1^+$  correspond remarquablement bien à celle que l'on peut déduire de l'analyse des résonances du Pu 239 à basse énergie (13)

M. DERRIEN se trouve actuellement au Laboratoire National d'Oak Ridge où il participe à l'analyse des résonances du Pu 239 à l'aide du formalisme de Adler.

- Temps de ralentissement des neutrons rapides dans les plaques minces de matière hydorgénée.

Les mesures faites auprès de l'accélérateur électrostatique Van de Graaff de 5 Mev du C. E. N. de Cadarache et auprès de l'accélérateur linéaire de Saclay ont été analysées. Les résultats expérimentaux sont en bon accord

avec les calculs effectués par la méthode de Monte Carlo (15).

- Analyse des mesures de sections efficaces totales, dans la région du kev, effectuées au Laboratoire National d'Oak Ridge avec la collaboration de D. PAYA (9)

Plusieurs noyaux pairs-impairs dans la région de la résonance 3 S de la fonction densité, ont été étudiés et les sections efficaces totales analysées.

Les résonances dans le Cr 53 et, dans une certaine mesure, le Fe 57 ont tendance à se grouper. C'est ainsi que la fonction densité de Cr 53, mesurée en-dessous de 10 kev, est assez importante (environ  $12.50^{-4}$ ) ; elle est plus basse (environ  $5.10^{-4}$ ) lorsqu'elle est mesurée entre 3 et 60 kev, et alors en accord avec les prédictions du modèle optique.

Ceci suggère que la valeur élevée de la fonction densité au sommet de la résonance 3 S (environ  $10.10^{-4}$ ) déduite de mesures similaires, peut provenir du fait que plusieurs noyaux voisins de Cr 53 peuvent présenter des valeurs élevées pour la fonction densité locale.

### 3. GROUPE DES NEUTRONS RAPIDES

J. L. LEROY

Les travaux décrits ci-après ont été effectués autour du Van de Graaff de 5 MV de Cadarache, par D. ABRAMSON, A. ARNAUD, J.C. BLUET, P. FARDEAU, G. FILIPPI, E. FORT, J. GENTIL, D. HEBERT, J. L. HUET, C. LE RIGOLEUR, J. L. LEROY, P. QUENTIN, I. SZABO.

#### 3.1. Commande de l'accélérateur et des expériences associées au moyen d'un calculateur électronique

Un calculateur C 90-10 a été installé au début de 1967 auprès du Van de Graaff. Il a pour rôle :

- de faire les réglages de l'accélérateur et des différents paramètres de

l'expérience tels que la position des compteurs, des échantillons étudiés, la durée des comptages, selon un programme établi à l'avance.

- de concentrer les données brutes pour fournir les grandeurs cherchées, et de présenter les résultats selon un mode qui permette au physicien de juger plus rapidement et plus exactement la qualité des résultats acquis.

L'unité centrale du système comprend 32.000 mots de 12 bits, avec un cycle de mémoire de 1,75  $\mu$ s.

Le réglage de l'énergie de l'accélérateur se fait par l'intermédiaire du réglage de l'analyseur magnétique, auquel l'accélérateur est asservi. Le champ magnétique est lui-même piloté par un dispositif basé sur la résonance magnétique nucléaire. Il suffit donc pour faire varier l'énergie de l'accélérateur que le calculateur fasse varier la fréquence d'oscillation du circuit de résonance magnétique, en agissant sur un condensateur variable, par l'intermédiaire d'un moteur pas à pas.

L'acquisition des données nucléaires brutes se fait dans des mémoires tampon constituées selon les cas par des échelles, des sélecteurs à 400 canaux, ou un bloc mémoire à 4096 canaux. Lorsque la durée de la séquence d'acquisition est écoulée, la calculatrice reçoit une interruption qui déclenche la lecture des mémoires tampon et le transfert de ces données sur un support extérieur, ruban perforé ou ruban magnétique. On procède ensuite au réglage des différents paramètres correspondant à la séquence suivante.

L'ensemble de ces opérations est réalisé au moyen du programme "ETOILE" écrit en langage symbolique.

Le choix de cette organisation nous a été dicté en grande partie par des considérations de programmation. Il nous a paru en effet essentiel que les programmes de réduction des données expérimentales, qui font partie

intégrante de l'expérience, soient écrits et puissent être modifiés facilement en cours d'expérience par les physiciens. Cela, bien entendu, n'est possible que grâce à l'utilisation d'un langage de programmation relativement simple comme le FORTRAN. Malheureusement, le compilateur FORTRAN qui nous a été fourni avec le calculateur est organisé de façon telle que l'utilisation des interruptions est impossible lorsqu'un programme FORTRAN est chargé en mémoire. De plus, les données expérimentales, lorsqu'elles apparaissent comme variables FORTRAN ne peuvent pas être implantées à un endroit fixe de la mémoire. Pour éviter ces difficultés il a fallu écrire un programme moniteur qui réside toujours en mémoire rapide et qui a simplement pour fonction d'aller chercher à tour de rôle sur une bande magnétique le programme ETOILE ou bien le programme FORTRAN de réduction des données et de le charger en mémoire. Le programme de réduction de donnée va relire le ruban perforé ou la bande magnétique, il effectue ensuite toutes les opérations mathématiques ou logiques nécessaires, et il sort les résultats sur imprimante, table traçante ou unité de visualisation oscilloscopique. Ensuite il rend le contrôle au moniteur qui charge à nouveau le programme ETOILE pour faire l'acquisition suivante, et ainsi de suite.

3. 2.

Mesures absolues de sections efficaces de référence :

Nous avons entrepris une étude approfondie des causes d'erreurs systématiques pouvant affecter les mesures de certaines sections efficaces de référence, dans le domaine d'énergie de 10 KeV à 1 MeV. Pour pouvoir faire des mesures de section efficace dans ce domaine il faut disposer d'un dispositif précis pour mesurer les flux de neutrons rapides. La méthode de la particule associée appliquée à la réaction  $T (p, n)^3 \text{He}$ , que nous avons mis au point les années précédentes (19), nous a servi à éta-

lonner, pour différentes énergies un dispositif que nous appellerons par la suite compteur directionnel étalon.

3.2.1. Etude et construction du compteur directionnel étalon (20)

Le compteur est représenté par la figure 16. C'est une version améliorée du "Long compteur". Les améliorations portent sur les points suivants :

- Une protection très efficace est placée tout autour de l'appareil de façon que les neutrons diffusés ne puissent être comptés.
- Le flux de neutrons à mesurer est admis par un collimateur dont la géométrie est définie avec précision, jusqu'au cœur d'un bloc de polyéthylène comportant deux gros compteurs à  $\text{BF}_3$ . Dans une telle géométrie la probabilité de fuite ou de retrodiffusion est très faible, et on peut s'attendre à ce que l'efficacité varie très peu en fonction de l'énergie. D'ailleurs, la géométrie étant très simple, il est possible d'obtenir l'efficacité du dispositif par un calcul de Monte Carlo très détaillé. Ce calcul a été fait pour des énergies allant de 0.1 KeV à 1 MeV, avec une statistique de  $\pm 7\%$ ; aucune variation significative d'efficacité n'a été trouvée dans ce domaine d'énergie.

Ensuite une étude expérimentale a été entreprise, pour des énergies comprises entre 100 KeV et 300 KeV l'efficacité du dispositif était obtenue par comparaison avec un scintillateur de verre au  $^6\text{Li}$  dont l'efficacité avait préalablement été mesurée par la méthode de la particule associée. A l'énergie de 2.7 MeV l'efficacité est obtenue en calculant le flux des neutrons produits par la réaction  $D(d, n)^3\text{He}$ , à partir de la mesure dans un angle solide défini du nombre de protons de la réaction  $D(d, p)^3\text{H}$ , et du rapport des sections efficaces de ces deux réactions (21). Les premiers résultats de ces mesures confirment que l'efficacité du compteur dépend peu de l'énergie.

3.2.2. Etude de la section efficace de la réaction  $^6\text{Li}$  ( $n, \alpha$ ) T entre 100 KeV et 400 KeV

Nous avons repris les mesures concernant cette réaction, en utilisant la technique de la particule associée (19). L'appareillage électronique a été amélioré et il était possible de déterminer quelle épaisseur de matière, devaient traverser les  $^3\text{He}$  avant de sortir de la cible. D'autre part, le scintillateur chargé au  $^6\text{Li}$  était placé plus près de la cible. De cette façon, la correction de diffusion coulombienne des particules  $^3\text{He}$ , qui était la principale cause d'incertitude est devenue très faible, et elle est basée sur des données plus précises.

Par ailleurs, il est apparu que les approximations faites dans le calcul de la correction d'efficacité due à la diffusion multiple des neutrons à l'intérieur du scintillateur, étaient trop grossières. Il s'ensuit que les valeurs de section efficace du  $^6\text{Li}$  que nous avons précédemment données (19) sont probablement un peu trop fortes surtout à basse énergie.

3.2.3. Mesure de la section efficace de fission de  $^{235}\text{U}$  entre 120 et 370 KeV (22)

Cette mesure a été faite en comparant le taux de comptage d'une chambre à fission qui nous avait aimablement été prêtée par P. H. WHITE, avec celui du compteur directionnel étalon. En se basant sur la calibration de cet appareil telle qu'elle est décrite au paragraphe 3.2.1., on obtient des résultats parfaitement compatibles avec ceux de WHITE. Les mesures seront poursuivies dans un domaine d'énergie plus étendu.

3.3. Mesure des distributions angulaires élastiques et inélastiques

On a construit et mis au point un système à 5 compteurs pour faire les distributions angulaires.

GROUPE DES REACTIONS PHOTONUCLEAIRES

R. BERGERE

Une installation de production de gammas monochromatiques (par annihilation en vol de positrons d'énergie variable de 5 à 40 MeV) a été installée en 1960 et perfectionnée en 1964 - 1965 par C. TZARA et son équipe (23).

Avec cette installation et un détecteur de photoneutrons à compteurs au BF<sup>3</sup> noyés dans la paraffine cette équipe a obtenu un certain nombre de sections efficaces relatives aux réactions

1/ ( $\gamma$ , n) sur les noyaux lourds (24)

2/ ( $\gamma$ , n) sur les noyaux légers (25)

3/ ( $\gamma$ ,  $\gamma$ ) et ( $\gamma$ ,  $\gamma'$ )

Cette installation a été reprise en 1966 par le groupe des réactions photonucléaires de la Section des Mesures Neutroniques Fondamentales. L'année 1967 a été partiellement consacrée à diverses améliorations de cette installation. En particulier, ont été mis en place :

1/ Un système à coupe de Faraday pour captation et mesure d'un courant de positrons pouvant descendre jusqu'à  $10^{-14}$  ampères (26)

2/ Un nouveau détecteur de photoneutrons constitué par une sphère Nuclear Enterprise contenant 500 litres de scintillateur liquide chargé à 0,5 % de Gadolinium. Les scintillations consécutives aux captures de neutrons par les noyaux de Gadolinium sont détectées par 2 bancs de

4 PM chacun, mis en coïncidence. Un tel détecteur détecté avec un rendement de  $60 \pm 0,3 \%$  et une stabilité de rendement meilleure que  $\pm 0,5 \%$  sur un mois, un spectre de neutrons de fission du Californium 252 (27)

3/ Un système électronique d'analyse de la multiplicité des événements détectés par le scintillateur liquide après chaque bouffée de gammas monochromatiques.

4/ Des systèmes de monitorage des divers bruits de fond : bruit des PM + bruit cosmique, bruit dû aux neutrons créés sur la cible de conversion électrons-positrons, bruit dû aux photoneutrons créés sur la collimation définissant le faisceau de gamma monochromatiques.

5/ Des systèmes divers de sortie automatique des résultats. Le schéma synoptique de l'expérience actuelle est représenté figure 17 .

L'installation ainsi améliorée a été utilisée fin 1967 pour déterminer de  $E_{\gamma} = 7 \text{ Mev}$ , jusqu'à  $E_{\gamma} = 30 \text{ Mev}$ , les sections efficaces des réactions ( $\gamma, n$ ), ( $\gamma, 2n$ ) et ( $\gamma, 3n$ ) sur un noyau lourd déformé ( $Tb_{159}$ ) et sur un noyau lourd sphérique ( $La_{139}$ ). Des analyses sont en cours pour représenter ces sections efficaces par 1, 2 ou 3 raies de Lorentz et en déduire l'absorption quadrupolaire éventuelle au-dessus de la résonance dipolaire géante ainsi que le moment quadrupolaire du noyau cible. Une analyse est également en cours pour l'évaluation, au-dessus du seuil ( $\gamma, 2n$ ) des pourcentages de photoneutrons d'évaporation et de photoneutrons d'émission directe.

REF E R E N C E S :

- ( 1) C. SIGNARBIEUX, M. RIBRAG : Rapport C. E. A. à paraître
- ( 2) C. SIGNARBIEUX, M. RIBRAG, H. NIFENECKER :  
Nucl. Phys. A99 (1967) 41
- ( 3) M. RIBRAG : Thèse de Doctorat d'Université (1967)
- ( 4) H. NIFENECKER, C. SIGNARBIEUX, M. RIBRAG, G. PERRIN,  
A. AUDIAS : J. de Phys. 29 C<sub>1</sub> (1968) 154
- ( 5) H. NIFENECKER et als : Nucl. Inst. and Meth., à paraître
- ( 6) H. NIFENECKER et als : Nucl. Inst. and Meth., à paraître
- ( 7) P. CARLOS et als : Nucl. Phys. à paraître
- ( 8) J. L. IRIGARAY et als : C. R. Acad. Sc. 265 B (1967) 701
- ( 9) W. M. GOOD, D. PAYA et als : Phys. Rev. 151 (1966) 912
- (10) X A. LOTTIN et als : Communication présentée à l'International  
(p184)  
Conference on Fast Critical Experiments and their Analysis"  
(Argonne, Octobre 1966)
- (11) D. PAYA et als : J. de Phys. 29 - C<sub>1</sub> (1968) 159
- (12) P. RIBON et als : J. de Phys. 29 - C<sub>1</sub> (1968) 203
- (13) A. MICHAUDON : J. de Phys. 29 - C<sub>1</sub> (1968) 51
- (14) A. FUBINI et als : à paraître
- (15) R. BAYER - rapport C. E. A. à paraître
- (16) H. TELLIER et als : C. R. Acad. Sc. : à paraître
- (17) A. MICHAUDON, R. JOLY, G. VENDRYES : B. I. S. T. 113  
(1967)
- (18) B. CAUVIN : B. I. S. T. 120 (1967)
- (19) E. FORT, J. L. LEROY : "Nuclear Data for Reactors"  
Conférence A. I. E. A. - CN 23/68 (Paris - Octobre 1966)

. / ...

- (20) J. L. LEROY, J. L. HUET, I. SZABO : Rapport DRP/SMNF 67/21
- (21) R. B. THEUS et als : Nucl. Phys. 80 (1966) 273
- (22) I. SZABO, P. QUENTIN : Rapport DRP/SMNF 67/20
- (23) J. MILLER, C. SCHUHL, C. TZARA : Nucl. Phys. 32 (1962)  
236
- (24) C. SCHUHL : Thèse 1962
- (25) J. MILLER : Thèse 1964
- (26) A. VEYSSIERE : Rapport C. E. A. - R/3276 (1967)
- (27) R. BERGERE, H. BEIL, A. VEYSSIERE : à paraître

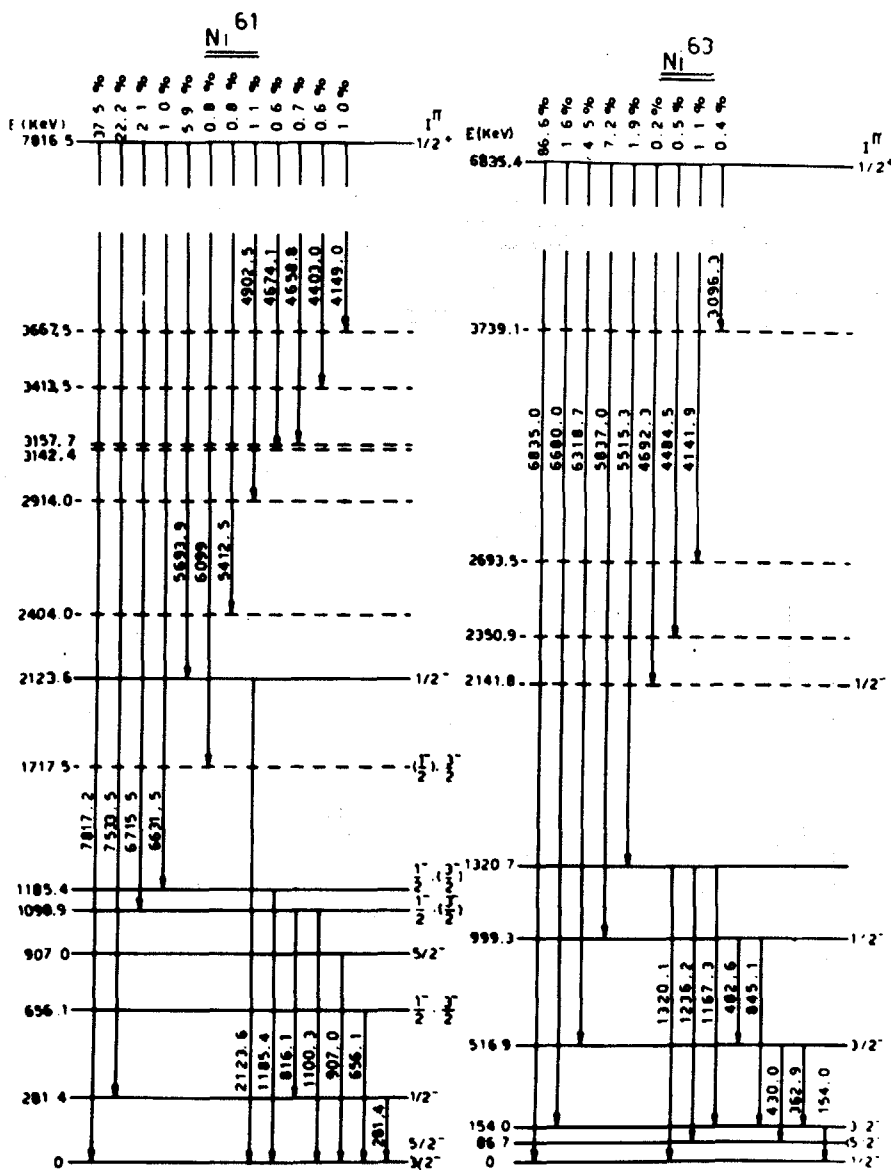


Fig. 2

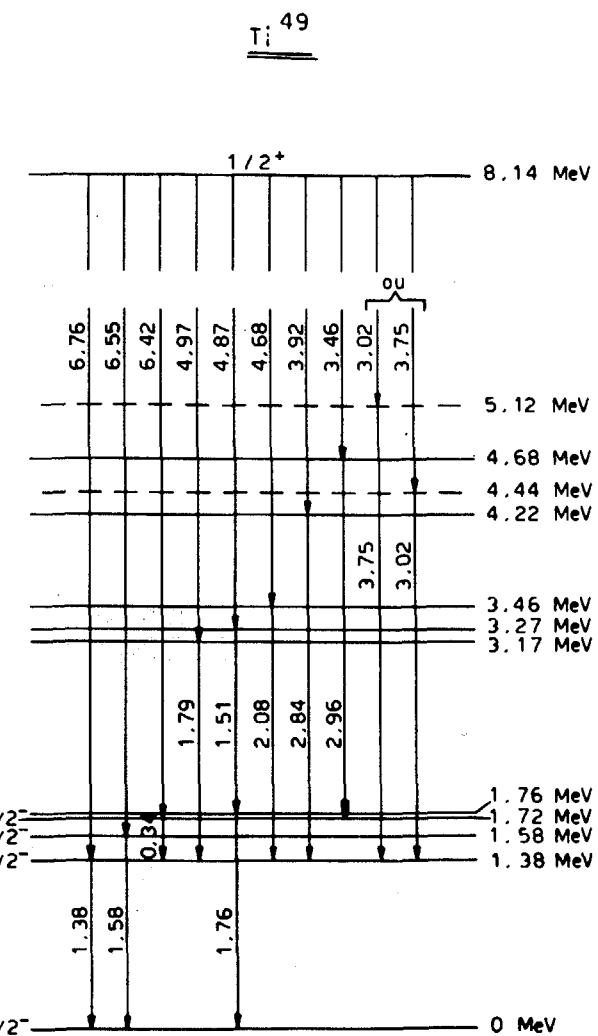
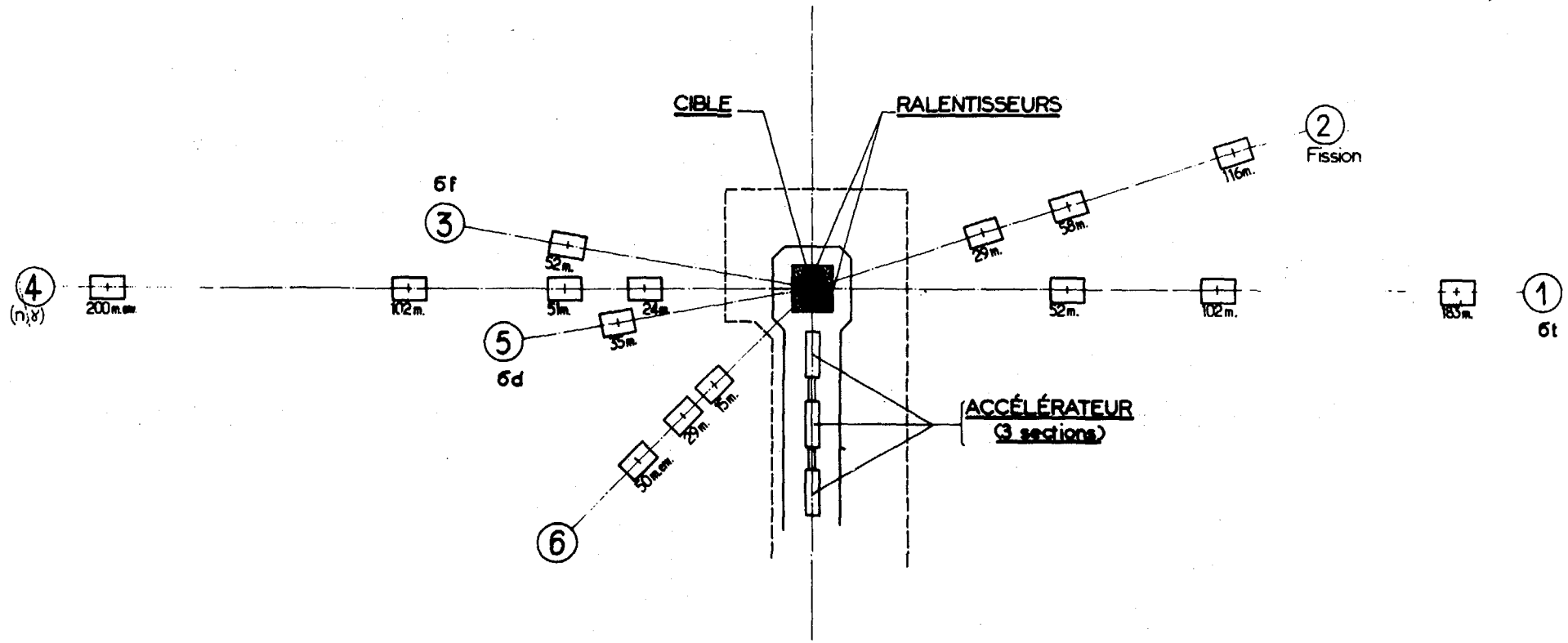


Fig. 1



IMPLANTATION DES BASES DE TEMPS DE VOL  
ACCÉLÉRATEUR LINÉAIRE DE 45 Mev.

Fig. 3

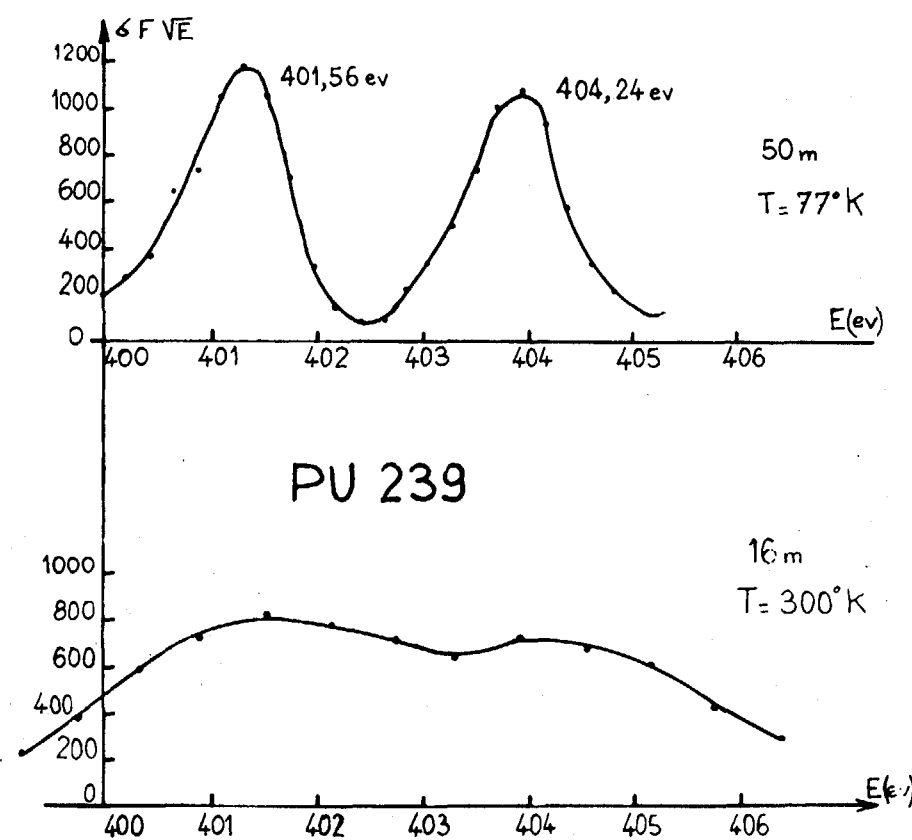
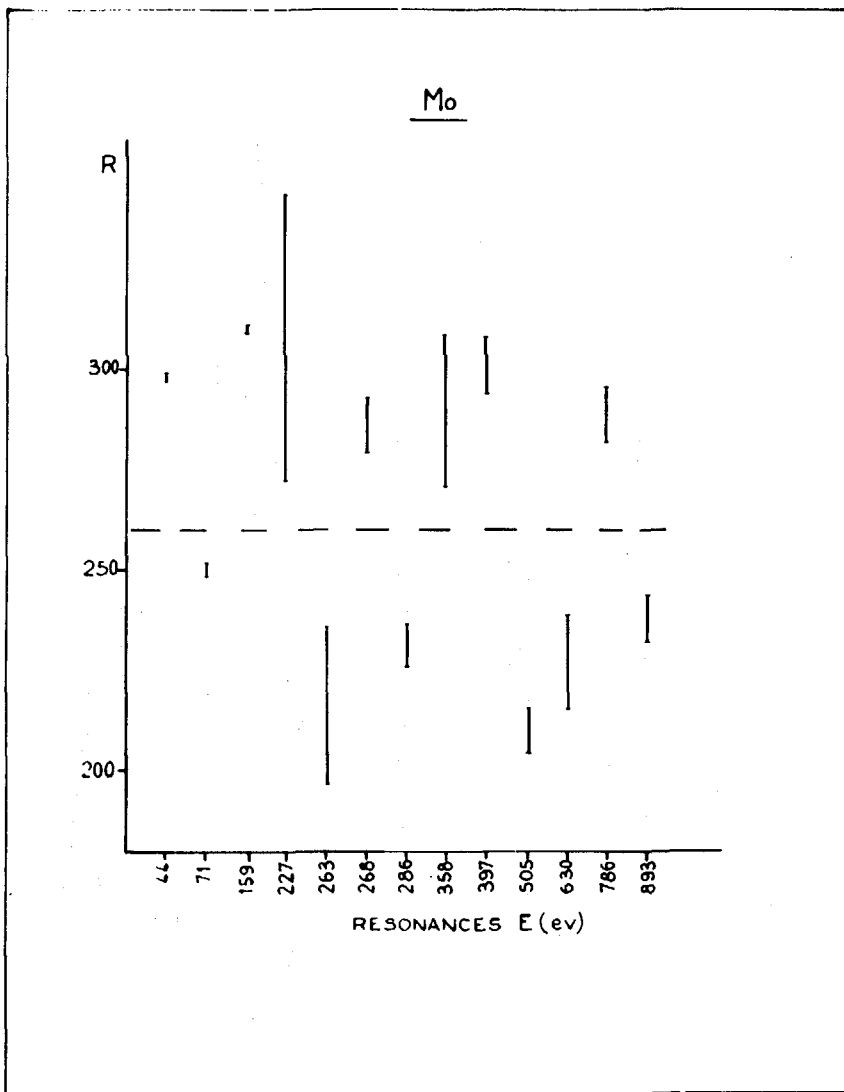


Fig. 4

Fig. 5

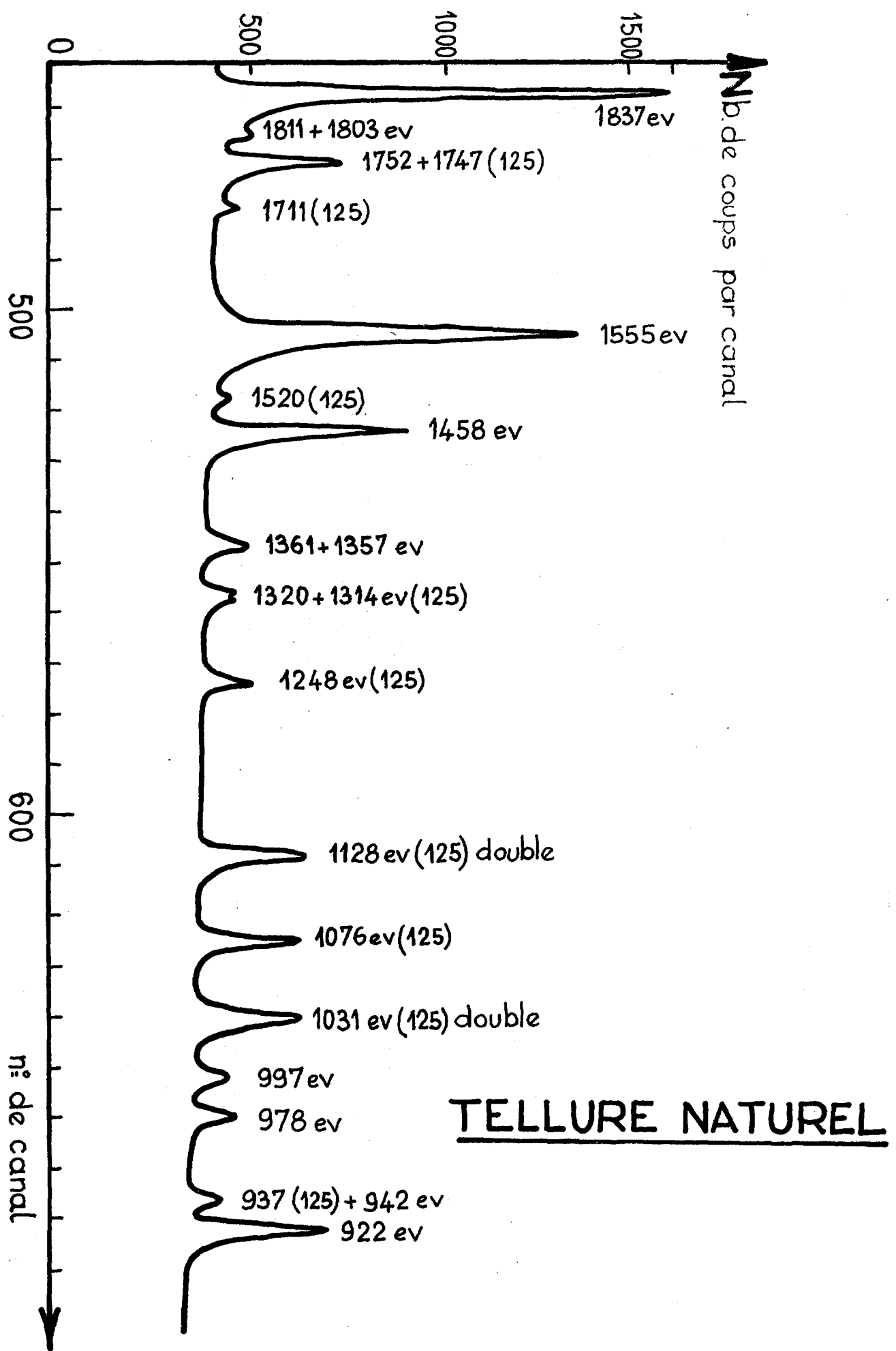


Fig. 6

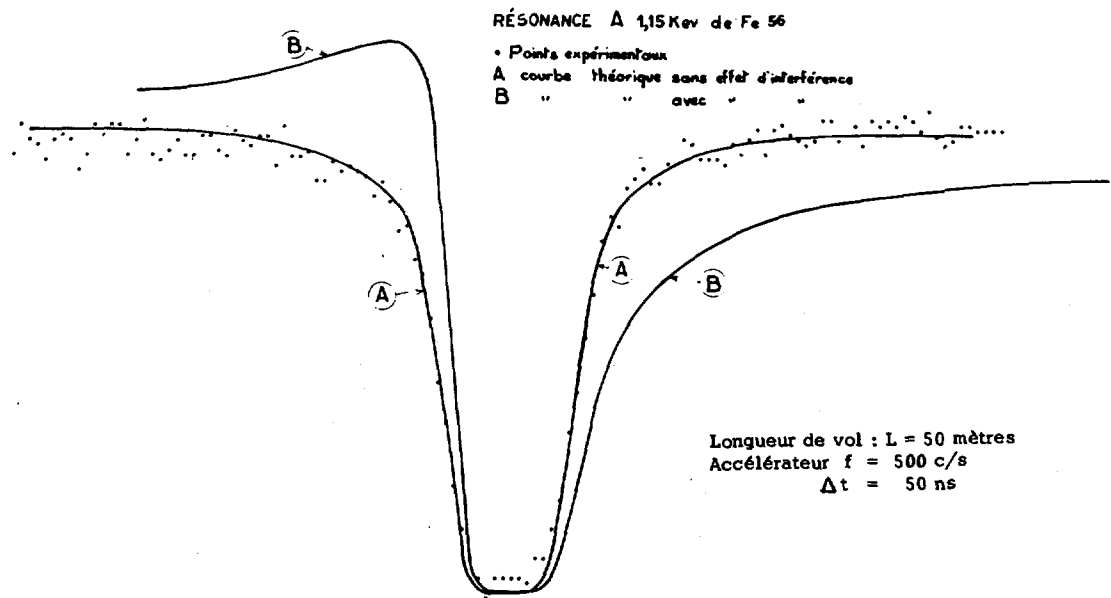


Fig. 8

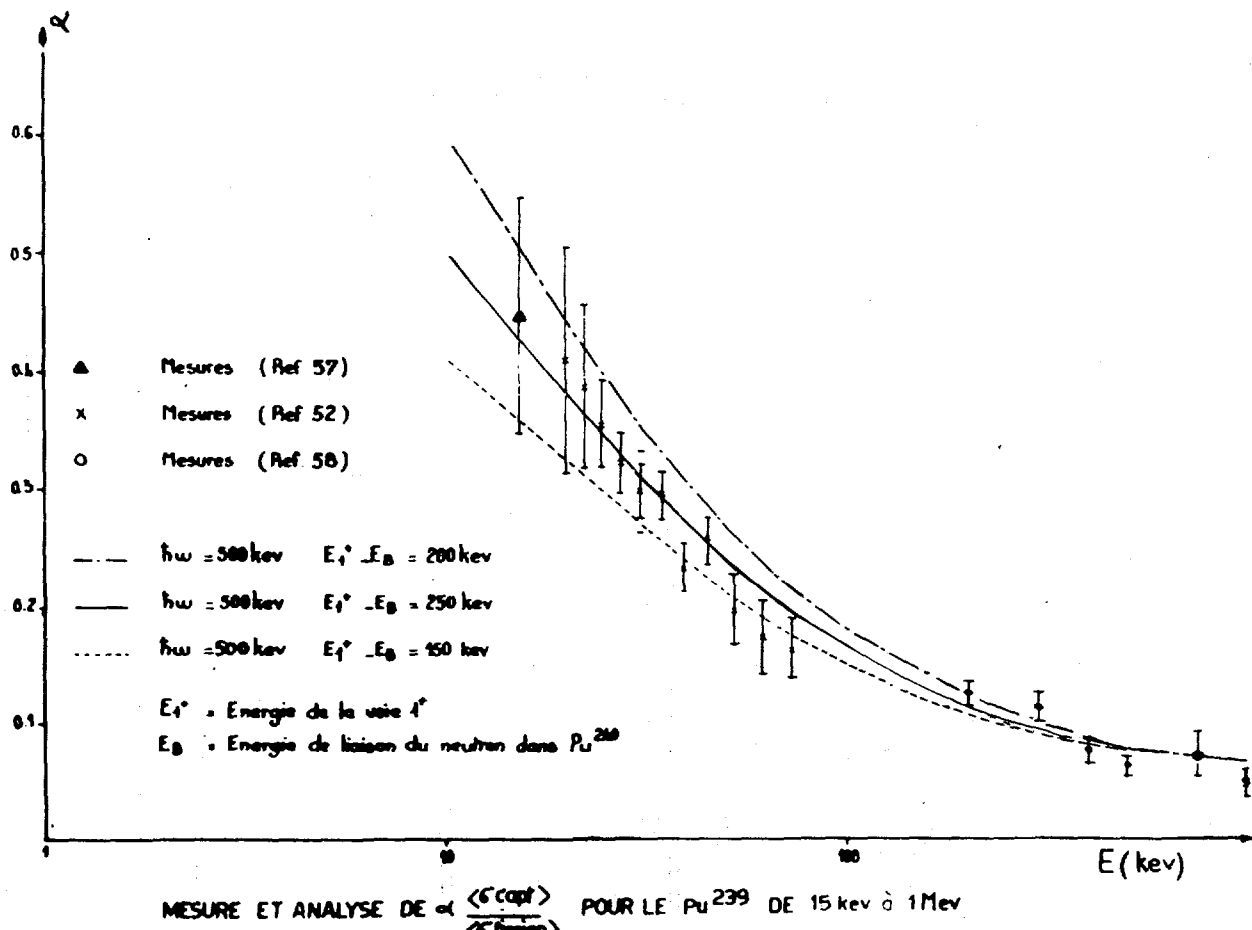


Fig. 7

Fig. 9

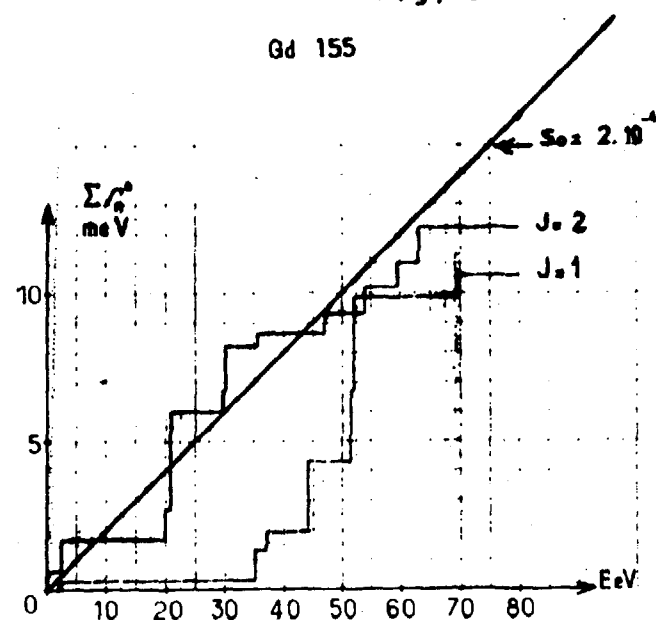
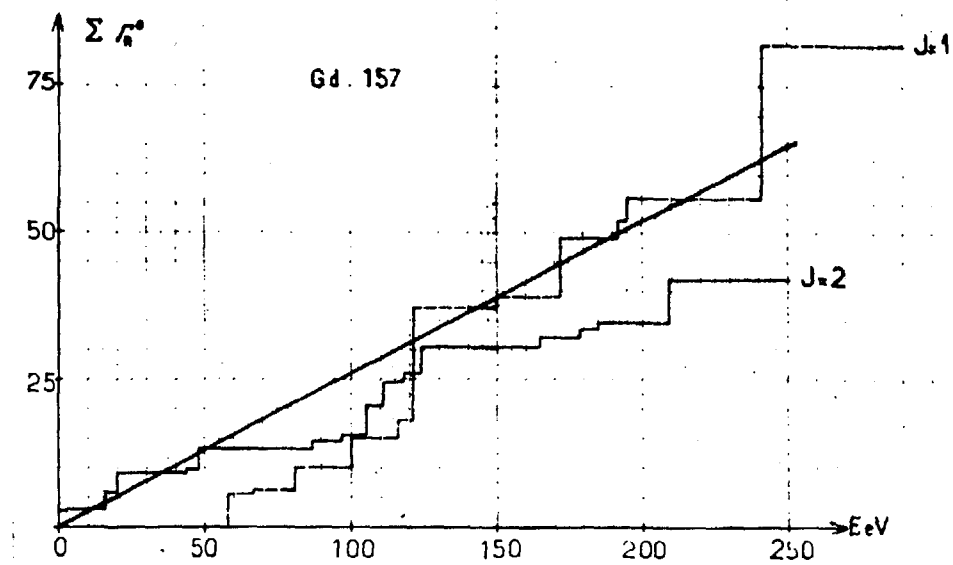


Fig. 10



-202-

Xe 131+n

Fig. 12

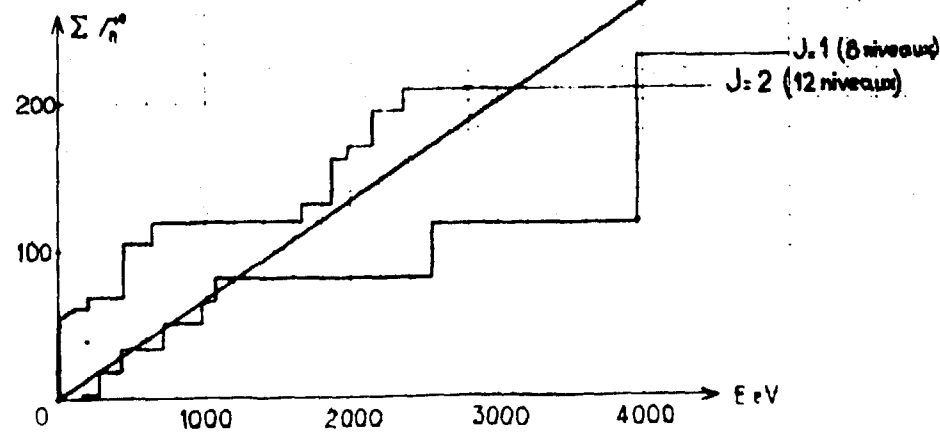
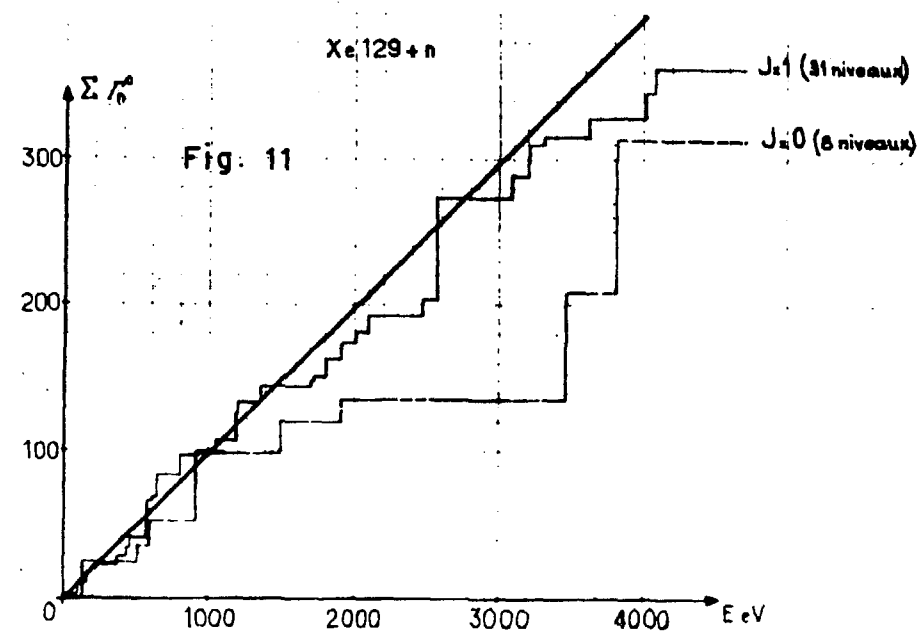


Fig. 11



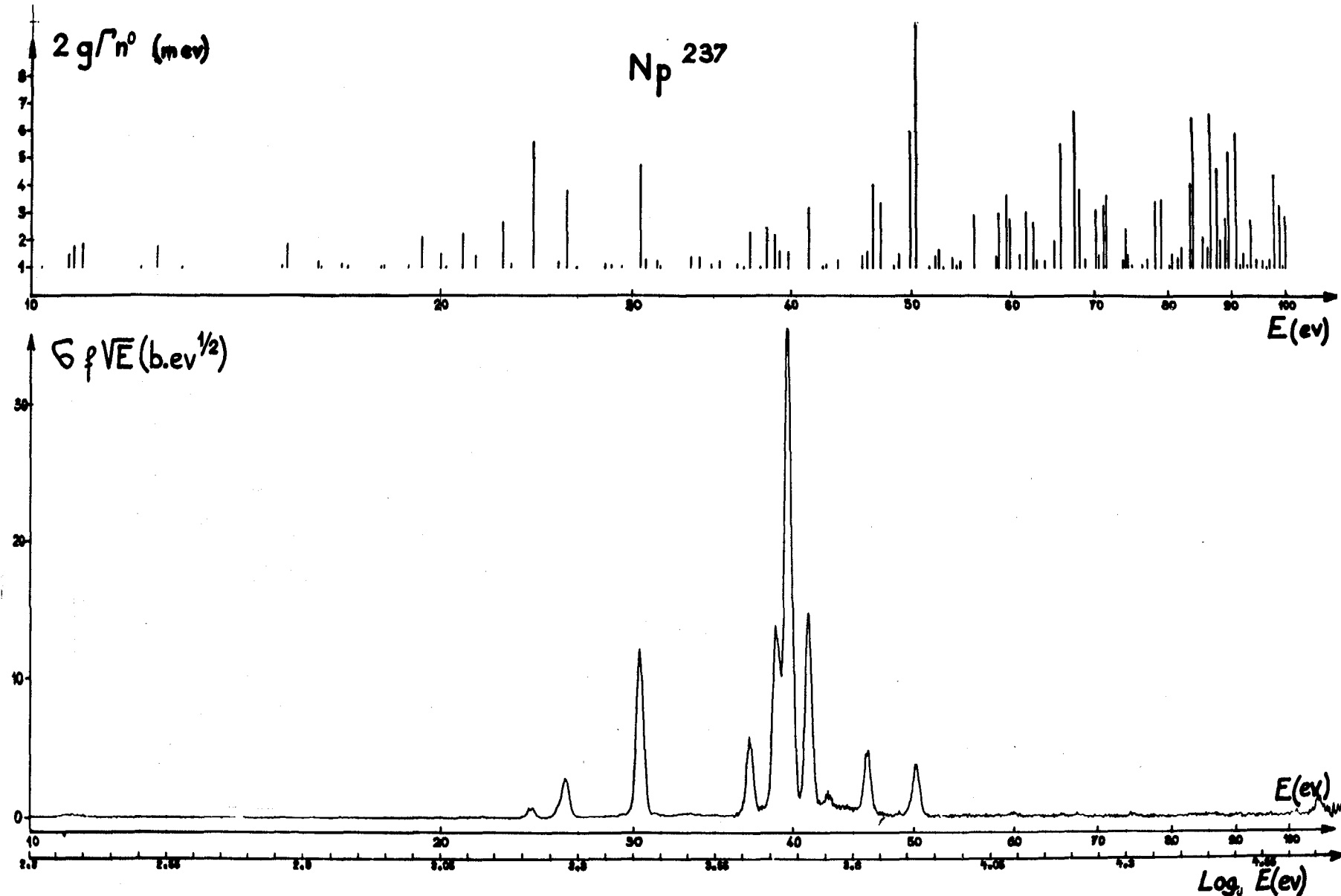


Fig. 13

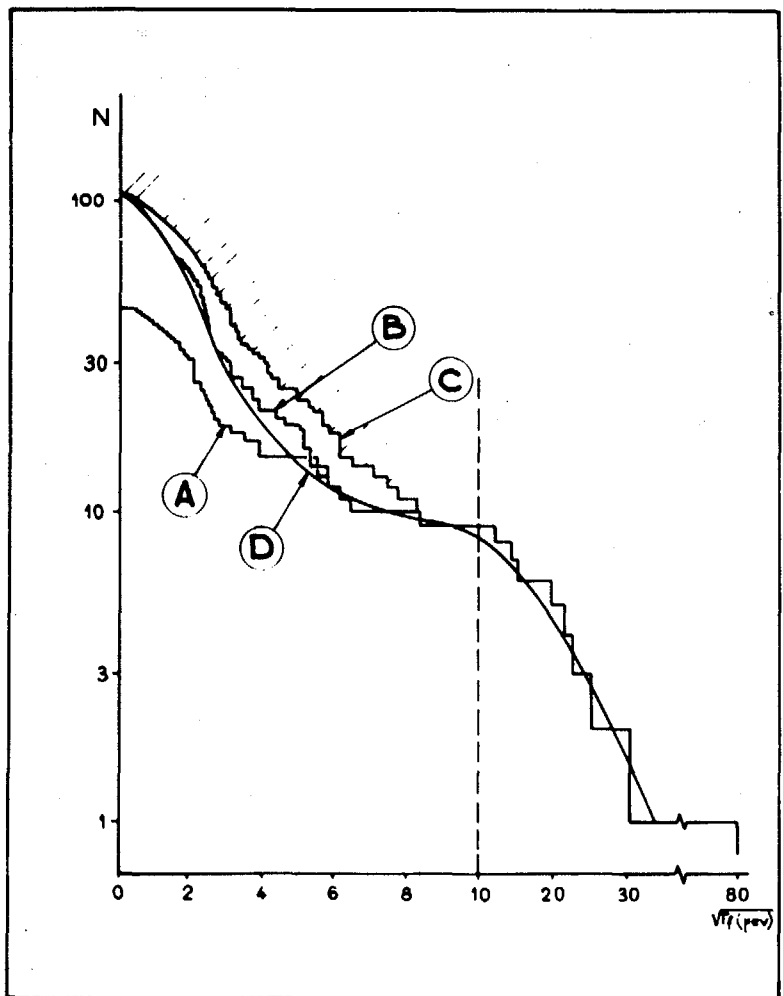


Fig. 15

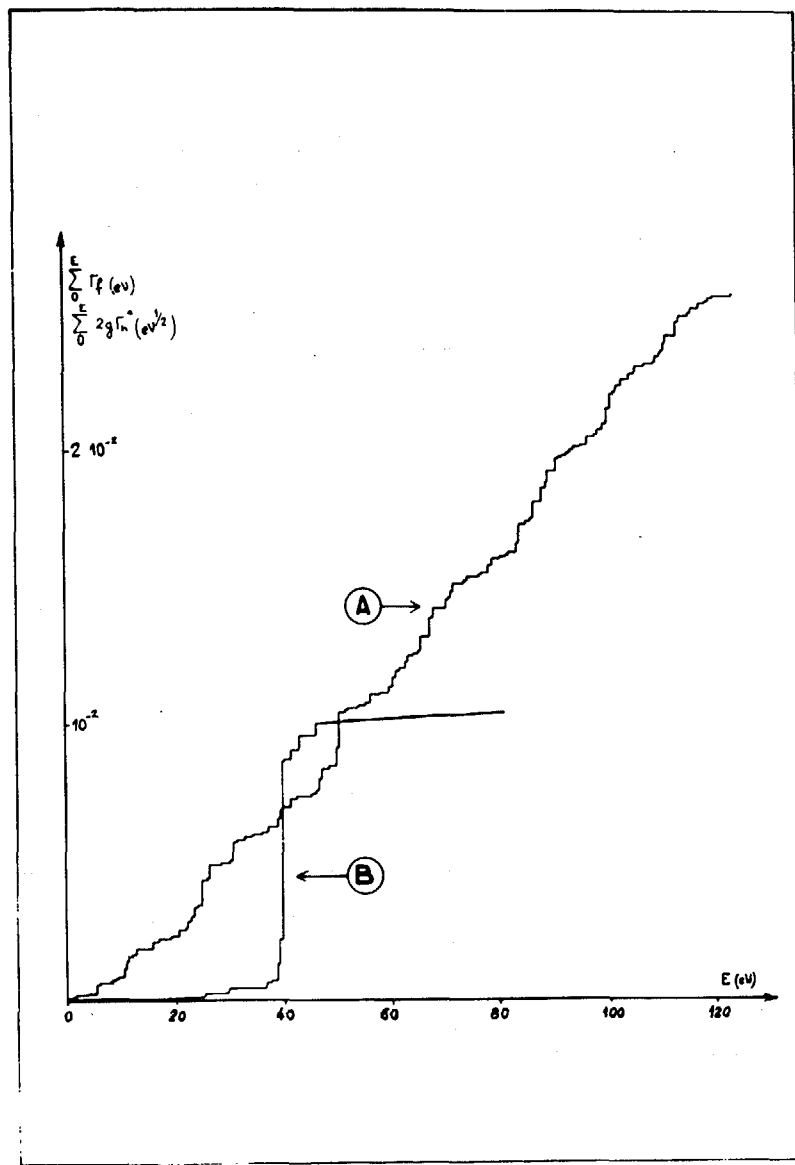


Fig. 14

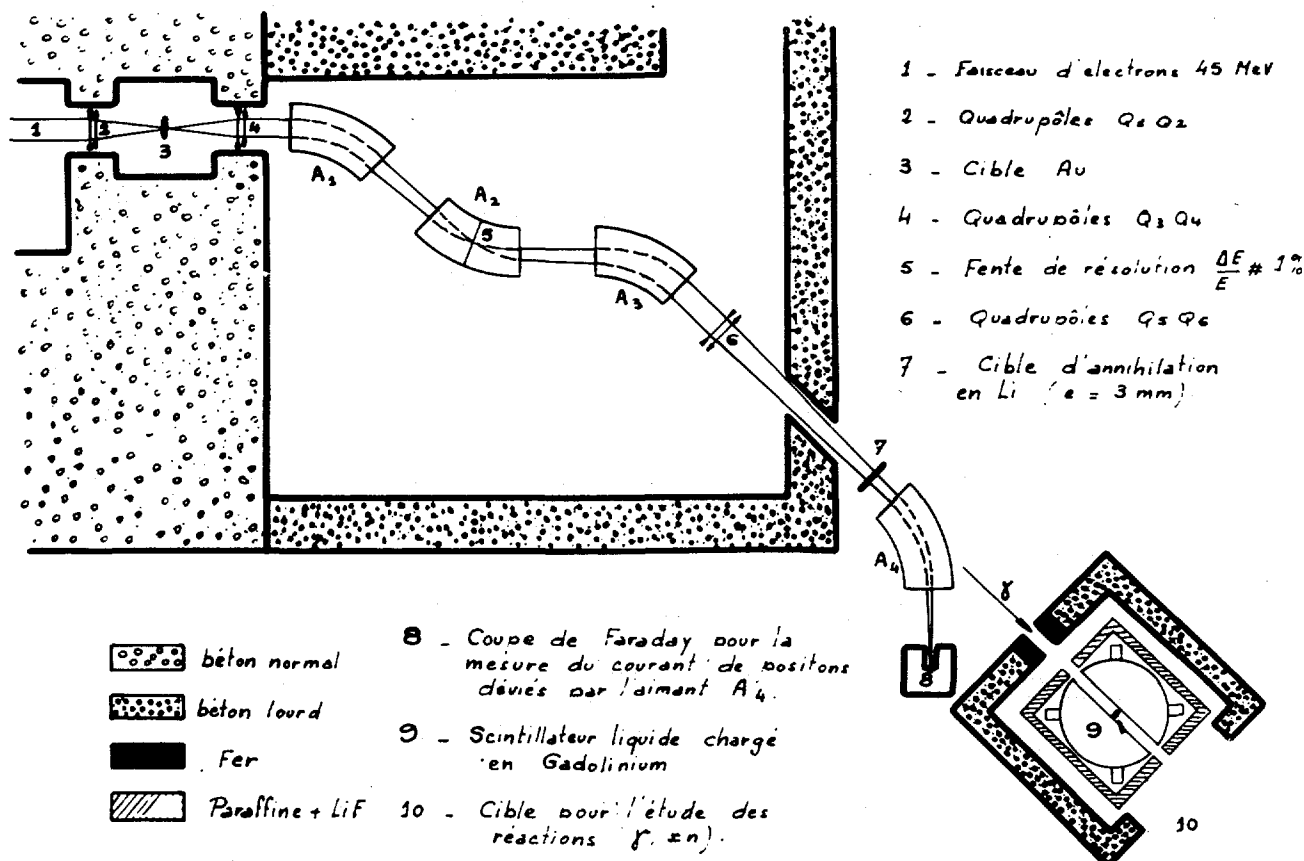
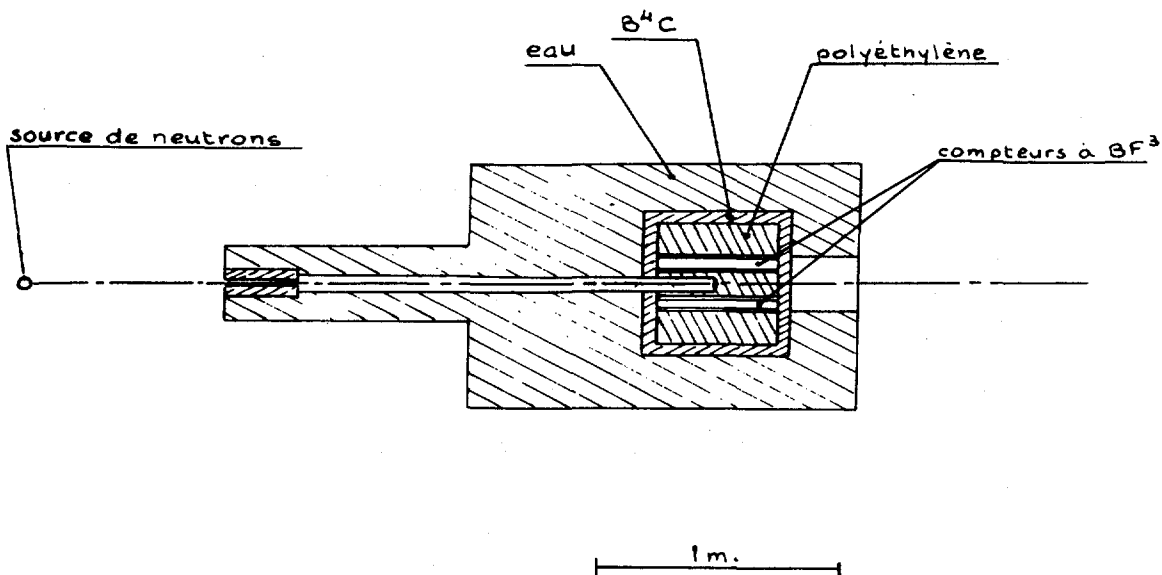


Fig. 17



Compteur directionnel étalon.

Fig. 16

**XXIV. DEPARTEMENT DE PHYSIQUE NUCLEAIRE**

**C. E. A. - SACLAY (FRANCE)**

J. JULIEN

Les expériences décrites ont été effectuées par R. ALVES, A. BLOCH, J. JULIEN, C. LOPATA, J. MORGENSENSTERN, C. SAMOUR.

**1. INFRASTRUCTURE**

Deux bases de temps-de-vol respectivement de 25 mètres et 14 mètres étaient dévolues aux expériences de capture de neutrons et une base aux expériences de transmission. L'appareillage utilisé et les méthodes d'analyse ont été décrits dans les précédents rapports.

**2. EXPERIENCES DE TRANSMISSION**

La base de temps-de-vol utilisée était de 103 ou 200 mètres suivant le noyau ou le domaine d'énergie étudiés. L'analyse de forme des résonances individuelles a permis d'obtenir les valeurs de  $S_0$ ,  $S_1$  et  $R'$  pour les éléments suivants :  $^{33,35}\text{Cl}$ ,  $^{51}\text{V}$ ,  $^{63}\text{Cu}$ ,  $^{65}\text{Cu}$ ,  $^{89}\text{Y}$ ,  $^{139}\text{La}$ , Nd,  $^{209}\text{Bi}$  (3,8).

Les valeurs obtenues complètent l'ensemble des valeurs publiées par ailleurs (1,2). Le tableau I résume l'ensemble des résultats obtenus. Les figures 1, 2 et 3 représentent respectivement les valeurs de  $S_0$ ,  $R'$  et  $S_1$  en fonction du nombre de masse. Les tableaux II et III donnent les paramètres des résonances de  $^{63}\text{Cu}$  et  $^{65}\text{Cu}$  étudiés à l'aide d'isotopes séparés.

**3. EXPERIENCES DE CAPTURE**

Les noyaux étudiés dans un domaine d'énergie de 1 eV à environ 500 eV suivant la base utilisée sont : Pt, W, Co, Au, Sn, Cd, Fe, Cu, Mn, Hg, Tm.

a) Entre 0 et 3 MeV un schéma détaillé des différents isotopes de ces noyaux a été établi avec quelquefois la valeur du spin quand le nombre des

résonances des deux états de spin est suffisant. La figure 4a représente un tel schéma pour  $^{195}\text{Pt} + n$  et  $^{197}\text{Au} + n$  (figure 4b).

b) La distribution des largeurs radiatives partielles pour 22 résonances de  $^{195}\text{Pt}$  et trois transitions donnait, pour le nombre de degrés de liberté, la valeur  $\nu = 1,25 \pm 0,35$  (4)  
 $- 0,27$

Il était intéressant d'étudier les distributions individuelles et la somme des transitions à deux niveaux très rapprochées. On a choisi  $^{183}\text{W}$ , l'échantillon des résonances étant 13. Pour la distribution correspondant à la somme des deux transitions, le degré de liberté  $\nu$  est :

$$\nu = 2,5 \quad + 1,6 \\ \quad \quad \quad - 1,2$$

ce qui montre que les deux transitions envisagées sont indépendantes. Le coefficient de corrélation entre ces deux transitions, pour ces 13 résonances, est voisin de zéro.

c) La valeur moyenne des largeurs radiatives partielles suit une loi en  $E_\gamma^5$  (5, 6, 7). Dans le platine, la valeur de la largeur radiative totale est fortement corrélée à la somme des largeurs radiatives partielles des transitions à l'état fondamental et aux états excités (5, 6). On trouve  
 $\rho = 0,75 \pm 0,17$  pour 13 résonances.  
 $- 0,30$

d) L'étude des résonances de l'étain (5, 6) a montré une intensité anormalement grande de certaines transitions M1. Les estimations de Blatt et Weisskopf présentent un rapport  $k(E1)/k(M1)$  supérieur à 3,5 soit :

$$k(E1) = \frac{\Gamma_i^2}{E_i^3 \cdot A^{2/3} \cdot D} \quad ; \quad k(M1) = \frac{\Gamma_i^2}{E_i^3 \cdot D}$$

Nos résultats expérimentaux montrent que ce rapport est 0,055 c'est-à-dire 60 fois plus faible que les prédictions théoriques.

e) Les figures 5a et 5b représentent les effets d'interférence relatifs aux transitions d'énergie 7920 et 6520 keV dans  $^{195}\text{Pt}$ . Ces effets sont négatifs.

Dans l'or on a trouvé un effet d'interférence positif entre les deux résonances situées entre 4,8 et 60 eV pour les quatre transitions de 6510, 6455, 6313 et 6245 keV. Toutefois, pour cette dernière, les données expérimentales ne peuvent être adaptées que si l'on introduit une section efficace de capture directe de 2 mb. La figure 6 représente l'adaptation des données expérimentales pour la transition d'énergie 6245 keV.

Dans le cobalt, une section efficace de capture directe de 10mb est nécessaire pour adapter les points expérimentaux de la transition d'énergie 7490 KeV.

Ce rapport est le dernier des auteurs dans le domaine des neutrons de faible énergie. Leurs activités se poursuivront auprès de l'accélérateur linéaire d'électrons de 300 MeV de Saclay.

REF E R E N C E S

- (1) J. MORGESTERN, S. DE BARROS, P. L. CHEVILLON,  
M. J. GAUTHIER, H. JACKSON, J. JULIEN et C. SAMOUR,  
Conf. I. A. E. A., Paris (1966) 183
- (2) J. MORGESTERN, S. DE BARROS, A. BLOCH,  
P. L. CHEVILLON, V. D. HUYNH, H. E. JACKSON, J. JULIEN,  
C. LOPATA et C. SAMOUR, Nucl. Phys. A 102 (1967) 602.
- (3) J. MORGESTERN, S. DE BARROS, P. L. CHEVILLON,  
V. D. HUYNH, H. E. JACKSON, J. JULIEN et SAMOUR,  
C. R. Acad. Sc. 265 (1967) 506
- (4) H. JACKSON, J. JULIEN, C. SAMOUR, A. BLOCH,  
C. LOPATA, J. MORGESTERN, H. MANN et G. E. THOMAS,  
Phys. Rev. Letters, 17 (1966) 656.  
C. SAMOUR, H. E. JACKSON, P. L. CHEVILLON, J. JULIEN  
et J. MORGESTERN, Conf. I. A. E. A., Paris (1966) 175.
- (5) C. SAMOUR, Thèse de Doctorat d'Etat, Paris (février 1968)
- (6) A paraître
- (7) J. JULIEN, Thèse de Doctorat d'Etat, Paris (mai 1967).
- (8) J. MORGESTERN, Thèse de Doctorat d'Etat, Paris  
(février 1968).

Tableau II

 $^{63}\text{Cu} + \text{n}$ 

$E_0$ eV	$g\Gamma_n$ eV	J	$\Gamma_n$ eV	$g\Gamma_n^0$ eV	$\Gamma_n^0$ eV
578	0,54				
650,9	0,0057				
807,1	0,0023				
994,3	0,0073				
2 042	15,44 ± 0,5	1	41,0	0,341	0,910
2 643	2,53 ± 0,07	2	4,0	0,049	0,078
4 386	1,94 ± 0,05	1	5,16	0,029	0,078
4 844	5,11 ± 0,15	1	13,60	0,073	0,195
5 374	22,93 ± 0,66	2	36,7	0,313	0,500
5 806	5,63 ± 0,33	2	9,0	0,074	0,118
6 820	0,10 ± 0,05			0,001	
7 062	0,49 ± 0,20			0,006	
7 543	6,30 ± 0,19	1	16,76	0,073	0,193
7 920	50,15 ± 2,5	2	80,2	0,563	0,900
8 327	2,27 ± 0,1	1	6,04	0,025	0,066
9 166	32,04 ± 1,6	2	51,3	0,333	0,535
9 886	35,64 ± 1,7	1	94,80	0,358	0,955
10 803	40,10 ± 2,0	2	64,2	0,387	0,620
12 480	5,09 ± 0,24	1	13,5	0,046	0,122
13 095	48,10 ± 2,4	2	77,0	0,419	0,671
13 645	10,80 ± 0,32	1	28,6	0,092	0,246
15 025	6,77 ± 0,33	1	18,0	0,055	0,147
15 739	8,60 ± 0,26	1	22,8	0,069	0,184
16 000	0,77 ± 0,25			0,006	
16 223	6,96 ± 0,70	1	18,5	0,055	0,147
17 787	30,0 ± 1,5	1	79,8	0,225	0,600
18 035	18,6 ± 0,9	2	29,8	0,138	0,221
20 806	0,74 ± 0,25			0,005	
20 900	44,18 ± 4,5	2	70,6	0,304	0,486
21 050	1,8 ± 0,8			0,012	
21 124	38,10 ± 3,8	1	101,0	0,252	0,672
21 619	2,6 ± 1,0			0,018	
22 672	58,0 ± 2,90	2	92,8	0,385	0,616
23 161	0,8 ± 0,4			0,005	
23 204	0,6 ± 0,3			0,004	
23 487	1,19 ± 0,5			0,008	
24 765	49,0 ± 2,4	2	78,4	0,312	0,499
25 618	16,7 ± 11,6	1	310	0,729	1,945
25 779	0,8 ± 0,4			0,005	
26 447	41,62 ± 8,0	1	110,7	0,256	0,690
29 359	15,57 ± 9,2	1	307,4	0,675	1,800
30 285	0,8 ± 0,4				
31 205	22,3 ± 1,1	2	35,6	0,126	0,202

Tableau III

 $^{65}\text{Cu} + \text{n}$ 

$E_0$ eV	$g\Gamma_n$ eV	J	$\Gamma_n$ eV	$g\Gamma_n^0$ eV	$\Gamma_n^0$ eV
230				0,001	
1 364					
2 529	9,79 ± 0,30	2	15,6	0,195	0,312
3 913	8,65 ± 0,30	1	23,0	0,138	0,368
4 476	5,59 ± 0,23	1	14,9	0,084	0,224
6 429	15,75 ± 0,60	2	25,2	0,196	0,314
7 604	13,30 ± 0,7	1	35,4	0,152	0,406
7 879	58,17 ± 3,4	2	93,0	0,658	1,055
8 369	0,21 ± 0,10			0,002	
9 785	0,75 ± 0,30			0,008	
12 086	0,66 ± 0,26			0,006	
13 192	54,84 ± 2,74	2	87,7	0,477	0,762
13 617	0,77 ± 0,25			0,006	
14 153	21,14 ± 1,2	2	33,8	0,178	0,285
16 060	18,50 ± 0,7	1	49,2	0,145	0,387
19 895	75,54 ± 4,5	2	120,9	0,535	0,856
21 921	3,44 ± 1,50			0,023	
23 681	20,53 ± 1,1	1	54,60	0,133	0,355
24 133	50,20 ± 3,0	1	133,5	0,323	0,861
25 017	22,7 ± 2,2	2	36,3	0,131	0,210
25 108	35 ± 3,5	1	93,1	0,194	0,517
25 784	5,21 ± 2,1			0,032	

Tableau I - Valeurs des fonctions densité et des rayons de diffusion.

Noyau étudié	Intervalle d'énergie analysé (eV)	$S_0 (10^{-4} \text{ eV}^{-\frac{1}{2}})$	R' (fm)	$S_1 (10^{-4} \text{ eV}^{\frac{1}{2}})$
$^{51}\text{V}$	0 - 130 000	$10,6 + 4,8$ $- 2,8$	$6,0 \pm 1,0$	$0,48 + 0,20$ $- 0,12$
$^{55}\text{Mn}$ (2)	0 - 75 000	$4,0 + 1,0$ $- 0,7$	$3,6 \pm 0,4$	
$^{59}\text{Co}$ (2)	0 - 120 000	$3,8 + 1,6$ $- 1,6$	$5,4 \pm 0,4$	$< 0,4$
$^{63}\text{Cu}$	0 - 30 000	$2,4 + 0,7$ $- 0,5$	$7,5 \pm 0,4$	
$^{65}\text{Cu}$	0 - 30 000	$1,2 + 0,5$ $- 0,3$	$6,9 \pm 0,4$	
$^{69}\text{Ga}$ (1)	0 - 2 500	$1,2 + 1,2$ $- 0,4$	$6,3 \pm 1$	
$^{75}\text{As}$ (1)	0 - 4 000	$1,75 + 0,4$ $- 0,3$	$7 \pm 0,8$	
$^{77}\text{Se}$ (1)	0 - 1 500	$1,5 + 1,0$ $- 0,5$		
$^{79,81}\text{Br}$ (1)	0 - 2 000	$1,5 + 0,38$ $- 0,28$	$7 \pm 0,8$	
$^{89}\text{Y}$ (1)	0 - 30 000	$0,39 + 0,27$ $- 0,12$	$6,6 \pm 0,3$	$4,4 + 2,0$ $- 1,2$
$^{91}\text{Zr}$ (1)	0 - 2 000	$0,8 + 1,3$ $- 0,3$	$7,10 \pm 0,35$	$5,8 + 7,9$ $- 2,1$
$^{93}\text{Nb}$ (1)	0 - 4 100	$0,35 + 0,10$ $- 0,07$	$7,1 \pm 0,3$	$5,0 + 1,5$ $- 1,0$
$^{107}\text{Ag}$ (1)	0 - 760	$0,37 + 0,10$ $- 0,07$		
$^{109}\text{Ag}$ (1)	0 - 760	$0,75 + 0,16$ $- 0,14$		
$^{133}\text{Ba}$ (1)	0 - 1 350	$0,80 + 0,35$ $- 0,20$	$5,8 \pm 0,8$	
$^{137}\text{Ba}$ (1)	0 - 1350	$0,30 + 0,70$ $- 0,18$	$5,8 \pm 0,8$	

Tableau I - Valeurs des fonctions densité et des rayons de diffusion (suite et fin).

Noyau étudié	Intervalle d'énergie analysé (eV)	$S_0 (10^{-4} \text{ eV}^{-\frac{1}{2}})$	R' (fm)	$S_1 (10^{-4} \text{ eV}^{\frac{1}{2}})$
$^{139}\text{La}$	0 - 10 000	$0,70 + 0,20$ $- 0,14$	$4,9 \pm 0,3$	$\lesssim 0,7$
$^{141}\text{Pr}$	0 - 6 000	$2,04 + 0,47$ $- 0,35$	$4,9 \pm 0,5$	
$^{143}\text{Nd}$	0 - 740	$4,1 + 2,5$ $- 1,2$	$7,5 \pm 0,8$	
$^{145}\text{Nd}$	0 - 740	$2,9 + 1,1$ $- 0,7$	$7,5 \pm 0,8$	
$^{169}\text{Tm}$ (1)	0 - 760	$1,50 + 0,27$ $- 0,21$	$7,7 \pm 0,8$	
$^{192}\text{Pt}$ (1)	0 - 580	$1,7 + 1,9$ $- 0,6$	$8,7 \pm 0,5$	
$^{194}\text{Pt}$ (1)	0 - 700	$1,4 + 2,4$ $- 0,5$	$8,7 \pm 0,5$	
$^{195}\text{Pt}$ (1)	0 - 825	$1,70 + 0,48$ $- 0,33$	$8,7 \pm 0,5$	
$^{197}\text{Au}$ (1)	0 - 1 000	$1,80 + 0,39$ $- 0,30$	$8,7 \pm 0,5$	
$^{198}\text{Hg}$ (1)	0 - 420	$1,5 + 2,1$ $- 0,5$	$9,8 \pm 0,7$	
$^{199}\text{Hg}$ (1)	0 - 700	$2,2 + 2,2$ $- 0,7$	$9,8 \pm 0,7$	
$^{201}\text{Hg}$ (1)	0 - 700	$1,3 + 1,3$ $- 0,4$	$9,8 \pm 0,7$	
$^{209}\text{Bi}$ (3)	0 - 70 000	$0,65 + 0,39$ $- 0,17$	$9,0 \pm 0,4$	$0,25 + 0,09$ $- 0,05$

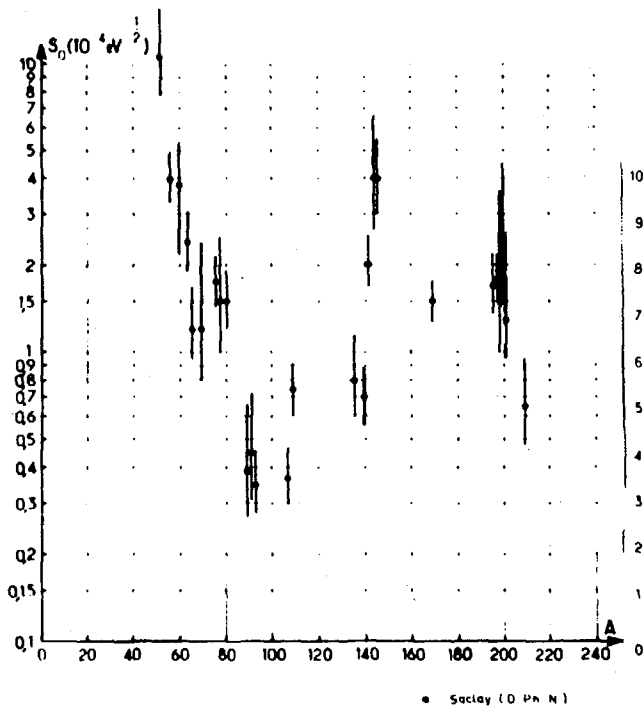


Fig. 1

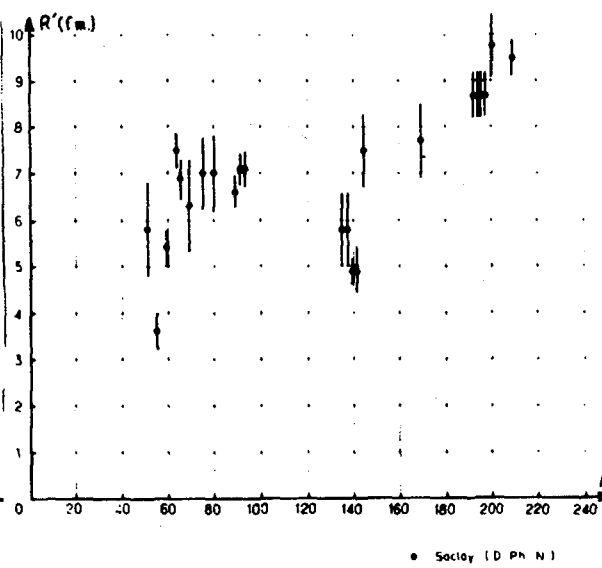


Fig. 2

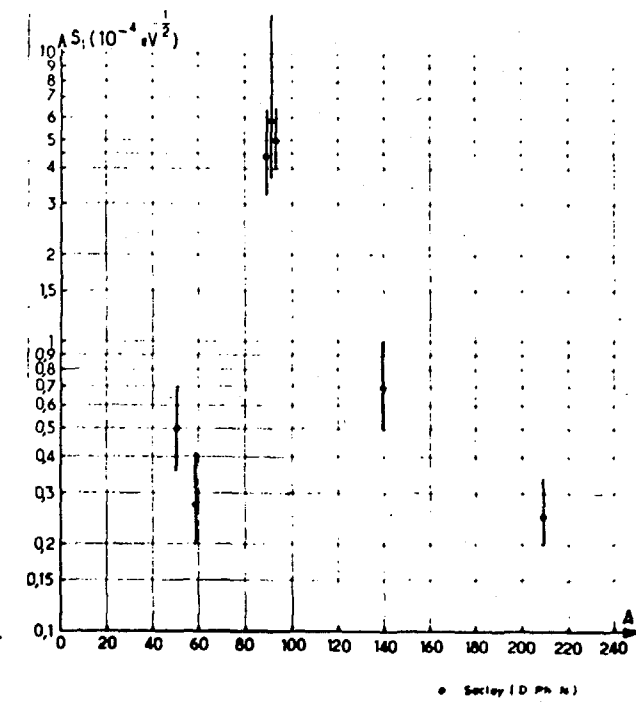


Fig. 3

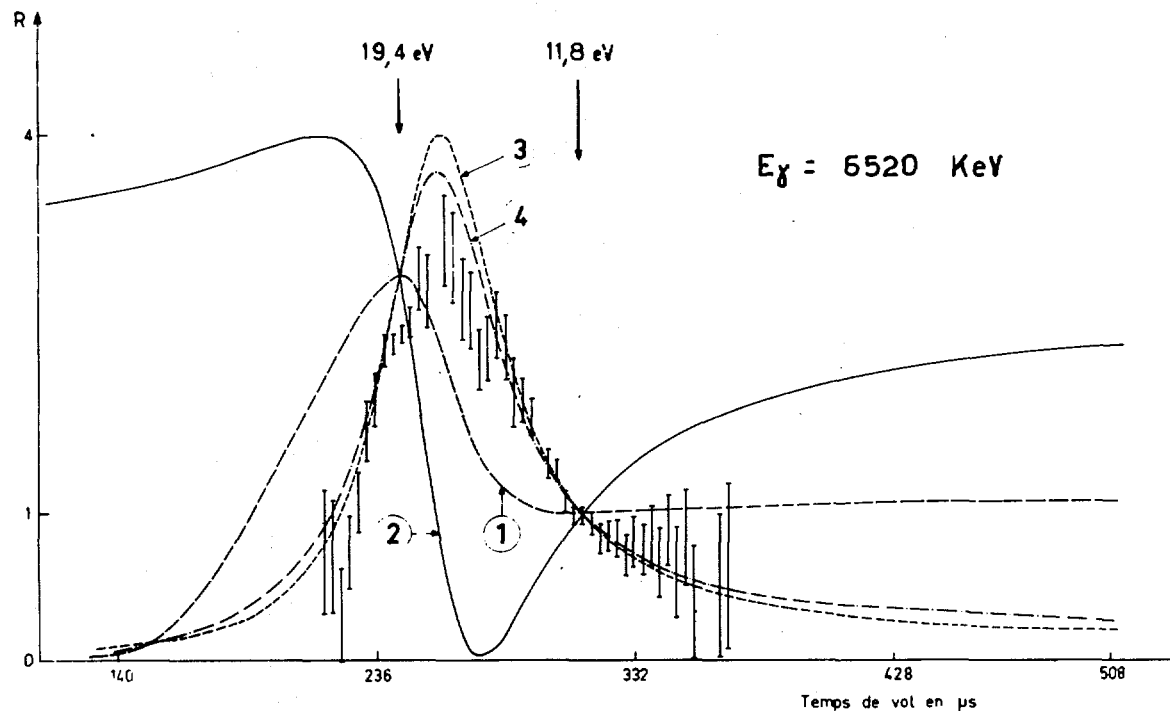


Fig. 5b

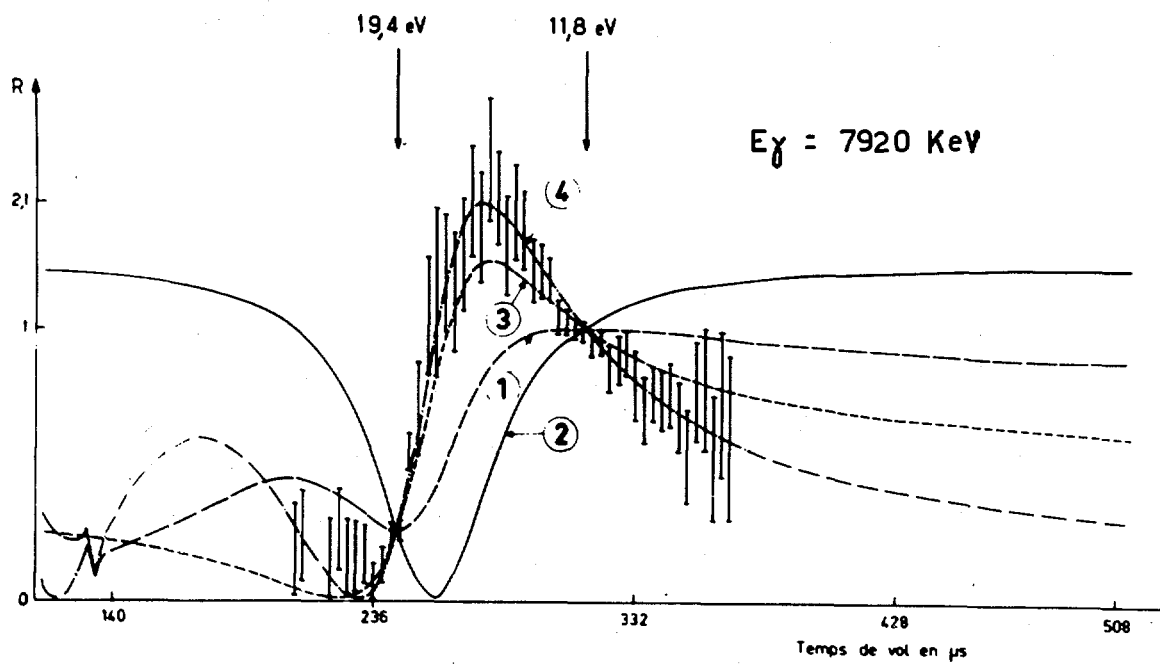


Fig. 5a



Fig. 4a

Fig. 4b

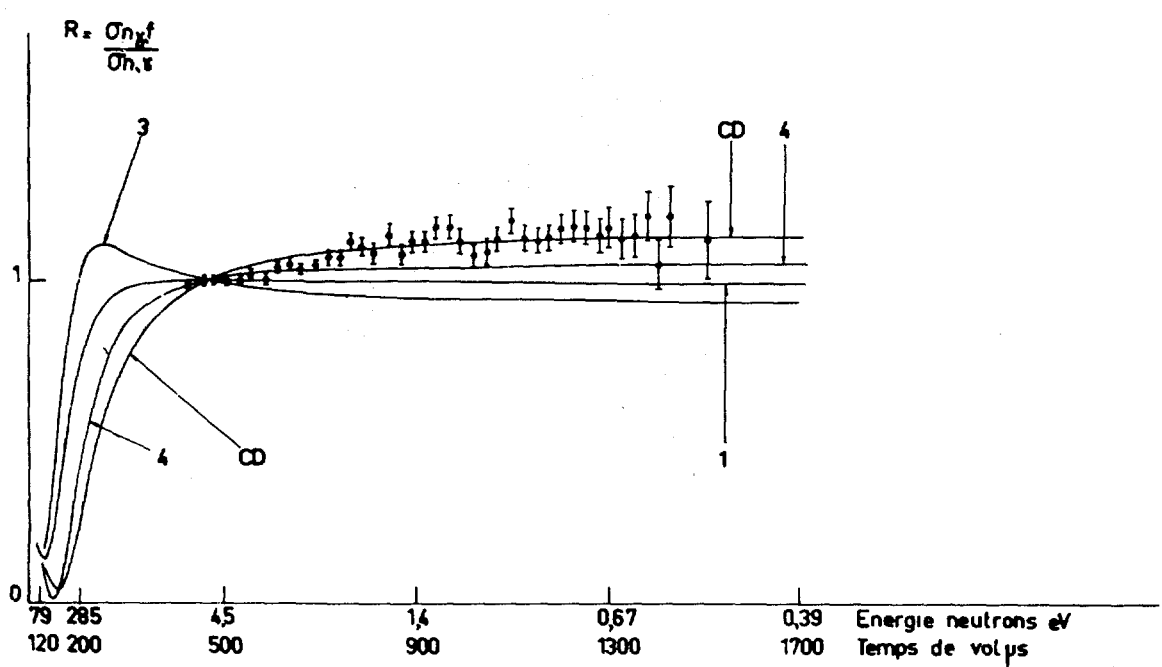


Fig. 6

**XXV. SECTIONS DE MESURES FONDAMENTALES DU COMMISSARIAT A L'ENERGIE ATOMIQUE (FRANCE)**

P. LEUBA, J. DIDIER.

**1. APPAREILLAGE**

**1.1. Accélérateur Van de Graaff Tandem 12 MeV**  
(A. DANDINE, J.D. CIRET)

**1.1.1. Amélioration de la pulsation du faisceau**

Le pulsateur actuel comprend un hacheur et en regroupeur disposés avant accélération qui permettent d'obtenir sur la cible des bouffées de protons d'intensité crête de 68 à 95  $\mu$  A, et de largeur à mi-hauteur 3, 7 à 5 nanosecondes suivant les énergies. Ce dispositif sera complété par un hacheur supplémentaire, disposé après accélération qui permettra de réduire la largeur à mi-hauteur des bouffées à 1 ou 2 nanosecondes.

**1.1.2. Installation d'une source d'ions négatifs à extraction directe**  
Comparée à la source à échange de charges actuelle, la source en projet d'installation délivre une intensité d'ions négatifs (protons) supérieure avec une dispersion en énergie environ dix fois plus faible. Il doit en résulter une amélioration notable des performances de l'accélérateur en régime continu et en fonctionnement pulsé.

**1.2. Acquisition et traitement de l'information**  
(PH. FERNIER, J. LABBE, J.P. LAGET, G. MARIN)

Au cours de l'année 1967, des améliorations importantes ont été apportées au système d'acquisition et de traitement utilisant un calculateur "C A E 510" elles concernent plus particulièrement :

**1.2.1. Acquisition à distance**

Des expériences effectuées sur un accélérateur distant de 1 km, on été connectées en ligne sur le "C A E 510" grâce à une transmission à fort débit (5 Mégabits).

**1.2.2. Exploitation en partage de temps**

La mise au point d'une version temps réel du compilateur "ALGOL" a permis d'étendre les possibilités de simultanéité du précédent système d'exploitation temps réel.

1.2.3. Projet de système de traitement d'informations

L'installation existante étant surchargée, nous étudions son remplacement par un système comprenant plusieurs ordinateurs interconnectés et reliés à un service de calcul extérieur au Centre par une liaison à 2 400 Bauds.

2. REACTIONS ENTRE PROTONS ET NOYAUX LEGERS

2.1. Diffusion élastique et inélastique des protons de 2 à 10 MeV, par le  $^7\text{Li}$

(G. BARDOLLE, J. CABE, M. LAURAT, M. LONGUEVE)

L'étude de la diffusion élastique et inélastique des protons par le  $^7\text{Li}$  a été effectuée systématiquement entre 2 et 10 MeV, 10 courbes d'excitation ont été tracées à des angles compris entre  $40^\circ$  et  $170^\circ$  dans le système du laboratoire.

Les protons étaient accélérés par un Van de Graaff Tandem 12 MeV ; la cible était constituée d'un dépôt de Lithium 7 sur un film de Carbone ; la masse de Lithium déposée était mesurée par la méthode du quartz (1), et le flux de protons incidents par un intégrateur de courant associé à une cage de Faraday. Les protons diffusés étaient détectés par des jonctions au Silicium.

Pour la diffusion élastique, l'incertitude sur la valeur absolue des sections efficaces est de 5 à 7 % suivant les points, et de 6 à 10 % pour la diffusion inélastique.

Les principales courbes d'excitation sont représentées sur les Fig. 1 - 2 et 3. Les distributions annulaires (Fig. 4 et 5) ont été développées en série de polynômes de Legendre :

$$\begin{aligned} L &= 4 \\ \frac{d\sigma}{d\Omega}(\theta) &= \sum A_L \cdot P_L(\cos\theta) \\ L &= 0 \end{aligned}$$

Les figures 6 et 7 représentent la variation avec l'énergie des coefficients  $A_L$  des développements limités à  $P_4$ . Il a été possible d'en déduire des précisions sur les niveaux du  $^8\text{Be}$  entre 19 et 25 MeV (2).

2.2. Etude de la réaction p +  $^{11}\text{B}$  à 1,4 MeV

(M. CADEAU, D. DIDIER, J.P. LAUGIER, G. MOUILHAYRAT, F. PERRAULT, J. SUDAROVICH)

Nous avons étudié la réaction p +  $^{11}\text{B}$  pour une énergie incidente de protons de 1,4 MeV. Cette énergie correspond à la résonnance à 17,23 MeV d'énergie d'excitation dans le  $^{12}\text{C}$  pour la particule  $a_1$  associée au 1er niveau excité du  $^8\text{Be}$ . Cette résonnance a pour caractéristique de spin et de parité  $J = 1^-$ .

D'après les résultats obtenus précédemment (3,4) nous nous attendions à observer une dépopulation sur la périphérie du diagramme de Dalitz dans la zone où deux particules a emportent toute l'énergie. D'autre part nous avons cherché à mettre en évidence un phénomène d'interférence dans la zone où les contributions du 1er Niveau excité du  $^8\text{Be}$  se croisent.

Pour cela nous avons utilisé la méthode des coïncidences avec enregistrement multiparamétrique.

Nous avons enregistré simultanément deux spectres de coïncidence en enregistrant pour chaque évènement quatre paramètres.

- l'énergie de la particule détectée sur une jonction notée 0 placée à  $90^\circ$  par rapport à la direction du faisceau incident.
  - Le numéro (1 ou 2) de la jonction placée du côté opposé de la jonction 0 par rapport à la direction du faisceau incident sur laquelle a été détectée une particule en coïncidence avec la particule détectée sur la jonction 0.
  - l'énergie de la particule détectée sur la jonction 1 (ou 2)
  - l'instant de détection de la particule sur la jonction 1 (ou 2)
- Le temps  $t = 0$  était celui où l'on a détecté une particule sur la jonction 0. Ces quatre paramètres sont regroupés pour former un mot binaire transmis en deux séquences sur un calculateur CAE 510.

Le calculateur reçoit les informations, les inscrit sur bande magnétique et parallèlement effectue un prétraitement.

Nous avons effectué un dépouillement préliminaire de tous les spectres enregistrés en utilisant la formalisme que nous avions mis au point précédemment (3). Les premiers résultats obtenus nous indiquent une variation continue de la largeur du 1er niveau excité du  $^8\text{Be}$ . Sur la périphérie du Diagramme de Dalitz nous observons le dépeuplement auquel nous nous attendions. Pour les spectres voisins la largeur utilisée pour le 1er niveau excité du  $^8\text{Be}$  est 1,45 MeV. Au fur et à mesure que l'on se rapproche de

... l'intersection des deux contributions de ce niveau la largeur décroît jusqu'à 0,9 MeV, cette largeur se stabilise ensuite à 1,45 MeV quand on s'éloigne à nouveau. Cette variation de largeur nous a conduit à introduire dans nos calculs un terme d'interférence. L'introduction de ce terme permet de reproduire nos 24 spectres en prenant la valeur  $\Gamma = 1,45$  MeV pour le premier niveau excité du  $^{8}\text{Be}$ .

Ces calculs ont été faits en collaboration avec M. MARQUEZ de la Faculté des Sciences de Bordeaux; nous en publierons les résultats prochainement.

3.

REACTIONS ENTRE DEUTERONS ET NOYAUX LEGERS

(G. BRUNO, J. DECHARGE, M.Y. DECHARGE, L. FAUGERE, A. PERRIN, G. SURGET)

On a poursuivi l'étude de la réaction  $^{7}\text{Li} (\text{d}, \alpha) ^5\text{He}$ ;  $^{5}\text{He} \rightarrow \alpha_2 + n$ . Une évaluation du spectre des  $\alpha_1$  a permis de tracer des fonctions d'excitation et des distributions angulaires pour la première étape de la réaction dans une gamme d'énergie comprise entre 0,6 et 2 MeV. L'interprétation des résonances observées doit permettre de préciser les caractéristiques des noyaux de  $^{9}\text{Be}$  mis en jeu. L'interprétation des spectres correspondant à la corrélation ( $\alpha_1, \alpha_2$ ) dans différentes conditions géométriques se poursuit.

Au cours d'essais de mesures de sections efficaces à basse énergie (inférieure ou égale à 100 keV) et en particulier de mesures par activation par particules chargées, on s'est heurté au problème de la contamination des cibles par les vapeurs organiques résiduelles. Différentes tentatives ont été faites pour déterminer les conditions dans lequel ce phénomène peut-être réduit au minimum.

4.

ETUDE DE LA REACTION D + n → p + n + n à 13,9 MeV

(M. CADEAU, D. DIDIER, J.P. LAUGIER, G. MOUILHAYRAT, F. PERRAULT, J. SUDAROVICH)

4.1.

Etude du spectre en énergie des protons de la réaction D (n,p)2n

La mesure précédente (EANDC E 66) a été reprise et précisée à l'aide d'un télescope comprenant un radiateur mince ( $4,5 \text{ mg/cm}^2$ ) de polyéthylène deutéré, un compteur proportionnel au  $\text{CO}_2$ , et deux détecteurs semi-conducteurs refroidis ( $\Delta E$  et  $E$ ). Le système ( $\frac{\Delta E}{\Delta X}$ ,  $E$ ) permet de séparer parfaitement (100%) le spectre des protons et les deutérons diffusés élastiquement.

La figure 8 représente la partie supérieure du spectre des particules chargées émises à  $0^\circ$ .

On y voit les protons de recul dus aux traces d'hydrogène (A), les deutérons de recul (B) et la partie supérieure du spectre de protons de rupture (C). Le maximum haute énergie de (C) est dû à l'interaction neutron-neutron. Les courbes continues correspondent aux résolutions calculées.

Une interprétation théorique en cours devrait permettre d'obtenir des renseignements sur l'interaction neutron-neutron.

Cette méthode basée sur la théorie des perturbations calcule dans l'approximation de Born le spectre des particules issues de la rupture du deutéron. Les potentiels nucléon-nucléon sont pris comme étant du type de Yukawa à cœur dur et la fonction d'onde initiale du deutéron est du type de Hulten. On a tenu compte des divers couplages de spin possibles ce qui conduit à un calcul de volume assez important. Un calcul de ce type a déjà été fait par D.R. KOEHLER et R.A. MANN (5) pour le spectre des protons de rupture. Nous nous proposons de calculer aussi le spectre des neutrons de rupture pour le comparer à nos résultats.

4.2. Etude du spectre en énergie des neutrons de la réaction  $D(n,2n)p$

Pour mesurer le spectre des neutrons émis à 20° par rapport au faisceau incident (figure 9) nous avons mis au point et utilisé un spectromètre à temps de vol dont la base de vol a 2,30 mètres de long et dont le détecteur neutron est un scintillateur liquide de 590 cm<sup>3</sup> vu par deux photomultiplicateurs 56 AVP mis en coïncidence. Un système de discrimination neutron gamma nous permet d'éliminer les gamma tout en ayant un seuil de détection de l'ordre de 0,5 MeV. Ce spectromètre est monté sur un goniomètre qui peut tourner autour de l'échantillon.

Dans le cas de notre mesure le diffuseur était constitué d'eau lourde. Nous avons soustrait le spectre des neutrons diffusé dans les mêmes conditions sur de l'eau ordinaire de façon à éliminer l'influence du boîtier et de l'oxygène. Les sections efficaces ont été mesurées par rapport à la diffusion sur l'hydrogène. Cette mesure confirme et précise celle de S. MESSELT (EANDC (UK) 39 L).

4.3. Etude biperamétrique du spectre des protons et des neutrons de rupture du deutérium.

Dans le montage précédent nous avons remplacé le diffuseur d'eau lourde par un scintillateur deutéré vu par un photomultiplicateur. Nous enregistrons simultanément le temps de vol des neutrons émis à 0° et l'énergie de protons associé. Dans le plan Ep

... En les interactions neutron-neutron et neutron-proton se traduisent par des amas de points distincts. Nous avons entrepris une première série de mesures pour  $\theta = 20^\circ$  et  $\theta = 40^\circ$ .

## 5. SECTIONS TOTALES NEUTRONIQUES

### 5.1. Recherche d'une structure intermédiaire dans la section totale neutronique du Titane

(G. BARDOLLE, J. CABE, M. CANCE, M. LAURAT, M. LONGUEVE)

Ces mesures de sections efficaces totales neutroniques concernent la recherche d'une structure intermédiaire dans les corps dont le Ti est voisin de 50 (6). La littérature antérieure ne donnait pour le Ti qu'une dizaine de points dans la gamme 300 - 1200 KeV. Nous avons effectué des mesures de 2 keV en 2 KeV avec une dispersion en énergie de 3 KeV environ (figure 10) afin de mettre en évidence la structure fine sur laquelle on pourra effectuer des moyennes.

L'échantillon utilisé était du Titane naturel contenant 8 % de  $^{46}\text{Ti}$ , 7 % de  $^{47}\text{Ti}$ , 74 % de  $^{48}\text{Ti}$ , 6 % de  $^{49}\text{Ti}$  et 5 % de  $^{50}\text{Ti}$  de 3 cm de diamètre et 3 ou 4 cm de long de façon à conserver une transmission de l'ordre de 50 %. L'erreur totale sur les mesures compte tenu de la statistique et de la géométrie est de l'ordre de 3 à 4 %.

Les moyennes effectuées sur des intervalles d'énergie  $\Delta E$  compris entre 10 KeV et 300 KeV (figure 11) font apparaître un maximum à une énergie d'environ 700 KeV qui se conserve en position et amplitude pour des moyennes comprises entre 60 KeV et 120 KeV. La largeur à mi-hauteur de ce maximum est d'une centaine de KeV.

### 5.2. Etude des niveaux du $^{29}\text{Si}$ entre 8,870 MeV et 9,640 MeV

(G. BARDOLLE, J. CABE, M. LAURAT, M. LONGUEVE)

Nous avons mesuré la section efficace totale neutronique du Silicium entre 400 KeV et 1200 KeV (figure 12). Ces mesures nous ont permis de mettre en évidence trois résonnances aux énergies neutroniques respectives de 536 KeV, 570 KeV et 804 KeV. Les deux premières résonnances avaient été signalées dans les références 7 et 8. Il y avait accord pour la valeur  $J = \frac{3}{2}^-$  attribuée au niveau dont l'énergie d'excitation dans le  $^{29}\text{Si}$  est 9,028 MeV (ce qui correspond à  $E_n = 570$  KeV). Par contre l'analyse de nos résultats à l'aide d'un programme de moindres carrés utilisant une formule de BREIT et WIGNER nous a donné pour la première

... résonnance  $J = \frac{1}{2}$ ,  $\Gamma = 1,7 + 0,3$  KeV tandis que les mesures de la référence 1 lui attribuaient  $J = \frac{5}{2}$ ,  $\Gamma = 0,32$  KeV. La dernière résonnance obtenue à  $E_n = 804$  KeV (ce qui correspond à 9,254 MeV d'excitation dans le  $^{29}Si$ ) est telle que son moment angulaire total  $J = \frac{3}{2}$  (+) et sa largeur  $\Gamma = 26,2 + 2$  KeV. Aucune mesure n'avait mis en évidence cette dernière résonnance.

6. DIFFUSION ELASTIQUE DES NEUTRONS DE 500 KeV A 1100 KeV PAR LE FER  
(G. BARDOLLE, J. CABE, M. LAURAT, M. LONGUEVE)

Ce travail fait suite à des mesures de sections efficaces totales sur le fer entre 400 KeV et 1200 KeV (figure 13) (9) et s'inscrit dans le cadre de la recherche d'une structure intermédiaire dans cette gamme d'énergie (10) (11). Une première série de mesures de diffusion élastique comprenant deux courbes d'excitation et trois distributions angulaires ont déjà été présentées (12). Nous complétons ces résultats par quatre courbes d'excitation à  $\theta = 20^\circ$ ;  $\theta = 54^\circ$ ;  $\theta = 90^\circ$  et  $\theta = 109^\circ$  (figure 14) ainsi que par trois distributions angulaires aux énergies respectives de 630 KeV, 770 KeV et 970 KeV (figure 15). Ces énergies correspondent aux minimums et maximums de la résonnance. La figure 16 présente ces mêmes distributions angulaires comparées à un développement en série de Polynômes de Legendre. Toutes ces mesures ont été effectuées avec une dispersion en énergie de 40 KeV de façon à recouvrir plusieurs pics de structure fine.

Les résultats sont corrigés de l'absorption dans l'échantillon ainsi que des diffusions multiples par une méthode de Monte-Carlo. Les erreurs expérimentales sont de l'ordre de 5%.

7. MESURE DE  $\bar{N}_p$  ET DE  $P(\bar{v})$  POUR  $^{235}U$ ,  $^{238}U$  ET  $^{239}Pu$  EN FISSIONS INDUITES PAR DES NEUTRONS D'ENERGIE COMPRISE ENTRE 1,5 ET 15 MeV  
(J. FREHAUT, J. GAURIAU, M. LABAT, J. PERCHEREAU, M. SOLEILHAC)

Nous avons mesuré  $\bar{N}_p$  (nombre moyen de neutrons prompts de fission) et les probabilités associées  $P(\bar{v})$  (probabilité d'émission de neutrons par fission) simultanément sur  $^{235}U$ ,  $^{238}U$ ,  $^{239}Pu$  en fissions provoquées par des neutrons d'énergie comprise entre 1,5 et 15 MeV. Ces trois matériaux fissiles sont contenues dans une chambre à fission à 45 électrodes parallèles qui renferme également le corps étalon ( $^{252}Cf$ ).

...Toutes les mesures ont été faites en utilisant le faisceau pulsé d'un accélérateur Tandem Van de Graaff 12 MeV. Les neutrons sont produits par réaction p-t ou d-d avec une cible gazeuse. Les résultats des 27 mesures effectuées dans le domaine d'énergie signalé sont en cours d'exploitation. Le Tableau I présente l'ensemble des  $\bar{V}_p$  obtenus pour les trois corps considérés (résultats provisoires). Pour l' $^{235}U$  une discontinuité assez nette (2%) apparaît au voisinage du seuil du phénomène n - n'f (6 MeV). Pour  $^{238}Pu$  cette discontinuité semble moins apparente. Par ailleurs la loi  $P(V=f)$  ( $V_p$ ) semble indépendante du matériau fissile (pour les 3 matériaux étudiés) et la variance de la distribution des probabilités augmente avec  $V_p$ .

#### 8. ETUDE DU RAYONNEMENT GAMMA PRODUIT PAR DIFFUSION INELASTIQUE

##### DES NEUTRONS DE 2,5 MeV ET DE 14 MeV

( G. HAOUAT, J. LACHKAR, J. SIGAUD)

Les gamma de désexcitation émis par divers matériaux, après diffusion inélastique des neutrons de 2,5 MeV et de 14 MeV ont été enregistrés. Des mesures ont été entreprises sur le Fer naturel (à En = 2,5 MeV), le carbone et l'hydrogène (à En = 14 MeV) et sur l' $^{197}Or$  (à En = 2,5 MeV et 14 MeV). Ces expériences ont permis de préciser ou de mettre en évidence certains niveaux d'énergie (figure 17 cas de  $^{197}Au$  (13)). La mesure des distributions angulaires des gamma de désexcitation émis par le Fer a permis de déterminer l'anisotropie des transitions les plus fournies (Table II)

La détection des  $\gamma$  a été réalisé au moyen d'un détecteur coaxial au Ge (Li) de 15 cm<sup>3</sup>. Les  $\gamma$  de désexcitation sont discriminés des neutrons diffusés par temps de vol à l'aide de la méthode de la particule associée (13).

Une méthode de déconvolution des spectres  $\gamma$  à l'aide d'un ordinateur est en préparation.

Références :

- (1) - J. Jouanigot, G. Bardolle, J. Cabe, J. Chretien, M. Laurat : Nucl. Inst. Méth. 47 (1967) 105 .
- (2) - M. Laurat : Thèse de Docteur-Ingénieur, Université de Paris (à paraître).
- (3) - Marquez et coll. Nucl. Phys. A 97 (1967) 321 .
- (4) - Phillips : Rev. Mod. Phys. 37 (1965) 409.
- (5) - D.R. Koehler, R.A. Mann : Phys. Rev. 135 B (1964) 91 .  
et Phys. Rev. 138 B (1965) 607 .
- (6) - J. Cabe, M. Laurat, P. Yvon, G. Bardolle : J. de Phys.  
(à paraître).
- (7) - R.E. Fields, M. Walt : Phys. Rev. 83 (1951) 479
- (8) - R.O. Lane, A.S. Langsdorf, J.R. Monahan, A.J. Elwyn :  
Phys. Rev. 126 (1962) 1105.
- (9) - J. Cabe, M. Laurat, P. Yvon, E.A.N.D.C. (E) - 57 U .
- (10)- J. Cabe, M. Laurat, P. Yvon, G. Bardolle : Nucl. Phys.  
A 102 (1967) 92.
- (11)- J. Cabe : Rapport C.E.A. 3279 (1967)
- (12)- J. Cabe, M. Laurat, G. Bardolle, M. Longueve : E.A.N.D.C.  
(E) - 76 U .
- (13)- G. Haouat, J. Lachkar, J. Sigaud (à paraître)

$E_n$ MeV	$\Delta E_n$ keV	(1) : $^{235}\text{U}$	(2) : $^{238}\text{U}$	(2) : $^{239}\text{Pu}$	$E_n$ MeV	$\Delta E_n$ keV	(1) : $^{235}\text{U}$	(2) : $^{238}\text{U}$	(2) : $^{239}\text{Pu}$
1,36	165	2,551	2,452	3,060	9,49	110	3,809	3,748	4,324
1,87	150	2,631	2,597	3,152	9,74	110	3,859	3,805	4,333
2,45	125	2,688	2,641	3,222	9,98	100	3,871	3,857	4,389
2,98	105	2,751	2,679	3,304	10,47	95	3,956	3,896	4,460
3,50	100	2,804	2,799	3,372	10,96	90	3,978	3,976	4,554
4,03	90	2,890	2,884	3,467	11,44	85	4,080	4,061	4,609
5,06	70	3,040	3,080	3,628	11,93	80	4,122	4,136	4,680
6,08	65	3,254	3,234	3,791	12,41	80	4,197	4,196	4,665
6,97	170	3,422	3,403	3,937	12,88	80	4,269	4,278	4,810
7,09	65	3,428	3,401	3,970	13,36	75	4,341	4,334	4,849
7,48	160	3,532	3,426	3,996	13,84	75	4,411	4,445	4,939
7,99	145	3,596	3,540	4,102	14,31	70	4,481	4,496	4,977
8,49	130	3,668	3,595	4,169	14,79	70	4,508	4,498	5,048
9,00	120	3,734	3,693	4,242					

TABLEAU I

(1) Demi largeur totale du spectre de neutrons issus de la source

(2) Référence :  $^{252}\text{cf} = 3,7820 \pm 0,0000$

La précision des mesures de  $\bar{\nu}_p$  est inférieure à  $\pm 1\%$ .

TABLE II

Isotope	$E_\gamma$ MeV	$\left(\frac{d\sigma}{d\Omega}\right)_{15^\circ}$ mb/ster	$\left(\frac{d\sigma}{d\Omega}\right)_{90^\circ}$ mb/ster	Anisotropie
$^{56}\text{Fe}$	0,845	$93 \pm 17$	$60 \pm 14$	$+0,5 \pm 0,3$
$^{56}\text{Fe}$	1,240	$13 \pm 6$	$11 \pm 4$	$+0,18 \pm 0,3$
$^{54}\text{Fe}$	1,14	$3 \pm 1$	$1,6 \pm 1$	$>0$
$^{54}\text{Fe}$	1,41	2 mb	2 mb	---

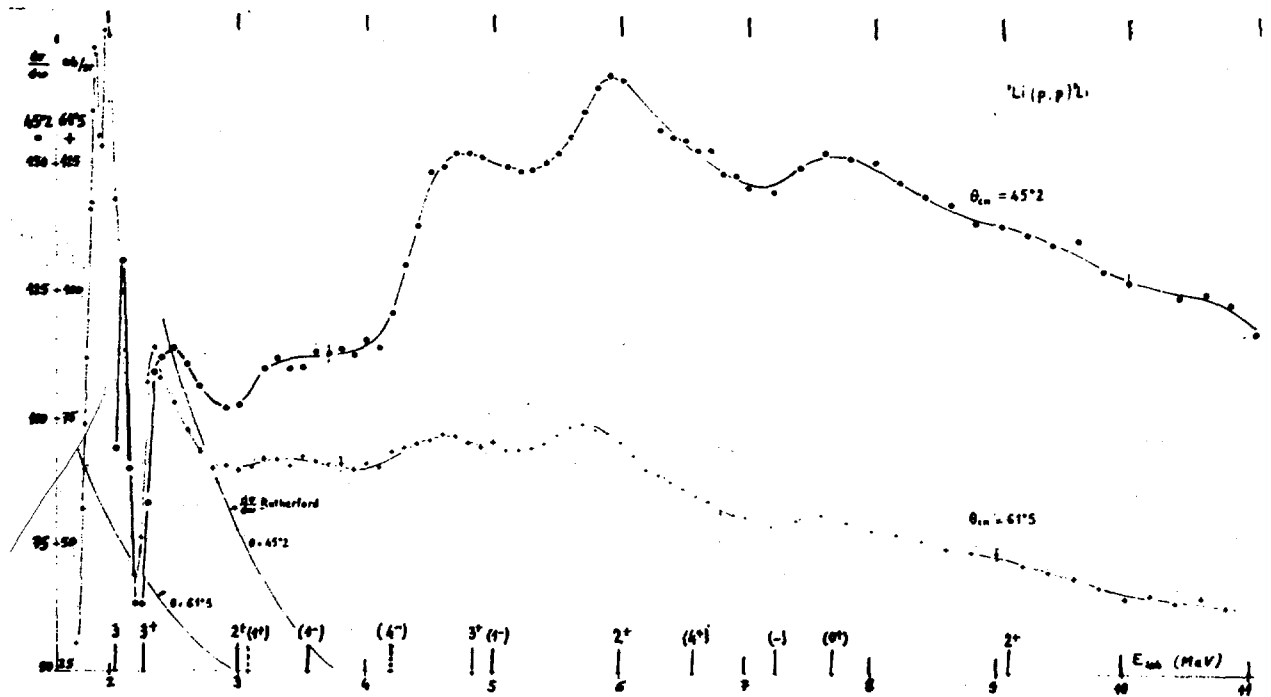


Figure.2

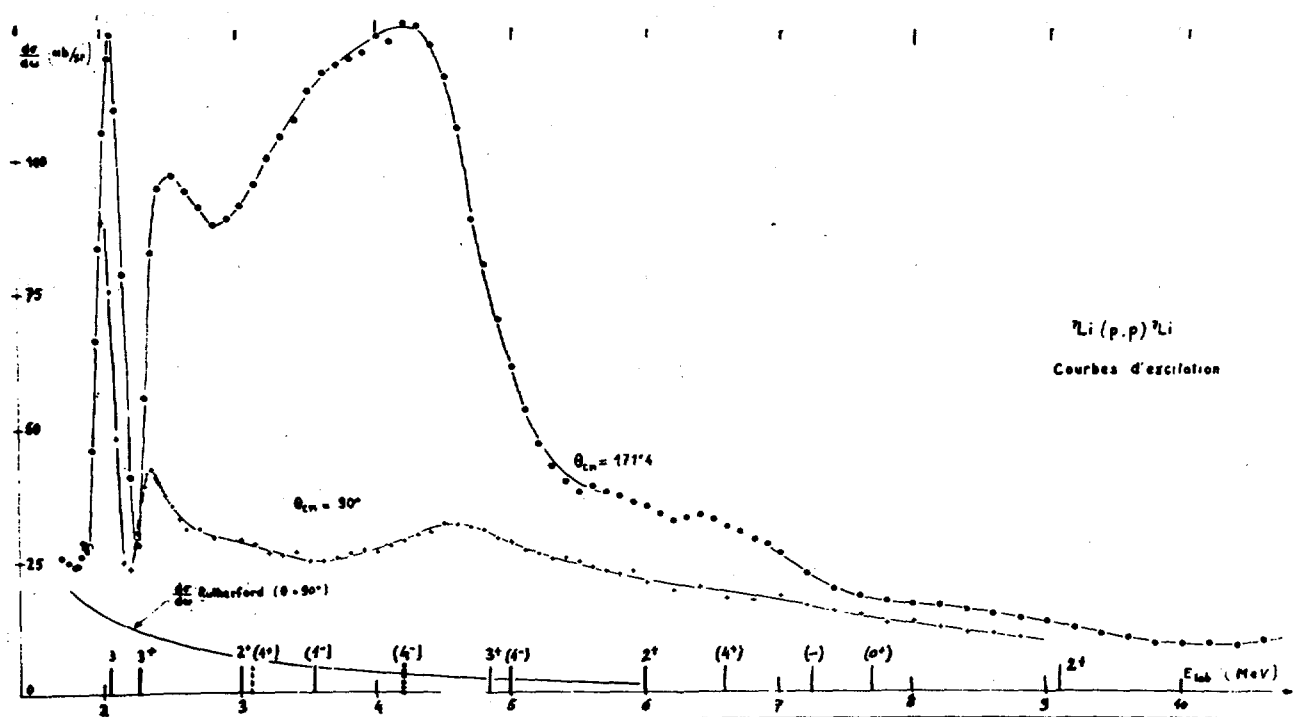


Figure.1

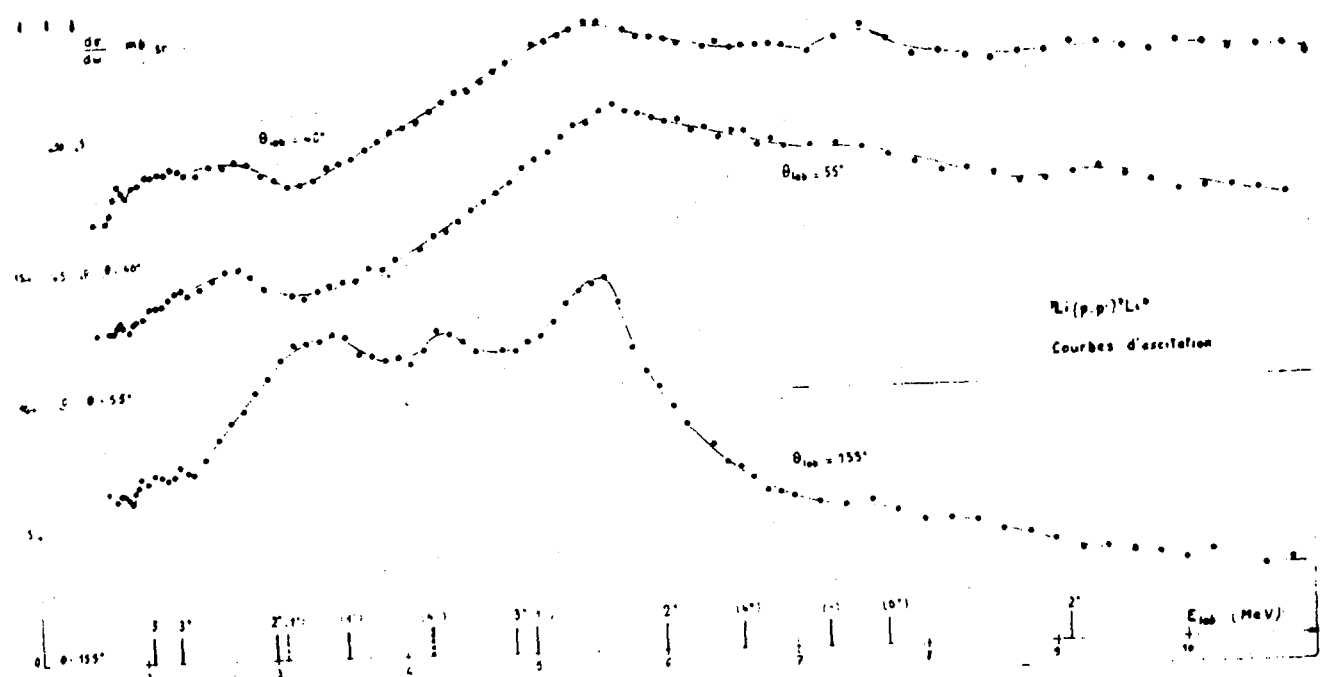


Figure 3

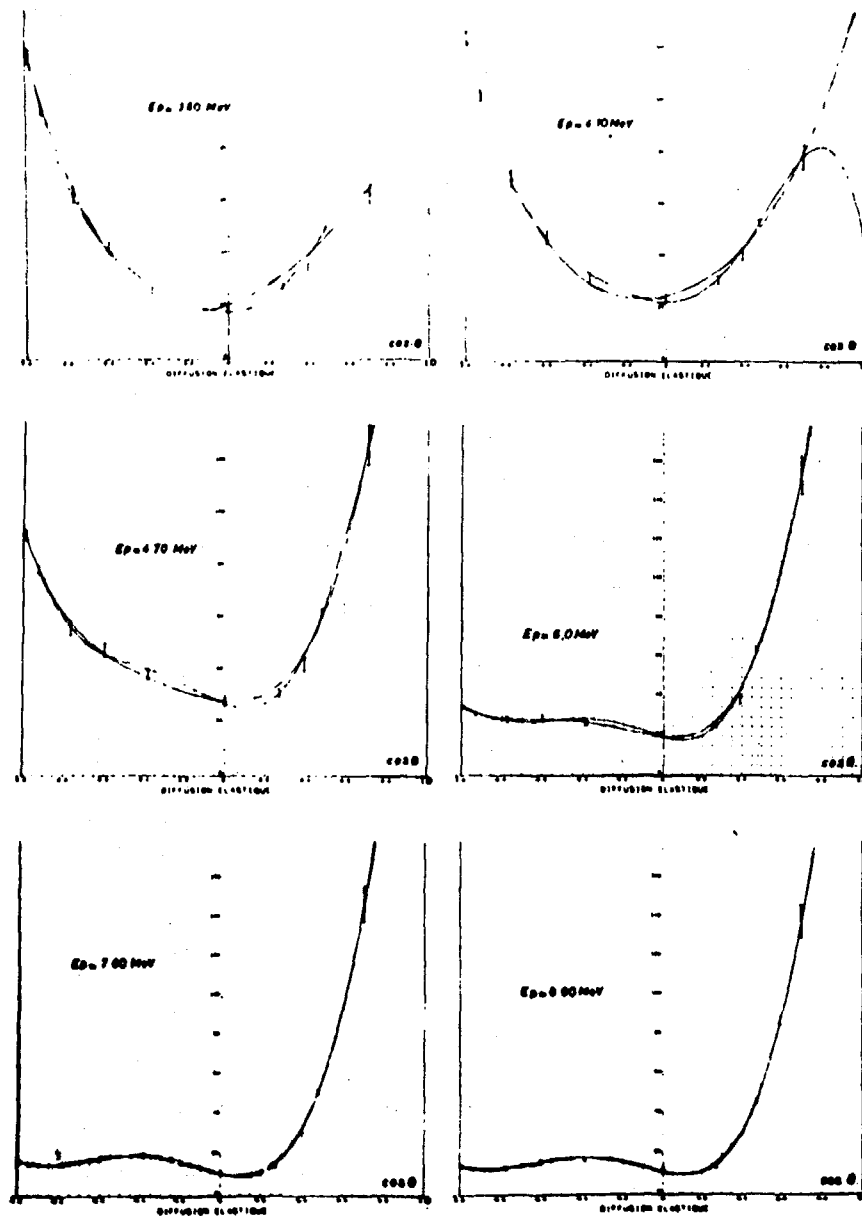


Figure 4

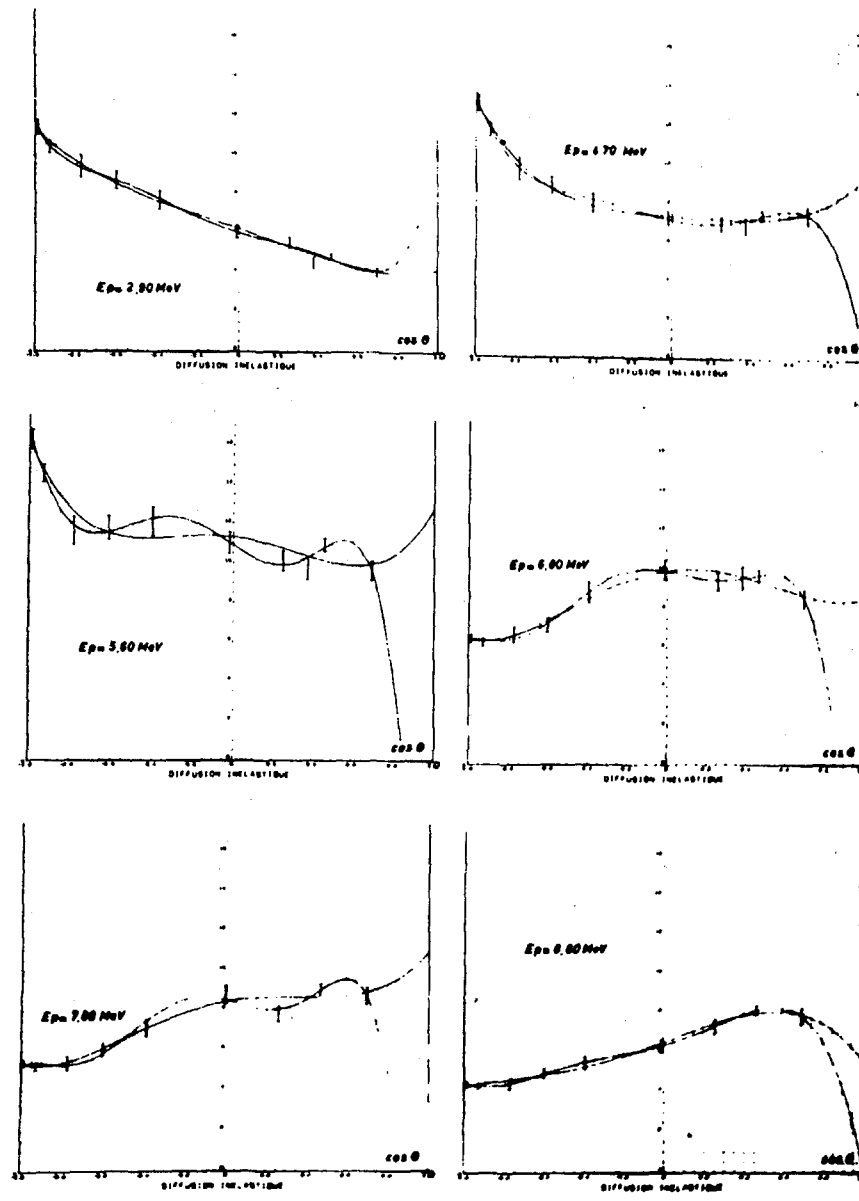


Figure 5

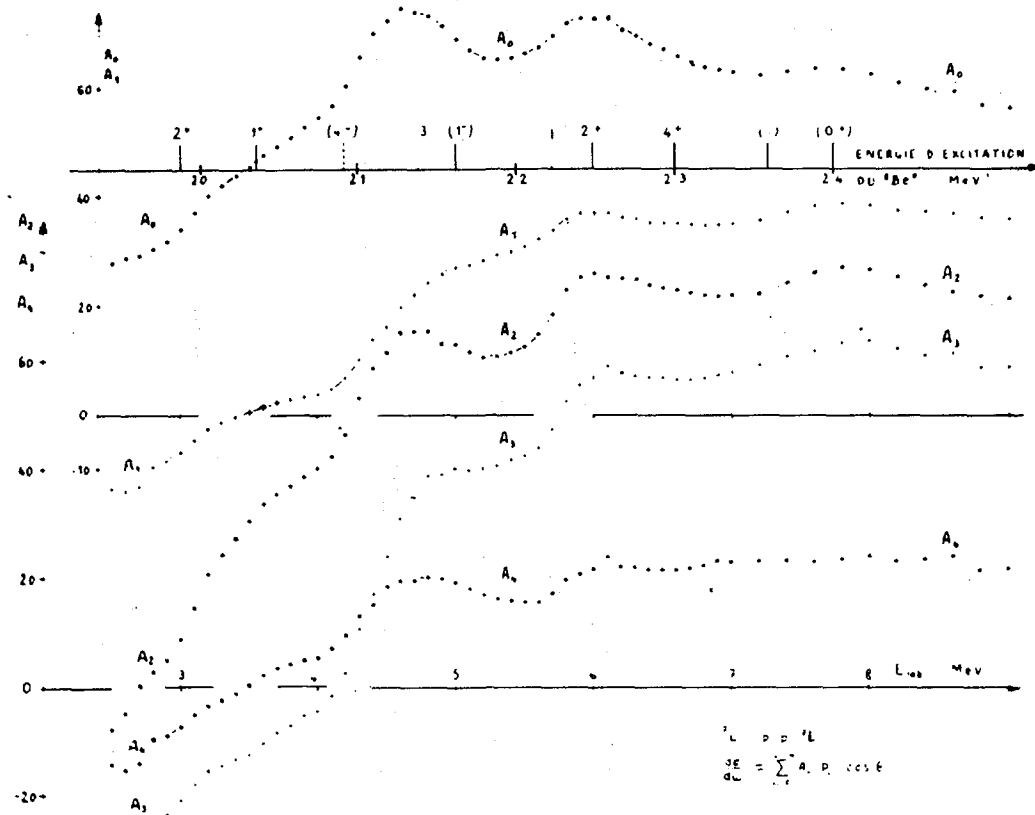
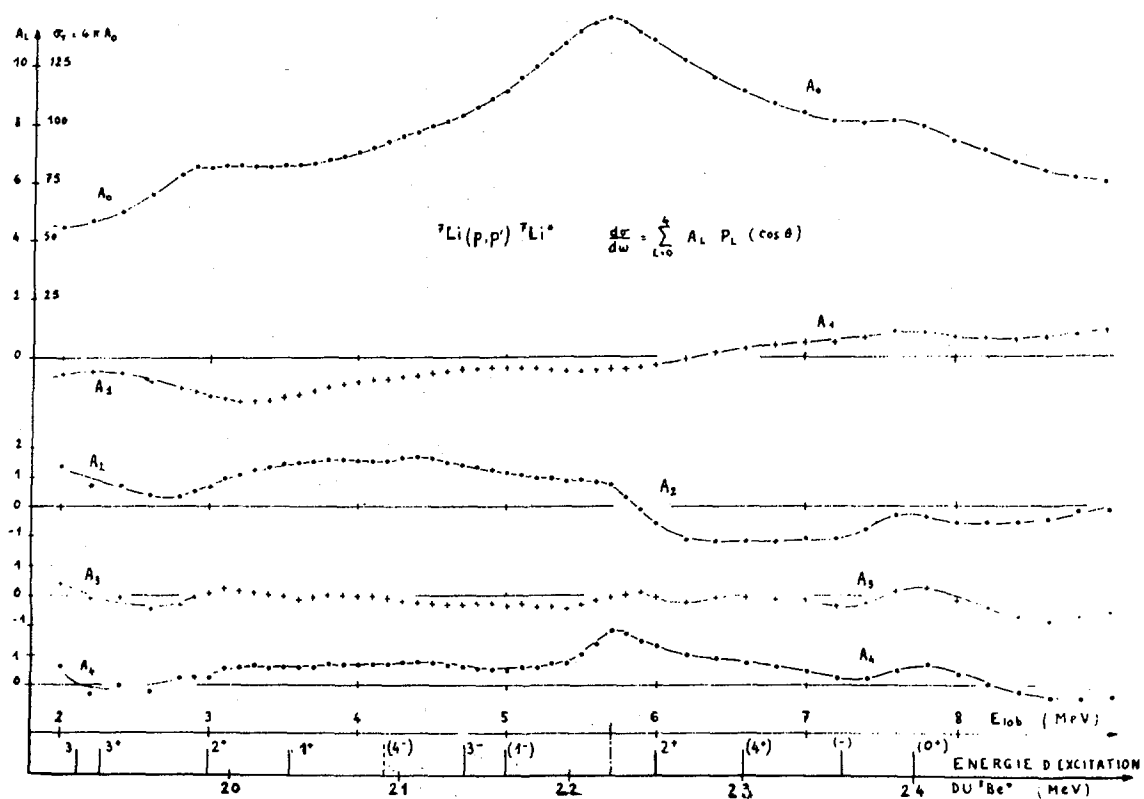


Figure 6



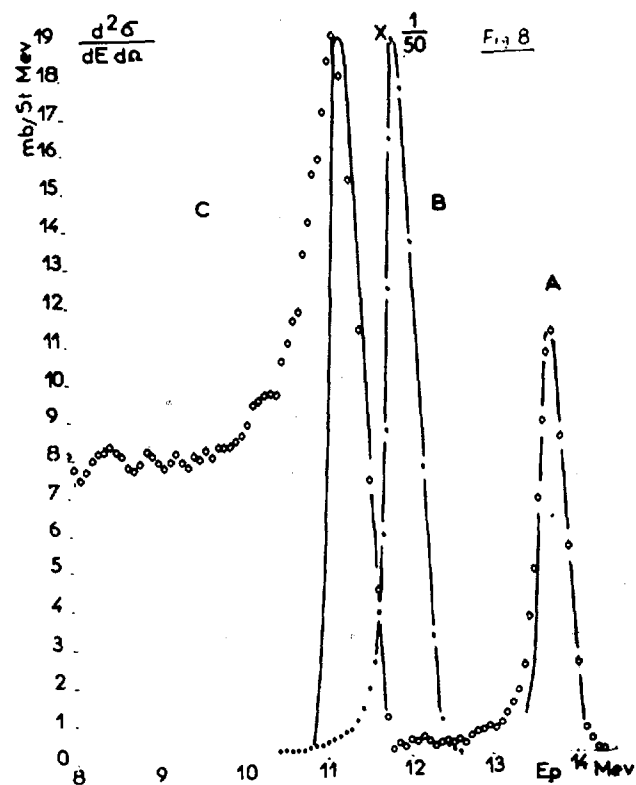
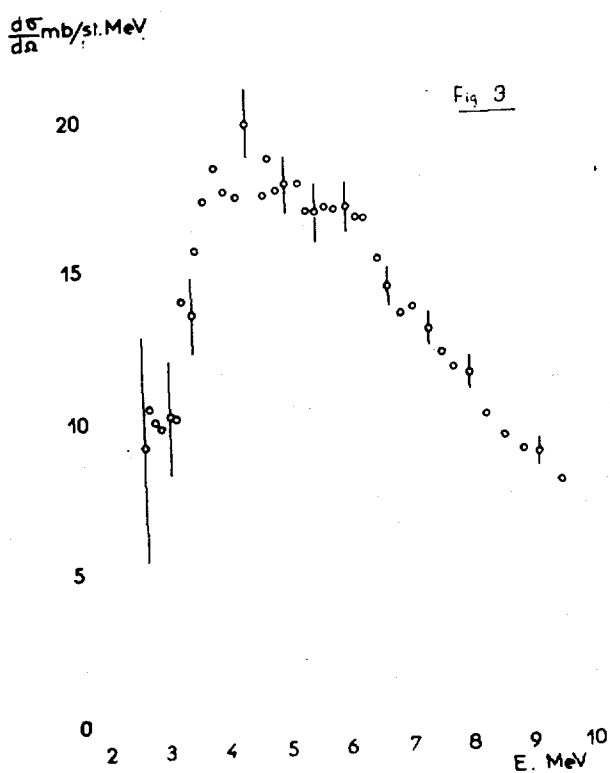


Figure. 10

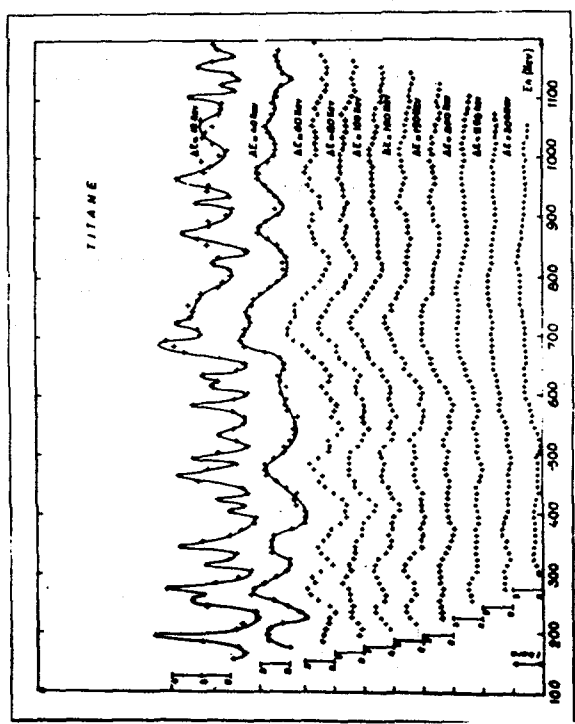


Figure. 11

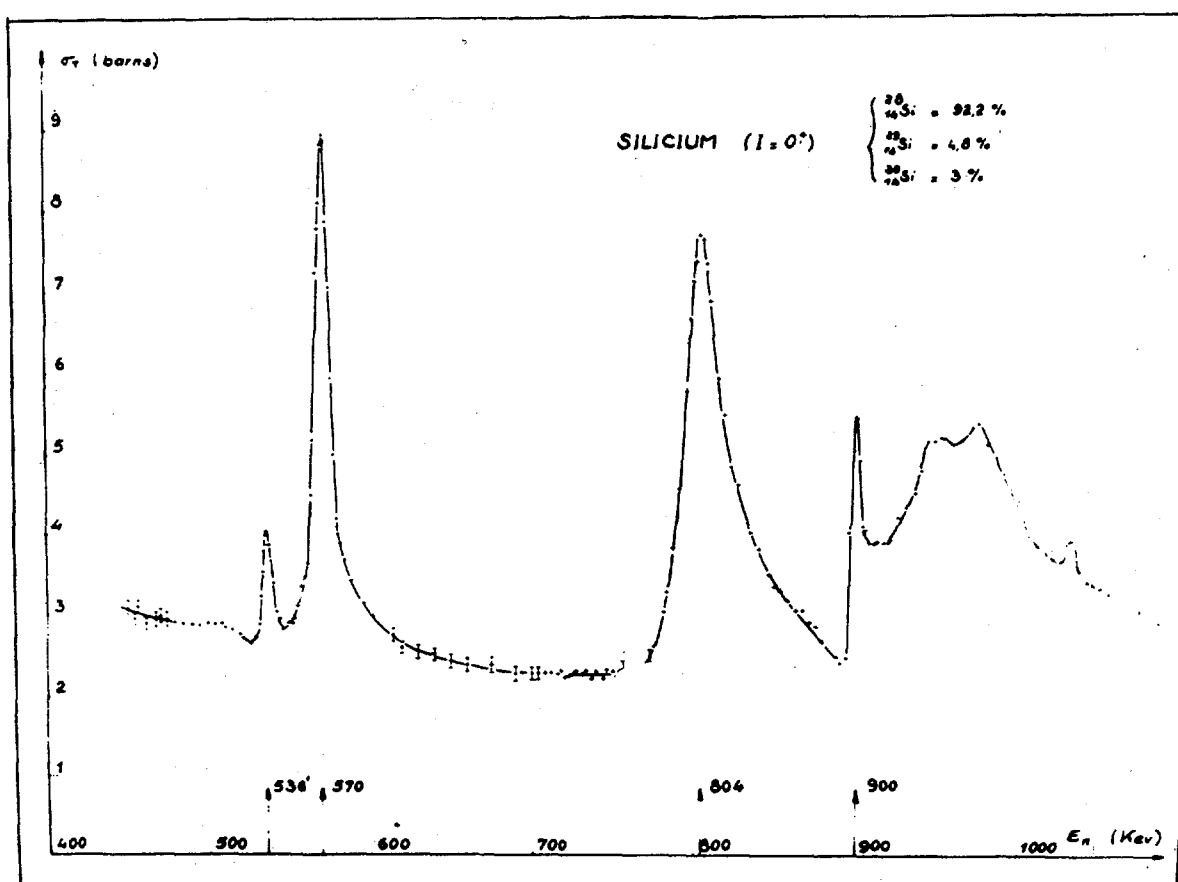


Figure 12

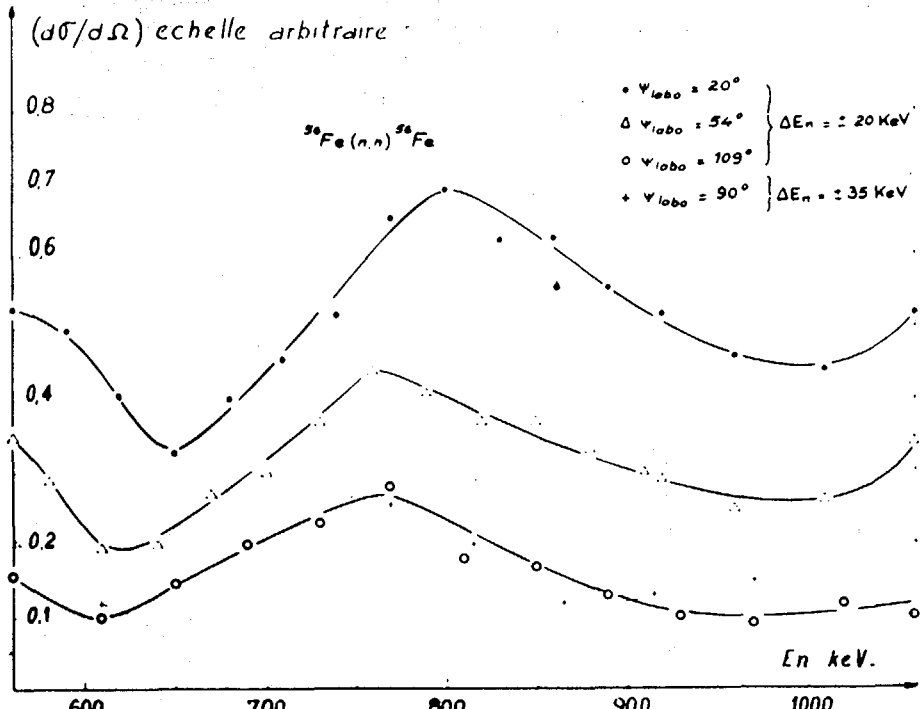


Figure 14

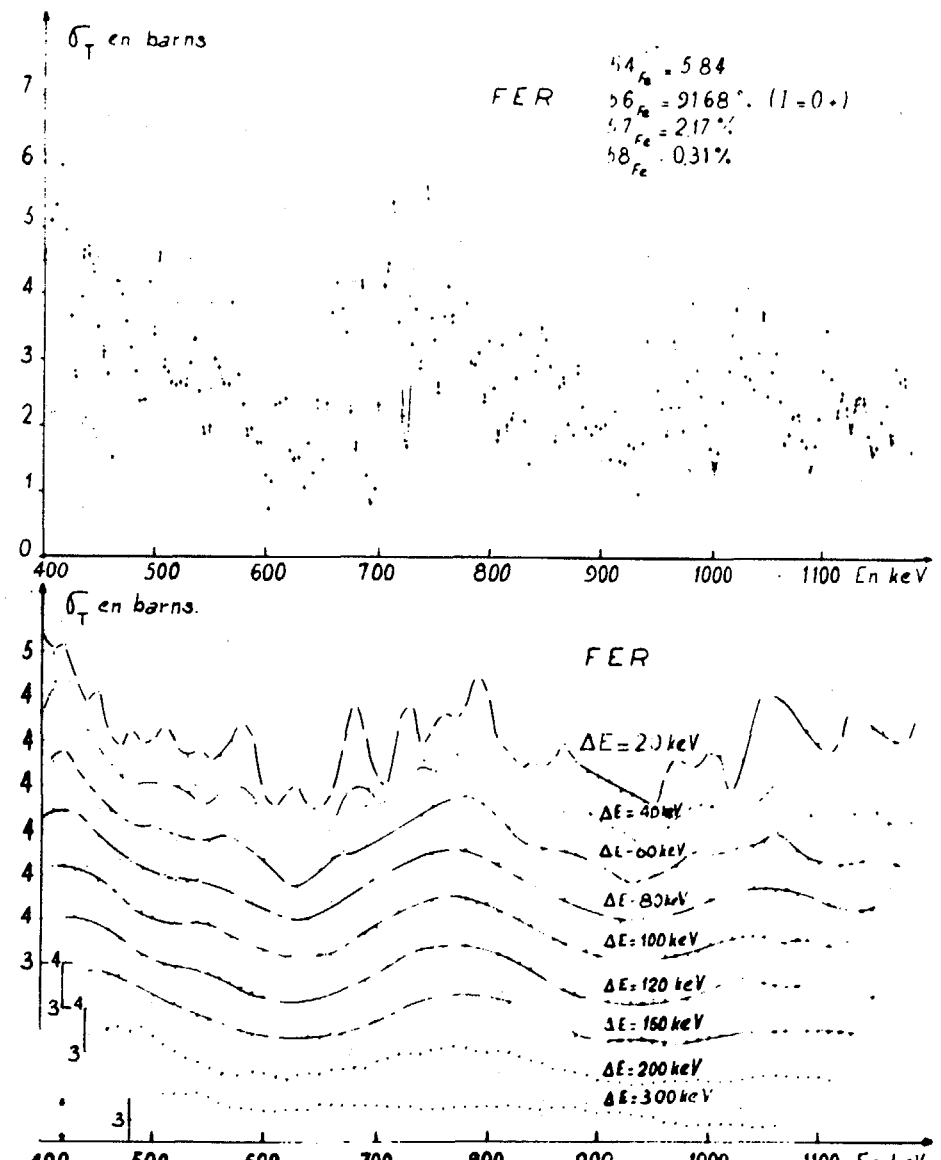


Figure 13

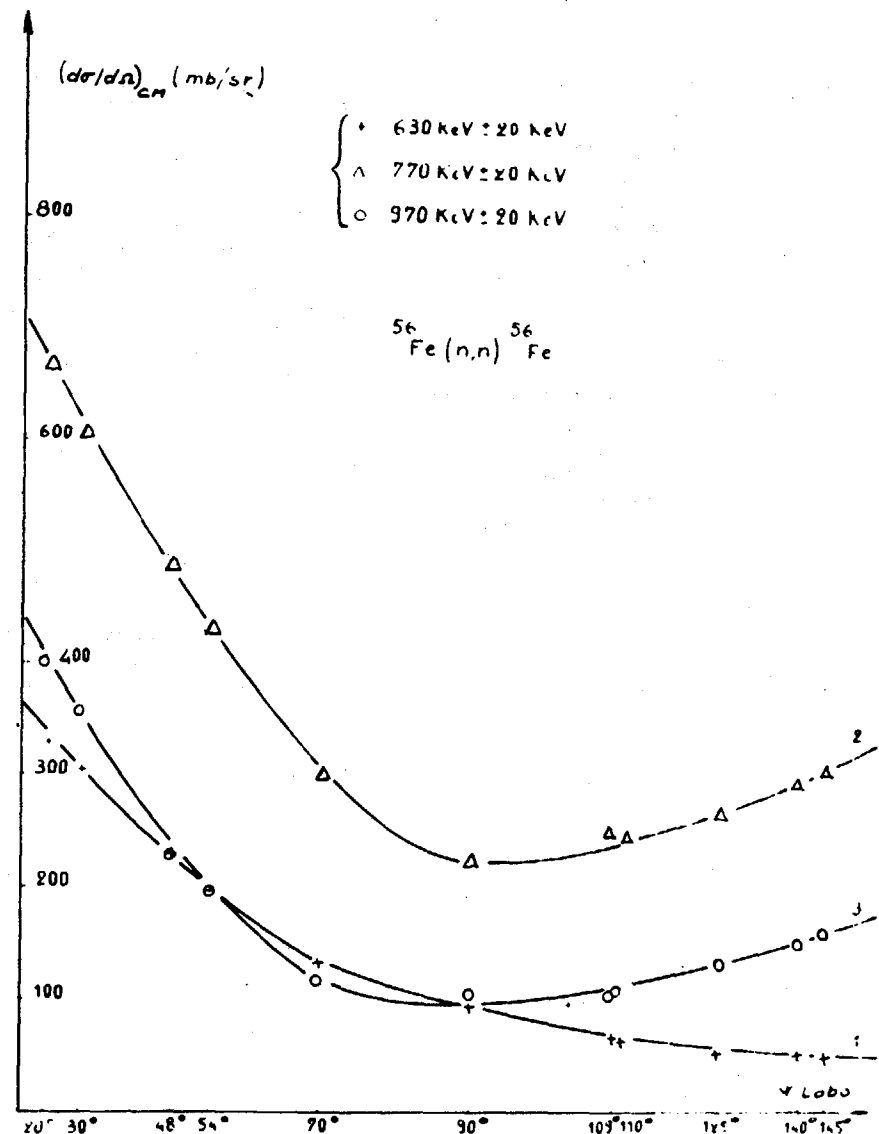
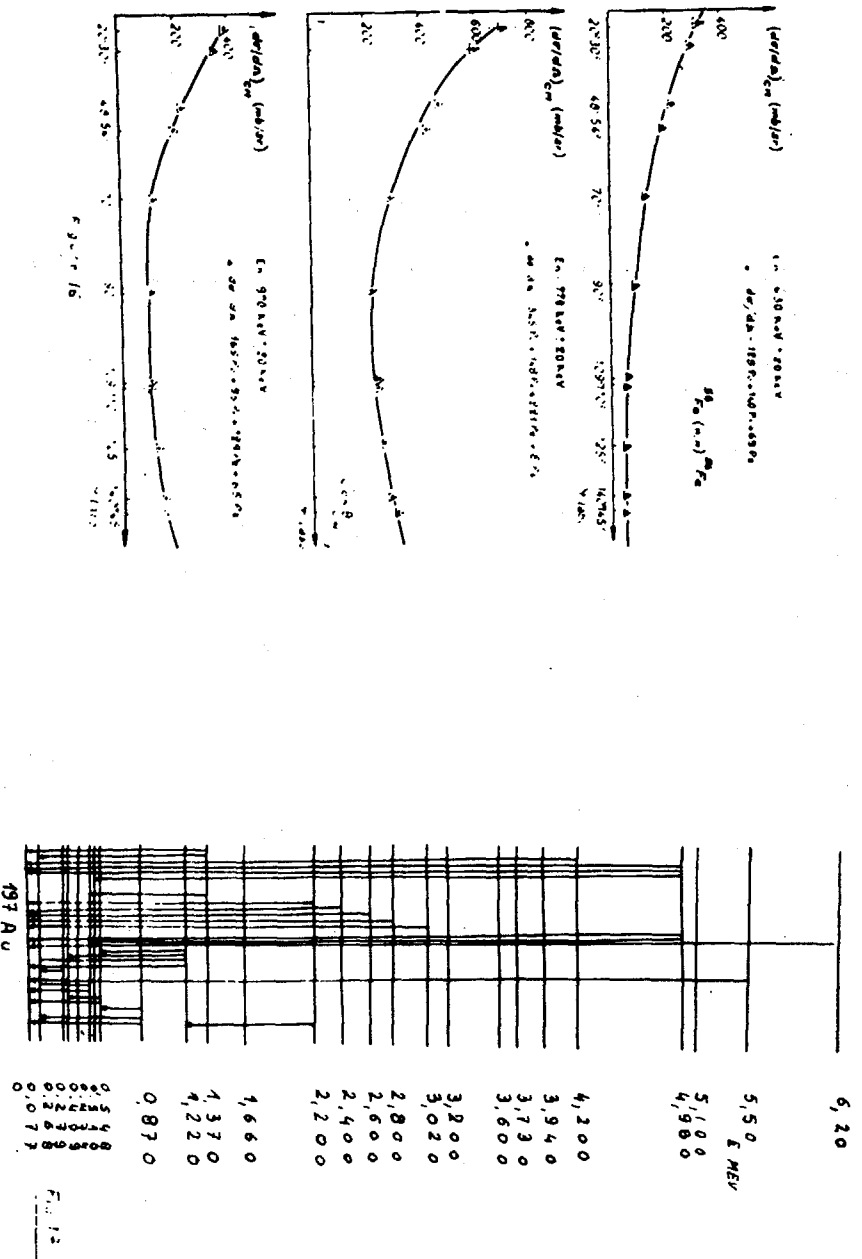


Figure 15

XXVI. SERVICE DE PHYSIQUE GENERALE DU COMMISSARIAT A L'ENERGIE ATONIQUE (FRANCE) -

F. DELOBEAU

La section de mesures nucléaires poursuit l'étude des spectres énergétiques de neutrons et de gammas : dans les réactions ( $n, n$ ) induites par des neutrons de 14 MeV, et dans les réactions ( $n, \gamma$ ) induites par des neutrons de 14 MeV ou de 5 à 9 MeV, ces derniers étant produits au moyen d'un accélérateur Van de Graaff tandem de 12 MeV. Les spectres neutroniques sont mesurés par temps de vol ; les spectres de gammas sont mesurés au moyen d'une chaîne de détection comprenant un "NaI".

Les réactions ( $n, n$ ) ont été étudiées sur le fer, le plutonium 239, l'uranium naturel, et le scandium (diffusion élastique seulement). Les résultats obtenus sur ces deux derniers corps ont fait l'objet de communications au congrès organisé en Mars à Bordeaux par la Société Française de Physique.

Les réactions ( $n, \gamma$ ) ont été étudiées sur ces mêmes éléments (Fe, U, Pu) et sont en cours d'étude ou en projet sur Au, N, O.

Sont également en projet pour 1968 :

- l'examen des distributions angulaires des gammas.
- le remplacement des NaI par des détecteurs en germanium.
- l'étude par double temps de vol des réactions ( $n, 2n$ ).

XXVII. LABORATOIRE DE PHYSIQUE NUCLEAIRE, CENTRE D'ETUDES NUCLEAIRES DE GRENOBLE - COMMISSARIAT A L'ENERGIE ATOMIQUE, et UNIVERSITE DE GRENOBLE (FRANCE).

R. BOUCHEZ.

1. REACTIONS NUCLEAIRES SUR NOYAUX LEGERS -

1.1.  $^6\text{Li}$  ( $n, n'$ ) 14 MeV (1) - Fig. 1.

On a mesuré la section efficace différentielle de la réaction  $^6\text{Li}$  ( $n, n'$ )  $^6\text{Li}$  (3,56 MeV), à  $15^\circ - 45^\circ - 60^\circ$  (L), et on a obtenu respectivement :

$$\sigma_c(\theta) = (4 \pm 1,5), (2,2 \pm 1), (1,4 \pm 0,6) \text{ mb/sr.}$$

Ce résultat reste bien supérieur aux valeurs correspondant aux réactions ( $p, p'$ ), ( $p, n$ ) ou ( $n, p$ ) arrivant aux états analogues  $0^+$  du triplet de spin isotopique  $T = 1$ .

Cette mesure a été effectuée avec une spectrométrie de neutrons rapides à temps-de-vol, améliorée par une identification  $n-\gamma$ .

1.2.  $^6\text{Li}$  ( $p, p'$ ) 14 MeV (2) - Fig. 2

L'Expérience a été faite avec le cyclotron de l'Université d'Ur-bana (Illinois) -USA-. On a étudié la diffusion élastique et inélastique ( $Q = -2,18$  et  $-3,56$  MeV) ; les sections efficaces différentes ont été mesurées de  $15^\circ$  à  $160^\circ$ , en valeur relative, puis normalisées avec les résultats de SHERR (Bull. Amer. Phys. Soc.. 1954, 1, 231). Les sections efficaces totales ainsi obtenues sont de  $(760 \pm 23)$  mb pour la diffusion élastique,  $(76,3 \pm 2)$  mb et  $(3,2 \pm 1)$  mb respectivement pour les diffusions inélastiques.

Nous pensons préciser ces valeurs par l'emploi d'une normalisation plus sûre.

1.3.  $\mathbf{D}(n, p)nn$  14 MeV (3) (4) - Fig. 3

Le spectre de protons à  $0^\circ$  a été étudié à l'aide d'un télescope à trois semi-conducteurs à faible bruit-de-fond ; l'on a mis en évidence à 11,4 MeV le pic dû à l'interaction  $n-n$  dans l'état final  $^1S_0$ .

Une analyse préliminaire indique une longueur de diffusion  $a_{nn} = -23 \pm 2$  fm.

1.4. Mise en évidence de l'interaction neutron-neutron dans la réaction  $\mathbf{D}(n, 2n)$  à 14,5 MeV par spectromètre à double temps-de-vol (5) fig.4

Dans une première expérience multiparamétrique, environ 3 000 événements  $\mathbf{D}(n, 2n)$  ont été sélectionnés. Les deux neutrons de l'état final ont été détectés vers l'avant au même angle ( $30^\circ$  L). Les résultats sont comparés à des modèles à l'aide d'une simulation de l'expérience basée sur la méthode de Monte-Carlo. La valeur de la longueur de diffusion ainsi obtenue est  $a_{nn} = -22 \pm 3$  fm.

R E F E R E N C E S

- (1) G. PERRIN - thèse 3ème Cycle - Grenoble 1967)
- (2) F. MERCHEZ, A.I. YAVIN : à paraître
- (3) J.M. HELLEBOID - Thèse Docteur-Ingénieur, Grenoble (1967)
- (4) G. BENEDETTI - Tèse 3ème Cycle, Grenoble (à paraître)
- (5) G. PERRIN, P. PERRIN, A. GIORNI, P. QUIVY, M. SALTMARSH,  
S. DESREUMAUX, R. BOUCHEZ : "International Symposium  
on lighy nuclei, few body problems and nuclear forces".  
Brela (Jugoslavija), July 1967.

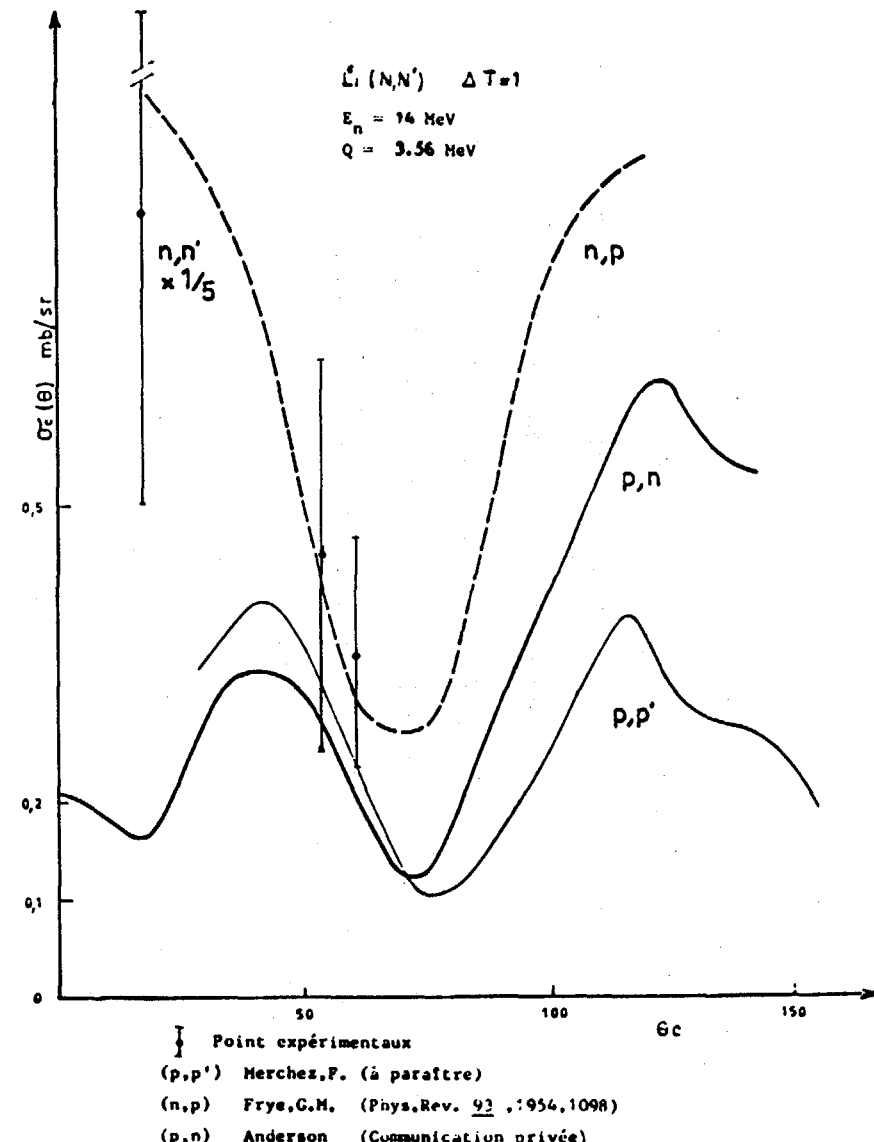
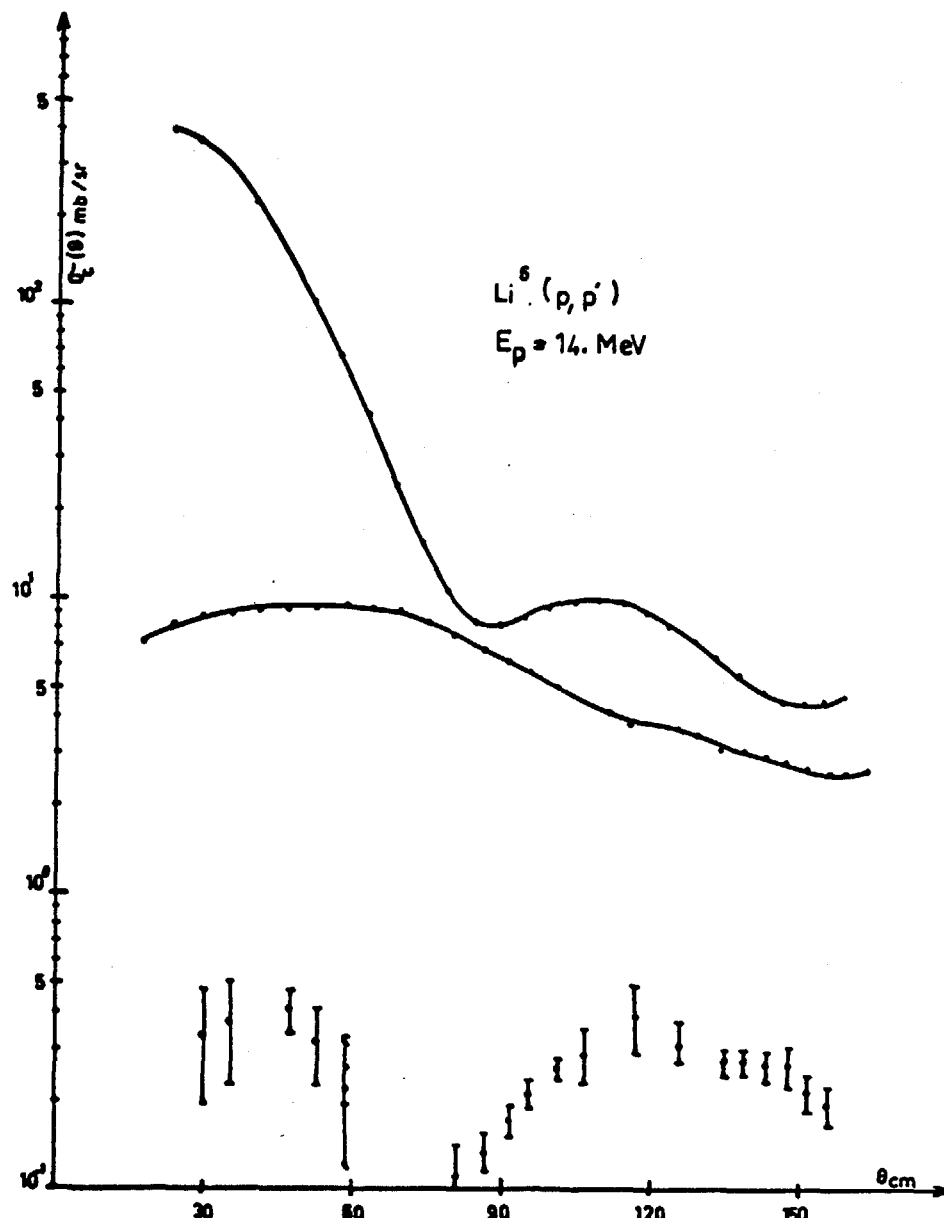


Fig. 1 Expériences \$(n, n'), (p, p'), (p, n)\$ sur  ${}^6\text{Li}$

Fig. 2 Diffusions élastique et inélastique  ${}^6\text{Li}(p, p')$  à 14 MeV

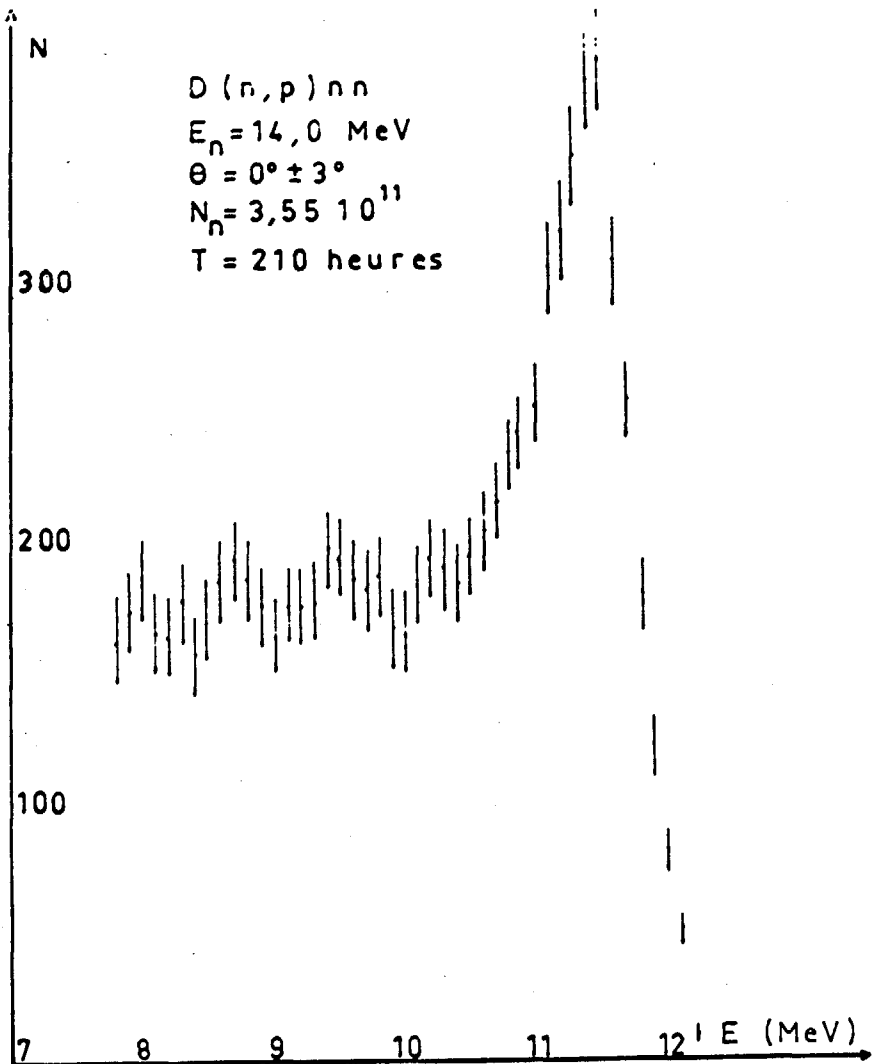


Fig. 3 Spectre des protons D( $n,p$ )nn à  $0^\circ$

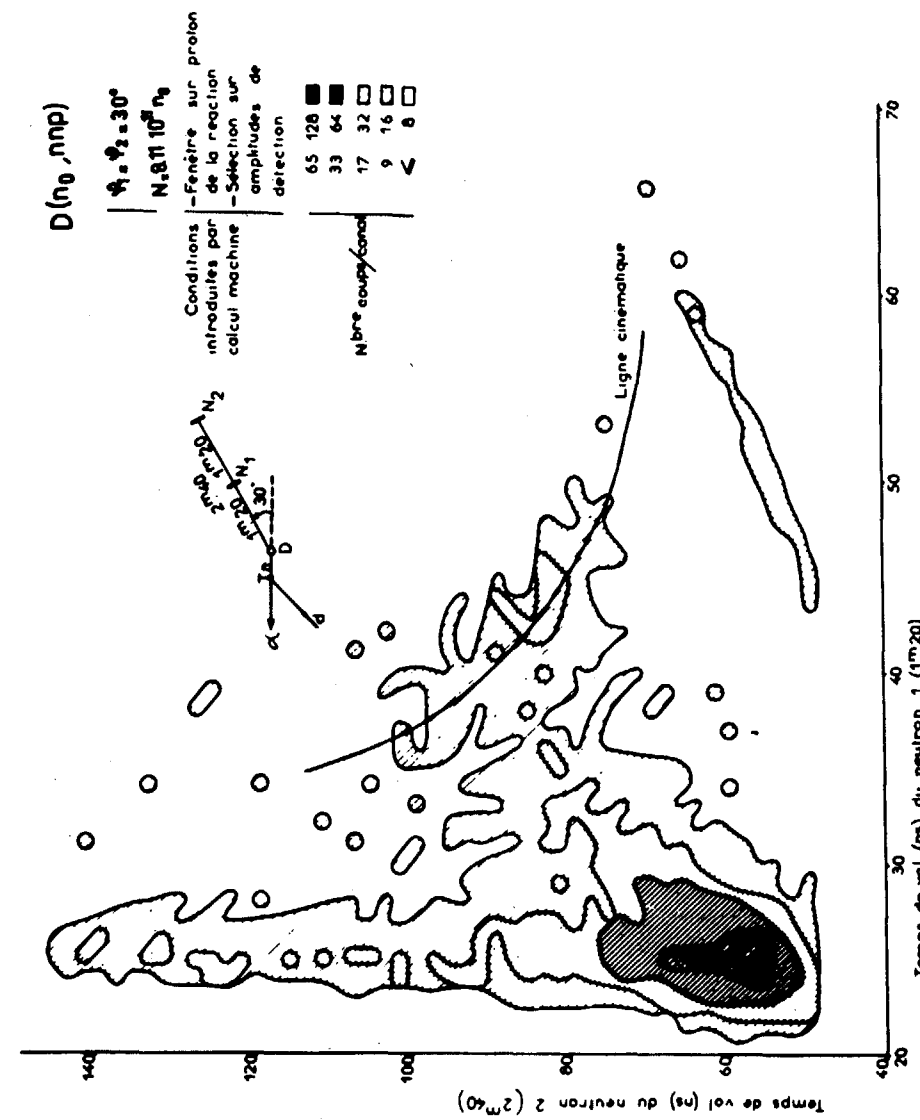


Fig. 4 Spectres biparamétriques ( $t_1, t_2$ )